

GEOTECHNICAL EARTHQUAKE ENGINEERING



STEVEN L. KRAMER

Geotechnical Earthquake Engineering

PRENTICE-HALL INTERNATIONAL SERIES
IN CIVIL ENGINEERING AND ENGINEERING MECHANICS
William J. Hall, Editor

- Au and Christiano, *Fundamentals of Structural Analysis*
Au and Christiano, *Structural Analysis*
Barson and Rolfe, *Fracture and Fatigue Control in Structures*, 2/e
Bathe, *Finite Element Procedures in Engineering Analysis*
Berg, *Elements of Structural Dynamics*
Biggs, *Introduction to Structural Engineering*
Chajes, *Structural Analysis*, 2/e
Chopra, *Dynamics of Structures: Theory and Applications to Earthquake Engineering*
Collins and Mitchell, *Prestressed Concrete Structures*
Cooper and Chen, *Designing Steel Structures*
Cording et al., *The Art and Science of Geotechnical Engineering*
Gallagher, *Finite Element Analysis*
Hendrickson and Au, *Project Management for Construction*
Higdon et al., *Engineering Mechanics*, 2nd Vector Edition
Hultz and Kovacs, *Introduction in Geotechnical Engineering*
Humar, *Dynamics of Structures*
Johnston, Lin, and Galambos, *Basic Steel Design*, 3/e
Kelkar and Sewell, *Fundamentals of the Analysis and Design of Shell Structures*
Kramer, *Geotechnical Earthquake Engineering*
MacGregor, *Reinforced Concrete: Mechanics and Design*, 2/e
Mehta and Monteiro, *Concrete: Structure, Properties and Materials*, 2/e
Melosh, *Structural Engineering Analysis by Finite Elements*
Meredith et al., *Design and Planning of Engineering Systems*, 2/e
Mindess and Young, *Concrete*
Nawy, *Prestressed Concrete*
Nawy, *Reinforced Concrete: A Fundamental Approach*, 2/e
Pfeffer, *Solid Waste Management*
Popov, *Engineering Mechanics of Solids*
Popov, *Introduction to the Mechanics of Solids*
Popov, *Mechanics of Materials*, 2/e
Schneider and Dickey, *Reinforced Masonry Design*, 2/e
Wang and Salmon, *Introductory Structural Analysis*
Weaver and Johnson, *Structural Dynamics by Finite Elements*
Wolf, *Dynamic Soil-Structure Interaction*
Wray, *Measuring Engineering Properties of Soils*
Yang, *Finite Element Structural Analysis*

Geotechnical Earthquake Engineering

Steven L. Kramer
University of Washington

Prentice-Hall International Series
in Civil Engineering and Engineering Mechanics



Prentice Hall
Upper Saddle River, New Jersey 07458

Library of Congress Cataloging-in-Publication Data

Kramer, Steven Lawrence.
Geotechnical earthquake engineering / Steven L. Kramer.
p. cm. -- (Prentice-Hall civil engineering and engineering
mechanics series)
Includes bibliographical references and index.
ISBN 0-13-374943-6
1. Earthquake engineering. 2. Engineering geology. I. Title.
II. Series.
TA654.6.K72 1996
624.1'762--dc20
95-33020
CIP

Acquisitions editor: **BILL STENQUIST**
Production editor: **IRWIN ZUCKER**
Cover director: **JAYNE CONTE**
Buyer: **JULIA MEEHAN**
Editorial assistant: **MEG WEIST**



©1996 by Prentice-Hall, Inc.
Simon & Schuster / A Viacom Company
Upper Saddle River, NJ 07458

All rights reserved. No part of this book may be
reproduced, in any form or by any means,
without permission in writing from the publisher.

The author and publisher of this book have used their best efforts in preparing this book. These efforts include the development, research, and testing of the theories and programs to determine their effectiveness. The author and publisher make no warranty of any kind, expressed or implied, with regard to these programs or the documentation contained in this book. The author and publisher shall not be liable in any event for incidental or consequential damages in connection with, or arising out of, the furnishing, performance, or use of these programs.

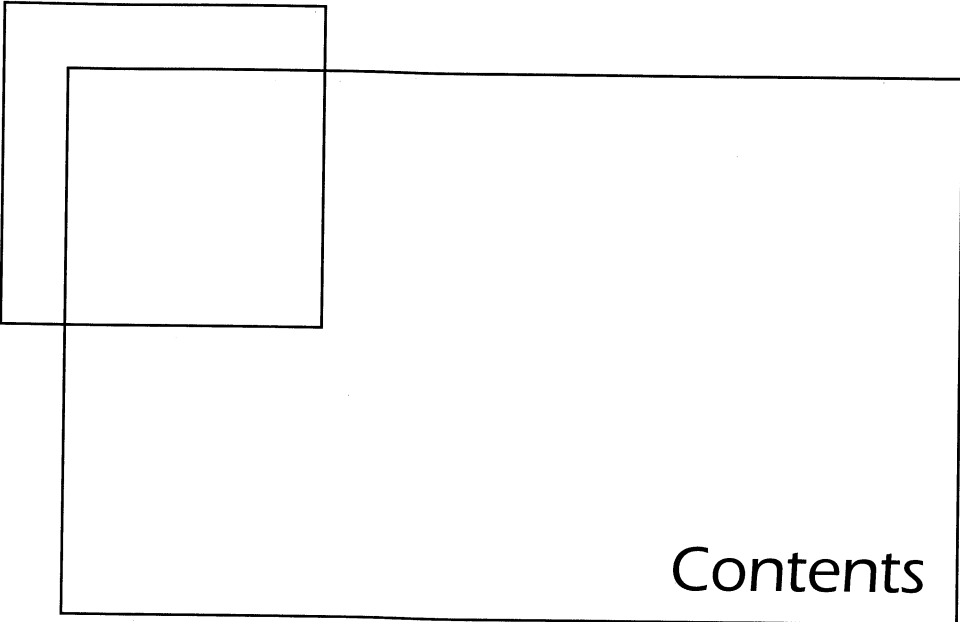
Printed in the United States of America

10 9 8 7 6 5 4 3

ISBN 0-13-374943-6

Prentice-Hall International (UK) Limited, London
Prentice-Hall of Australia Pty. Limited, Sydney
Prentice-Hall Canada Inc., Toronto
Prentice-Hall Hispanoamericana, S.A., Mexico
Prentice-Hall of India Private Limited, New Delhi
Prentice-Hall of Japan, Inc., Tokyo
Simon & Schuster Asia Pte. Ltd., Singapore
Editora Prentice-Hall do Brasil, Ltda., Rio de Janeiro

To my parents



Contents

Preface**xv****1 Introduction to Geotechnical Earthquake Engineering****1**

1.1	Introduction	1
1.2	Background	1
1.3	Seismic Hazards	2
1.3.1	<i>Ground Shaking</i> ,	2
1.3.2	<i>Structural Hazards</i> ,	3
1.3.3	<i>Liquefaction</i> ,	5
1.3.4	<i>Landslides</i> ,	9
1.3.5	<i>Retaining Structure Failures</i> ,	11
1.3.6	<i>Lifeline Hazards</i> ,	11
1.3.7	<i>Tsunami and Seiche Hazards</i> ,	13
1.4	Mitigation of Seismic Hazards	14
1.5	Significant Historical Earthquakes	14

vii

2	Seismology and Earthquakes	18
2.1	Introduction	18
2.2	Internal Structure of the Earth	18
2.2.1	<i>Seismic Waves, 19</i>	
2.2.2	<i>Internal Structure, 20</i>	
2.3	Continental Drift and Plate Tectonics	23
2.3.1	<i>Plate Tectonics, 24</i>	
2.3.2	<i>Plate Boundaries, 29</i>	
2.4	Faults	33
2.4.1	<i>Fault Geometry, 33</i>	
2.4.2	<i>Fault Movement, 34</i>	
2.5	Elastic Rebound Theory	36
2.5.1	<i>Relationship to Earthquake Recurrence, 39</i>	
2.5.2	<i>Relationship to Tectonic Environment, 41</i>	
2.5.3	<i>Seismic Moment, 42</i>	
2.6	Other Sources of Seismic Activity	42
2.7	Geometric Notation	43
2.8	Location of Earthquakes	44
2.9	Size of Earthquakes	45
2.9.1	<i>Earthquake Intensity, 45</i>	
2.9.2	<i>Earthquake Magnitude, 46</i>	
2.9.3	<i>Earthquake Energy, 50</i>	
2.10	Summary	51
3	Strong Ground Motion	54
3.1	Introduction	54
3.2	Strong-Motion Measurement	56
3.2.1	<i>Seismographs, 56</i>	
3.2.2	<i>Data Acquisition and Digitization, 59</i>	
3.2.3	<i>Strong-Motion Processing, 61</i>	
3.2.4	<i>Strong-Motion Instrument Arrays, 62</i>	
3.2.5	<i>Strong-Motion Records, 64</i>	
3.3	Ground Motion Parameters	65
3.3.1	<i>Amplitude Parameters, 66</i>	
3.3.2	<i>Frequency Content Parameters, 70</i>	
3.3.3	<i>Duration, 79</i>	
3.3.4	<i>Other Measures of Ground Motion, 82</i>	
3.3.5	<i>Discussion, 84</i>	

3.4	Estimation of Ground Motion Parameters	84	
3.4.1	<i>Magnitude and Distance Effects,</i>	85	
3.4.2	<i>Development of Predictive Relationships,</i>	86	
3.4.3	<i>Estimation of Amplitude Parameters,</i>	88	
3.4.4	<i>Estimation of Frequency Content Parameters,</i>	91	
3.4.5	<i>Estimation of Duration,</i>	95	
3.4.6	<i>Estimation of Other Parameters,</i>	95	
3.5	Spatial Variability of Ground Motions	100	
3.6	Summary	102	
4	Seismic Hazard Analysis		106
4.1	Introduction	106	
4.2	Identification and Evaluation of Earthquake Sources	107	
4.2.1	<i>Geologic Evidence,</i>	107	
4.2.2	<i>Tectonic Evidence,</i>	113	
4.2.3	<i>Historical Seismicity,</i>	113	
4.2.4	<i>Instrumental Seismicity,</i>	114	
4.3	Deterministic Seismic Hazard Analysis	114	
4.4	Probabilistic Seismic Hazard Analysis	117	
4.4.1	<i>Earthquake Source Characterization,</i>	118	
4.4.2	<i>Predictive Relationships,</i>	126	
4.4.3	<i>Temporal Uncertainty,</i>	127	
4.4.4	<i>Probability Computations,</i>	129	
4.5	Summary	138	
5	Wave Propagation		143
5.1	Introduction	143	
5.2	Waves in Unbounded Media	144	
5.2.1	<i>One-Dimensional Wave Propagation,</i>	144	
5.2.2	<i>Three-Dimensional Wave Propagation,</i>	149	
5.3	Waves in a Semi-infinite Body	156	
5.3.1	<i>Rayleigh Waves,</i>	156	
5.3.2	<i>Love Waves,</i>	162	
5.3.3	<i>Higher-Mode Surface Waves,</i>	164	
5.3.4	<i>Dispersion of Surface Waves,</i>	164	
5.3.5	<i>Phase and Group Velocities,</i>	165	
5.4	Waves in a Layered Body	165	
5.4.1	<i>One-Dimensional Case: Material Boundary in an Infinite Rod,</i>	165	
5.4.2	<i>Three-Dimensional Case: Inclined Waves,</i>	170	
5.5	Attenuation of Stress Waves	174	
5.5.1	<i>Material Damping,</i>	175	
5.5.2	<i>Radiation Damping,</i>	179	
5.6	Summary	180	

6	Dynamic Soil Properties	184
6.1	Introduction	184
6.2	Representation of Stress Conditions by the Mohr Circle	185
6.2.1	<i>Principal Stresses</i> , 187	
6.2.2	<i>Stress Paths</i> , 188	
6.3	Measurement of Dynamic Soil Properties	191
6.3.1	<i>Field Tests</i> , 191	
6.3.2	<i>Laboratory Tests</i> , 215	
6.3.3	<i>Interpretation of Observed Ground Response</i> , 228	
6.4	Stress–Strain Behavior of Cyclically Loaded Soils	228
6.4.1	<i>Some Basic Aspects of Particulate Matter Behavior</i> , 228	
6.4.2	<i>Equivalent Linear Model</i> , 230	
6.4.3	<i>Cyclic Nonlinear Models</i> , 240	
6.4.4	<i>Discussion</i> , 244	
6.5	Strength of Cyclically Loaded Soils	244
6.5.1	<i>Definitions of Failure</i> , 244	
6.5.2	<i>Cyclic Strength</i> , 245	
6.5.3	<i>Monotonic Strength</i> , 246	
6.6	Summary	248
7	Ground Response Analysis	254
7.1	Introduction	254
7.2	One-Dimensional Ground Response Analysis	255
7.2.1	<i>Linear Approach</i> , 256	
7.2.2	<i>Nonlinear Approach</i> , 275	
7.2.3	<i>Comparison of One-Dimensional Ground Response Analyses</i> , 279	
7.3	Two-Dimensional Ground Response Analysis	280
7.3.1	<i>Dynamic Finite-Element Analysis</i> , 281	
7.3.2	<i>Equivalent Linear Approach</i> , 284	
7.3.3	<i>Nonlinear Approach</i> , 286	
7.3.4	<i>Other Approaches to Two-Dimensional Ground Response Problems</i> , 286	
7.3.5	<i>Comparison of Two-Dimensional Ground Response Analyses</i> , 291	
7.4	Three-Dimensional Ground Response Analysis	291
7.4.1	<i>Equivalent Linear Finite-Element Approach</i> , 292	
7.4.2	<i>Nonlinear Finite-Element Approach</i> , 292	
7.4.3	<i>Shear Beam Approach</i> , 293	
7.4.4	<i>Comparison of Three-Dimensional Ground Response Analyses</i> , 294	
7.5	Soil–Structure Interaction	294
7.5.1	<i>Illustration of Soil–Structure Interaction Effects</i> , 295	
7.5.2	<i>Methods of Analysis</i> , 300	
7.6	Summary	303

8 Local Site Effects and Design Ground Motions	308
8.1 Introduction 308	
8.2 Effects of Local Site Conditions on Ground Motion 309	
8.2.1 <i>Evidence from Theoretical Ground Response Analyses</i> , 309	
8.2.2 <i>Evidence from Measured Amplification Functions</i> , 310	
8.2.3 <i>Evidence from Measured Surface Motions</i> , 312	
8.2.4 <i>Compilations of Data on Local Site Effects</i> , 317	
8.2.5 <i>Effects of Surface Topography and Basin Geometry</i> , 319	
8.3 Design Parameters 323	
8.3.1 <i>Design Earthquakes</i> , 324	
8.3.2 <i>Design Spectra</i> , 325	
8.4 Development of Design Parameters 327	
8.4.1 <i>Site-Specific Development</i> , 327	
8.4.2 <i>Code-Based Development</i> , 328	
8.5 Development of Ground Motion Time Histories 340	
8.5.1 <i>Modification of Actual Ground Motion Records</i> , 340	
8.5.2 <i>Time-Domain Generation</i> , 341	
8.5.3 <i>Frequency-Domain Generation</i> , 343	
8.5.4 <i>Green's Function Techniques</i> , 343	
8.5.5 <i>Limitations of Artificial Ground Motions</i> , 345	
8.6 Summary 345	
9 Liquefaction	348
9.1 Introduction 348	
9.2 Liquefaction-Related Phenomena 349	
9.2.1 <i>Flow Liquefaction</i> , 349	
9.2.2 <i>Cyclic Mobility</i> , 349	
9.3 Evaluation of Liquefaction Hazards 350	
9.4 Liquefaction Susceptibility 351	
9.4.1 <i>Historical Criteria</i> , 352	
9.4.2 <i>Geologic Criteria</i> , 353	
9.4.3 <i>Compositional Criteria</i> , 354	
9.4.4 <i>State Criteria</i> , 355	
9.5 Initiation of Liquefaction 361	
9.5.1 <i>Flow Liquefaction Surface</i> , 361	
9.5.2 <i>Influence of Excess Pore Pressure</i> , 366	
9.5.3 <i>Evaluation of Initiation of Liquefaction</i> , 368	
9.6 Effects of Liquefaction 397	
9.6.1 <i>Alteration of Ground Motion</i> , 398	
9.6.2 <i>Development of Sand Boils</i> , 400	
9.6.3 <i>Settlement</i> , 402	
9.6.4 <i>Instability</i> , 408	
9.7 Summary 417	

10 Seismic Slope Stability	423
10.1 Introduction	423
10.2 Types of Earthquake-Induced Landslides	424
10.3 Earthquake-Induced Landslide Activity	426
10.4 Evaluation of Slope Stability	429
10.5 Static Slope Stability Analysis	430
<i>10.5.1 Limit Equilibrium Analysis, 430</i>	
<i>10.5.2 Stress-Deformation Analyses, 433</i>	
10.6 Seismic Slope Stability Analysis	433
<i>10.6.1 Analysis of Inertial Instability, 433</i>	
<i>10.6.2 Analysis of Weakening Instability, 450</i>	
10.7 Summary	462
11 Seismic Design of Retaining Walls	466
11.1 Introduction	466
11.2 Types of Retaining Walls	466
11.3 Types of Retaining Wall Failures	467
11.4 Static Pressures on Retaining Walls	469
<i>11.4.1 Rankine Theory, 469</i>	
<i>11.4.2 Coulomb Theory, 472</i>	
<i>11.4.3 Logarithmic Spiral Method, 474</i>	
<i>11.4.4 Stress-Deformation Analysis, 476</i>	
11.5 Dynamic Response of Retaining Walls	477
11.6 Seismic Pressures on Retaining Walls	477
<i>11.6.1 Yielding Walls, 478</i>	
<i>11.6.2 Nonyielding Walls, 484</i>	
<i>11.6.3 Effects of Water on Wall Pressures, 486</i>	
<i>11.6.4 Finite-Element Analysis, 489</i>	
11.7 Seismic Displacements of Retaining Walls	489
<i>11.7.1 Richards–Elms Method, 489</i>	
<i>11.7.2 Whitman–Liao Method, 492</i>	
<i>11.7.3 Finite-Element Analysis, 493</i>	
11.8 Seismic Design Considerations	494
<i>11.8.1 Gravity Walls, 494</i>	
<i>11.8.2 Cantilever Walls, 495</i>	
<i>11.8.3 Braced Walls, 495</i>	
<i>11.8.4 Reinforced Soil Walls, 500</i>	
11.9 Summary	503

12 Soil Improvement for Remediation of Seismic Hazards 506

- 12.1 Introduction 506
- 12.2 Densification Techniques 507
 - 12.2.1 *Vibro Techniques*, 508
 - 12.2.2 *Dynamic Compaction*, 510
 - 12.2.3 *Blasting*, 512
 - 12.2.4 *Compaction Grouting*, 513
 - 12.2.5 *Areal Extent of Densification*, 514
- 12.3 Reinforcement Techniques 515
 - 12.3.1 *Stone Columns*, 515
 - 12.3.2 *Compaction Piles*, 516
 - 12.3.3 *Drilled Inclusions*, 516
- 12.4 Grouting and Mixing Techniques 517
 - 12.4.1 *Grouting*, 518
 - 12.4.2 *Mixing*, 519
- 12.5 Drainage Techniques 521
- 12.6 Verification of Soil Improvement 522
 - 12.6.1 *Laboratory Testing Techniques*, 522
 - 12.6.2 *In Situ Testing Techniques*, 523
 - 12.6.3 *Geophysical Testing Techniques*, 523
- 12.7 Other Considerations 524
- 12.8 Summary 524

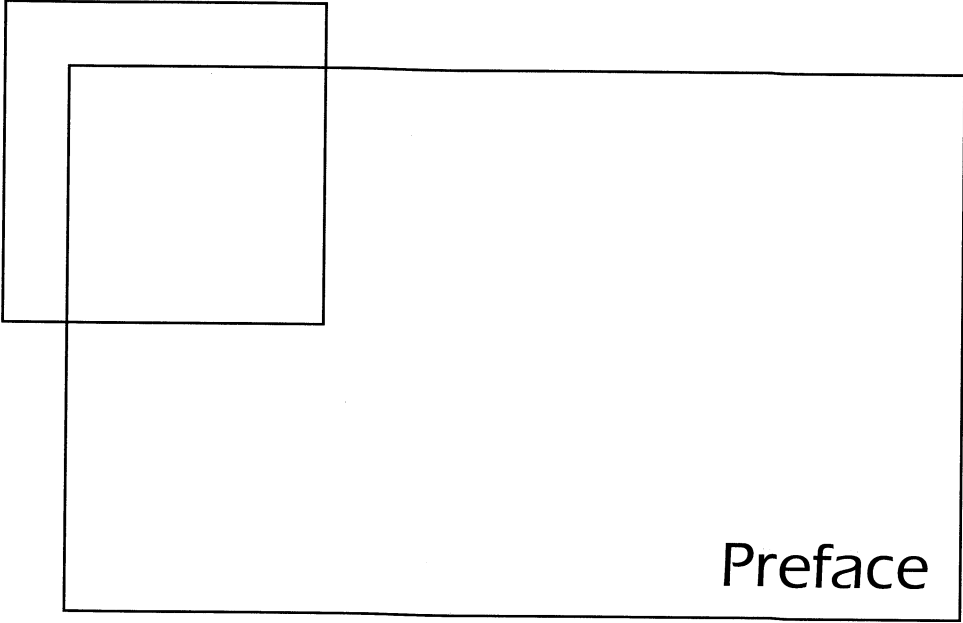
A Vibratory Motion 527

- A.1 Introduction 527
- A.2 Types of Vibratory Motion 527
 - A.2.1 *Simple Harmonic Motion*, 528
 - A.2.2 *Trigonometric Notation for Simple Harmonic Motion*, 529
 - A.2.3 *Other Measures of Motion*, 533
- A.3 Fourier Series 536
 - A.3.1 *Trigonometric Form*, 536
 - A.3.2 *Exponential Form*, 539
 - A.3.3 *Discrete Fourier Transform*, 541
 - A.3.4 *Fast Fourier Transform*, 541
 - A.3.5 *Power Spectrum*, 542

B Dynamics of Discrete Systems 543

- B.1 Introduction 543
- B.2 Vibrating Systems 544
- B.3 Single-Degree-of-Freedom Systems 544

B.4	Equation of Motion for SDOF System	545
B.4.1	<i>Equation of Motion: External Loading,</i>	545
B.4.2	<i>Equation of Motion: Vibration of Supports (Base Shaking),</i>	547
B.5	Response of Linear SDOF Systems	547
B.5.1	<i>Undamped Free Vibrations,</i>	548
B.5.2	<i>Damped Free Vibrations,</i>	551
B.5.3	<i>Response of SDOF Systems to Harmonic Loading,</i>	553
B.5.4	<i>Response of SDOF Systems to Periodic Loading,</i>	561
B.5.5	<i>Response of SDOF Systems to General Loading,</i>	564
B.6	Damping	567
B.6.1	<i>Viscous Damping,</i>	567
B.6.2	<i>Other Measures of Energy Dissipation,</i>	569
B.6.3	<i>Complex Stiffness,</i>	570
B.7	Response Spectra	571
B.8	Response of Nonlinear SDOF Systems to General Loading	572
B.8.1	<i>Incremental Equation of Motion,</i>	572
B.8.2	<i>Numerical Integration,</i>	574
B.9	Multiple-Degree-of-Freedom Systems	575
B.9.1	<i>Equations of Motion,</i>	575
B.9.2	<i>Undamped Free Vibrations,</i>	577
B.9.3	<i>Mode Superposition Method,</i>	579
B.9.4	<i>Response Spectrum Analysis,</i>	581
B.9.5	<i>Discussion,</i>	582
C	Probability Concepts	583
C.1	Introduction	583
C.2	Sample Spaces and Events	583
C.3	Axioms of Probability	584
C.4	Probabilities of Events	585
C.5	Random Variables	588
C.6	Expected Values and Standard Deviations	589
C.7	Common Probability Distributions	590
C.7.1	<i>Uniform Distribution,</i>	590
C.7.2	<i>Normal Distribution,</i>	591
C.7.3	<i>Lognormal Distribution,</i>	594
References		596
Index		643



Preface

Compared to most disciplines of civil engineering, geotechnical earthquake engineering is quite young. While the damaging effects of earthquakes have been known for centuries, the strong contribution of soils to the magnitude and pattern of earthquake damage was not widely appreciated until relatively recently. Following damaging earthquakes in 1964 in Niigata, Japan and Alaska, and spurred by the growth of the nuclear power industry in the 1960s and 1970s, the field of geotechnical earthquake engineering has grown rapidly. Although much remains to be learned, the field has matured to the point where generally accepted theories and analytical procedures now exist for many important problems.

The purpose of this book is to introduce the reader to the concepts, theories, and procedures of geotechnical earthquake engineering. It is intended for use as a text in graduate courses on geotechnical earthquake engineering and as a reference book for practicing engineers. Recognizing that geotechnical earthquake engineering is a broad, multidisciplinary field, the book draws from seismology, geology, structural engineering, risk analysis, and other technical disciplines.

The book is written at a level suitable for students with knowledge equivalent to that of a senior (fourth-year) civil engineering student. The student should have had basic courses in soil mechanics, structural engineering, and hydraulics; introductory courses in geology and probability/statistics would also be helpful. Many graduate students will have

had courses in structural dynamics or soil dynamics by the time they begin study of geotechnical earthquake engineering. For those readers without prior exposure, introductions to the nomenclature and mathematics of dynamic systems, structural dynamics, and probability are presented in three appendices.

ORGANIZATION

The subject matter falls into two main categories. The appendices and the first six chapters present fundamental principles of seismology, ground motion, dynamics, and soil behavior. Applications of these principles to the practical problems most commonly encountered in geotechnical earthquake engineering practice are presented in the last six chapters.

Chapter 1 introduces the reader to the types of damage that can occur during earthquakes and to the problems they present to geotechnical earthquake engineers. Basic concepts of earthquake seismology and the terminology used to describe earthquakes and their effects are described in Chapter 2. Chapter 3 describes ground motion measurement, the parameters used to characterize strong ground motion, and methods for prediction of those parameters. Deterministic and probabilistic seismic hazard analyses are presented in Chapter 4. Chapter 5 introduces the reader to wave propagation, beginning with simple one-dimensional body waves in homogeneous materials and extending to surface waves and multidimensional, layered systems. The properties of soil that control their wave propagation behavior are described in Chapter 6. Field and laboratory techniques for measurement of these properties are also described.

Chapter 7 presents methods for analysis of ground response during earthquakes, beginning with one-dimensional ground response analysis and moving through two- and three-dimensional dynamic response analyses. Both frequency- and time-domain approaches are described. Chapter 7 concludes with an introduction to the basic concepts and effects of soil-structure interaction. The effects of local soil conditions on ground motions and earthquake damage are described in Chapter 8. Chapter 8 also introduces the concept of design ground motions, and how they are obtained from site-specific analyses and from building codes. Chapter 9 deals with liquefaction—it begins with a conceptual framework for understanding various liquefaction-related phenomena and then presents practical procedures for evaluation of liquefaction hazards. Seismic stability of slopes is covered in Chapter 10, and seismic design of retaining structures in Chapter 11. Chapters 10 and 11 address their respective topics initially from pseudo-static and then from permanent displacement standpoints. Chapter 12 introduces commonly used soil improvement techniques for mitigation of seismic hazards.

PEDAGOGY

This book is the first to deal explicitly with the topic of geotechnical earthquake engineering. During its preparation, a great deal of time and effort was devoted to decisions regarding content and organization. The final form naturally reflects my own preference, but the text has been reviewed by many engineers from both academia and professional practice. Preparation of the text also involved a great deal of interpretation of information from a

wide variety of sources. While the text reflects my own interpretation of this information, it is heavily referenced to allow readers to explore background or more detailed information on various geotechnical earthquake engineering topics.

A couple features are noteworthy. Two ground motions from the Loma Prieta earthquake, one from a rock outcrop and one from the surface of a nearby deep soil deposit, are used to illustrate a number of concepts throughout the book. Differences in the amplitudes, frequency contents, and durations of the motions are emphasized in Chapter 3. The reasons for these differences later become apparent in Chapters 7 and 8. The book also emphasizes the use of transfer functions, particularly in the solution of ground response problems. The transfer function approach helps students form a more complete understanding of ground response—in the frequency domain as well as the time domain. With the advent of computer programs such as MATLAB, MathCad, and Mathematica, the Fourier analyses required in the transfer function approach are quite simple; students use MATLAB extensively in my soil dynamics and geotechnical earthquake engineering courses.

The book contains worked examples and homework problems. The example problems are intended to illustrate the basic concepts of the problems they address; to allow the results to be checked, a number involve calculations carried out to more significant figures than the accuracy of the procedures (and typical input data) would justify. Many of the important problems of geotechnical earthquake engineering, however, do not lend themselves to the type of short, well-defined homework problem that is readily placed in a book. My preference is to assign longer, project-oriented assignments based on actual case histories, and I recommend that the homework problems in this book be supplemented by such assignments.

UNITS

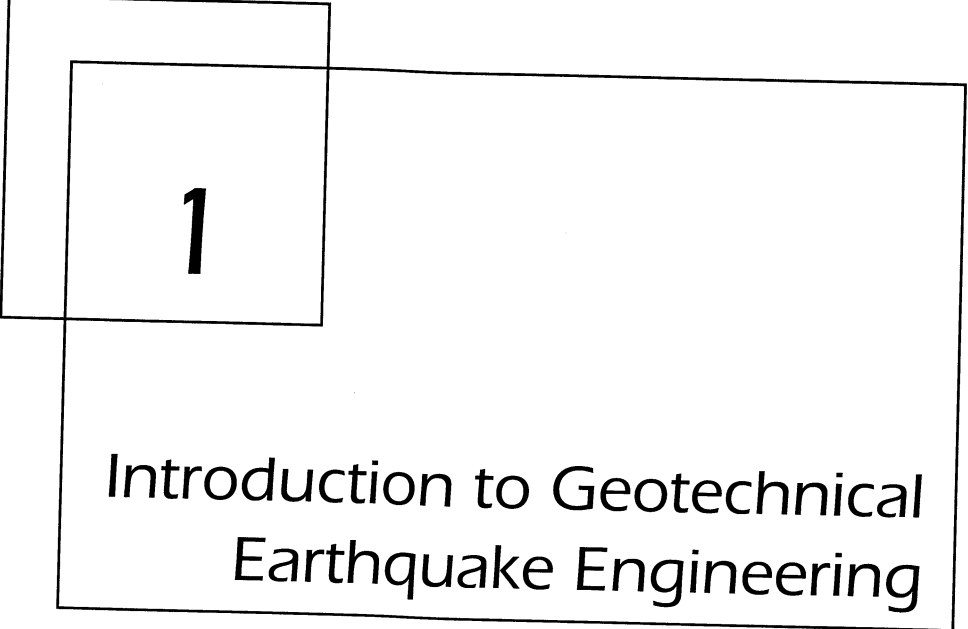
As in many other fields, the use of units in geotechnical earthquake engineering is neither uniform nor consistent. The current state of knowledge in geotechnical earthquake engineering has resulted from advances in a variety of technical fields and a variety of countries, many of which customarily use different units. Fortunately, most conform to relatively standard metric or British systems. Rather than attempt to force the use of one system or the other, this book uses dual units. In recognition of their origins, the most common units for each quantity is listed first with the alternative following in parentheses. The approach is intended to allow all readers to proceed through the material without stopping to convert (mentally or otherwise) from one set of units to another. To encourage familiarity with both sets of units, some example and homework problems are specified in metric units and some in British units.

ACKNOWLEDGMENTS

A number of people have helped directly and indirectly in the preparation of this book. The professional and academic portions of my career have benefited greatly from a number of people that I have worked closely with, particularly (in chronological order) Bill Houston, Tom Tejima, H.B. Seed, Joe Mahoney, and Bob Holtz. Their assistance, advice, and encouragement has taken many forms, and I am grateful to each.

As this book evolved from a collection of lecture notes and handouts, it was continually improved by comments and suggestions from many students in my soil dynamics and geotechnical earthquake engineering courses. Their assistance is greatly appreciated. I am also grateful to many colleagues who provided constructive critical reviews of different parts of the book, including Dr. Donald G. Anderson, Dr. Juan Baez, Mr. David Baska, Dr. Gopal Biswas, Prof. Ross W. Boulanger, Dr. C.B. Crouse, Prof. Emeritus William J. Hall, Ms. Karen Henry, Prof. Carlton L. Ho, Prof. William D. Kovacs, Prof. Roberto T. Leon, Prof. Gregory R. MacRae, Dr. Lelio H. Mejia, Dr. Robert Pyke, Prof. Peter K. Robertson, Prof. Raj Siddharthan, Prof. Stewart Smith, Prof. Timothy D. Stark, and Prof. George M. Turkiyyah. Each made suggestions that improved the quality of the book. Prof. Geoffrey R. Martin and Prof. T. Leslie Youd reviewed substantial portions of the book; their efforts are particularly appreciated.

Finally, I am most grateful to my wife, Diane, and to my daughters, Katie and Megan. Preparation of this book involved several years of long working hours; I could not have done it without their cheerful understanding and encouragement.



1

Introduction to Geotechnical Earthquake Engineering

1.1 INTRODUCTION

Earthquake engineering deals with the effects of earthquakes on people and their environment and with methods of reducing those effects. It is a very young discipline, many of its most important developments having occurred in the past 30 to 40 years. Earthquake engineering is a very broad field, drawing on aspects of geology, seismology, geotechnical engineering, structural engineering, risk analysis, and other technical fields. Its practice also requires consideration of social, economic, and political factors. Most earthquake engineers have entered the field from structural engineering or geotechnical engineering backgrounds, a fact that is reflected in the practice of earthquake engineering. This book covers geotechnical aspects of earthquake engineering. Although its primary audience is geotechnical engineering students and practitioners, it contains a great deal of information that should be of interest to the structural engineer and the engineering seismologist.

1.2 BACKGROUND

The study of earthquakes dates back many centuries. Written records of earthquakes in China date as far back as 3000 years. Japanese records and records from the eastern Mediterranean region go back nearly 1600 years. In the United States the historical record of

earthquakes is much shorter, about 350 years. On the seismically active west coast of the United States, earthquake records go back only about 200 years. Compared with the millions of years over which earthquakes have been occurring, humankind's experience with earthquakes is very brief.

Today, hundreds of millions of people throughout the world live with a significant risk to their lives and property from earthquakes. Billions of dollars of public infrastructure are continuously at risk of earthquake damage. The health of many local, regional, and even national economies are also at risk from earthquakes. These risks are not unique to the United States, Japan, or any other country. Earthquakes are a global phenomenon and a global problem.

Earthquakes have occurred for millions of years and will continue in the future as they have in the past. Some will occur in remote, undeveloped areas where damage will be negligible. Others will occur near densely populated urban areas and subject their inhabitants and the infrastructure they depend on to strong shaking. It is impossible to prevent earthquakes from occurring, but it is possible to mitigate the effects of strong earthquake shaking: to reduce loss of life, injuries, and damage.

1.3 SEISMIC HAZARDS

A number of naturally occurring events, such as earthquakes, hurricanes, tornados, and floods, are capable of causing deaths, injuries, and property damage. These *natural hazards* cause tremendous damage around the world each year. Hazards associated with earthquakes are commonly referred to as *seismic hazards*. The practice of earthquake engineering involves the identification and mitigation of seismic hazards. The most important seismic hazards are described in the following sections.

1.3.1 Ground Shaking

When an earthquake occurs, seismic waves radiate away from the source and travel rapidly through the earth's crust. When these waves reach the ground surface, they produce shaking that may last from seconds to minutes. The strength and duration of shaking at a particular site depends on the size and location of the earthquake and on the characteristics of the site. At sites near the source of a large earthquake, ground shaking can cause tremendous damage. In fact, ground shaking can be considered to be the most important of all seismic hazards because all the other hazards are caused by ground shaking. Where ground shaking levels are low, these other seismic hazards may be low or nonexistent. Strong ground shaking, however, can produce extensive damage from a variety of seismic hazards.

Although seismic waves travel through rock over the overwhelming majority of their trip from the source of an earthquake to the ground surface, the final portion of that trip is often through soil, and the characteristics of the soil can greatly influence the nature of shaking at the ground surface. Soil deposits tend to act as "filters" to seismic waves by attenuating motion at certain frequencies and amplifying it at others. Since soil conditions often vary dramatically over short distances, levels of ground shaking can vary significantly within a small area. One of the most important aspects of geotechnical earthquake engineering practice involves evaluation of the effects of local soil conditions on strong ground motion. In this book, Chapter 3 presents methods for quantifying the most important

characteristics of strong ground motions, and Chapters 4 through 7 provide the background and techniques for site-specific ground motion prediction.

1.3.2 Structural Hazards

Without doubt the most dramatic and memorable images of earthquake damage are those of structural collapse. From the predictable collapse of the unreinforced masonry and adobe structures in which many residents of underdeveloped areas of the world live (Figure 1.1) to the surprising destruction of more modern construction (Figures 1.2 to 1.4), structural damage is the leading cause of death and economic loss in many earthquakes. However, structures need not collapse to cause death and damage. Falling objects such as brick facings and parapets on the outside of a structure or heavy pictures and shelves within a structure have caused casualties in many earthquakes. Interior facilities such as piping, lighting, and storage systems can also be damaged during earthquakes.

Over the years, considerable advances have been made in earthquake-resistant design of structures, and seismic design requirements in building codes have steadily improved. As earthquake-resistant design has moved from an emphasis on structural strength to emphases on both strength and ductility, the need for accurate predictions of ground motions has increased. In current design practice, the geotechnical earthquake engineer is often responsible for providing the structural engineer with appropriate design ground motions. In this book, Chapter 8 describes the effects of local soil conditions on ground motions and provides guidance for the development of site-specific design ground motions.



Figure 1.1 Damage to buildings in Huaras, Peru following the 1970 Peru earthquake. The adobe structures in the foreground were destroyed, but the reinforced concrete structure in the background suffered little damage (photo by G. Plafker, courtesy of USGS).

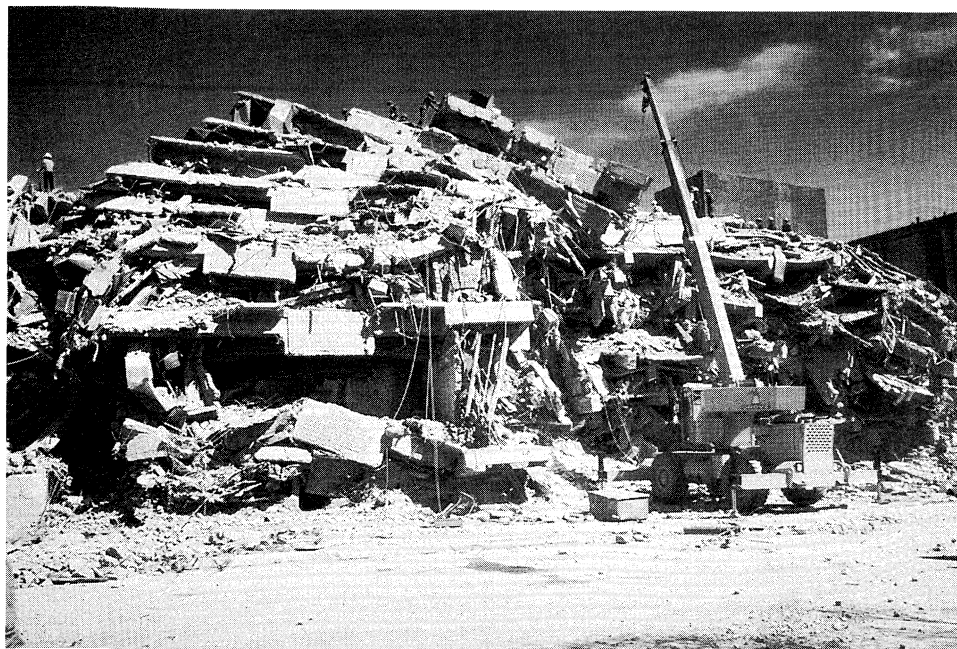


Figure 1.2 Collapsed portion of the reinforced concrete Hospital Juarez in Mexico City following the 1985 Mexico earthquake (photo by E.V. Leyendecker, courtesy of EERI).

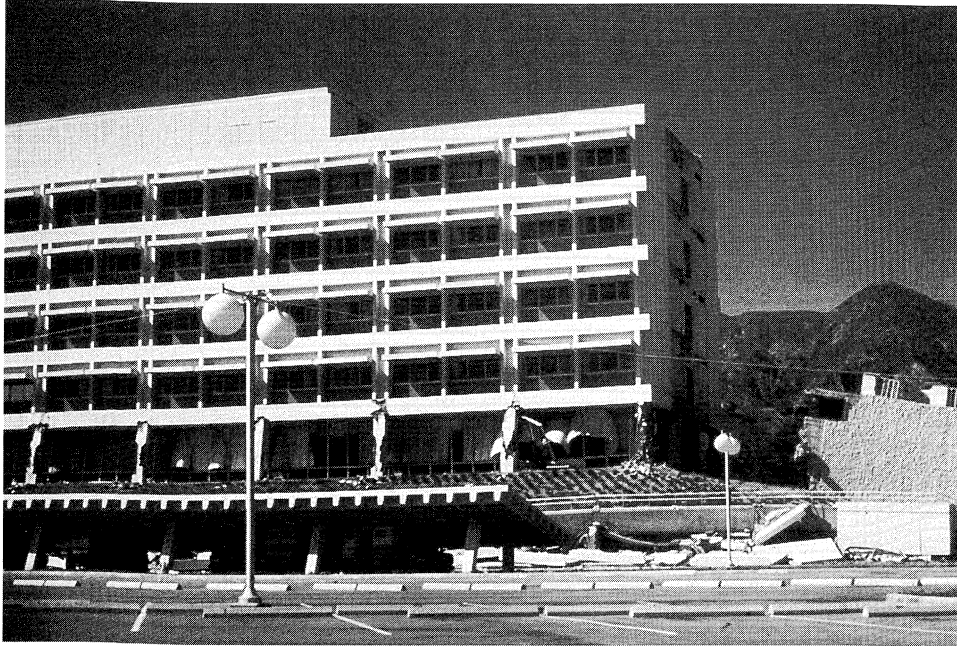


Figure 1.3 Effects of column failures at Olive View Hospital in the 1971 San Fernando earthquake. Collapse of the canopy in the foreground pinned the ambulances beneath them, rendering them useless (courtesy of EERI).

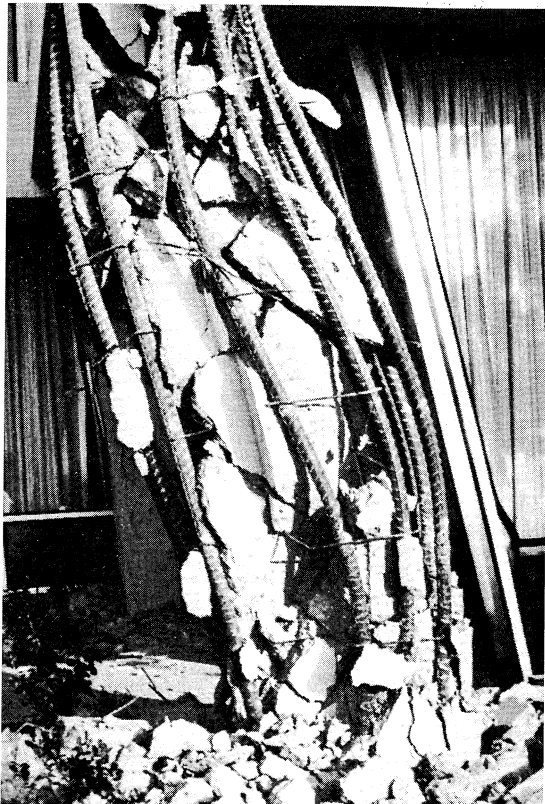


Figure 1.4 Reinforced concrete column at Olive View Hospital following the 1971 San Fernando earthquake. Insufficient transverse reinforcement was unable to provide adequate confinement (courtesy of USGS).

1.3.3 Liquefaction

Some of the most spectacular examples of earthquake damage have occurred when soil deposits have lost their strength and appeared to flow as fluids. In this phenomenon, termed *liquefaction*, the strength of the soil is reduced, often drastically, to the point where it is unable to support structures or remain stable. Because it only occurs in saturated soils, liquefaction is most commonly observed near rivers, bays, and other bodies of water.

The term *liquefaction* actually encompasses several related phenomena. Flow failures, for example, can occur when the strength of the soil drops below the level needed to maintain stability under static conditions. Flow failures are therefore driven by static gravitational forces and can produce very large movements. Flow failures have caused the collapse of earth dams (Figure 1.5) and other slopes, and the failure of foundations (Figure 1.6). The 1971 San Fernando earthquake caused a flow failure in the upstream slope of the Lower San Fernando Dam (Figure 1.7) that nearly breached the dam. Thousands could have been killed in the residential area immediately below the dam. Lateral spreading is a related phenomenon characterized by incremental displacements during earthquake shaking. Depending on the number and strength of the stress pulses that exceed the strength of the soil, lateral spreading can produce displacements that range from negligible to quite large. Lateral spreading is quite common near bridges, and the displacements it produces can damage the abutments, foundations, and superstructures of bridges (Figures 1.8 and 1.9). Finally, the



Figure 1.5 Liquefaction failure of Shefield Dam following the 1925 Santa Barbara earthquake (K. Steinbrugge collection; courtesy of EERC, Univ. of California).



Figure 1.6 Liquefaction-induced bearing capacity failures of the Kawagishi-cho apartment buildings following the 1964 Niigata earthquake (courtesy of USGS).

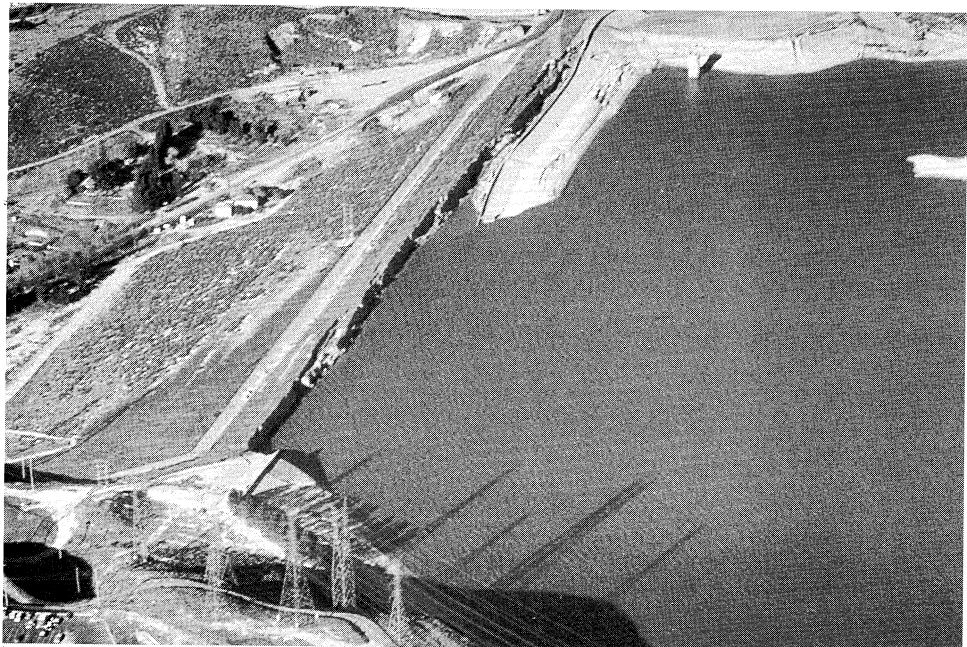


Figure 1.7 Lower San Fernando Dam following liquefaction failure of its upstream slope in the 1971 San Fernando earthquake (K. Steinbrugge collection; courtesy of EERC, Univ. of California).

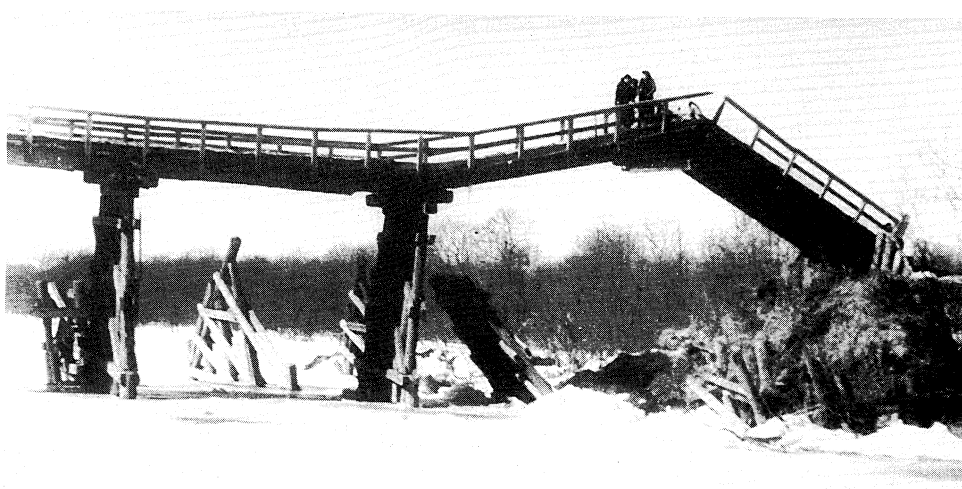


Figure 1.8 Effect of lateral spreading on a small bridge in Japan following the 1952 Tokachi-Oki earthquake. Lateral spreading of the soil at the abutment buckled the bridge deck (K. Steinbrugge collection; courtesy of EERC, Univ. of California).



Figure 1.9 The Showa Bridge following the 1964 Niigata earthquake. Lateral spreading caused bridge pier foundations to move and rotate sufficiently for simply supported bridge spans to fall (courtesy of USGS).

phenomenon of level-ground liquefaction does not involve large lateral displacements but is easily identified by the presence of sand boils (Figure 1.10) produced by groundwater rushing to the surface. Although not particularly damaging by themselves, sand boils indicate the presence of high groundwater pressures whose eventual dissipation can produce subsidence and damaging differential settlements.

Liquefaction is a complicated phenomenon, but research has progressed to the point where an integrated framework of understanding can be developed. Chapter 9 of this book presents the basic concepts with which the susceptibility, triggering conditions, and effects of all liquefaction phenomena can be understood, together with practical procedures for evaluation of liquefaction hazards.

1.3.4 Landslides

Strong earthquakes often cause landslides. Although the majority of such landslides are small, earthquakes have also caused very large slides. In a number of unfortunate cases, earthquake-induced landslides have buried entire towns and villages (Figure 1.11). More commonly, earthquake-induced landslides cause damage by destroying buildings, or disrupting bridges and other constructed facilities (Figures 1.12 and 1.13). Many earthquake-induced landslides result from liquefaction phenomena, but many others simply represent the failures of slopes that were marginally stable under static conditions. Various types of seismic slope failures, their frequency of occurrence, and procedures for their analysis are described in Chapter 10.



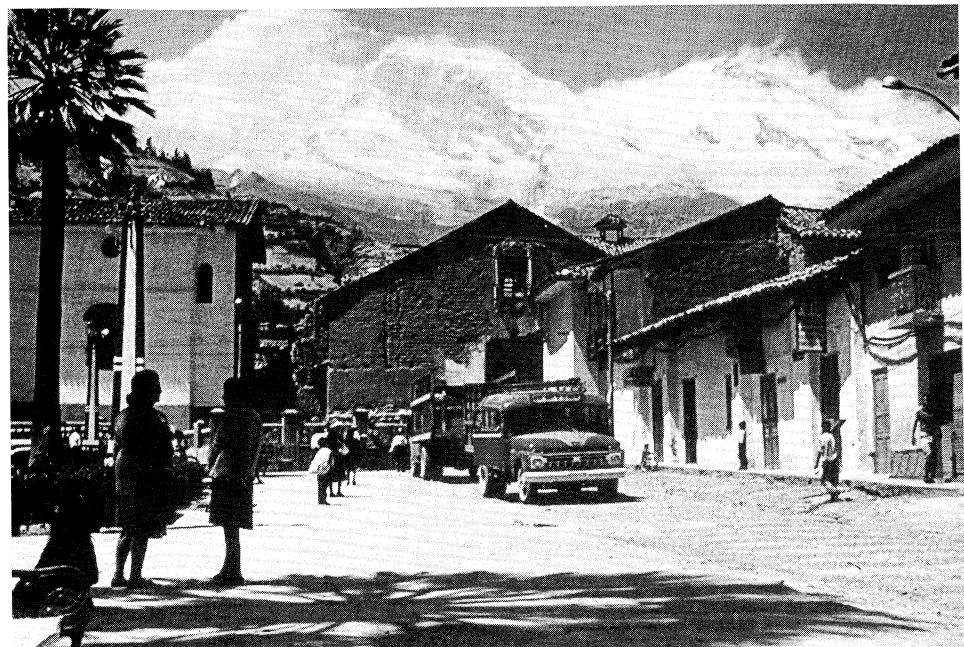
Figure 1.10 Sand boil in rice field following the 1964 Niigata earthquake (K. Steinbrugge collection; courtesy of EERC, Univ. of California).

1.3.5 Retaining Structure Failures

Anchored bulkheads, quay walls, and other retaining structures are frequently damaged in earthquakes. Damage is usually concentrated in waterfront areas such as ports and harbors (Figure 1.14). Because such facilities are often essential for the movement of goods upon which local economies often rely, the business losses associated with their failure can go far beyond the costs of repair or reconstruction. The seismic design of retaining structures is covered in Chapter 11.

1.3.6 Lifeline Hazards

A network of facilities that provide the services required for commerce and public health can be found in virtually any developed area. These networks, which include electrical power and telecommunications, transportation, water and sewage, oil and gas distribution, and waste storage systems, have collectively come to be known as *lifelines*. Lifeline systems may include power plants, transmission towers, and buried electrical cables; roads, bridges, harbors, and airports; water treatment facilities, reservoirs and elevated water tanks, and buried water distribution systems; liquid storage tanks and buried oil and gas pipelines; and municipal solid waste and hazardous waste landfills. Lifeline systems and the facilities that comprise them provide services that many take for granted but which are essential in modern industrial areas. Lifeline failures not only have severe economic consequences but can also adversely affect the environment and quality of life following an earthquake.



(a)



(b)

Figure 1.11 Village of Yungay, Peru, (a) before and (b) after being buried by a giant landslide in the 1970 Peruvian earthquake. The same palm trees are visible at the left side of both photographs. The landslide involved 50 million cubic meters of material that eventually covered an area of some 8000 square kilometers. About 25,000 people were killed by this landslide, over 18,000 in the villages of Yungay and Ranrahirca (K. Steinbrugge collection; courtesy of EERC, Univ. of California).



Figure 1.12 A wing of Government Hill School in Anchorage, Alaska, straddled the head scarp of the Government Hill landslide in the 1964 Good Friday earthquake (K. Steinbrugge collection; courtesy of EERC, Univ. of California).

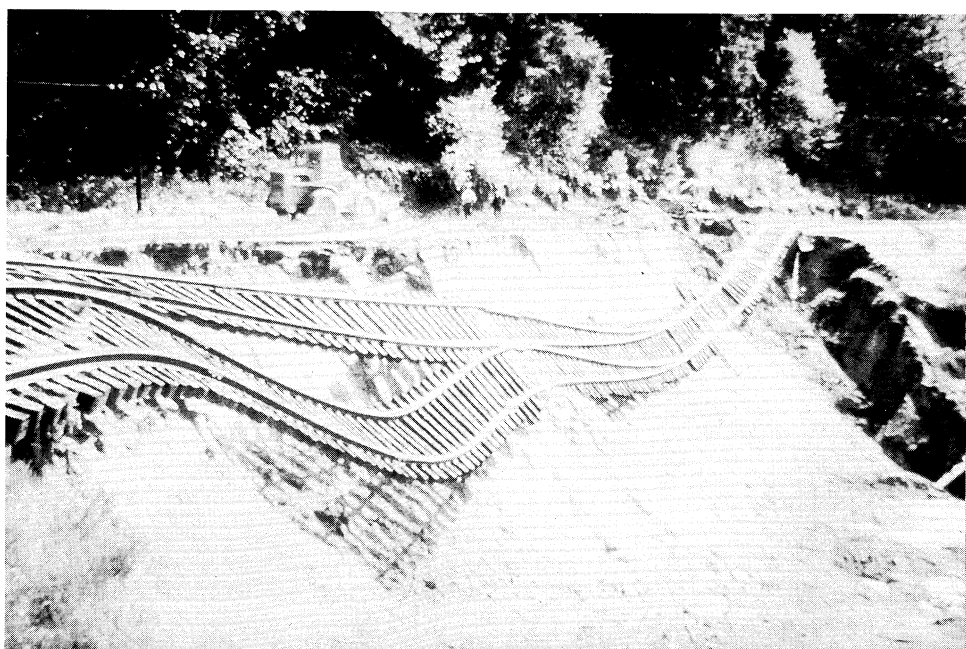


Figure 1.13 Earthquake-induced landslide along railroad tracks near Olympia, Washington (photo by G.W. Thorsen).



Figure 1.14 Failure of a quay wall on Rokko Island in Kobe, Japan in the 1995 Hyogo-Ken Nanbu earthquake (photo by S. L. Kramer).

Lifeline failure can cause disruption and economic losses that greatly exceed the cost of repairing facilities directly damaged by earthquake shaking. The 1989 Loma Prieta and 1994 Northridge earthquakes caused economic losses estimated at \$8 billion and \$30 billion in the state of California alone. These losses had severe local and regional repercussions but had only minor effects on most U.S. citizens. The 1972 Managua earthquake, on the other hand, caused losses of \$2 billion, 40% of Nicaragua's gross national product that year. The high costs of reconstruction produced a national debt that triggered inflation, increased unemployment, and eventually contributed to the destabilization of the Nicaraguan government. More recently, the Hyogo-Ken Nanbu earthquake devastated the city of Kobe, Japan; total damages have been estimated in excess of \$100 billion.

Lifeline failures can also hamper emergency response and rescue efforts immediately following damaging earthquakes. Most of the damage in the 1906 San Francisco earthquake, for example, was caused by a fire that could not be fought properly because of broken water mains. Eighty-three years later, television allowed the world to watch another fire in San Francisco following the Loma Prieta earthquake. These fires were caused by broken natural gas pipes, and again, firefighting was hampered by broken water mains. The Loma Prieta earthquake also caused the collapse and near collapse of several elevated highways and the collapse of a portion of the San Francisco–Oakland Bay Bridge. Loss of these transportation lifelines caused gridlock throughout the area. Some of the elevated highways were still out of service five years after the earthquake.

1.3.7 Tsunami and Seiche Hazards

Rapid vertical seafloor movements caused by fault rupture during earthquakes can produce long-period sea waves called *tsunamis*. In the open sea, tsunamis travel great distances at high speeds but are difficult to detect—they usually have heights of less than 1 m and wavelengths (the distance between crests) of several hundred kilometers. As a tsunami approaches shore, however, the decreasing water depth causes its speed to decrease and the height of the wave to increase. In some coastal areas, the shape of the seafloor may amplify the wave, producing a nearly vertical wall of water that rushes far inland and causes devastating damage (Figure 1.15). The Great Hoei Tokaido–Nonhaido tsunami killed 30,000 people in Japan in 1707. The 1960 Chilean earthquake produced a tsunami that not only killed 300 people in Chile, but also killed 61 people in Hawaii and, 22 hours later, 199 people in distant Japan (Iida et al., 1967).

Earthquake-induced waves in enclosed bodies of water are called *seiches*. Typically caused by long-period seismic waves that match the natural period of oscillation of the water in a lake or reservoir, seiches may be observed at great distances from the source of an earthquake. The 1964 Good Friday earthquake in Alaska, for example, produced damaging waves up to 5 ft high in lakes in Louisiana and Arkansas (Spaeth and Berkman, 1967). Another type of seiche can be formed when faulting causes permanent vertical displacements within a lake or reservoir. In 1959, vertical fault movement within Hebgen Lake produced a seiching motion that alternately overtopped Hebgen Dam and exposed the lake bottom adjacent to the dam in 1959 (Steinbrugge and Cloud, 1962).



Figure 1.15 Tsunami damage in Kodiak, Alaska, following the 1964 Good Friday earthquake (courtesy of USGS).

1.4 MITIGATION OF SEISMIC HAZARDS

Ultimately, the goal of the earthquake engineer is to mitigate seismic hazards. For new construction, hazard mitigation is embedded in the process of earthquake-resistant design. Details of earthquake-resistant design of structures are beyond the scope of this book, but some aspects of earthquake loading of structures are described in Chapter 8. Earthquake-resistant design of slopes, dams, embankments, and retaining structures is based on topics presented in Chapters 9 to 11. Mitigation of existing seismic hazards is also very important. The important topic of remediation of soil deposits for seismic hazard mitigation is covered in Chapter 12.

1.5 SIGNIFICANT HISTORICAL EARTHQUAKES

Earthquakes occur almost continuously around the world. Fortunately, most are so small that they cannot be felt. Only a very small percentage of earthquakes are large enough to cause noticeable damage, and a small percentage of those are large enough to be considered major earthquakes. Throughout recorded history, some of these major earthquakes can be regarded as being particularly significant, either because of their size and the damage they produced or because of what scientists and engineers were able to learn from them. A partial list of significant earthquakes, admittedly biased toward U.S. earthquakes and earthquakes with significant geotechnical earthquake engineering implications, is given in Table 1-1.

TABLE 1-1 Significant Historical Earthquakes

Date	Location	Magnitude	Deaths	Comments
780 B.C.	China			One of the first reliable written accounts of a strong earthquake; produced widespread damage west of Xian in Shaanxi Province
A.D. 79	Italy			Sixteen years of frequent earthquakes culminating with the eruption of Mt. Vesuvius, which buried the city of Pompeii
893	India		180,000	Widespread damage; many killed in collapse of earthen homes
1556	China	8.0 (est.)	530,000	Occurred in densely populated region near Xian; produced thousands of landslides, which killed inhabitants of soft rock caves in hillsides; death estimate of questionable accuracy
1755	Portugal	8.6	60,000	Lisbon earthquake; first scientific description of earthquake effects
1783	Italy		50,000	Calabria earthquake; first scientific commission for earthquake investigation formed

TABLE 1-1 Significant Historical Earthquakes (continued)

1811–1812	Missouri	7.5, 7.3, 7.8	Several	Three large earthquakes in less than two months in New Madrid area; felt all across central and eastern United States
1819	India		1,500	Cutch earthquake; first well-documented observations of faulting
1857	California	8.3	1	Fort Tejon earthquake; one of the largest earthquakes known to have been produced by the San Andreas Fault; fault ruptured for 250 miles (400 km) with up to 30 ft (9 m) offset
1872	California	8.5	27	Owens Valley earthquake; one of the strongest ever to have occurred in the United States
1886	South Carolina	7.0	110	Strongest earthquake to strike east coast of United States; produced significant liquefaction
1906	California	7.9	700	First great earthquake to strike densely populated area in United States; produced up to 21 ft (7 m) offset in 270-mile (430-km) rupture of San Andreas Fault; most damage caused by fire; extent of ground shaking damage correlated to geologic conditions in postearthquake investigation
1908	Italy	7.5	83,000	Messina and surrounding area devastated; Italian government appointed engineering commission that recommended structures be designed for equivalent static lateral loads
1923	Japan	7.9	99,000	Kanto earthquake; caused major damage in Tokyo-Yokohama area, much due to fire in Tokyo and tsunami in coastal regions; strongly influenced subsequent design in Japan
1925	California	6.3	13	Santa Barbara earthquake; caused liquefaction failure of Sheffield Dam; led to first explicit provisions for earthquake resistance in U.S. building codes

TABLE 1-1 Significant Historical Earthquakes (continued)

1933	California	6.3	120	Considerable building damage; schools particularly hard-hit, with many children killed and injured; led to greater seismic design requirements in building codes, particularly for public school buildings
1940	California	7.1	9	Large ground displacements along Imperial Fault near El Centro; first important accelerogram for engineering purposes was recorded
1959	Montana	7.1	28	Hebgen Lake earthquake; faulting within reservoir produced large seiche that overtopped earth dam
1960	Chile	9.5	2,230	Probably the largest earthquake ever recorded
1964	Alaska	9.2	131	The Good Friday earthquake; caused severe damage due to liquefaction and many earthquake-induced landslides
1964	Japan	7.5	26	Widespread liquefaction caused extensive damage to buildings, bridges, and port facilities in Niigata; along with Good Friday earthquake in Alaska, spurred intense interest in the phenomenon of liquefaction
1967	Venezuela	6.5	266	Caused collapse of relatively new structures in Caracas; illustrated effects of local soil conditions on ground motion and damage
1971	California	6.6	65	San Fernando earthquake; produced several examples of liquefaction, including near collapse of Lower San Fernando Dam; caused collapse of several buildings and highway bridges; many structural lessons learned, particularly regarding need for spiral reinforcement of concrete columns; many strong motion records obtained
1975	China	7.3	1,300	Evacuation following successful prediction saved thousands of lives in Haicheng, Liaoning Province
1976	China	7.8	700,000	Thought to be the most deadly earthquake in history; destroyed city of Tangshan, Hebei Province; not predicted; death estimate of questionable accuracy

Sec. 1.5 Significant Historical Earthquakes

17

TABLE 1-1 Significant Historical Earthquakes (continued)

1985	Mexico	8.1	9,500	Epicenter off Pacific Coast, but most damage occurred over 220 miles (360 km) away in Mexico City; illustrated effect of local soil conditions on ground motion amplification and damage; subsequent studies led to better understanding of dynamic properties of fine-grained soils
1989	California	7.1	63	Loma Prieta earthquake; extensive ground motion amplification and liquefaction damage in San Francisco Bay area
1994	California	6.8	61	Northridge earthquake; occurred on previously unknown fault beneath heavily populated area; buildings, bridges, lifelines extensively damaged; produced extraordinarily strong shaking at several locations
1995	Japan	6.9	5,300	Hyogo-Ken Nanbu earthquake; caused tremendous damage to Kobe, Japan; widespread liquefaction in reclaimed lands constructed for port of Kobe; landslides and damage to retaining walls and underground subway stations also observed

2

Seismology and Earthquakes

2.1 INTRODUCTION

The study of geotechnical earthquake engineering requires an understanding of the various processes by which earthquakes occur and their effects on ground motion. The field of *seismology* (from the Greek *seismos* for earthquake and *logos* for science) developed from a need to understand the internal structure and behavior of the earth, particularly as they relate to earthquake phenomena. Although earthquakes are complex phenomena, advances in seismology have produced a good understanding of the mechanisms and rates of occurrence of earthquakes in most seismically active areas of the world. This chapter provides a brief introduction to the structure of the earth, the reasons why earthquakes occur, and the terminology used to describe them. More complete descriptions of these topics may be found in a number of seismology texts, such as Gutenberg and Richter (1954), Richter (1958), Bullen (1975), Bath (1979), Bullen and Bolt (1985), Gubbins (1990), and Lay and Wallace (1995). A very readable description of seismology and earthquakes is given by Bolt (1993).

2.2 INTERNAL STRUCTURE OF THE EARTH

The earth is roughly spherical, with an equatorial diameter of 12,740 km (7918 miles) and a polar diameter of 12,700 km (7893 miles), the higher equatorial diameter being caused by

higher equatorial velocities due to the earth's rotation. The earth weighs some 5.4×10^{21} tons (4.9×10^{24} kg), which indicates an average specific gravity of about 5.5. Since the specific gravity of surficial rocks is known to be on the order of 2.7 to 3, higher specific gravities are implied at greater depths.

One of the first important achievements in seismology was the determination of the internal structure of the earth. Large earthquakes produce enough energy to cause measurable shaking at points all around the world. As the different types of seismic waves travel through the earth, they are refracted and reflected at boundaries between different layers, reaching different points on the earth's surface by different paths. Studies of these refractions and reflections early in this century revealed the layered structure of the earth and provided insight into the characteristics of each layer.

2.2.1 Seismic Waves

When an earthquake occurs, different types of seismic waves are produced: *body waves* and *surface waves*. Although seismic waves are discussed in detail in Chapter 5, the brief description that follows is necessary to explain some of the concepts of Chapters 2 to 4.

Body waves, which can travel through the interior of the earth, are of two types: *p-waves* and *s-waves* (Figure 2.1). P-waves, also known as primary, compressional, or longitudinal waves, involve successive compression and rarefaction of the materials through which they pass. They are analogous to sound waves; the motion of an individual particle that a p-wave travels through is parallel to the direction of travel. Like sound waves, p-waves can travel through solids and fluids. S-waves, also known as secondary, shear, or transverse waves, cause shearing deformations as they travel through a material. The motion of an individual particle is perpendicular to the direction of s-wave travel. The direction of particle movement can be used to divide s-waves into two components, SV (vertical

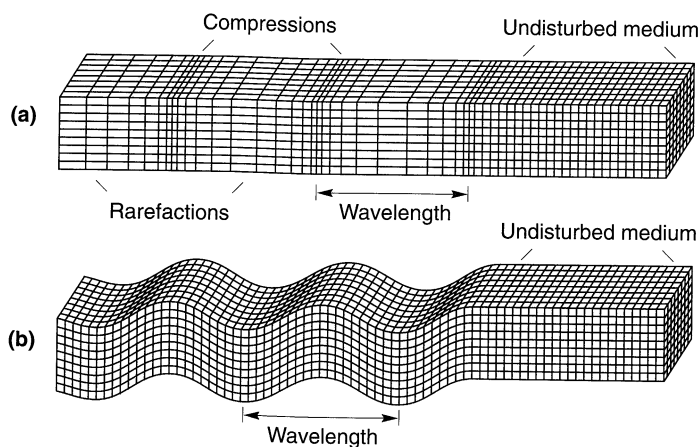


Figure 2.1 Deformations produced by body waves: (a) p-wave; (b) SV-wave. From *Earthquakes* by Bolt. Copyright © 1993 by W.H. Freeman and Company. Used with permission.

plane movement) and SH (horizontal plane movement). The speed at which body waves travel varies with the stiffness of the materials they travel through. Since geologic materials are stiffest in compression, p-waves travel faster than other seismic waves and are therefore the first to arrive at a particular site. Fluids, which have no shearing stiffness, cannot sustain s-waves.

Surface waves result from the interaction between body waves and the surface and surficial layers of the earth. They travel along the earth's surface with amplitudes that decrease roughly exponentially with depth (Figure 2.2). Because of the nature of the interactions required to produce them, surface waves are more prominent at distances farther from the source of the earthquake. At distances greater than about twice the thickness of the earth's crust, surface waves, rather than body waves, will produce peak ground motions. The most important surface waves, for engineering purposes, are *Rayleigh waves* and *Love waves*. Rayleigh waves, produced by interaction of p- and SV-waves with the earth's surface, involve both vertical and horizontal particle motion. They are similar, in some respects, to the waves produced by a rock thrown into a pond. Love waves result from the interaction of SH-waves with a soft surficial layer and have no vertical component of particle motion.

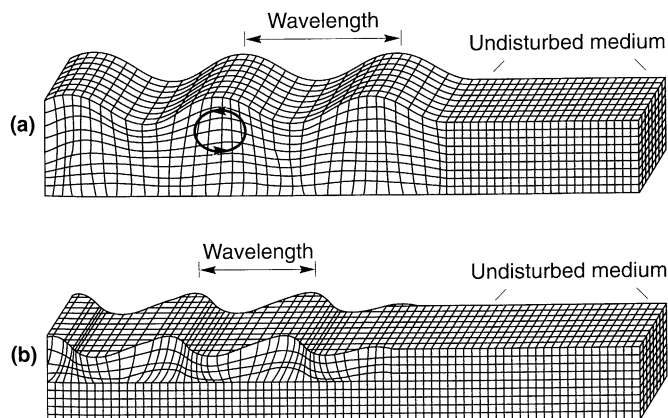


Figure 2.2 Deformations produced by surface waves: (a) Rayleigh wave; and (b) Love wave. From *Earthquakes* by Bolt. Copyright ©1993 by W.H. Freeman and Company. Used with permission.

2.2.2 Internal Structure

The *crust*, on which human beings live, is the outermost layer of the earth. The thickness of the crust ranges from about 25 to 40 km (15 to 25 miles) beneath the continents (although it may be as thick as 60 to 70 km (37 to 44 miles) under some young mountain ranges) to as thin as 5 km (3 miles) or so beneath the oceans—only a very small fraction of the earth's diameter (Figure 2.3). The internal structure of the crust is complex but can be represented by a basaltic layer that is overlain by a granitic layer at continental locations. Since it is

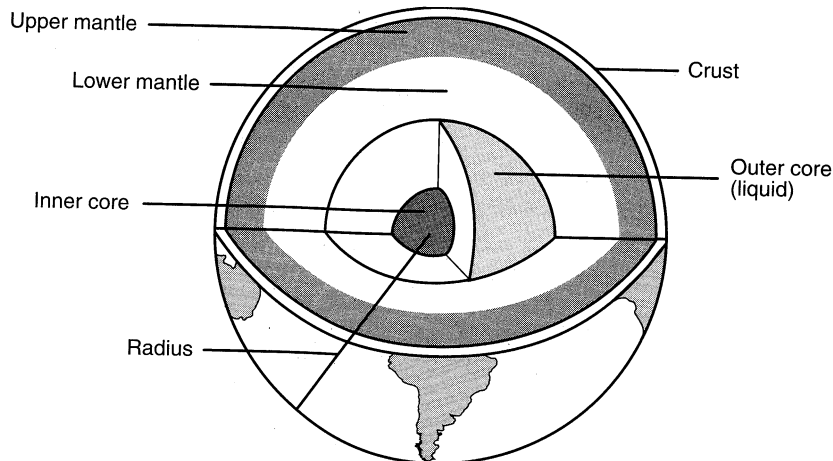


Figure 2.3 Internal structure of the earth.

exposed to the oceans or the atmosphere, the crust is cooler than the materials below it (Figure 2.4). In addition to being thinner, the oceanic crust is generally more uniform and more dense than the continental crust.

A distinct change in wave propagation velocity marks the boundary between the crust and the underlying *mantle*. This boundary is known as the *Mohorovičić discontinuity*, or the *Moho*, named after the seismologist who discovered it in 1909. Although the specific nature of the Moho itself is not well understood, its role as a reflector and refractor of seismic waves is well established. The mantle is about 2850 km (1770 miles) thick and can be

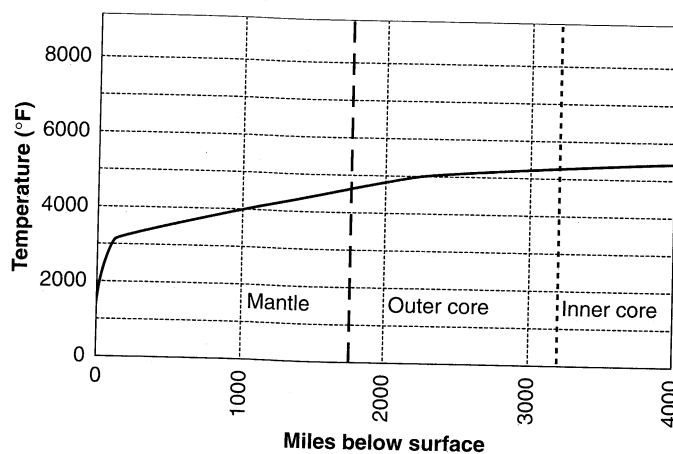


Figure 2.4 Estimated variation of temperature below the surface of the earth. (After Verhoogen, 1960.)

divided into the *upper mantle* (shallower than about 650 km (404 miles)) and the *lower mantle*. No earthquakes have been recorded in the lower mantle, which exhibits a uniform velocity structure and appears to be chemically homogeneous, except near its lower boundary. The mantle is cooler near the crust than at greater depths but still has an average temperature of about 4000°F. As a result, the mantle materials are in a viscous, semimolten state. They behave as a solid when subjected to rapidly applied stresses, such as those associated with seismic waves, but can slowly flow like a fluid in response to long-term stresses. The mantle material has a specific gravity of about 4 to 5.

The *outer core*, or *liquid core*, is some 2260 km (1400 miles) thick. As a liquid, it cannot transmit s-waves. As shown in Figure 2.5, the s-wave velocity drops to zero at the core-mantle boundary, or *Gutenberg discontinuity*; note also the precipitous drop in p-wave velocity. The outer core consists primarily of molten iron (which helps explain its high specific gravity of 9 to 12). The *inner core*, or *solid core*, is a very dense (specific gravity up to about 15), solid nickel–iron material compressed under tremendous pressures. The temperature of the inner core is estimated to be relatively uniform at over 5000°F.

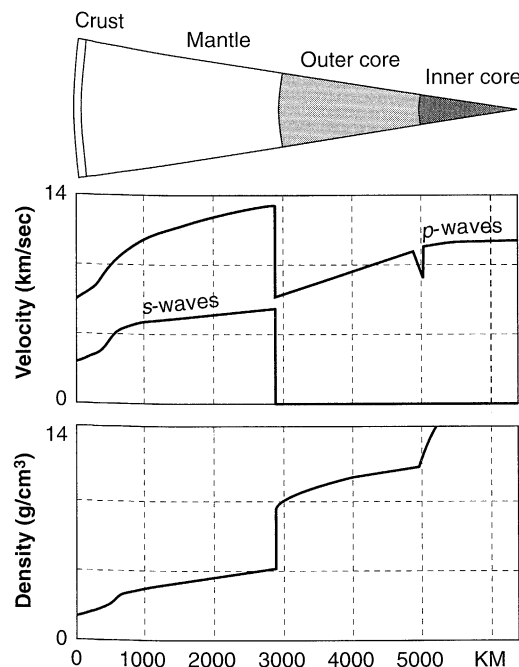


Figure 2.5 Variation of p- and s-wave velocity and density within the earth. (After Eiby, 1980.)

Figure 2.6 shows the influence of the earth's structure on the distribution of seismic waves during earthquakes. Since wave propagation velocities generally increase with depth, wave paths are usually refracted back toward the earth's surface. An exception is at the core–mantle boundary, where the outer core velocity is lower than the mantle velocity.

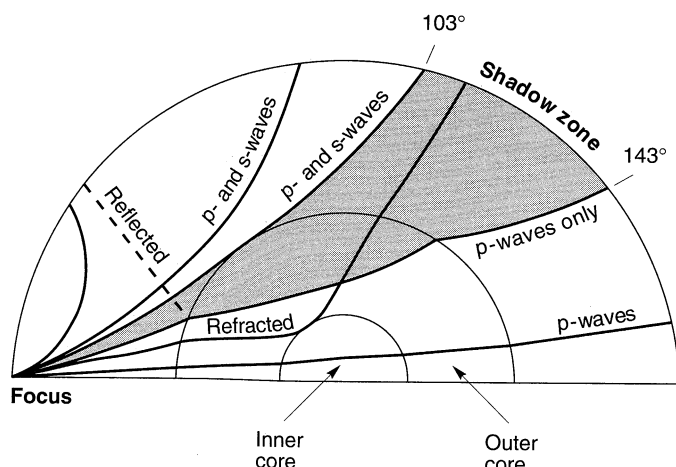


Figure 2.6 Seismic wave paths illustrating reflection and refraction of seismic waves from the source (focus) of the earthquake by the different layers of the earth. Note that p- and s-waves can reach the earth's surface between 0 and 103°, but the liquid nature of the outer core allows only p-waves to reach the surface between 143 and 180°. In the shadow zone between angles of 103 and 143°, only paths reflected from the inner core can reach the earth's surface. (From Sumner, 1969.)

2.3 CONTINENTAL DRIFT AND PLATE TECTONICS

Although observations of similarity between the coastlines and geology of eastern South America and the western Africa and the southern part of India and northern part of Australia had intrigued scientists since the seventeenth century (Glen 1975; Kearey and Vine, 1990), the theory that has come to be known as *continental drift* was not proposed until the early twentieth century (Taylor, 1910; Wegener, 1915). Wegener, for example, believed that the earth had only one large continent called Pangaea 200 million years ago. He believed that Pangaea broke into pieces that slowly drifted (Figure 2.7) into the present configuration of the continents. A more detailed view of the current similarity of the African and South American coasts is shown in Figure 2.8.

The theory of continental drift did not receive much attention until about 1960, when the current worldwide network of seismographs was able to define earthquake locations accurately, and to confirm that long-term deformations were concentrated in narrow zones between relatively intact blocks of crust. Also, exploration of the ocean floor did not begin in earnest until after World War II, when new techniques such as deep-water echo sounding, seismic refraction, and piston coring became available. The geology of the ocean floor is young, representing only about 5% of the earth's history (Gubbins, 1990), and relatively simple. Its detailed study provided strong supporting evidence of the historical movement of the continents as assumed in the theory of continental drift. Within 10 years, the theory of continental drift had become widely accepted and acknowledged as the greatest advance in the earth sciences in a century.

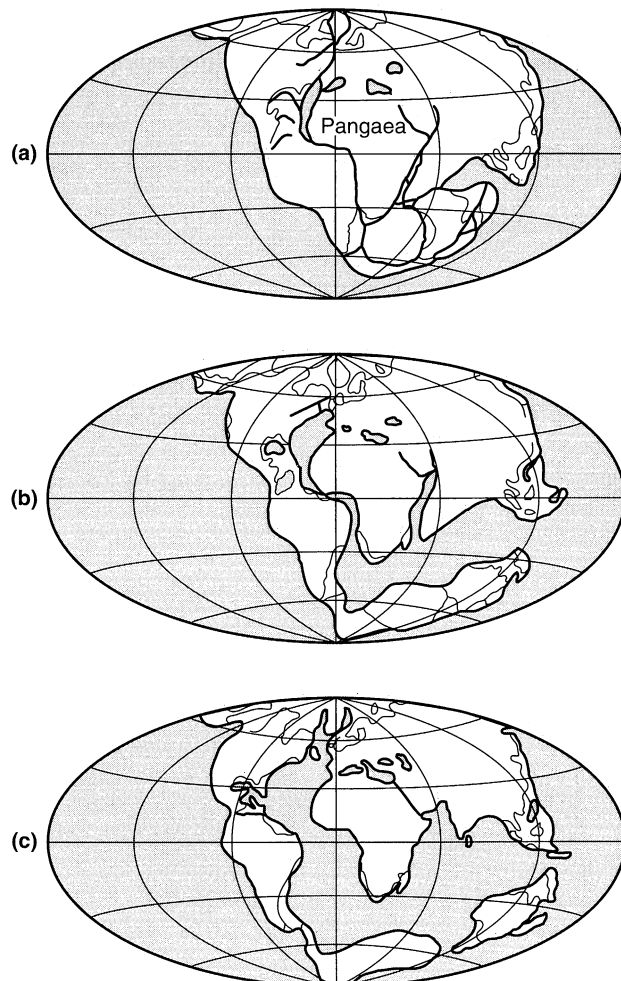


Figure 2.7 Wegener's theory of continental drift: (a) 270 million years ago; (b) 150 million years ago; (c) 1 million years ago. (After Verney, 1979.)

2.3.1 Plate Tectonics

The original theory of continental drift suggested images of massive continents pushing through the seas and across the ocean floor. It was well known, however, that the ocean floor was too strong to permit such motion, and the theory was originally discredited by most earth scientists. From this background, however, the modern theory of *plate tectonics* began to evolve. The basic hypothesis of plate tectonics is that the earth's surface consists of a number of large, intact blocks called *plates*, and that these plates move with respect to

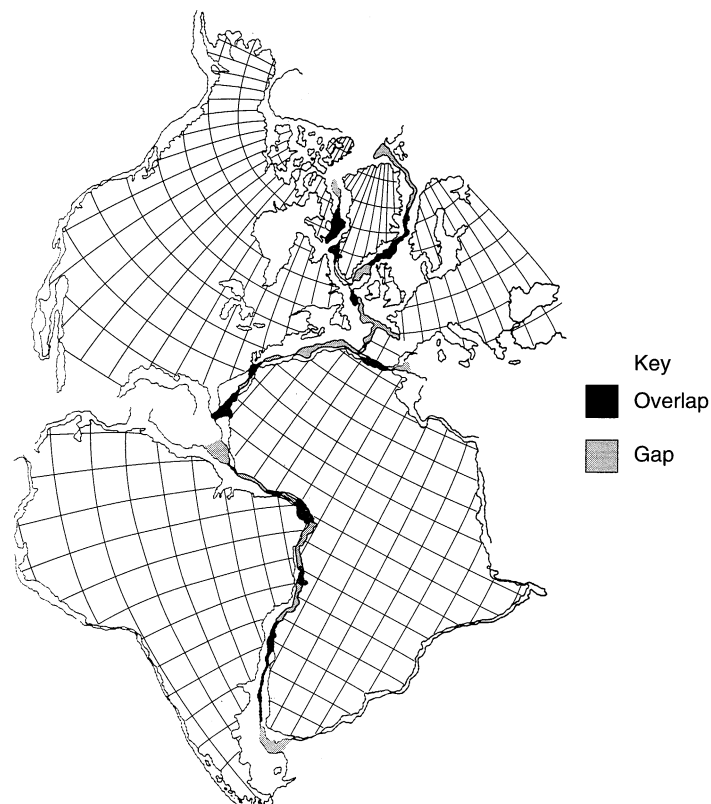


Figure 2.8 Statistical spherical fit of several continents using the continental slopes rather than the coastlines. (After Bullard et al., 1965, with permission of the Royal Society.)

each other. The earth's crust is divided into six continental-sized plates (African, American, Antarctic, Australia-Indian, Eurasian, and Pacific) and about 14 of subcontinental size (e.g., Caribbean, Cocos, Nazca, Philippine, etc.). The major plates are shown in Figure 2.9. Smaller *platelets*, or *microplates*, have broken off from the larger plates in the vicinity of many of the major plate boundaries but are not shown here. The relative deformation between plates occurs only in narrow zones near their boundaries. This deformation of the plates can occur slowly and continuously (*aseismic deformation*) or can occur spasmodically in the form of earthquakes (*seismic deformation*). Since the deformation occurs predominantly at the boundaries between the plates, it would be expected that the locations of earthquakes would be concentrated near plate boundaries. The map of earthquake epicenters shown in Figure 2.10 confirms this expectation, thereby providing strong support for the theory of plate tectonics.

The theory of plate tectonics is a kinematic theory (i.e., it explains the geometry of plate movement without addressing the cause of that movement). Something must drive the movement, however, and the tremendous mass of the moving plates requires that the

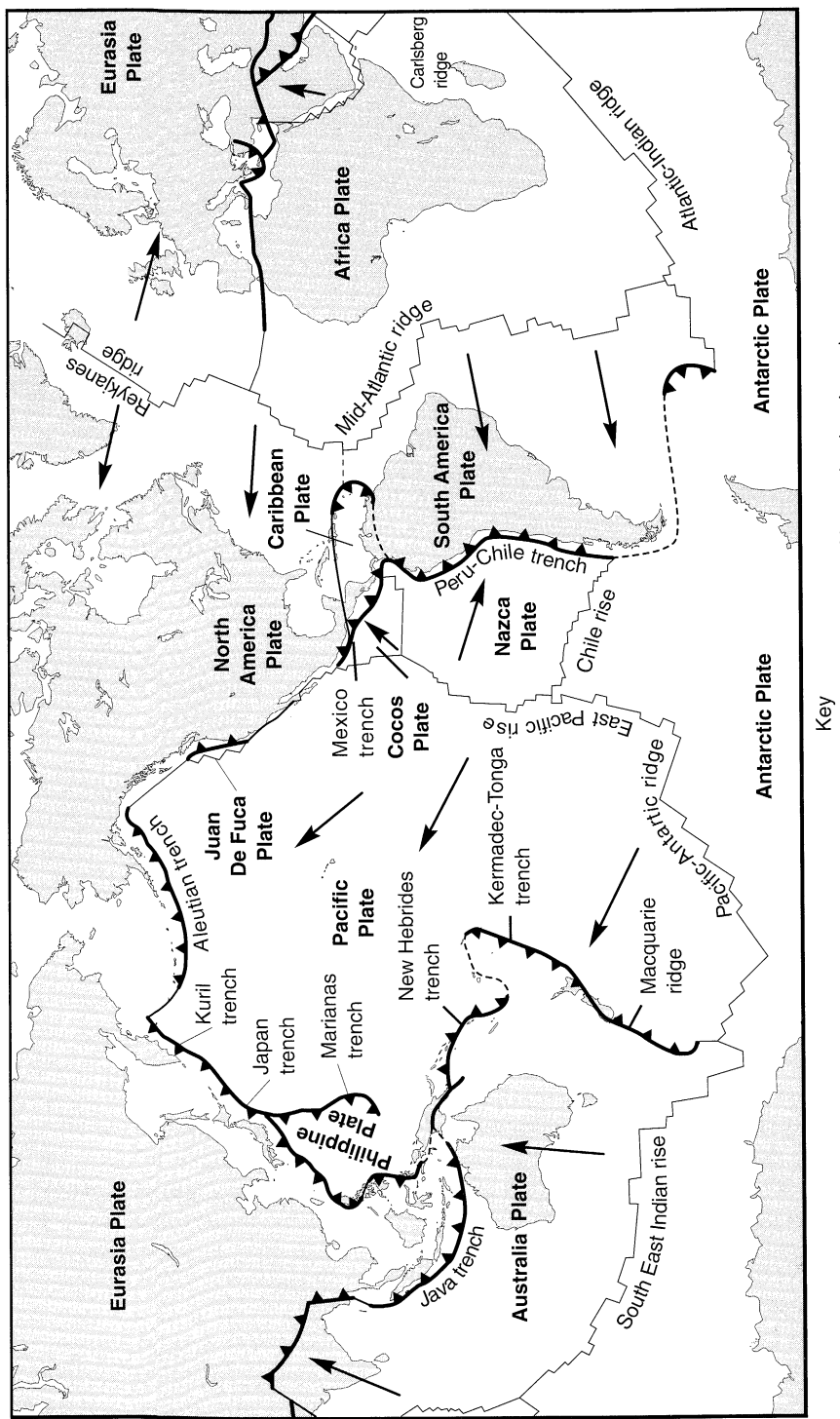


Figure 2.9 The major tectonic plates, mid-oceanic ridges, trenches, and transform faults of the earth. Arrows indicate directions of plate movement. (After Fowler, 1990.)

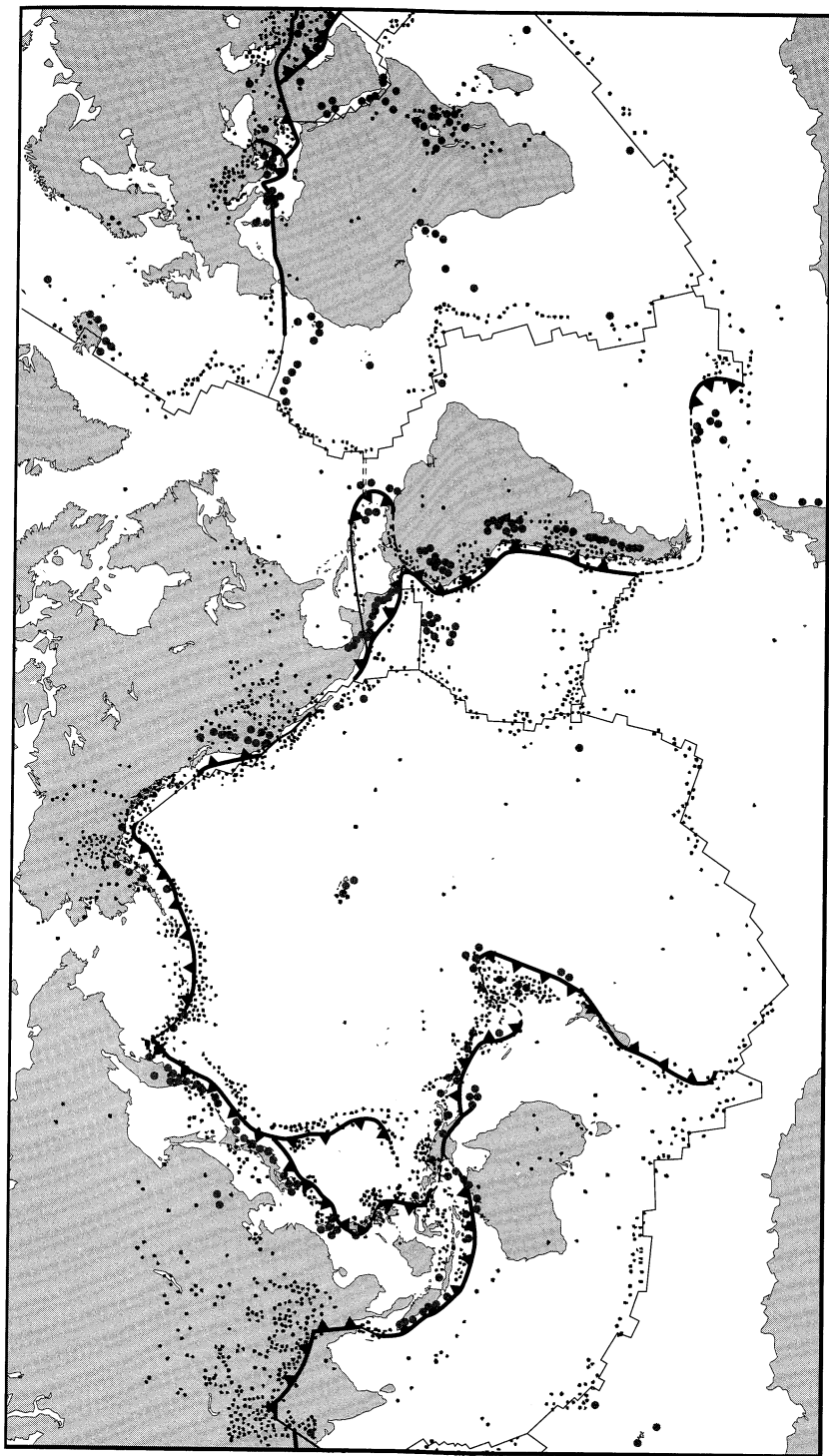


Figure 2.10 Worldwide seismic activity. The dots represent the epicenters of significant earthquakes. It is apparent that the locations of the great majority of earthquakes correspond to the boundaries between plates. (After Bolt, 1988.)

driving forces be very large. The most widely accepted explanation of the source of plate movement relies on the requirement of thermomechanical equilibrium of the earth's materials. The upper portion of the mantle is in contact with the relatively cool crust while the lower portion is in contact with the hot outer core. Obviously, a temperature gradient must exist within the mantle (see Figure 2.4). The variation of mantle density with temperature produces the unstable situation of denser (cooler) material resting on top of less dense (warmer) material. Eventually, the cooler, denser material begins to sink under the action of gravity and the warmer, less dense material begins to rise. The sinking material gradually warms and becomes less dense; eventually, it will move laterally and begin to rise again as subsequently cooled material begins to sink. This process is the familiar one of *convection*.

Convection currents in the semimolten rock of the mantle, illustrated schematically in Figure 2.11, impose shear stresses on the bottom of the plates, thus "dragging" them in various directions across the surface of the earth. Other phenomena, such as *ridge push* or *slab pull*, may also contribute to the movement of plates (Hager, 1978).

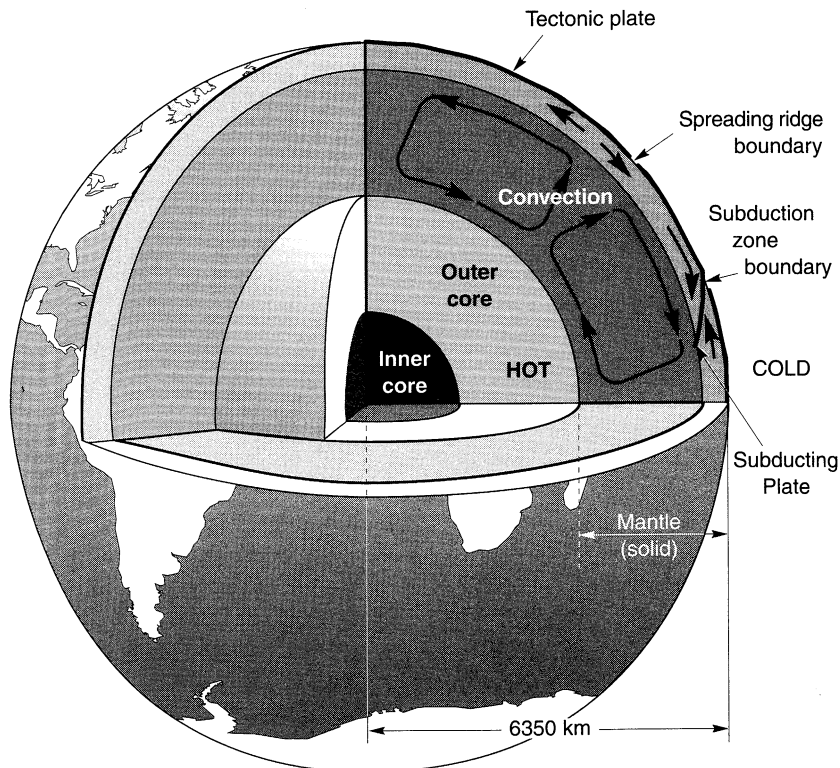


Figure 2.11 Convection currents in mantle. Near the bottom of the crust, horizontal component of convection currents impose shear stresses on bottom of crust, causing movement of plates on earth's surface. The movement causes the plates to move apart in some places and to converge in others. (After Nason et al., 1988.)

2.3.2 Plate Boundaries

Three distinct types of plate boundaries have been identified, and understanding the movement associated with each will aid in the understanding of plate tectonics. The characteristics of the plate boundaries also influence the nature of the earthquakes that occur along them.

2.3.2.1 Spreading Ridge Boundaries

In certain areas the plates move apart from each other (Figure 2.12) at boundaries known as *spreading ridges* or *spreading rifts*. Molten rock from the underlying mantle rises to the surface where it cools and becomes part of the spreading plates. In this way, the plates “grow” at the spreading ridge. Spreading rates range from approximately 2 to 18 cm/yr (1 to 7 in/yr); the highest rates are found in the Pacific Ocean ridges and the lowest along the Mid-Atlantic Ridge. It is estimated (Garfunkel, 1975) that new oceanic crust is currently formed at a rate of about $3.1 \text{ km}^2/\text{yr}$ (1.2 miles $^2/\text{yr}$) worldwide. The crust, mainly young, fresh basalt, is thin in the vicinity of the spreading ridges. It may be formed by relatively slow upward movement of magma, or it may be ejected quickly during seismic activity. Underwater photographs have shown formations of pillow lava and have even recorded lava eruptions in progress. Volcanic activity, much of which occurs beneath the ocean surface, is common in the vicinity of spreading-ridge boundaries. Spreading ridges can protrude above the ocean; the island of Iceland, where volcanic activity is nearly continuous (there are 150 active volcanos), is such an example.

The mantle material cools after it reaches the surface in the gap between the spreading plates. As it cools, it becomes magnetized (*remnant magnetism*) with a polarity that depends on the direction of the earth’s magnetic field at that time. The magnetic field of the earth is not constant on a geological time scale; it has fluctuated and reversed at irregular historical intervals, thus imposing magnetic anomalies (reversals of polarity) in the rock that forms at the

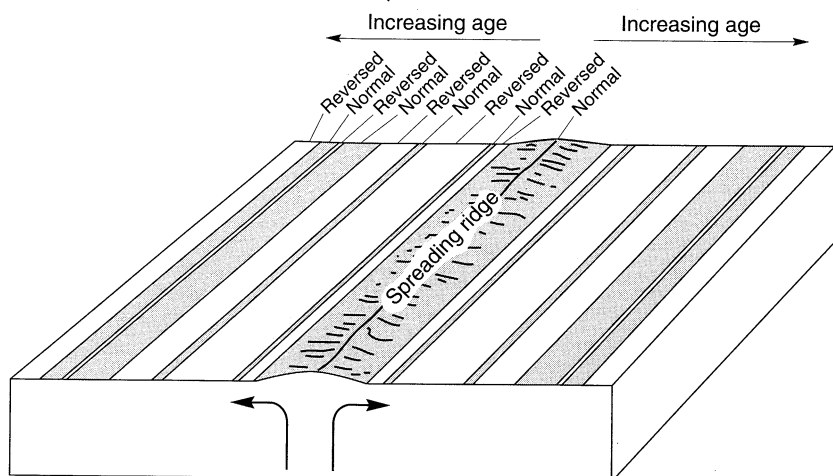


Figure 2.12 Spreading ridge boundary. Magma rises to surface and cools in gap formed by spreading plates. Magnetic anomalies are shown as stripes of normal and reversed magnetic polarity. (After Foster, 1971.)

spreading ridge boundaries. Measurement of the magnetic field in a direction perpendicular to a spreading ridge plate boundary reveals a fluctuating pattern of magnetic intensity, as illustrated for the eastern Pacific Ocean region in Figure 2.13. These magnetic anomalies have allowed large portions of the major plates to be dated. Comparison of the ages of various materials allows identification of the geometry and movement of various plates and has proven invaluable in the verification and acceptance of the theory of plate tectonics.

2.3.2.2 Subduction Zone Boundaries

Since the size of the earth remains constant, the creation of new plate material at spreading ridges must be balanced by the consumption of plate material at other locations. This occurs at *subduction zone* boundaries where the relative movement of two plates is toward each other. At the point of contact, one plate plunges, or *subducts*, beneath the other,

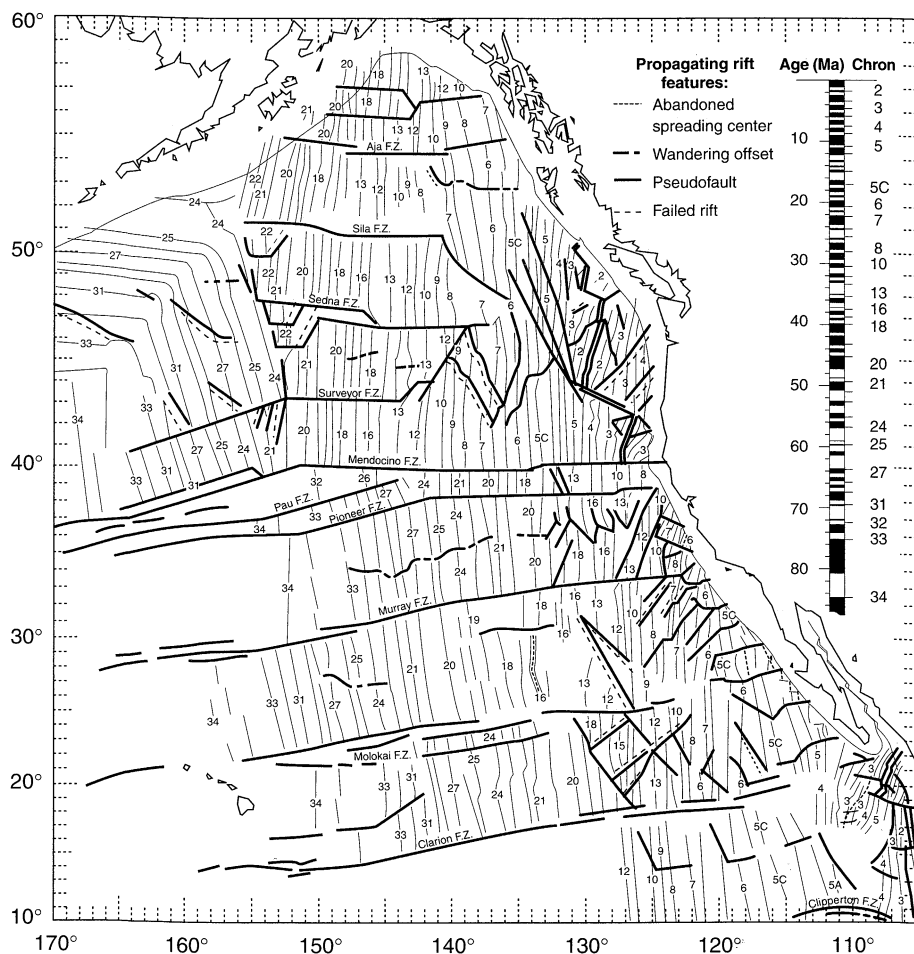


Figure 2.13 Magnetic anomalies in the eastern Pacific Ocean. The dark lines represent bands of common magnetic polarity. (After Atwater and Sveringhaus, 1989.)

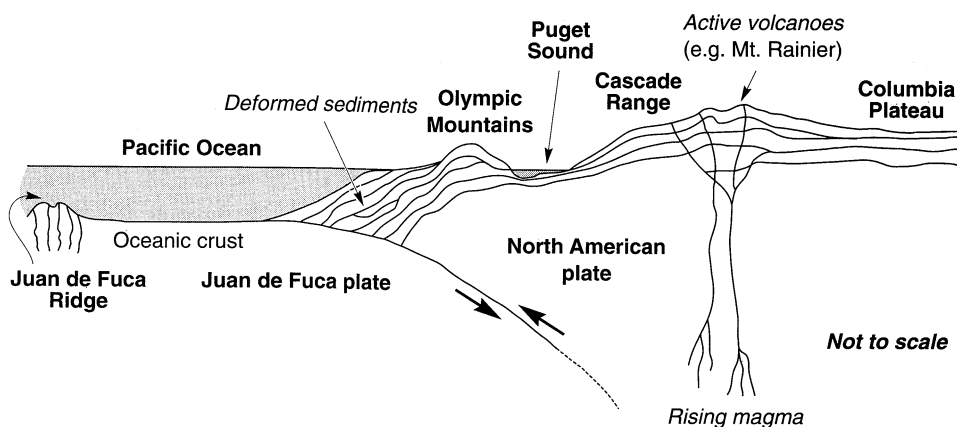


Figure 2.14 Cascadia subduction zone off the coasts of Washington and Oregon. The Juan de Fuca plate originates at the Juan de Fuca spreading ridge and subducts beneath the North American plate. Magma rising from the deeper part of the subduction zone has formed a series of volcanoes that run roughly parallel to the subduction zone. One of these, Mt. St. Helens, erupted explosively in 1980. (After Noson et al., 1988.)

as shown in Figure 2.14. Subduction zone plate boundaries exist off the western coasts of Mexico and Chile, south of the Aleutian Island chain of Alaska, and off the eastern coast of Japan. The Cascadia subduction zone off the coast of Washington and British Columbia is shown in Figure 2.14.

Subduction zone boundaries are often found near the edges of continents. Because the oceanic crust is generally cold and dense, it sinks under its own weight beneath the lighter continental crust. When the rate of plate convergence is high, a trench is formed at the boundary between plates. In fact, subduction zone boundaries are sometimes called trench boundaries. Earthquakes are generated in the sloping *Benioff zone* at the interface between the subducting and overriding plates. When the rate of convergence is slow, sediments accumulate in an *accretionary wedge* on top of the crustal rock, thus obscuring the trench.

The subducting plate warms and becomes less brittle as it sinks. Eventually, it becomes so ductile as to be incapable of producing earthquakes; the greatest recorded earthquake depth of approximately 700 km (435 miles) supports this hypothesis. Portions of the subducting plate melt, producing magma that can rise to the surface to form a line of volcanoes roughly parallel to the subduction zone on the overriding plate.

When plates carrying continents move toward each other, *continental collisions* can lead to the formation of mountain ranges. The Himalayas consist of two crustal layers that have formed as the Australia–Indian plate has collided with the Eurasian plate. Continental collision of the plates carrying Africa and Europe are currently reducing the size of the Mediterranean Sea and will eventually lead to the formation of a collision-type mountain range (McKenzie, 1970).

2.3.2.3 Transform Fault Boundaries

Transform faults occur where plates move past each other without creating new crust or consuming old crust. They are usually found offsetting spreading ridges as illustrated in Figure 2.15. These transform faults are identified by offsets in magnetic anomalies and, where preserved, scarps on the surface of the crust. Magnetic anomaly offsets defining *fracture zones* may be observed over thousands of kilometers; however, it is only the segment of the fracture zone between the spreading ridges that is referred to as the transform fault. As illustrated in Figure 2.15, the motion on the portions of the fracture zone that extend beyond the transform fault is in the same direction on either side of the fracture zone; hence there is generally no relative motion. These inactive portions of the fracture zone can be viewed as fossil faults that are not producing earthquakes.

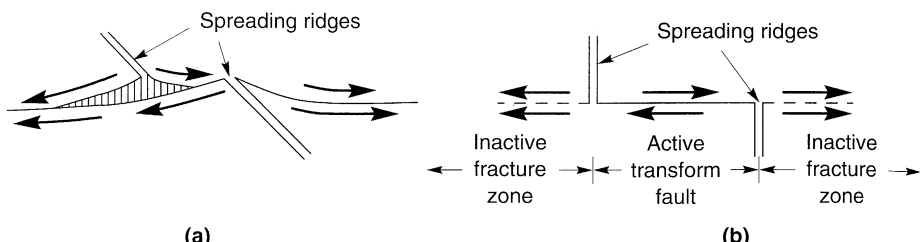


Figure 2.15 (a) Oblique and (b) plan views of transform fault and adjacent inactive fracture zones.

The San Andreas fault, for example, has been characterized as a transform fault (Wilson, 1965) connecting the East Pacific ridge off the coast of Mexico with the Juan de Fuca ridge off the coast of Washington state. In reality, the geometry of transform faults is usually quite complex with many bends and kinks, and they are often divided into a number of *fault segments*. Their depth is typically limited but can extend horizontally over very long distances. Other important transform faults include the Motagua fault (which separates the North American and Caribbean plates), the Alpine fault of New Zealand, and the Dead Sea fault system that connects the Red Sea to the Bitlis Mountains of Turkey (Kearey and Vine, 1990).

Plate tectonics provides a very useful framework for understanding and explaining movements on the earth's surface and the locations of earthquakes and volcanoes. Plate tectonics accounts for the formation of new and consumption of old crustal materials in terms of the three types of plate movement illustrated in Figure 2.16. It does not, however, explain all observed tectonic seismicity. For example, it is known that *intraplate earthquakes* (earthquakes that occur within a plate, away from its edges) have occurred on most continents. Well-known North American examples are the series of midplate earthquakes that occurred in the vicinity of New Madrid, Missouri, in 1811–1812, and the 1886 Charleston (South Carolina) earthquake. The 1976 Tangshan (China) and 1993 Marathawada (India) earthquakes are more recent examples of damaging intraplate earthquakes.

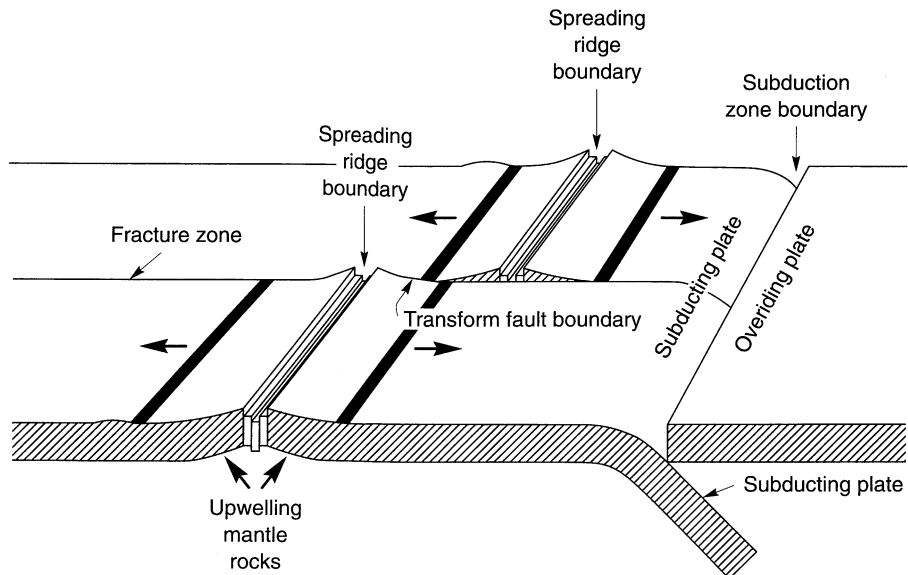


Figure 2.16 Interrelationships among spreading ridge, subduction zone, and transform fault plate boundaries.

2.4 FAULTS

While the theory of plate tectonics generally assigns the relative movement of plates to one of the three preceding types of plate boundaries, examination on a smaller scale reveals that the movement at a particular location can be quite complicated. In some regions, plate boundaries are distinct and easy to identify, while in others they may be spread out with the edges of the plates broken to form smaller *platelets* or *microplates* trapped between the larger plates. Locally, the movement between two portions of the crust will occur on new or preexisting offsets in the geologic structure of the crust known as *faults*.

Faults may range in length from several meters to hundreds of kilometers and extend from the ground surface to depths of several tens of kilometers. Their presence may be obvious, as reflected in surficial topography, or they may be very difficult to detect. The presence of a fault does not necessarily mean that earthquakes can be expected; movement can occur aseismically, or the fault may be inactive. The lack of observable surficial faulting, on the other hand, does not imply that earthquakes cannot occur; in fact, fault rupture does not reach the earth's surface in most earthquakes. The activity of faults is discussed in more detail in Chapter 4.

2.4.1 Fault Geometry

Standard geologic notation is used to describe the orientation of a fault in space. While the surface of a large fault may be irregular, it can usually be approximated, at least over short distances, as a plane. The orientation of the fault plane is described by its *strike* and *dip*. The

strike of a fault is the horizontal line produced by the intersection of the fault plane and a horizontal plane as shown in Figure 2.17. The azimuth of the strike (e.g., N60°E) is used to describe the orientation of the fault with respect to due north. The downward slope of the fault plane is described by the *dip angle*, which is the angle between the fault plane and the horizontal plane measured perpendicular to the strike. A vertical fault would have a dip angle of 90°.

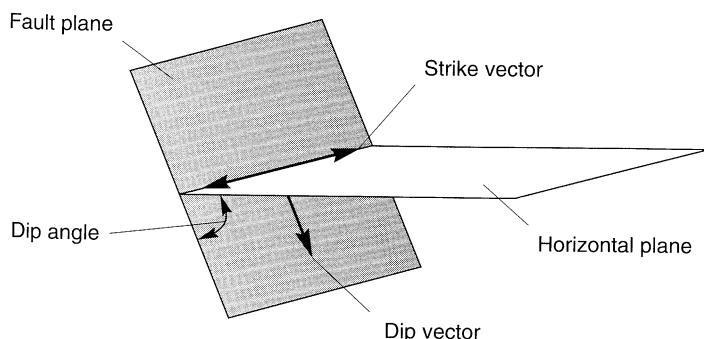


Figure 2.17 Geometric notation for description of fault plane orientation.

2.4.2 Fault Movement

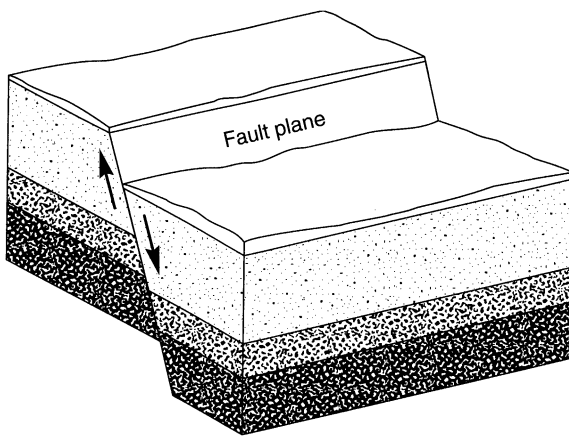
The type of movement occurring on a fault is usually reduced to components in the directions of the strike and dip. While some movement in both directions is inevitable, movement in one direction or the other will usually predominate.

2.4.2.1 Dip Slip Movement

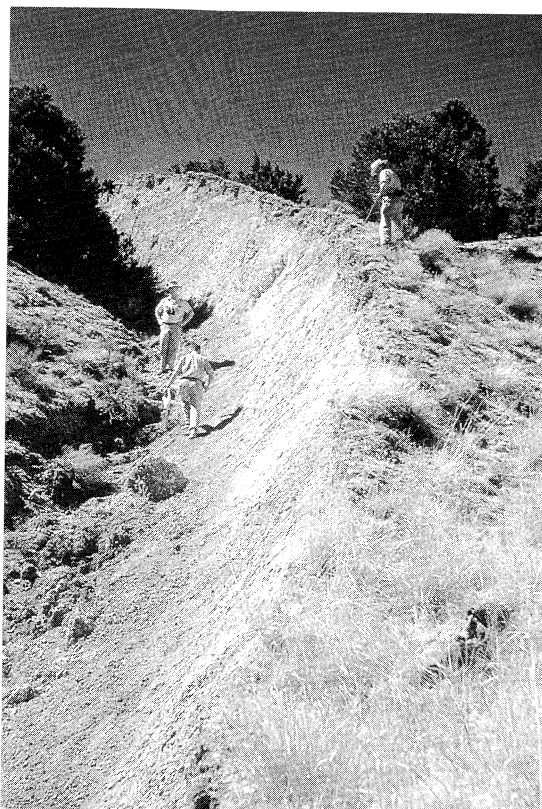
Fault movement that occurs primarily in the direction of the dip (or perpendicular to the strike) is referred to as *dip slip* movement. There are different types of dip slip movements, classified according to the direction of movement and the dip angle of the fault. *Normal faults*, illustrated in Figure 2.18, occur when the horizontal component of dip slip movement is extensional and when the material above the inclined fault (sometimes referred to as the *hanging wall*) moves downward relative to the material below the fault (the *foot wall*). Normal faulting is generally associated with tensile stresses in the crust and results in a horizontal lengthening of the crust. When the horizontal component of dip slip movement is compressional and the material above the fault moves upward relative to the material below the fault, *reverse faulting* is said to have occurred. Movement on reverse faults, illustrated in Figure 2.19, results in a horizontal shortening of the crust. A special type of reverse fault is a *thrust fault*, which occurs when the fault plane has a small dip angle. Very large movements can be produced by thrust faulting; the European Alps are an excellent example of thrust structure.

2.4.2.2 Strike-Slip Movement

Fault movement occurring parallel to the strike is called *strike-slip* movement. Strike-slip faults are usually nearly vertical and can produce large movements. Strike-slip faults are further categorized by the relative direction of movement of the materials on either side of the fault. An observer standing near a *right lateral strike-slip fault* would observe the ground on



(a)



(b)

Figure 2.18 (a) Normal faulting (after Noson et al., 1988); (b) scarp of the normal fault that produced the 1954 Dixie-Fairview earthquake in Nevada (K. Steinbrugge collection; courtesy of EERC, Univ. of California).

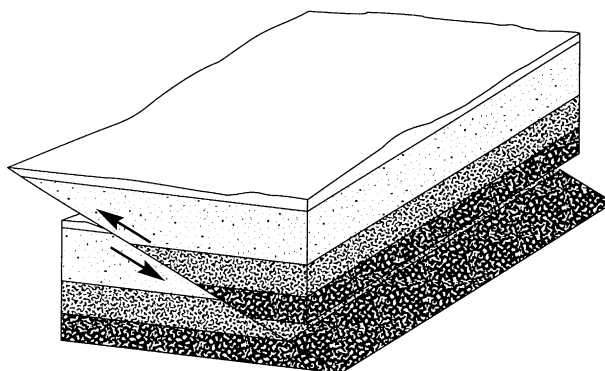


Figure 2.19 Reverse faulting. Because the dip angle is so small, this reverse fault would probably be classified as a thrust fault. (After Noson et al., 1988.)

the other side of the fault moving to the right. Similarly, an observer adjacent to a *left lateral strike-slip fault* would observe the material on the other side moving to the left. The strike-slip fault shown in Figure 2.20a would be characterized as a left lateral strike-slip fault. The San Andreas fault in California is an excellent example of right lateral strike-slip faulting; in the 1906 San Francisco earthquake, several roads and fences north of San Francisco were offset by nearly 6 m (20 ft) (Figure 2.20b).

Oblique fault movement (i.e., movement with both dip-slip and strike-slip components) often occurs. The 1971 San Fernando earthquake ruptured the ground surface over a length of 15 km (9 miles). The maximum vertical displacement (produced by reverse fault movement) was 1.46 m (4.8 ft), and the maximum horizontal displacement (from left lateral strike-slip movement) was 2.13 m (7.0 ft) (Berlin, 1980).

2.5 ELASTIC REBOUND THEORY

The plates of the earth are in constant motion, and plate tectonics indicates that the majority of their relative movement occurs near their boundaries. The long-term effects of this movement can be observed in the geologic record, which reflects deformations that have occurred over very long periods of time. With the advent of modern electronic distance measurement equipment, however, movements can also be observed over much shorter time scales. Figure 2.21 shows a set of survey lines established across the San Andreas and Calaveras faults by the California Department of Water Resources and Division of Mines and Geology. The shortening of chords 17 and 19, and the lengthening of 20 and 23, indicate that fault movement is occurring. Chord 21, which lies entirely east of the Calaveras fault, shows very little change in length.

As relative movement of the plates occurs, *elastic strain energy* is stored in the materials near the boundary as shear stresses increase on the fault planes that separate the plates. When the shear stress reaches the shear strength of the rock along the fault, the rock fails and the accumulated strain energy is released. The effects of the failure depend on the nature of the rock along the fault. If it is weak and ductile, what little strain energy that could be stored

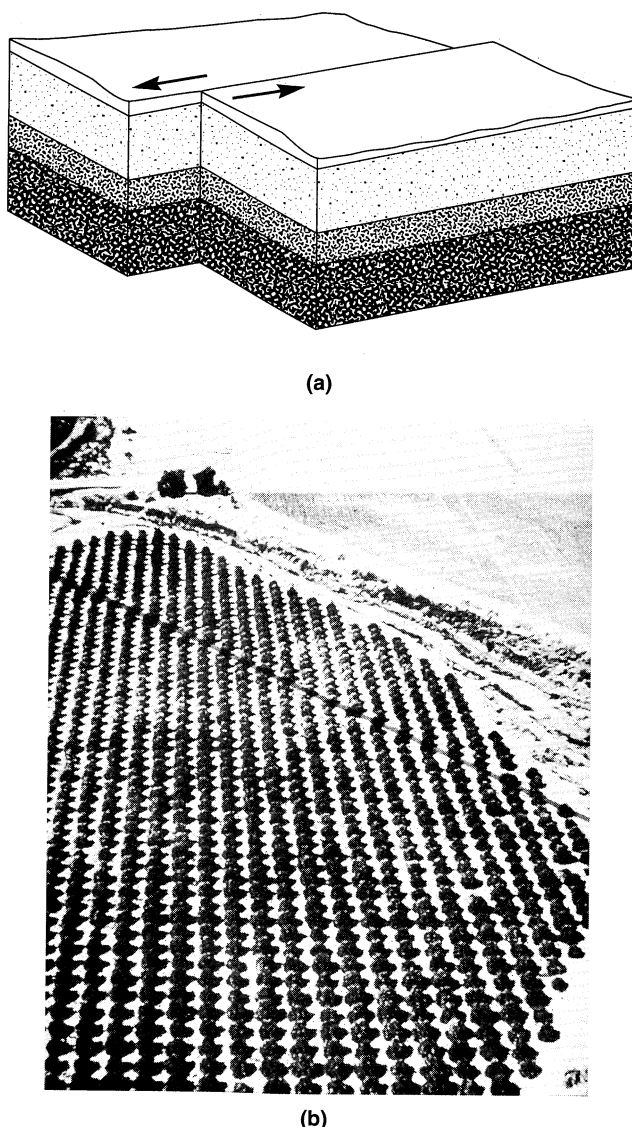


Figure 2.20 (a) Left lateral strike-slip faulting (from Noson et al., 1988); (b) trees offset by strike-slip faulting through citrus grove in 1940 Imperial Valley earthquake (courtesy of U.S. Geological Survey).

will be released relatively slowly and the movement will occur aseismically. If, on the other hand, the rock is strong and brittle, the failure will be rapid. Rupture of the rock will release the stored energy explosively, partly in the form of heat and partly in the form of stress waves that are felt as earthquakes. The theory of *elastic rebound* (Reid, 1911) describes this

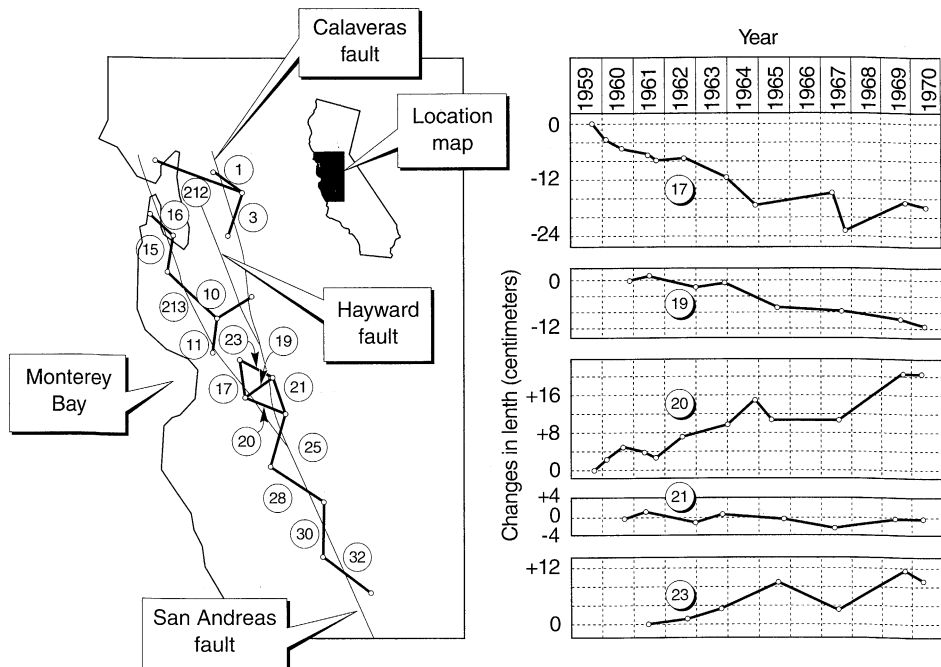


Figure 2.21 (a) Survey lines across San Andreas and Calaveras faults in California;
 (b) change in chord length (extension positive). (From *Earthquakes* by Bolt. Copyright
 © 1993 by W.H. Freeman and Company. Used with permission.)

process of the successive buildup and release of strain energy in the rock adjacent to faults. It is often illustrated as shown in Figure 2.22.

The nature of the buildup and release of stress is of interest. Faults are not uniform, either geometrically or in terms of material properties—both strong and weak zones can exist over the surface of a fault. The stronger zones, referred to as *asperities* by some (Kanamori and Stewart, 1978) and *barriers* by others (Aki, 1979), are particularly important. The *asperity model* of fault rupture assumes that the shear stresses prior to an earthquake are not uniform across the fault because of stress release in the weaker zones by creep or *foreshocks*. Release of the remaining stresses held by the asperities produces the main earthquake that leaves the rupture surface in a state of uniform stress. In the *barrier model*, the pre-earthquake stresses on the fault are assumed to be uniform. When the main earthquake occurs, stresses are released from all parts of the fault except for the stronger barriers; *aftershocks* then occur as the rock adjusts to the new uniform stress field. Since both foreshocks and aftershocks are commonly observed, it appears that some strong zones behave as asperities and others as barriers (Aki, 1984). The engineering significance of asperities and barriers lies in their influence on ground-shaking characteristics close to the fault. A site located close to one of these strong zones may experience stronger shaking than a site equally close

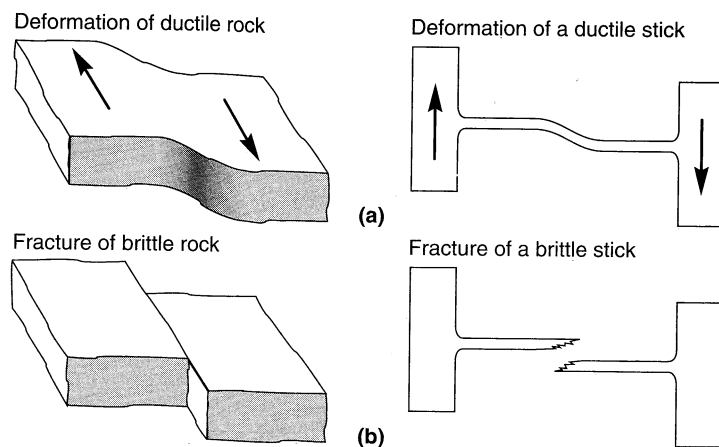


Figure 2.22 Elastic rebound theory of earthquakes. In (a) the slow deformation of rock in the vicinity of a plate boundary results in a buildup of strain energy in the rock in the same way that strain energy builds up in a ductile stick deformed as shown on the right. If the strength of the rock is exceeded, it will rupture, releasing strain energy in the form of vibrations, much as the energy in the stick would be released when the stick breaks. After the earthquake, the rock is displaced from its original position. The total relative displacement of the plates is the sum of the slip displacement at the fault and possible displacements due to warping distortion of the edges of the plates near the fault. (After Foster, R.J., General Geology, 5/e, © 1988. Adapted by permission of Prentice Hall, Upper Saddle River, New Jersey.)

to the fault but farther from a strong zone. At larger distances from the fault the effects of fault nonuniformity decrease. Unfortunately, methods for locating these strong zones prior to rupture have not yet been developed.

Rupture generally progresses across a fault as a series of dislocations (some *multiple-event* earthquakes can be thought of as a series of small earthquakes that occur in close spatial and temporal proximity). Small earthquakes can be modeled as point processes since their rupture surfaces usually span only a few kilometers. Large earthquakes, however, can rupture over distances of tens, or even hundreds, of kilometers, and the nature of ground shaking can be influenced by the characteristics of the rupture process. For example, waves emanate from the fault with different strengths in different directions; such *directivity* effects can produce azimuthal differences in ground motion characteristics (Benioff, 1955; Ben-Menachem, 1961). Constructive interference of waves produced by successive dislocations can produce strong pulses of large displacement called *fling* (Figure 2.23) at nearby sites toward which the rupture is progressing (Benioff, 1955; Singh, 1985).

2.5.1 Relationship to Earthquake Recurrence

The theory of elastic rebound implies that the occurrence of earthquakes will relieve stresses along the portion of a fault on which rupture occurs, and that subsequent rupture

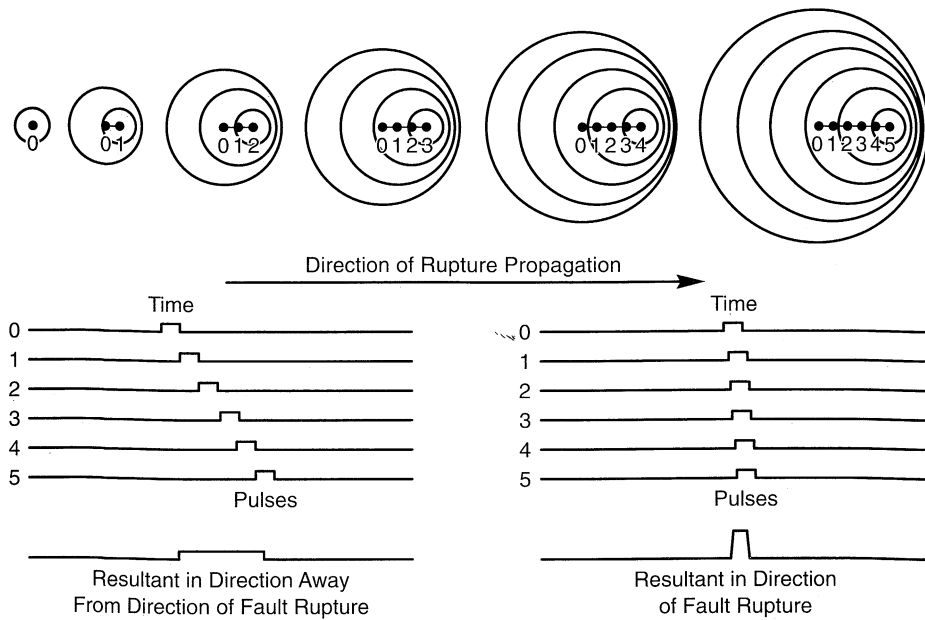


Figure 2.23 Schematic illustration of directivity effect on ground motions at sites toward and away from direction of fault rupture. Overlapping of pulses can lead to strong fling pulse at sites toward which the fault ruptures. (After Singh, 1985; used by permission of EERI).

will not occur on that segment until the stresses have had time to build up again. The chances of an earthquake occurring on a particular fault segment should therefore be related in some way to the time that has elapsed since the last earthquake and, perhaps, to the amount of energy that was released. In a probabilistic sense, then, individual earthquakes on a particular fault segment should not be considered as random, independent events. This characteristic is important in seismic hazard analysis.

Because earthquakes relieve the strain energy that builds up on faults, they should be more likely to occur in areas where little or no seismic activity has been observed for some time. By plotting fault movement and historical earthquake activity along a fault, it is possible to identify *gaps* in seismic activity at certain locations along faults. According to elastic rebound theory, either the movement is occurring aseismically or strain energy is building in the vicinity of these seismic gaps. In areas where the latter is known to be the case, seismic gaps should represent the most likely locations for future earthquakes. A number of seismic gaps have been identified around the world and large earthquakes have subsequently been observed on several of them. The 1989 Loma Prieta earthquake occurred on a segment of the San Andreas fault that had previously been identified as a gap, as shown in Figure 2.24. The use of seismic gaps offers promise for improvement in earthquake prediction capabilities and seismic risk evaluation.

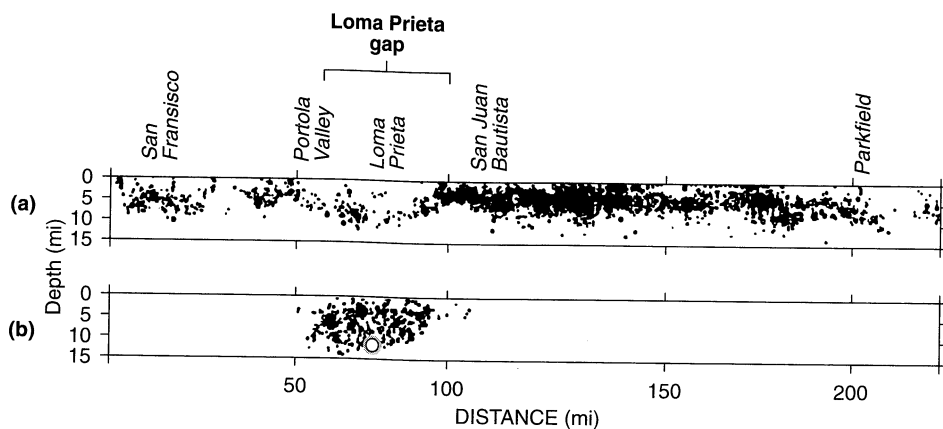


Figure 2.24 Cross section of the San Andreas fault from north of San Francisco to south of Parkfield: (a) seismicity in the 20 years prior to the 1989 Loma Prieta earthquake is shown with the Loma Prieta gap highlighted; (b) main shock (open circle) and aftershocks of the Loma Prieta earthquake. Note the remaining gaps between San Francisco and Portola Valley and south of Parkfield. (After Housner et al., 1990.)

2.5.2 Relationship to Tectonic Environment

Elastic rebound also implies that tectonic environments capable of storing different amounts of energy will produce earthquakes of different size. Consider, for example, the tectonic environment in the vicinity of a spreading ridge plate boundary. First, the crust is thin; hence the volume of rock in which strain energy can build up is small. Second, the horizontal component of the relative plate movement is extensional; hence the normal stress on the fault plane, and with it the rupture strength, is low. Third, the rock is relatively warm and ductile, so it will not release strain energy suddenly. Taken together, these factors limit the total strain energy that can build up and be suddenly released at a spreading ridge boundary. These factors explain the observed absence of very large earthquakes at spreading ridge boundaries.

By the time the oceanic crust has moved from a spreading ridge to a subduction zone, it has cooled and become much thicker and stronger. Relative movement of the plates is toward each other, so high compressive normal stresses increase the rupture strength on the fault plane. Because subduction zone plate boundaries are inclined, the potential rupture area is large. All of these factors support the potential buildup of very large amounts of strain energy that, when suddenly released, can produce great earthquakes. In fact, the largest recorded earthquakes have been produced by subduction zones.

At transform faults, the rock is generally cool and brittle, but large compressive stresses do not usually develop because the faults are often nearly vertical and movement is typically of a strike-slip nature. Because the depth of transform faulting is limited, the total

amount of strain energy that can be stored is controlled by the length of rupture. Very large earthquakes involving rupture lengths of hundreds of kilometers have been observed on transform faults, but truly “great” earthquakes may not be possible.

2.5.3 Seismic Moment

The concept of elastic rebound theory can be used to develop a useful measure of the size of an earthquake. The *seismic moment* of an earthquake is given by

$$M_0 = \mu A \bar{D} \quad (2.1)$$

where μ is the rupture strength of the material along the fault, A the rupture area, and \bar{D} the average amount of slip. The seismic moment is named for its units of force times length; however, it is more a measure of the work done by the earthquake. As such, the seismic moment correlates well with the energy released during an earthquake. The seismic moment can be estimated from geologic records for historical earthquakes, or obtained from the long-period components of a seismogram (Bullen and Bolt, 1985).

2.6 OTHER SOURCES OF SEISMIC ACTIVITY

The sudden release of strain energy by rupture of the rock at plate boundaries is the primary cause of seismic activity around the world. There are, however, other sources of seismic activity that produce smaller earthquakes that may be important in localized regions.

Earthquakes have been associated with volcanic activity. Shallow volcanic earthquakes may result from sudden shifting or movement of magma. In 1975, a magnitude 7.2 earthquake on the big island of Hawaii produced significant damage and was followed shortly by an eruption of the Kilauea volcano. The 1980 eruption of Mt. St. Helens in southern Washington was actually triggered by a small ($M_s = 5.1$), shallow, volcanic earthquake that triggered a massive landslide on the north slope of the volcano. The unloading of the north slope allowed the main eruption to occur approximately 30 sec later. Volcanic eruptions themselves can release tremendous amounts of energy essentially at the earth’s surface and may produce significant ground motion.

Seismic waves may be produced by underground detonation of chemical explosives or nuclear devices (Bolt, 1975). Many significant developments in seismology during the Cold War years stemmed from the need to monitor nuclear weapons testing activities of other countries. Collapse of mine or cavern roofs, or *mine bursts*, can cause small local earthquakes, as can large landslides. A 1974 landslide involving $1.6 \times 10^9 \text{ m}^3$ ($2.1 \times 10^9 \text{ yd}^3$) of material along the Montaro River in Peru produced seismic waves equivalent to those of a magnitude 4.5 earthquake (Bolt, 1989).

Reservoir-induced earthquakes have been the subject of considerable study and some controversy. Local seismicity increased significantly after the filling of Lake Mead behind Hoover Dam on the Nevada–Arizona border in 1935. When the Koyna Dam (India) reservoir was filled, local shallow earthquakes became common in an area previously thought to have been virtually aseismic. In 1967, five years after filling of the Koyna reservoir had

begun, a magnitude 6.5 earthquake killed 177 persons and injured more than 2000 more. Local seismicity has been observed to increase seasonally with seasonal increases in reservoir level. In 1975, seven years after the filling of Oroville Dam in an area of low historical seismicity in northern California, a swarm of earthquakes culminated in a magnitude 5.7 main shock. After construction of the High Dam, a magnitude 5.6 earthquake occurred in Aswan, Egypt where very little significant seismic activity had been observed in the 3000-year history of the area. In these cases, seismic activity appears to have been triggered by the presence of the reservoir. While the effect of the weight of the impounded water is likely to be negligible at the depths of the induced seismic activity, an increase in porewater pressure that migrates as a “pulse” away from the reservoir after filling may have been sufficient to reduce the strength of the rock to the point where rupture could occur.

2.7 GEOMETRIC NOTATION

To describe the location of an earthquake, it is necessary to use accepted descriptive terminology. Earthquakes result from rupture of the rock along a fault, and even though the rupture may involve thousands of square kilometers of fault plane surface, it must begin somewhere. The point at which rupture begins and the first seismic waves originate is called the *focus*, or *hypocenter*, of the earthquake (Figure 2.25). From the focus, the rupture spreads across the fault at velocities of 2 to 3 km/sec (1.2 to 1.9 miles/sec) (Bolt, 1989). Although fault rupture can extend to the ground surface, the focus is located at some *focal depth* (or *hypocentral depth*) below the ground surface. The point on the ground surface directly above the focus is called the *epicenter*. The distance on the ground surface between an observer or site and the epicenter is known as the *epicentral distance*, and the distance between the observer and the focus is called the *focal distance* or *hypocentral distance*.

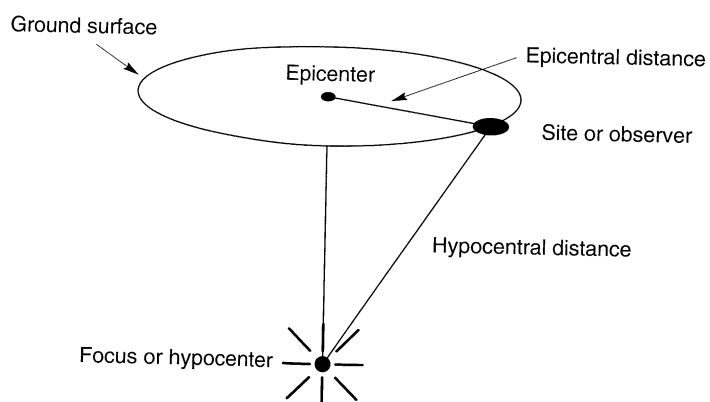


Figure 2.25 Notation for description of earthquake location.

2.8 LOCATION OF EARTHQUAKES

The location of an earthquake is often initially specified in terms of the location of its epicenter. Preliminary epicentral location is a simple and straightforward matter, but refinement of the final location can be considerably more complex. Preliminary location is based on the relative arrival times of p- and s-waves at a set of at least three seismographs.

Since p-waves travel faster than s-waves, they will arrive first at a given seismograph. The difference in arrival times will depend on the difference between the p- and s-wave velocities, and on the distance between the seismograph and the focus of the earthquake, according to

$$d = \frac{\Delta t_{p-s}}{1/v_s - 1/v_p} \quad (2.2)$$

where Δt_{p-s} is the difference in time between the first p- and s-wave arrivals, and v_p and v_s are the p- and s-wave velocities, respectively. In bedrock, p-wave velocities are generally 3 to 8 km/sec (1.9 to 5 miles/sec) and s-wave velocities range from 2 to 5 km/sec (1.2 to 3.1 miles/sec). At any single seismograph it is possible to determine the epicentral distance but not the direction of the epicenter. This limited knowledge is expressed graphically by plotting a circle of radius equal to the epicentral distance. When the epicentral distance from a second seismograph is plotted as a circle about its location, the possible location of the epicenter is narrowed to the two points of intersection of the circles. Obviously, a third seismograph is necessary to identify the most likely location of the epicenter as illustrated in Figure 2.26. More refined estimates of the epicentral, or hypocentral, location are made using multiple seismographs, a three-dimensional seismic velocity model of the earth, and numerical optimization techniques. The accuracy of these techniques depends on the number, quality, and geographic distribution of the seismographs and on the accuracy of the seismic velocity model (Dewey, 1979).

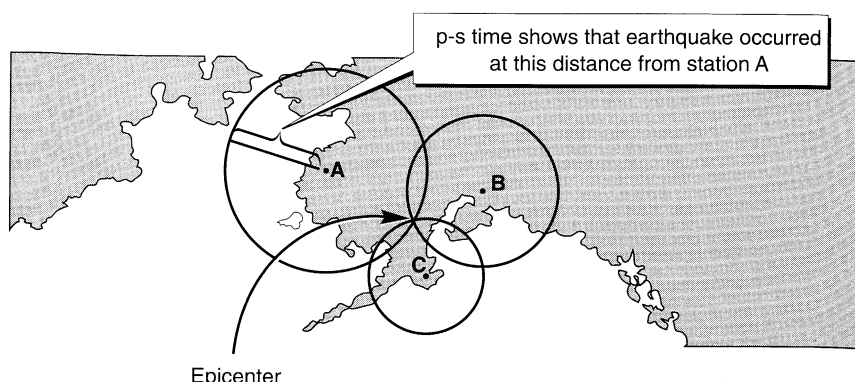


Figure 2.26 Preliminary location of epicenter from differential wave-arrival-time measurements at seismographs A, B, and C. Most likely epicentral location is at the intersection of the three circles. (After Foster, R.J., *General Geology*, 5/e, © 1988. Adapted by permission of Prentice Hall, Upper Saddle River, New Jersey.)

2.9 SIZE OF EARTHQUAKES

The “size” of an earthquake is obviously a very important parameter, and it has been described in different ways. Prior to the development of modern instrumentation, methods for characterizing the size of earthquakes were based on crude and qualitative descriptions of the effects of the earthquakes. More recently, modern seismographs have allowed the development of a number of quantitative measures of earthquake size. Since several of these measures are commonly used in both seismology and earthquake engineering, the distinguishing features of each should be understood.

2.9.1 Earthquake Intensity

The oldest measure of earthquake size is the earthquake *intensity*. The intensity is a qualitative description of the effects of the earthquake at a particular location, as evidenced by observed damage and human reactions at that location. Because qualitative descriptions of the effects of earthquakes are available throughout recorded history, the concept of intensity can be applied to historical accounts to estimate the locations and sizes of earthquakes that occurred prior to the development of modern seismic instruments (*preinstrumental* earthquakes). This application has been very useful in characterizing the rates of recurrence of earthquakes of different sizes in various locations, a critical step in evaluation of the likelihood of seismic hazards. Intensities can also be used to estimate strong ground motion levels (Section 3.3.1.1), for comparison of earthquake effects in different geographic regions, and for earthquake loss estimation.

The Rossi–Forel (RF) scale of intensity, describing intensities with values ranging from I to X, was developed in the 1880s and used for many years. It has largely been replaced in English-speaking countries by the modified Mercalli intensity (MMI) scale originally developed by the Italian seismologist Mercalli and modified in 1931 to better represent conditions in California (Richter, 1958). The MMI scale is illustrated in Table 2-1. The qualitative nature of the MMI scale is apparent from the descriptions of each intensity level.

The Japanese Meteorological Agency (JMA) has its own intensity scale, and the Medvedev–Spoonheuer–Karnik (MSK) scale is used in central and eastern Europe. A comparison of the RF, MMI, JMA, and MSK scales is shown in Figure 2.27.

Earthquake intensities are usually obtained from interviews of observers after the event. The interviews are often done by mail, but in some seismically active areas, permanent observers are organized and trained to produce rational and unemotional accounts of ground shaking. Since human observers and structures are scattered more widely than any seismological observatory could reasonably hope to scatter instruments, intensity observations provide information that helps characterize the distribution of ground shaking in a region. A plot of reported intensities at different locations on a map allows contours of equal intensity, or *isoseisms*, to be plotted. Such a map is called an *isoseismal map* (Figure 2.28). The intensity is generally greatest in the vicinity of the epicenter of the earthquake, and the term *epicentral intensity* is often used as a crude description of earthquake size. Isoseismal maps show how the intensity decreases, or attenuates, with increasing epicentral distance.

Table 2-1 Modified Mercalli Intensity Scale of 1931

I	Not felt except by a very few under especially favorable circumstances
II	Felt by only a few persons at rest, especially on upper floors of buildings; delicately suspended objects may swing
III	Felt quite noticeably indoors, especially on upper floors of buildings, but many people do not recognize it as an earthquake; standing motor cars may rock slightly; vibration like passing of truck; duration estimated
IV	During the day felt indoors by many, outdoors by few; at night some awakened; dishes, windows, doors disturbed; walls make cracking sound; sensation like heavy truck striking building; standing motor cars rocked noticeably
V	Felt by nearly everyone, many awakened; some dishes, windows, etc., broken; a few instances of cracked plaster; unstable objects overturned; disturbances of trees, piles, and other tall objects sometimes noticed; pendulum clocks may stop
VI	Felt by all, many frightened and run outdoors; some heavy furniture moved; a few instances of fallen plaster or damaged chimneys; damage slight
VII	Everybody runs outdoors; damage negligible in buildings of good design and construction, slight to moderate in well-built ordinary structures, considerable in poorly built or badly designed structures; some chimneys broken; noticed by persons driving motor cars
VIII	Damage slight in specially designed structures, considerable in ordinary substantial buildings, with partial collapse, great in poorly built structures; panel walls thrown out of frame structures; fall of chimneys, factory stacks, columns, monuments, walls; heavy furniture overturned; sand and mud ejected in small amounts; changes in well water; persons driving motor cars disturbed
IX	Damage considerable in specially designed structures; well-designed frame structures thrown out of plumb; great in substantial buildings, with partial collapse; buildings shifted off foundations; ground cracked conspicuously; underground pipes broken
X	Some well-built wooden structures destroyed; most masonry and frame structures destroyed with foundations; ground badly cracked; rails bent; landslides considerable from river banks and steep slopes; shifted sand and mud; water splashed over banks
XI	Few, if any (masonry) structures remain standing; bridges destroyed; broad fissures in ground; underground pipelines completely out of service; earth slumps and land slips in soft ground; rails bent greatly
XII	Damage total; practically all works of construction are damaged greatly or destroyed; waves seen on ground surface; lines of sight and level are distorted; objects thrown into the air

2.9.2 Earthquake Magnitude

The possibility of obtaining a more objective, quantitative measure of the size of an earthquake came about with the development of modern instrumentation for measuring ground motion during earthquakes. In the past 60 years, the development of seismic instruments, and our understanding of the quantities they measure, have increased dramatically. Seismic instruments allow an objective, quantitative measurement of earthquake size called *earthquake magnitude* to be made. Most measurements of earthquake magnitude are instrumental (i.e., based on some measured characteristic of ground shaking).

MMI	I	II	III	IV	V	VI	VII	VIII	IX	X	XI	XII
RF	I	II	III	IV	V	VI	VII	VIII	IX	X		
JMA	I			II			III			IV		
MSK	I	II	III	IV	V	VI	VII	VIII	IX	X	XI	XII

Figure 2.27 Comparison of intensity values from modified Mercalli (MMI), Rossi–Forel (RF), Japanese Meteorological Agency (JMA), and Medvedev–Spoonheuer–Karnik (MSK) scales. (After Richter (1958) and Murphy and O’Brien (1977).)

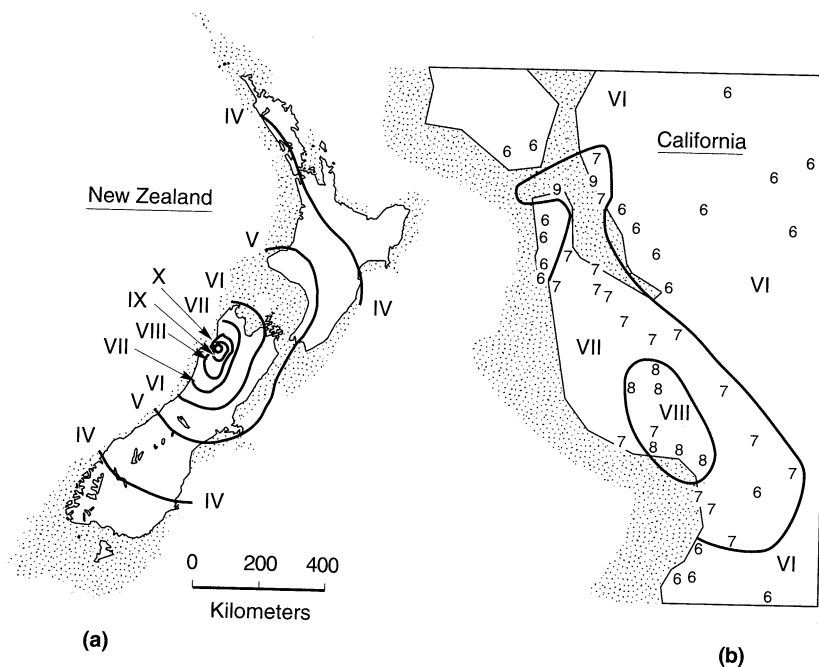


Figure 2.28 Isoseismal maps from (a) the 1968 Inangahua earthquake in New Zealand (After Eiby, 1980) and (b) the 1989 Loma Prieta earthquake in northern California (Modified Mercalli intensities). (After Housner, 1990.)

2.9.2.1 Richter Local Magnitude

In 1935, Charles Richter used a Wood–Anderson seismometer to define a *magnitude* scale for shallow, local (epicentral distances less than about 600 km (375 miles)) earthquakes in southern California (Richter, 1935). Richter defined what is now known as the *local magnitude* as the logarithm (base 10) of the maximum trace amplitude (in micrometers) recorded on a Wood–Anderson seismometer located 100 km (62 miles) from the epicenter of the earthquake. The Richter local magnitude (M_L) is the best known magnitude scale, but it is not always the most appropriate scale for description of earthquake size.

2.9.2.2 Surface Wave Magnitude

The Richter local magnitude does not distinguish between different types of waves. Other magnitude scales that base the magnitude on the amplitude of a particular wave have been developed. At large epicentral distances, body waves have usually been attenuated and scattered sufficiently that the resulting motion is dominated by surface waves. The *surface wave magnitude* (Gutenberg and Richter, 1936) is a worldwide magnitude scale based on the amplitude of Rayleigh waves with a period of about 20 sec. The surface wave magnitude is obtained from

$$M_s = \log A + 1.66 \log \Delta + 2.0 \quad (2.3)$$

where A is the maximum ground displacement in micrometers and Δ is the epicentral distance of the seismometer measured in degrees (360° corresponding to the circumference of the earth). Note that the surface wave magnitude is based on the maximum ground displacement amplitude (rather than the maximum trace amplitude of a particular seismograph); therefore, it can be determined from any type of seismograph. The surface wave magnitude is most commonly used to describe the size of shallow (less than about 70 km (44 miles) focal depth), distant (farther than about 1000 km (622 miles)) moderate to large earthquakes.

2.9.2.3 Body Wave Magnitude

For deep-focus earthquakes, surface waves are often too small to permit reliable evaluation of the surface wave magnitude. The *body wave magnitude* (Gutenberg, 1945) is a worldwide magnitude scale based on the amplitude of the first few cycles of p-waves which are not strongly influenced by the focal depth (Bolt, 1989). The body wave magnitude can be expressed as

$$m_b = \log A - \log T + 0.01 \Delta + 5.9 \quad (2.4)$$

where A is the p-wave amplitude in micrometers and T is the period of the p-wave (usually about one sec). Body wave magnitude can also be estimated from the amplitude of one-second-period, higher-mode Rayleigh waves (Nuttli, 1973); the resulting magnitude, m_{bLg} , is commonly used to describe intraplate earthquakes.

2.9.2.4 Other Instrumental Magnitude Scales

Magnitude scales using different parts of the instrumental record have also been proposed. The *coda* of an earthquake motion are the backscattered waves (Aki, 1969) that follow passage of the primary (unreflected) body and surface waves. Aki (1969), showing that certain characteristics of the coda are independent of the travel path, developed a *coda magnitude*, M_c , that could be obtained from those characteristics. The *duration magnitude*,

M_D , which is based on the total duration of the earthquake, can be used to describe small earthquakes that are often of more interest to seismologists than engineers (Real and Teng, 1973). The Japanese Meteorological Agency uses long-period waves to determine a local magnitude scale, M_{JMA} , for Japanese earthquakes.

2.9.2.5 Moment Magnitude

It is important to realize that the previously described magnitude scales are empirical quantities based on various instrumental measurements of ground-shaking characteristics. As the total amount of energy released during an earthquake increases, however, the ground-shaking characteristics do not necessarily increase at the same rate. For strong earthquakes, the measured ground-shaking characteristics become less sensitive to the size of the earthquake than for smaller earthquakes. This phenomenon is referred to as *saturation*; the body wave and Richter local magnitudes saturate at magnitudes of 6 to 7 and the surface wave magnitude saturates at about $M_s = 8$. To describe the size of very large earthquakes, a magnitude scale that does not depend on ground-shaking levels, and consequently does not saturate, would be desirable. The only magnitude scale that is not subject to saturation is the *moment magnitude* (Kanamori, 1977; Hanks and Kanamori, 1979) since it is based on the seismic moment, which is a direct measure of the factors that produce rupture along the fault. The moment magnitude is given by

$$M_w = \frac{\log M_0}{1.5} - 10.7 \quad (2.5)$$

where M_0 is the seismic moment (Section 2.5.3) in dyne-cm.

The relationship between the various magnitude scales can be seen in Figure 2.29. Saturation of the instrumental scales is indicated by their flattening at higher magnitude

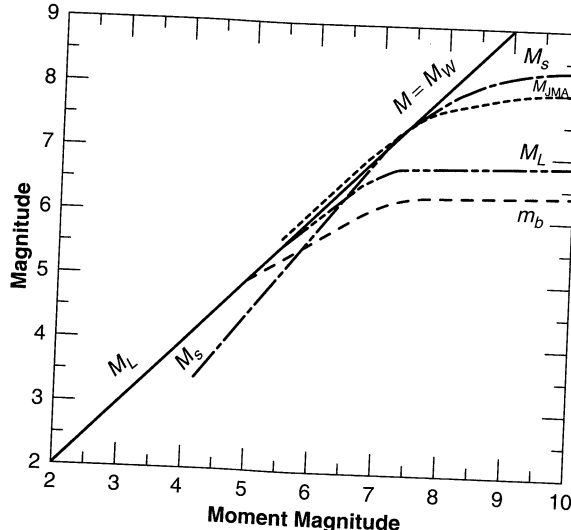


Figure 2.29 Saturation of various magnitude scales: M_w (moment magnitude), M_L (Richter local magnitude), M_s (surface wave magnitude), m_b (short-period body wave magnitude), M_B (long-period body wave magnitude), and M_{JMA} (Japanese Meteorological Agency magnitude). (After Idriss, 1985.)

values. As an example of the effects of magnitude saturation, both the 1906 San Francisco and 1960 Chile earthquakes produced ground shaking that led to surface wave magnitudes of 8.3, even though the sizes of their rupture surfaces, illustrated by the shaded areas in Figure 2.30, were vastly different. The great disparity in energy release was, however, reflected in the moment magnitudes of the earthquakes: 7.9 for San Francisco and 9.5 for Chile.

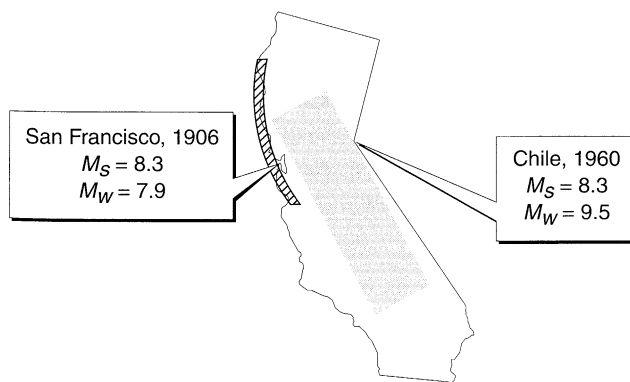


Figure 2.30 Comparison of relative areas of fault rupture (shaded) and magnitudes for 1906 San Francisco and 1960 Chile earthquakes. Although the shaking of both earthquakes produced surface wave magnitudes of 8.3, the amounts of energy released were very different, as reflected in their moment magnitudes. (After Boore, 1977. The motion of the ground during earthquakes, Scientific American, Vol. 237, No. 6, used with permission.)

Bolt (1989) suggests that M_L or m_b be used for shallow earthquakes of magnitude 3 to 7, M_s for magnitudes 5 to 7.5, and M_w for magnitudes greater than 7.5.

2.9.3 Earthquake Energy

The total seismic energy released during an earthquake is often estimated from the relationship (Gutenberg and Richter, 1956)

$$\log E = 11.8 + 1.5M_s \quad (2.6)$$

where E is expressed in ergs. This relationship was later shown (Kanamori, 1983) to be applicable to moment magnitude as well. It implies that a unit change in magnitude corresponds to a $10^{1.5}$ or 32-fold increase in seismic energy. A magnitude 5 earthquake therefore would release only about 0.001 times the energy of a magnitude 7 earthquake, thereby illustrating the ineffectiveness of small earthquakes in relieving the buildup of strain energy that causes very large earthquakes. Combining equations (2.5) and (2.6) (using M_w) shows that the amount of energy released during an earthquake is proportional to the seismic moment.

The amount of energy released by earthquakes is often difficult to comprehend; although a single erg is small ($1 \text{ erg} = 7.5 \times 10^{-8} \text{ ft-lb}$), the energy released in an atomic bomb of the size used at Hiroshima (20,000-ton TNT equivalent) would correspond to a magnitude 6.0 earthquake. On that basis, the 1960 Chile earthquake ($M_w = 9.5$) released as much energy as 178,000 such atomic bombs (Figure 2.31).

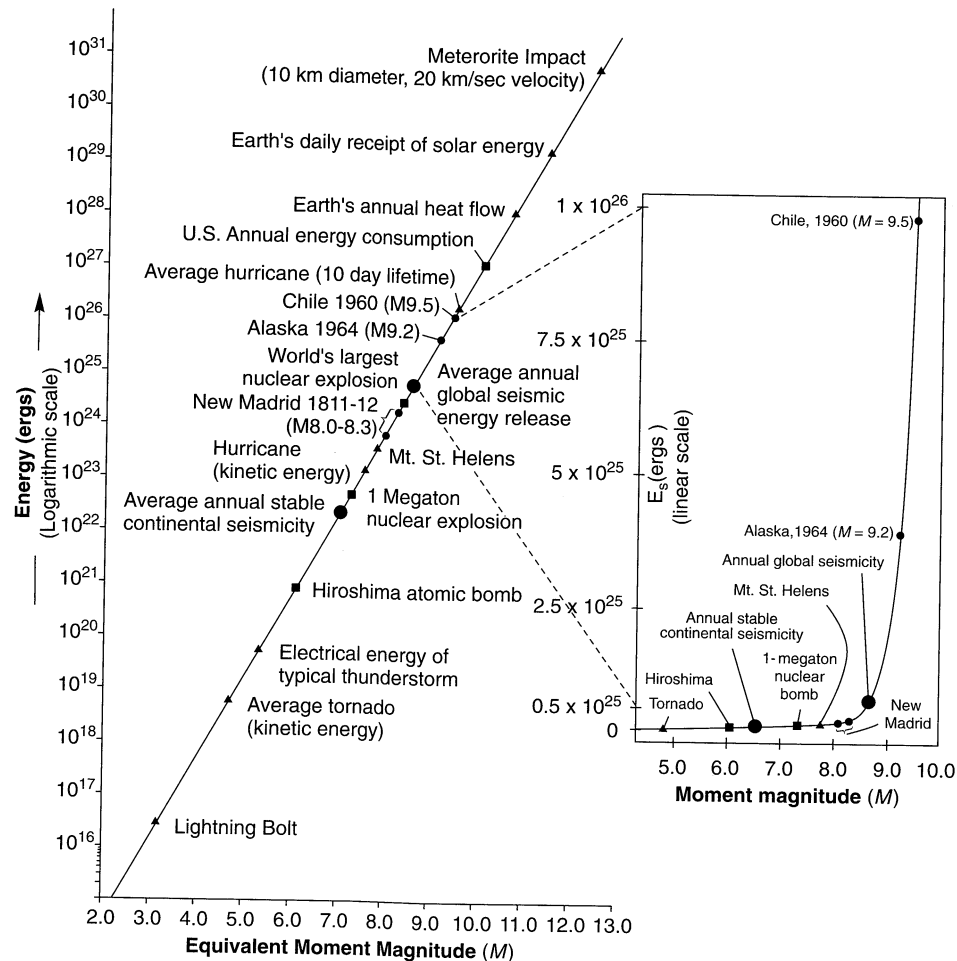


Figure 2.31 Relative energy of various natural and human-made phenomena. (After Johnston, 1990. Reprinted by permission of USGS.)

2.10 SUMMARY

1. The earth has a layered structure—the surficial crust is underlain in turn by the mantle, the outer core, and the inner core. The temperature of each layer increases with depth. The temperature gradient in the mantle causes the semimolten rock to move slowly by convection.
2. The crust is broken into a number of large plates and smaller platelets. Shear stresses on the bottoms of the plates, caused by lateral movement of the convecting mantle, and gravitational forces cause the plates to move with respect to each other.
3. Relative movement of the plates causes stresses to build up on their boundaries. As movement occurs, strain energy accumulates in the vicinity of the boundaries. This

energy is eventually dissipated: either smoothly and continuously or in a stick-slip manner that produces earthquakes. The size of an earthquake depends on the amount of energy released.

4. There are three different types of plate boundaries and their characteristics influence the amount of strain energy that can build up near them. As a result, the different types of boundaries have different earthquake capabilities: subduction zone boundaries can produce the largest earthquakes, followed by transform fault boundaries and then spreading ridge boundaries.
5. The surfaces on which relative movements occur are called faults. At a particular location, a fault is assumed to be planar with an orientation described by its strike and dip. Fault movement is divided into dip-slip components (normal and reverse faulting) and strike-slip components (left lateral and right lateral faulting).
6. The energy-releasing function of earthquakes suggests that a period of time for strain energy accumulation should be expected between large earthquakes at the same location. It also suggests that earthquakes should be most likely to occur along portions of a fault for which little seismic activity has been observed—unless the plate movement has occurred aseismically.
7. Earthquake intensity is a qualitative measure of the effects of an earthquake at a particular location. It is related to the size of the earthquake but is also influenced by other factors. Isoseismal maps can be used to describe the spatial variation of intensity for a given earthquake. Because no instrumental measurements are required, historical accounts can be used to estimate intensity values for preinstrumental earthquakes.
8. Earthquake magnitude is a quantitative measure of the size of an earthquake. Most magnitude scales are based on measured ground motion characteristics. The local magnitude is based on the trace amplitude of a particular seismometer, the surface wave magnitude on the amplitude of Rayleigh waves, and the body wave magnitude on the amplitude of p-waves. Because these amplitudes tend to reach limiting values, these magnitude scales may not accurately reflect the size of very large earthquakes. The moment magnitude, which is not obtained from ground motion characteristics, is able to describe the size of any earthquake.
9. Earthquake magnitude scales are logarithmic, hence a unit change in magnitude corresponds to a 10-fold change in the magnitude parameter (ground motion characteristic or seismic moment). The energy released by an earthquake is related to magnitude in such a way that a unit change in magnitude corresponds to a 32-fold change in energy.

HOMEWORK PROBLEMS

- 2.1 Convection caused by thermal gradients in the upper mantle is thought to be a primary cause of continental drift. Estimate the average thermal gradient in the upper mantle.
- 2.2 The coefficient of thermal expansion of the upper mantle is about $2.5 \times 10^{-5}/^{\circ}\text{K}$. Estimate the ratio of the density at the top of the upper mantle to that at the bottom on the upper mantle.

- 2.3** Using the data from Figure 2.21, determine whether the San Andreas and Calaveras faults are undergoing right lateral or left lateral strike slip faulting.
- 2.4** Using the data from Figure 2.21, estimate the average rate of relative movement along the San Andreas and Calaveras faults during the period from 1959 to 1970.
- 2.5** Assuming p- and s-waves traveled through the crust at 6 km/sec and 3 km/sec, respectively, estimate the epicentral location (latitude and longitude) of the hypothetical earthquake whose characteristics are given below:

Seismograph			
Latitude	Longitude	p-wave arrival time	s-wave arrival time
37°22'30"	121°52'30"	06:11:18.93	06:11:26.90
37°45'00"	122°20'00"	06:11:14.84	06:11:18.71
37°52'33"	121°43'38"	06:11:17.26	06:11:23.53

- 2.6** Using a map of California, determine which fault the hypothetical earthquake of Problem 2.5 would most likely have occurred on?
- 2.7** An earthquake causes an average of 2.5 m strike-slip displacement over an 80 km long, 23 km deep portion of a transform fault. Assuming that the rock along the fault had an average rupture strength of 175 kPa, estimate the seismic moment and moment magnitude of the earthquake.

3

Strong Ground Motion

3.1 INTRODUCTION

The earth is far from quiet—it vibrates almost continuously at periods ranging from milliseconds to days and amplitudes ranging from nanometers to meters. The great majority of these vibrations are so weak that they cannot be felt or even detected without specialized measurement equipment. Such *microseismic activity* is of greater importance to seismologists than engineers. Earthquake engineers are interested primarily in *strong ground motion* (i.e., motion of sufficient strength to affect people and their environment). Evaluation of the effects of earthquakes at a particular site requires objective, quantitative ways of describing strong ground motion.

The ground motions produced by earthquakes can be quite complicated. At a given point, they can be completely described by three components of translation and three components of rotation. In practice, the rotational components are usually neglected; three orthogonal components of translational motion are most commonly measured. Typical ground motion records, such as the acceleration-time histories shown in Figure 3.1, contain a tremendous amount of information. To express all of this information precisely (i.e., to reproduce each of the three time histories exactly), every twist and turn in each plot must be described. The motions shown in Figure 3.1, for example, were determined from 2000 acceleration values measured at time increments of 0.02 sec. This large amount of information makes precise description of a ground motion rather cumbersome.

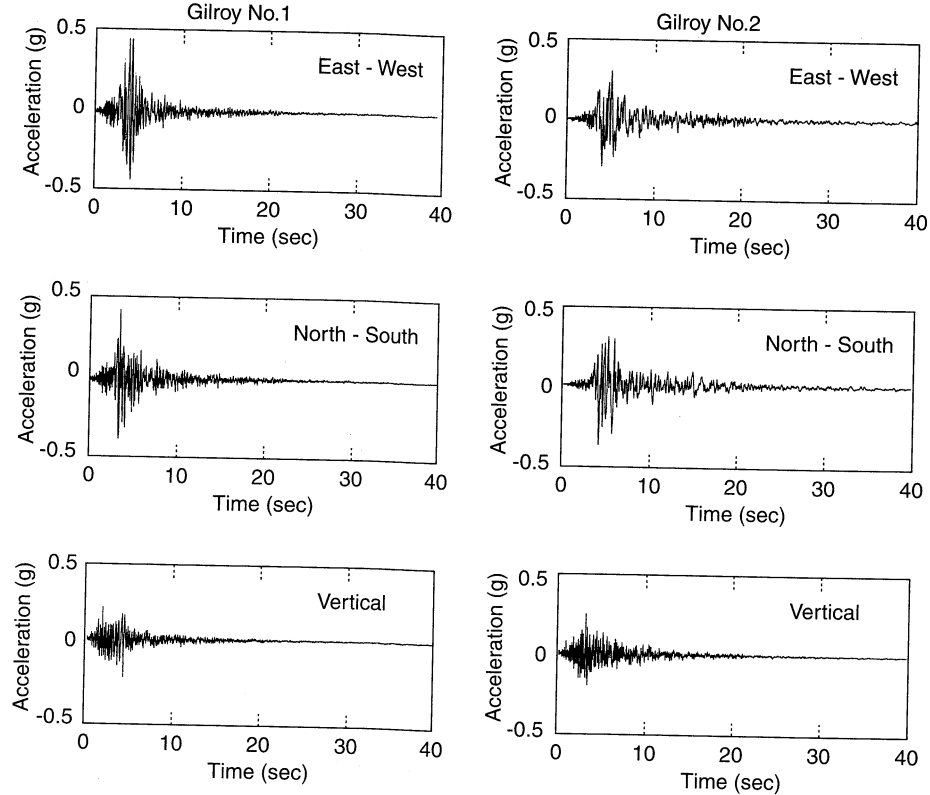


Figure 3.1 Acceleration time histories recorded at two sites in Gilroy, California during the 1989 Loma Prieta earthquake. The Gilroy No. 1 instrument was located on an outcrop of Franciscan sandstone, while the Gilroy No. 2 instrument was underlain by 165 m (540 ft) of stiff, alluvial soils. The Gilroy No. 1 (rock) and Gilroy No. 2 (soil) sites were located at epicentral distances of 21.8 km (13.5 miles) and 22.8 km (14.2 miles), respectively.

Fortunately, it is not necessary to reproduce each time history exactly to describe the ground motion adequately for engineering purposes. It is necessary, however, to be able to describe the characteristics of the ground motion that are of engineering significance and to identify a number of *ground motion parameters* that reflect those characteristics. For engineering purposes, three characteristics of earthquake motion are of primary significance: (1) the *amplitude*, (2) *frequency content*, and (3) *duration* of the motion. A number of different ground motion parameters have been proposed, each of which provides information about one or more of these characteristics. In practice, it is usually necessary to use more than one of these parameters to characterize a particular ground motion adequately.

This chapter describes the instruments and techniques used to measure strong ground motion, and the procedures by which measured motions are corrected. It then presents a variety of parameters that can be used to characterize the amplitude, frequency content, and duration of strong ground motions. Relationships that can be used to predict these parameters are also presented. The chapter concludes with a brief description of the spatial variability of

ground motions. Before proceeding further, the reader should review the topics discussed in Appendices A and B—familiarity with the concepts presented in those appendices is assumed in this chapter and the remainder of the book.

3.2 STRONG-MOTION MEASUREMENT

The identification and evaluation of ground motion parameters requires access to measurements of strong ground motions in actual earthquakes. Accurate, quantitative measurement of strong ground motion is critical for both seismological and earthquake engineering applications. As stated by the National Research Council Committee on Earthquake Engineering Research (Housner, 1982): “The recording of strong ground motion provides the basic data for earthquake engineering. Without a knowledge of the ground shaking generated by earthquakes, it is not possible to assess hazards rationally or to develop appropriate methods of seismic design.”

3.2.1 Seismographs

Although written descriptions of earthquakes date back as far as 780 B.C., the first accurate measurements of destructive ground motions were made during the 1933 Long Beach, California earthquake (Hudson, 1984). Measurement of ground motion has advanced considerably since then, most rapidly in the past 20 years or so.

Various instruments are available for ground motion measurement. *Seismographs* are used to measure relatively weak ground motion; the records they produce are called *seismograms*. Strong ground motions are usually measured by *accelerographs* and expressed in the form of *accelerograms*. The simplest type of seismograph can be illustrated by a mass–spring–damper single-degree-of-freedom (SDOF) system, as shown in Figure 3.2. A rotating drum is connected to the seismograph housing with a stylus attached to a mass. The mass is connected to the housing by a spring and dashpot arranged in parallel, and the housing is connected to the ground. Since the spring and dashpot are not rigid, the motion of the mass will not be identical to the motion of the ground during an earthquake. The relative movement of the mass and the ground will be indicated by the *trace* made by the stylus on

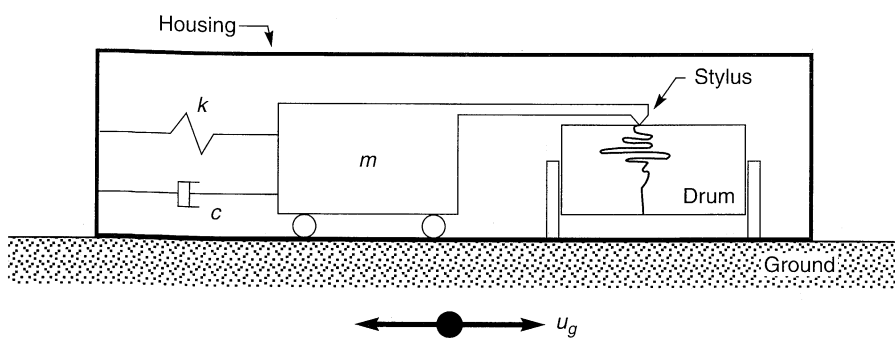


Figure 3.2 Simple mass–spring–dashpot type of seismograph. The housing is firmly connected to the ground. When the ground shakes, the stylus marks a trace on the rotating drum that shows the relative displacement between the mass and the ground. Most modern instruments are more complicated than the one shown here.

the rotating drum. A typical seismograph station may have three seismographs oriented to record motion in the vertical and two perpendicular horizontal directions.

Seismographs can be designed to measure various ground motion characteristics. To understand how this can be done it is necessary to consider the dynamic response of a simple seismograph such as the one shown in Figure 3.2. This seismograph is a SDOF oscillator whose response to shaking is given by the equation of motion (Appendix B)

$$m\ddot{u} + c\dot{u} + ku = -m\ddot{u}_g \quad (3.1)$$

where u is the seismograph trace displacement (the relative displacement between the seismograph and the ground) and u_g is the ground displacement.

If the ground displacement is simple harmonic at a circular frequency ω_g , the displacement response ratio (the ratio of trace displacement amplitude to ground displacement amplitude) will be

$$\frac{|u|}{|u_g|} = \frac{\beta^2}{\sqrt{(1-\beta^2)^2 + (2\xi\beta)^2}} \quad (3.2)$$

where $\beta (= \omega_g/\omega_0)$ is the *tuning ratio*, $\omega_0 (= \sqrt{k/m})$ is the *undamped natural circular frequency*, and $\xi (= c/2\sqrt{km})$ is the *damping ratio*. Figure 3.3a shows how the displacement response ratio varies with frequency and damping. For ground motion frequencies well above the natural frequency of the seismograph (i.e., large values of β), the trace amplitude is equal to the ground motion amplitude. The lowest frequency for which this equality holds (within a given range of accuracy) depends on the damping ratio. Because the frequency response is flat and phase angles are preserved at damping ratios of 60%, SDOF displacement seismographs are usually designed with damping ratios in that range (Richart et al., 1970).

Similarly, the acceleration response ratio (the ratio of trace displacement amplitude to ground acceleration amplitude) is given by

$$\frac{|u|}{|\ddot{u}_g|} = \frac{1}{\omega_0^2 \sqrt{(1-\beta^2)^2 + (2\xi\beta)^2}} \quad (3.3)$$

The variation of acceleration response ratio with frequency and damping is shown in Figure 3.3b. The trace amplitude is proportional to the ground acceleration amplitude for frequencies well below the natural frequency of the seismograph (i.e., low values of β). A seismograph with 60% damping will accurately measure accelerations at frequencies up to about 55% of its natural frequency. Most seismographs of this type have natural frequencies of about 25 Hz with damping ratios near 60%, with desirable flat response (constant acceleration response ratio) at frequencies up to about 13 Hz.

The preceding paragraphs show how the same physical system can act as both a displacement seismograph and an accelerograph. It measures displacements at frequencies well above and accelerations at frequencies well below its natural frequency. The Wood-Anderson seismograph, used by Richter to develop the first earthquake magnitude scale, used a small mass suspended eccentrically on a thin tungsten torsion wire. A mirror attached to the wire allowed optical recording with a ground motion magnification of about 3000. Damping was provided electromagnetically at 80% of critical; the damped natural period was about 0.8 sec.

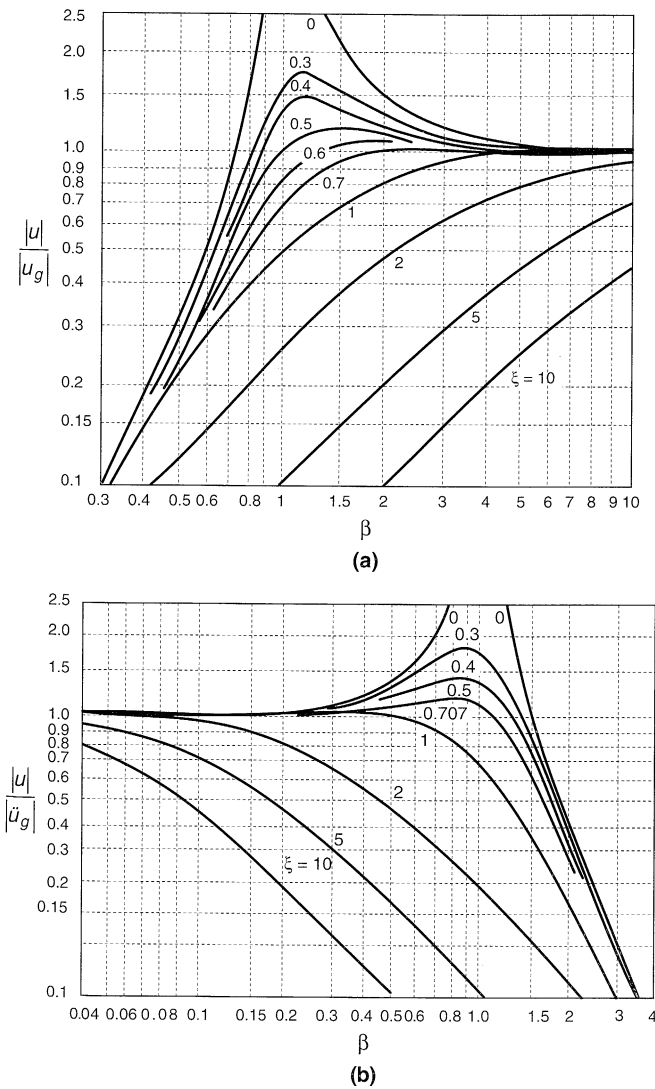


Figure 3.3 (a) Displacement response ratio and (b) acceleration response ratio ($\omega_0 = 1$ rad/sec) for SDOF system subjected to simple harmonic base motion.

In most modern seismographs, an electronic transducer often referred to as a *seismometer* senses the motion and produces an analog (continuous) electrical signal that is recorded for subsequent processing. Most accelerographs currently in use are *accelerometers*, electronic transducers that produce an output voltage proportional to acceleration. A number of different types of accelerometers are available. *Servo* (or *force balance*) accelerometers use a suspended mass to which a displacement transducer is attached. When the housing is accelerated, the signal produced by the relative displacement between the

housing and mass is used to generate a restoring force that pushes the mass back toward its equilibrium position. The restoring force is proportional to the acceleration and can be measured electronically. Servo accelerometers can provide very good accuracy over the range of frequencies of greatest interest in earthquake engineering. *Piezoelectric accelerometers* use a mass attached to a piezoelectric material (usually quartz, tourmaline, or a ferroelectric ceramic) to sense accelerations. The piezoelectric material acts as the spring in the diagram of Figure 3.2; damping is generally negligible. When accelerated, the inertial force of the mass strains the piezoelectric material, which develops an electrical charge on its surfaces. The resulting voltage is (if the dielectric constant does not vary with charge) proportional to acceleration. Because piezoelectric materials are quite stiff, their natural frequencies are very high, so they are particularly useful for high-frequency measurements. Their response at low frequencies, however, can be strongly influenced by signal conditioning system characteristics. Triaxial accelerometers, in which three orthogonal components of acceleration are measured with a common time base, are commonly used. From the three components, the acceleration in any direction can be computed. Some seismographs use velocity transducers, or *geophones*, in addition or as an alternative to accelerometers.

Seismographs, accelerographs, and ancillary equipment are protected by an instrument shelter (Figure 3.4). An important component of a seismograph or accelerograph is an accurate clock, particularly when more than one component of motion is measured or when the ground motion at one location is being compared with that at another. Most modern instruments maintain time accuracy by synchronizing on a daily basis with radio time signals transmitted by a standard time service or by recording such signals along with the ground-motion data. Universal Coordinated Time (the scientific equivalent of Greenwich Mean Time) is used as a common worldwide time basis.

A *seismoscope* (Hudson, 1958) is a relatively inexpensive ground motion instrument. Seismoscopes are conical pendulums (Figure 3.5a) in which a metal stylus attached to a suspended mass inscribes a record of ground motion on a smoked glass plate, producing a two-dimensional record of the type shown in Figure 3.5b. Scott (1972) found that small oscillations of the trace were related to the instrument rather than the earthquake and that they could be used to provide a time scale to the seismoscope trace. The time scale allows accelerograms to be computed from the seismoscope trace.

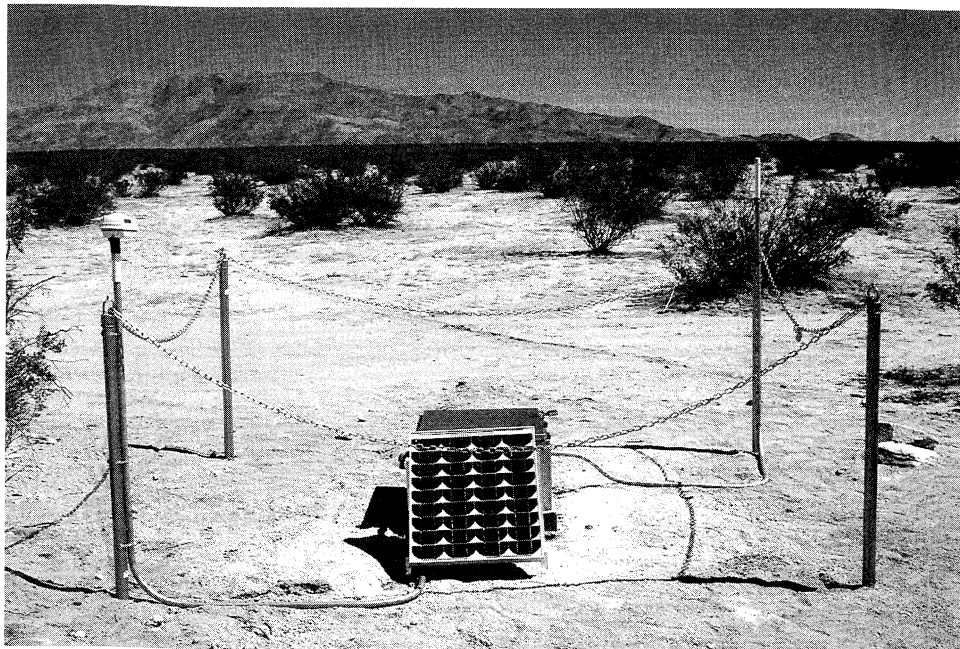
3.2.2 Data Acquisition and Digitization

Early ground motion instruments transformed the motion of the ground to the motion of a physical mechanism. The mechanism, perhaps in the form of a pen or stylus or reflective mirror, caused the motion to be recorded in analog form on paper or photographic film attached to a rotating drum. Later-generation instruments recorded motions electronically in analog form on magnetic tape. Rather than record continuously, instruments of these types lay dormant until triggered by the exceedance of a small threshold acceleration at the beginning of the earthquake motion. As a result, any vibrations that may have preceded triggering were not recorded, thereby introducing a *baseline error* into the acceleration record.

To use the recorded ground motions for engineering computations, the analog ground motion records must be digitized. Originally, digitization was performed manually with paper, pencil, and an engineering scale. Semiautomatic digitizers, with which a user moved a lens with crosshairs across an accelerogram mounted on a digitizing table, were commonly used in the late



(a)



(b)

Figure 3.4 (a) Modern digital strong motion instrument (solar-powered, 16-bit resolution, 250 samples/sec, GPS timing, and cellular modem) mounted in cast-in-place reinforced concrete vault, and (b) completed installation with insulated cover and solar panel (courtesy of Terra Technology Corp, Redmond, Washington).

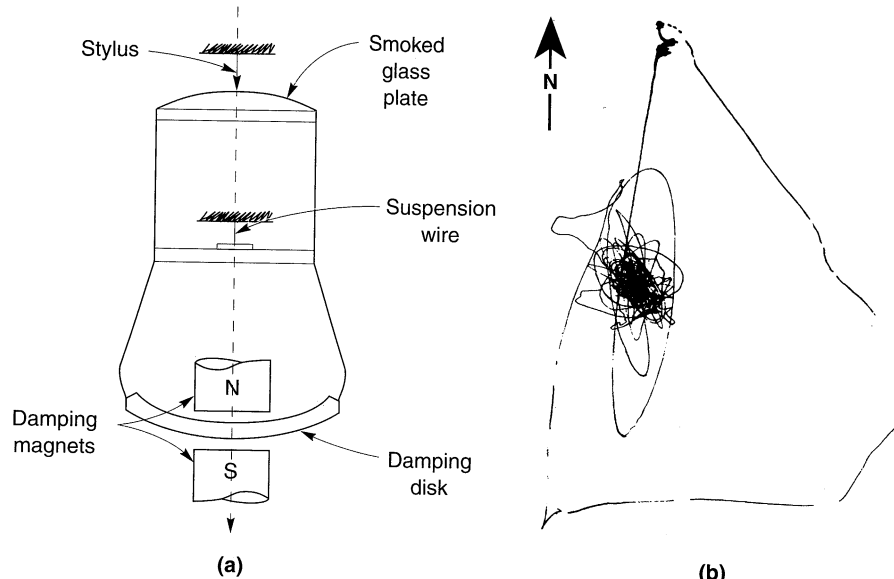


Figure 3.5 (a) Typical Wilmot-type seismoscope in which a fixed stylus scribes a record of relative motion on a smoked glass plate mounted on the suspended seismoscope; (b) typical seismoscope record. (After Newmark and Rosenblueth, 1971.)

1970s. By pressing a foot-operated switch, the coordinates of the crosshairs were recorded. These forms of digitizing involved exacting and tiring work; operator accuracy and fatigue were important considerations (Hudson, 1979). Fully automatic computer-based digitization, typically at sampling rates of 200 or more samples per second, is now commonplace.

In recent years, *digital seismographs* have become much more commonly used. Although they use analog transducers, digital instruments convert the analog signal to digital form in the field. They record ground motions continuously at rates of 200 to 1000 samples/sec with 12- to 16-bit resolution, saving the recorded data only if a triggering acceleration is exceeded. Their on-board memories can typically save 4 to 6 Mb worth of data, from before an earthquake begins until after it ends, thereby preserving the initial portion of the record that is lost with triggered analog systems. Because digital systems are more complex, more expensive, and more difficult to maintain in the field, they have not yet replaced analog systems.

3.2.3 Strong-Motion Processing

The raw data obtained from a strong-motion instrument may include errors from several possible sources, each of which must be carefully evaluated and corrected to produce an accurate record of the actual ground motion. Raw data often include background noise from different sources. Microseisms from ocean waves can be detected by sensitive instruments. Other noise may be caused by traffic, construction activity, wind (transmitted to the ground by vibration of trees, buildings, etc.), and even atmospheric pressure changes. Obviously, this range of sources can produce nonseismic noise at both low and high frequencies. To isolate the motion actually produced by the earthquake, background noise must be removed or at least suppressed.

All accelerographs have their own dynamic response characteristics, or *instrument response*, that can influence the motions they measure. Consequently, instrument response must be corrected for in strong-motion processing. Instrument response corrections are usually performed by modeling the instrument itself as a SDOF system and using the SDOF model to decouple the response of the instrument from the actual ground motion. For most modern accelerographs with flat frequency response up to about 12 to 13 Hz, the instrument correction is only important for frequencies above the usual range of engineering interest. However, some accelerographs are located in buildings (usually on the ground floor or in the basement) or near the abutments of dams or bridges. The motions they record can be affected at frequencies of interest by the response of the structure in or near which they are located. Even the motions recorded by strong motion instruments located in the *free field* (away from the influence of large structures) may be influenced by the response of their instrument shelter (Bycroft, 1978; Crouse et al., 1984), although these effects are usually important only at relatively high frequencies (Crouse and Hushmand, 1989) for typical instrument shelters.

Another correction is required to reduce the effects of errors in ground motion measurement, such as those associated with the triggering of analog seismographs. If a seismograph does not start until some triggering level of motion is reached, the entire accelerogram is in error by the level of motion at the time of triggering. Integration of an uncorrected acceleration time history, for example, will produce a linear error in velocity and a quadratic error in displacement. An acceleration error as small as $0.001g$ at the beginning of a 30-second-long accelerogram would erroneously predict a permanent displacement of 441 cm at the end of the motion. Correction of such errors, termed *baseline correction*, was originally accomplished by subtracting a best-fit parabola from the accelerogram before integrating to velocity and displacement but is now performed using high-pass filters and modern data processing techniques (Joyner and Boore, 1988). The motions shown in Figure 3.1, for example, were bandpass filtered to remove frequencies below 0.08 Hz and frequencies above 23 Hz. Computer software for processing strong-ground-motion records (Converse, 1992) is available from the U.S. Geological Survey (USGS).

3.2.4 Strong-Motion Instrument Arrays

Large earthquakes produce ground motions with different characteristics at different points on the ground surface. The spatial variation of ground motion, whether on worldwide, regional, or local scales, is important in both seismology and earthquake engineering. Arrays and networks of strong motion instruments have proven useful in determining the spatial variation of strong ground motion.

3.2.4.1 Worldwide and Regional Arrays

Understanding of earthquake and tectonic processes improved dramatically with the establishment of the *Worldwide Standard Seismograph Network* (WWSSN) in 1961. The WWSSN was originally developed, in large part, to monitor compliance with nuclear weapons testing bans. Before that time, worldwide seismicity data were obtained from a wide variety of very different types of instruments operated by many different organizations. Differences in instruments and operating procedures made comparison of results difficult. WWSSN stations use standardized instruments; each station has at least two three-component analog seismographs to monitor both short- and long-period motions. The capabilities of the WWSSN instruments, however, are limited by modern standards (Aki and Richards,

1980), and they are being replaced by digital instruments such as those of the *Global Digital Seismometer Network* (GDSN) and the *Global Seismographic Network* (GSN). The Incorporated Research Institutions for Seismology (IRIS), a consortium of U.S. and foreign research institutions, oversees operation of the GSN and a set of portable instruments that can be deployed to monitor aftershocks following large earthquakes.

Regional arrays of seismographs are now operating in most seismically active countries. In the United States, for example, the USGS operates regional arrays in different parts of the country. In the California Strong Motion Instrumentation Program (CSMIP), the California Division of Mines and Geology operates an extensive array of free-field seismographs (Figure 3.6) as well as seismographs in buildings and bridges.

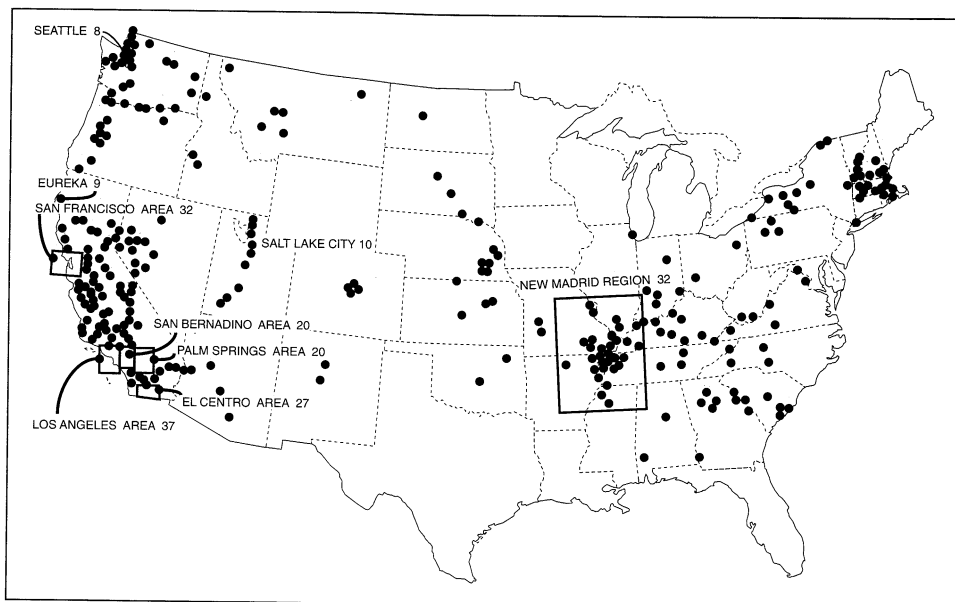


Figure 3.6 Locations of strong motion instruments operated by the U.S. Geological Survey in cooperation with other agencies as of April, 1990. Boxes in northern and southern California indicate areas with high instrument density. (After Joyner and Boore, Geotechnical News, March, 1991, p. 24. Used by permission of BiTech Publishers, Ltd..)

3.2.4.2 Local and Dense Arrays

While widely spaced regional and worldwide arrays are useful for studying earthquake mechanisms and the spatial distribution of many important earthquake parameters, geotechnical earthquake engineering often requires spatial distribution information on a smaller areal scale and below the ground surface. In recent years a number of local and dense arrays, some with downhole instrumentation, have been installed at various locations around the world.

Japan has been very active in the installation of local strong-motion instrument arrays. The three-dimensional dense accelerometer array at Chiba (Katayama and Sato, 1982), for example, includes 44 three-component accelerometers, 15 of which are at the ground surface and the remainder at depths of up to 40 m (130 ft.). In Taiwan, the SMART-1 dense accelerometer array near Lotung (Figure 3.7) consists of a central accelerometer surrounded

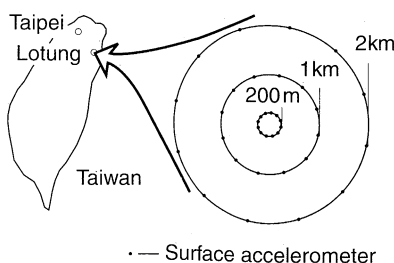


Figure 3.7 Original configuration of SMART-1 array in Lotung, Taiwan.

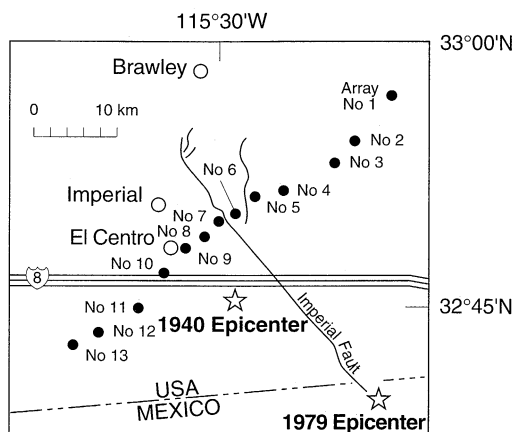


Figure 3.8 The El Centro Array in southern California. The El Centro Differential Array is located near Station 9.

by three rings of 12 accelerometers each at radii of 200 m (650 ft), 1 km (0.6 mi), and 2 km (1.2 mi). A few years after the SMART-1 array was installed, $\frac{1}{4}$ - and $\frac{1}{12}$ -scale models of nuclear containment structures were constructed in its midst (Tang, 1987). The structures were instrumented to record their response during earthquakes, and additional surface and downhole (to depths of 47 m (154 ft)) ground motion instruments were installed adjacent to the $\frac{1}{4}$ -scale model and in the free-field.

In the United States, one of the most important local arrays has been the El Centro Array, a 45-km-long (28 mi) array of 13 stations that crosses the Imperial and Brawley faults in southern California (Figure 3.8). It also contains the El Centro Differential Array, a dense array consisting of six three-component accelerometers along a 305-m (1000 ft) line. Shortly after installation, the arrays recorded the 1979 Imperial Valley earthquake ($M_s = 6.9$), which occurred only 5.6 km away and produced very useful information on near-field ground motions. Near Anza, California, an array of ten three-component stations along a 30-km (19 mi) stretch of the San Jacinto fault was installed to study various earthquake characteristics (Berger et al., 1984). Data are telemetered by digital VHF radio to a nearby mountain peak station and then on to another station in La Jolla, California.

These are but a few of the many strong-motion arrays that have been installed in seismically active countries around the world. The rapid proliferation of local, regional, and worldwide seismograph arrays in recent years has come hand in hand with technological advances in data acquisition, storage, and communication. The ability to acquire and store large quantities of digital seismic data at high speeds, and to retrieve the data from remote locations by telemetry, has and will continue to make such data more plentiful.

3.2.5 Strong-Motion Records

Strong-motion records can now be easily obtained from a number of sources. The U.S. Geological Survey, for example, published a compact disk (Seekins et al., 1992) that contained uncorrected strong motion records from North American earthquakes between 1933 and 1986; more than 4000 records were included. A number of strong-motion databases can be accessed over the Internet, with individual records downloaded by anonymous ftp (file transfer protocol)

procedures. The Gilroy records shown in Figure 3.1 were obtained from the database maintained by the Lamont–Doherty Earth Observatory at Columbia University in conjunction with the National Center for Earthquake Engineering Research at SUNY Buffalo. An example of the information provided with such records is shown in Figure 3.9. A useful World Wide Web site with links to many sources of ground motion and earthquake information is maintained at the University of Washington (<http://www.geophys.washington.edu/seismosurfing.html>). A variety of geotechnical earthquake engineering information can be found at a web site maintained at the University of Southern California (<http://rccg01.usc.edu/eqdata/home.html>).

Figure 3.9 Event, size, and record information preceding the digitized acceleration data for the Gilroy No. 1 (rock) strong-motion record.

3.3 GROUND MOTION PARAMETERS

Ground motion parameters are essential for describing the important characteristics of strong ground motion in compact, quantitative form. Many parameters have been proposed

to characterize the amplitude, frequency content, and duration of strong ground motions; some describe only one of these characteristics, while others may reflect two or three. Because of the complexity of earthquake ground motions, identification of a single parameter that accurately describes all important ground motion characteristics is regarded as impossible (Jennings, 1985; Joyner and Boore, 1988).

3.3.1 Amplitude Parameters

The most common way of describing a ground motion is with a time history. The motion parameter may be acceleration, velocity, or displacement, or all three may be displayed as shown in Figure 3.10. Typically, only one of these quantities is measured directly with the others computed from it by integration and/or differentiation. Note the different predominant frequencies in the acceleration, velocity, and displacement time histories. The acceleration time history shows a significant proportion of relatively high frequencies. Integration produces a smoothing or filtering effect [in the frequency domain, $\tilde{v}(\omega) = \tilde{a}(\omega)/\omega$ and

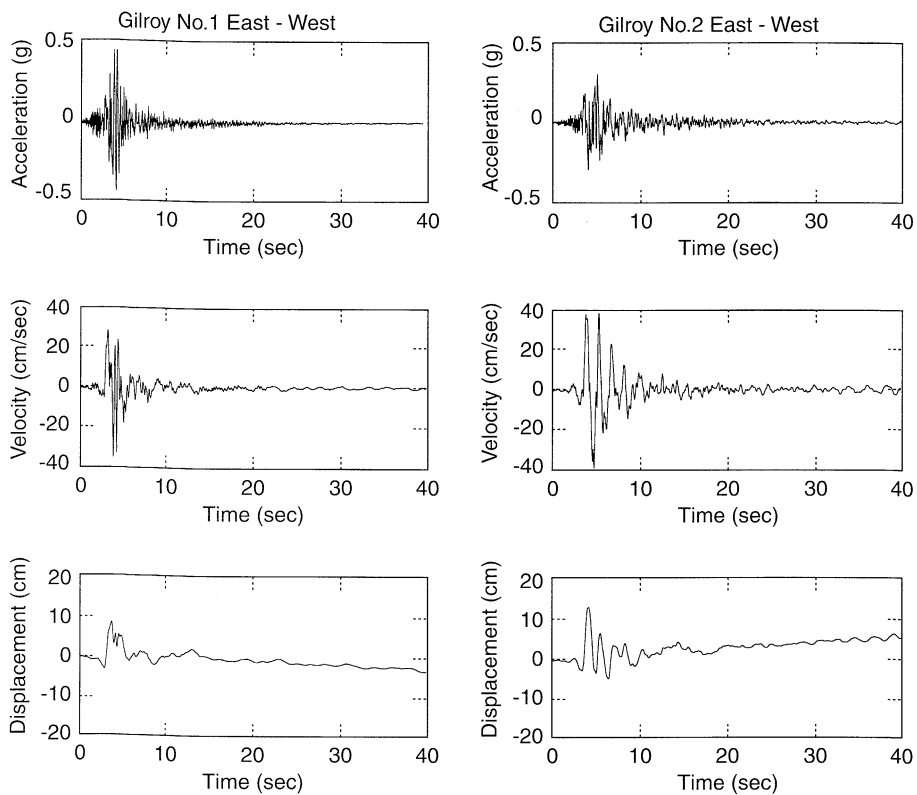


Figure 3.10 Acceleration, velocity, and displacement time histories for the E-W components of the Gilroy No. 1 (rock) and Gilroy No. 2 (soil) strong motion records. The velocities and displacements were obtained by integrating the acceleration records shown in Figure 3.1 using the trapezoidal rule. Note that the Gilroy No. 1 (rock) site experienced higher accelerations, but the Gilroy No. 2 (soil) site experienced higher velocities and displacements.

$\tilde{u}(\omega) = \tilde{v}(\omega)/\omega$, where \tilde{u} , \tilde{v} , and \tilde{a} are the transformed displacement, velocity, and acceleration, respectively]. Therefore, the velocity time history shows substantially less high-frequency motion than the acceleration time history. The displacement time history, obtained by another round of integration, is dominated by relatively low frequency motion.

3.3.1.1 Peak Acceleration

The most commonly used measure of the amplitude of a particular ground motion is the peak horizontal acceleration (PHA). The PHA for a given component of motion is simply the largest (absolute) value of horizontal acceleration obtained from the accelerogram of that component. By taking the vector sum of two orthogonal components, the maximum resultant PHA (the direction of which will usually not coincide with either of the measured components) can be obtained.

Horizontal accelerations have commonly been used to describe ground motions because of their natural relationship to inertial forces; indeed, the largest dynamic forces induced in certain types of structures (i.e., very stiff structures) are closely related to the PHA. The PHA can also be correlated to earthquake intensity (e.g., Trifunac and Brady, 1975a; Murphy and O'Brien, 1977; Krinitzsky and Chang, 1987). Although this correlation is far from precise, it can be very useful for estimation of PHA when only intensity information is available, as in the cases of earthquakes that occurred before strong motion instruments were available (preinstrumental earthquakes). A number of intensity–acceleration relationships have been proposed, several of which are shown in Figure 3.11. The use of intensity–attenuation relationships also allows estimation of the spatial variability of peak acceleration from the isoseismal maps of historical earthquakes.

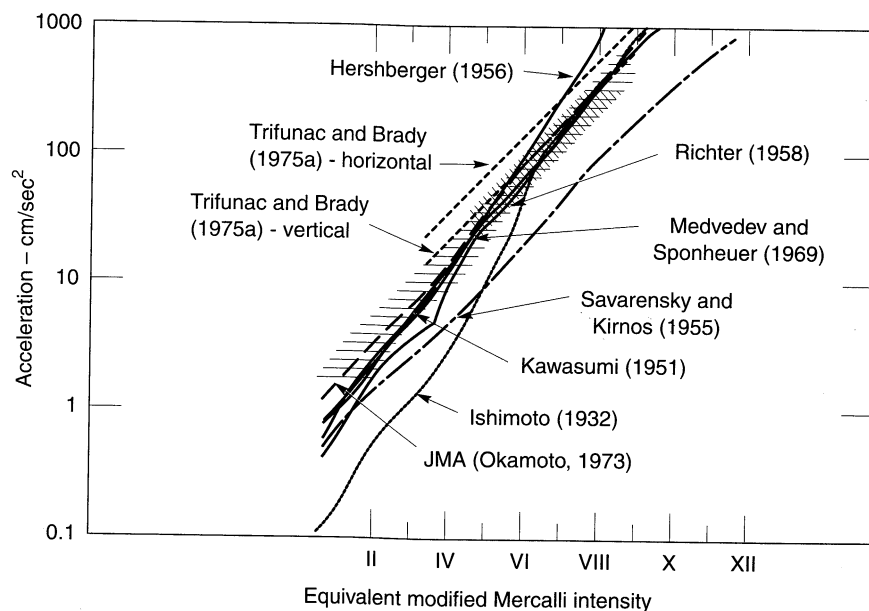


Figure 3.11 Proposed relationships between PHA and MMI. (After Trifunac and Brady, 1975a. Used by permission of the Seismological Society of America.)

Vertical accelerations have received less attention in earthquake engineering than horizontal accelerations, primarily because the margins of safety against gravity-induced static vertical forces in constructed works usually provide adequate resistance to dynamic forces induced by vertical accelerations during earthquakes. For engineering purposes, the peak vertical acceleration (PVA) is often assumed to be two-thirds of the PHA (Newmark and Hall, 1982). The ratio of PVA to PHA, however, has more recently been observed to be quite variable but generally to be greater than two-thirds near the source of moderate to large earthquakes and less than two-thirds at large distances (Campbell, 1985; Abrahamson and Litehiser, 1989). Peak vertical accelerations can be quite large; a PVA of $1.74g$ was measured between the Imperial and Brawley faults in the 1979 Imperial Valley earthquake.

Ground motions with high peak accelerations are usually, but not always, more destructive than motions with lower peak accelerations. Very high peak accelerations that last for only a very short period of time may cause little damage to many types of structures. A number of earthquakes have produced peak accelerations in excess of $0.5g$ but caused no significant damage to structures because the peak accelerations occurred at very high frequencies and the duration of the earthquake was not long. Although peak acceleration is a very useful parameter, it provides no information on the frequency content or duration of the motion; consequently, it must be supplemented by additional information to characterize a ground motion accurately.

3.3.1.2 Peak Velocity

The peak horizontal velocity (PHV) is another useful parameter for characterization of ground motion amplitude. Since the velocity is less sensitive to the higher-frequency components of the ground motion, as illustrated in Figure 3.10, the PHV is more likely than the PHA to characterize ground motion amplitude accurately at intermediate frequencies. For structures or facilities that are sensitive to loading in this intermediate-frequency range (e.g., tall or flexible buildings, bridges, etc.), the PHV may provide a much more accurate indication of the potential for damage than the PHA. PHV has also been correlated to earthquake intensity (e.g., Trifunac and Brady, 1975a; Krinitzsky and Chang, 1987).

3.3.1.3 Peak Displacement

Peak displacements are generally associated with the lower-frequency components of an earthquake motion. They are, however, often difficult to determine accurately (Campbell, 1985; Joyner and Boore, 1988), due to signal processing errors in the filtering and integration of accelerograms and due to long-period noise. As a result, peak displacement is less commonly used as a measure of ground motion than is peak acceleration or peak velocity.

Example 3.1

Determine the peak accelerations, velocities, and displacements for the E-W components of the Gilroy No. 1 (rock) and Gilroy No. 2 (soil) ground motions.

Solution The peak amplitude values can be estimated graphically from Figure 3.9. The actual peak values, based on the data from which Figure 3.9 was plotted, are:

Parameter	Gilroy No. 1 (Rock)	Gilroy No. 2 (Soil)
Peak acceleration	$0.442g$	$0.332g$
Peak velocity (cm/sec)	33.7	39.2
Peak displacement (cm)	8.5	13.3

3.3.1.4 Other Amplitude Parameters

Although the parameters discussed previously are easily determined, they describe only the peak amplitudes of single cycles within the ground motion time history. In some cases, damage may be closely related to the peak amplitude, but in others it may require several repeated cycles of high amplitude to develop. Newmark and Hall (1982) described the concept of an *effective acceleration* as “that acceleration which is most closely related to structural response and to damage potential of an earthquake. It differs from and is less than the peak free-field ground acceleration. It is a function of the size of the loaded area, the frequency content of the excitation, which in turn depends on the closeness to the source of the earthquake, and to the weight, embedment, damping characteristic, and stiffness of the structure and its foundation.”

Some time histories are characterized by single-cycle peak amplitudes that are much greater than the amplitudes of other cycles. An example of such a case is the Stone Canyon record shown in Figure 3.12a. These single cycles often occur at high frequencies and consequently have little effect on structures with lower natural frequencies. In other time histories, such as the Koyna record of Figure 3.12b, a number of peaks of similar amplitude are observed.

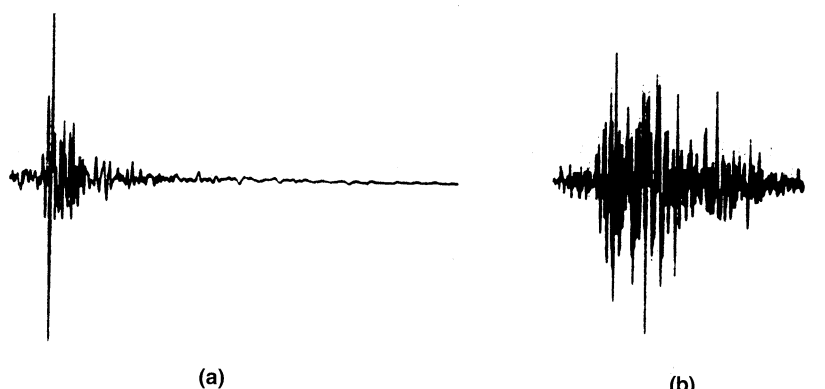


Figure 3.12 Accelerograms from (a) the N29W Melendy Ranch record of the 1972 Stone Canyon ($M = 4.6$) earthquake and (b) the longitudinal record from the 1967 Koyna ($M = 6.5$) earthquake. The time and acceleration scales are identical for both records. Peak accelerations are very close, illustrating the limitations of using peak amplitude as a sole measure of strong ground motion. (After Hudson, 1979; used by permission of EERI.)

Sustained Maximum Acceleration and Velocity. Nuttli (1979) used lower peaks of the accelerogram to characterize strong motion by defining the *sustained maximum acceleration* for three (or five) cycles as the third (or fifth) highest (absolute) value of acceleration in the time history. The *sustained maximum velocity* was defined similarly. Although the PHA values for the 1972 Stone Canyon earthquake and 1967 Koyna earthquake records (Figure 3.12) were nearly the same, a quick visual inspection indicates that their sustained maximum accelerations (three- or five-cycle) were very different. For a structure that required several repeated cycles of strong motion to develop damage, the

Koyna motion would be much more damaging than the Stone Canyon motion, even though they had nearly the same PHA. For these motions, the sustained maximum acceleration would be a better indicator of damage potential than the PHA.

Example 3.2

Determine the three- and five-cycle sustained maximum accelerations and velocities for the E-W components of the Gilroy No. 1 (rock) and Gilroy No. 2 (soil) ground motions.

Solution The sustained maximum acceleration and velocity values can be obtained graphically from Figure 3.10. The actual values, based on the data from which Figure 3.10 was plotted, are:

Parameter	Gilroy No. 1 (Rock)	Gilroy No. 2 (Soil)
Sustained maximum acceleration		
Three-cycle	0.434g	0.312g
Five-cycle	0.418g	0.289g
Sustained maximum velocity (cm/sec)		
Three-cycle	31.6	38.4
Five-cycle	29.9	38.2

Effective Design Acceleration. The notion of an effective design acceleration, with different definitions, has been proposed by at least two researchers. Since pulses of high acceleration at high frequencies induce little response in most structures, Benjamin and Associates (1988) proposed that an *effective design acceleration* be taken as the peak acceleration that remains after filtering out accelerations above 8 to 9 Hz. Kennedy (1980) proposed that the effective design acceleration be 25% greater than the third highest (absolute) peak acceleration obtained from a filtered time history.

3.3.2 Frequency Content Parameters

Only the simplest of analyses (see Section B.5.3 of Appendix B) are required to show that the dynamic response of compliant objects, be they buildings, bridges, slopes, or soil deposits, is very sensitive to the frequency at which they are loaded. Earthquakes produce complicated loading with components of motion that span a broad range of frequencies. The *frequency content* describes how the amplitude of a ground motion is distributed among different frequencies. Since the frequency content of an earthquake motion will strongly influence the effects of that motion, characterization of the motion cannot be complete without consideration of its frequency content.

3.3.2.1 Ground Motion Spectra

Any periodic function (i.e., any function that repeats itself exactly at a constant interval) can be expressed using Fourier analysis as the sum of a series of simple harmonic terms of different frequency, amplitude, and phase. Using the Fourier series (see Section A.3 of Appendix A), a periodic function, $x(t)$, can be written as

$$x(t) = c_0 + \sum_{n=1}^{\infty} c_n \sin(\omega_n t + \phi_n) \quad (3.4)$$

In this form, c_n and ϕ_n are the amplitude and phase angle, respectively, of the n th harmonic of the Fourier series [see equations (A.10) and (A.11) for their definitions]. The Fourier series provides a complete description of the ground motion since the motion can be completely recovered by the inverse Fourier transform.

Fourier Spectra. A plot of Fourier amplitude versus frequency [c_n versus ω_n from equation (3.4)] is known as a *Fourier amplitude spectrum*; a plot of Fourier phase angle (ϕ_n versus ω_n) gives the *Fourier phase spectrum*. The Fourier amplitude spectrum of a strong ground motion shows how the amplitude of the motion is distributed with respect to frequency (or period). It expresses the frequency content of a motion very clearly.

The Fourier amplitude spectrum may be narrow or broad. A narrow spectrum implies that the motion has a dominant frequency (or period), which can produce a smooth, almost sinusoidal time history. A broad spectrum corresponds to a motion that contains a variety of frequencies that produce a more jagged, irregular time history. The Fourier amplitude spectra for the E-W components of the Gilroy No. 1 (rock) and Gilroy No. 2 (soil) motions shown in Figure 3.13. The jagged shapes of the spectra are typical of those observed for

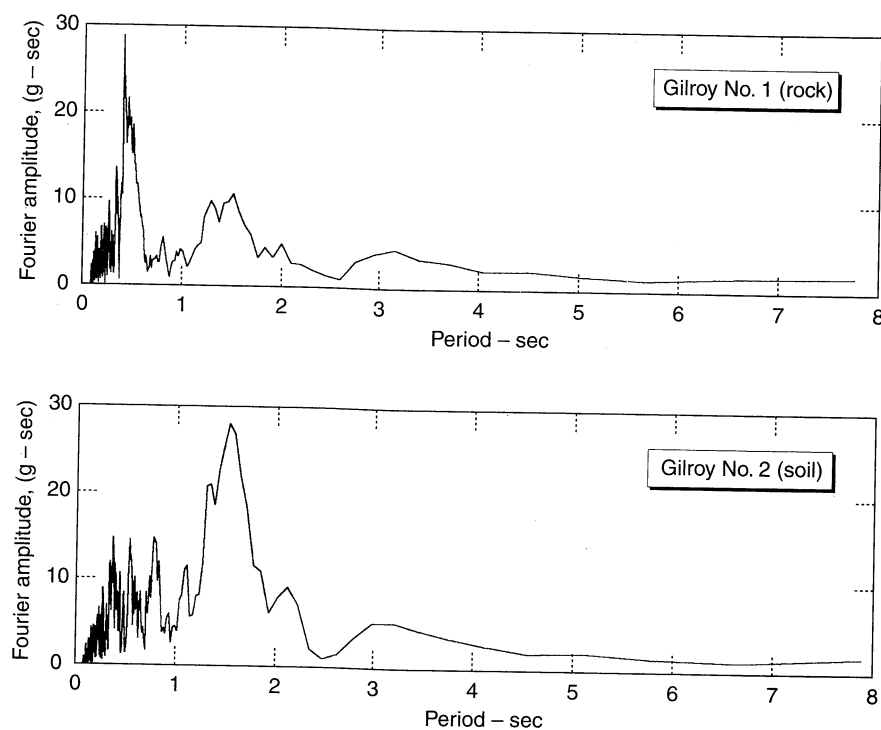


Figure 3.13 Fourier amplitude spectra for the E-W components of the Gilroy No. 1 (rock) and Gilroy No. 2 (soil) strong motion records. Fourier spectra were obtained by discrete Fourier transform (Section A.3.3 of Appendix A) and consequently have units of velocity. Fourier amplitude spectra can also be plotted as functions of frequency (see Figure E3.3).

individual ground motions. The shapes of the spectra are quite different: the Gilroy No. 1 (rock) spectrum is strongest at low periods (or high frequencies) while the reverse is observed for the Gilroy No. 2 (soil) record. A difference in frequency content can be detected by closely examining the motions in the time domain (Figure 3.1), but the difference is explicitly illustrated by the Fourier amplitude spectra.

When the Fourier amplitude spectra of actual earthquake motions are smoothed and plotted on logarithmic scales, their characteristic shapes can be seen more easily. As illustrated in Figure 3.14, Fourier acceleration amplitudes tend to be largest over an intermediate range of frequencies bounded by the *corner frequency* f_c on the low side and the *cutoff frequency* f_{\max} on the high side. The corner frequency can be shown theoretically (Brune, 1970, 1971) to be inversely proportional to the cube root of the seismic moment. This result indicates that large earthquakes produce greater low-frequency motions than do smaller earthquakes. The cutoff frequency is not well understood; it has been characterized both as a near-site effect (Hanks, 1982) and as a source effect (Papageorgiou and Aki, 1983) and is usually assumed to be constant for a given geographic region.

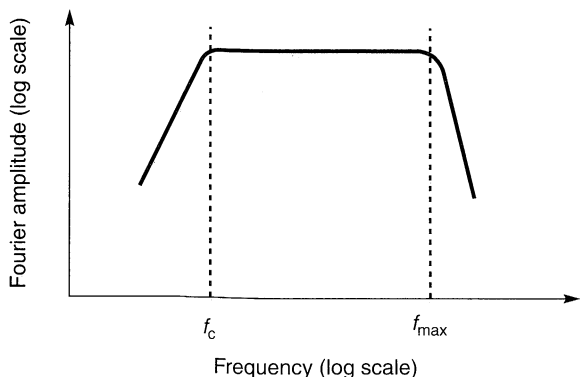


Figure 3.14 Idealized shape of smoothed Fourier amplitude spectrum illustrating the corner frequency, f_c , and cutoff frequency, f_{\max} .

Since phase angles control the times at which the peaks of harmonic motions occur (Appendix A), the Fourier phase spectrum influences the variation of ground motion with time. In contrast to Fourier amplitude spectra, Fourier phase spectra from actual earthquake records do not display characteristic shapes.

Power Spectra. The frequency content of a ground motion can also be described by a *power spectrum* or *power spectral density function*. The power spectral density function can also be used to estimate the statistical properties of a ground motion and to compute stochastic response using random vibration techniques (Clough and Penzien, 1975; Vanmarcke, 1976; Yang, 1986).

The total intensity of a ground motion of duration T_d is given in the time domain by the area under the time history of squared acceleration:

$$I_0 = \int_0^{T_d} [a(t)]^2 dt \quad (3.5)$$

Using Parseval's theorem, the total intensity can also be expressed in the frequency domain, as

$$I_0 = \frac{1}{\pi} \int_0^{\omega_N} c_n^2 d\omega \quad (3.6)$$

where $\omega_N = \pi / \Delta t$ is the *Nyquist frequency* (the highest frequency in the Fourier series). The average intensity, λ_0 , can be obtained by dividing equations (3.5) and (3.6) by the duration.

$$\lambda_0 = \frac{1}{T_d} \int_0^{T_d} [a(t)]^2 dt = \frac{1}{\pi T_d} \int_0^{\omega_N} c_n^2 d\omega \quad (3.7)$$

Notice that the average intensity is equal to the mean-squared acceleration. The *power spectral density*, $G(\omega)$, is defined such that

$$\lambda_0 = \int_0^{\omega_N} G(\omega) d\omega \quad (3.8)$$

from which we can easily see, by comparing equations (3.7) and (3.8), that

$$G(\omega) = \frac{1}{\pi T_d} c_n^2 \quad (3.9)$$

The close relationship between the power spectral density function and the Fourier amplitude spectrum is apparent from equation (3.9). The power spectral density is often normalized by dividing its values by the area beneath it

$$G^n(\omega) = \frac{1}{\lambda_0} G(\omega) \quad (3.10)$$

where λ_0 , as before, is the mean-squared acceleration.

The power spectral density function is useful in characterizing the earthquake as a random process. The power spectral density function by itself can describe a *stationary random process* (i.e., one whose statistical parameters do not vary with time). Actual strong motion accelerograms, however, frequently show that the intensity builds up to a maximum value in the early part of the motion, then remains approximately constant for a period of time, and finally decreases near the end of the motion. Such *nonstationary random process* behavior is often modeled by multiplying a stationary time history by a deterministic intensity function (e.g., Hou, 1968; Shinozuka, 1973; Saragni and Hart, 1983). Changes in frequency content during the motion have been described using an *evolutionary power spectrum* approach (Priestley, 1965, 1967; Liu, 1970).

Response Spectra. A third type of spectrum is used extensively in earthquake engineering practice. The *response spectrum* describes the maximum response of a single-degree-of-freedom (SDOF) system to a particular input motion as a function of the natural frequency (or natural period) and damping ratio of the SDOF system (Section B.7 of Appendix B). Computed response spectra for the Gilroy No. 1 (rock) and Gilroy No. 2 (soil) records are illustrated in Figure 3.15.

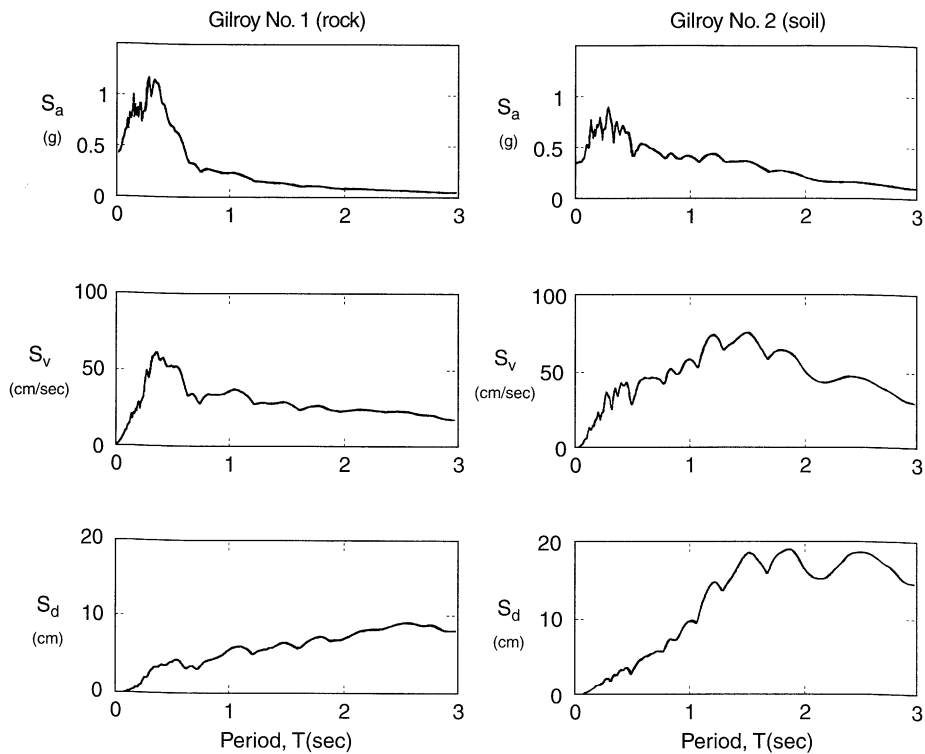


Figure 3.15 Response spectra (5% damping) for Gilroy No. 1 (rock) and Gilroy No. 2 (soil) strong motion records. The frequency contents of the two motions are reflected in the response spectra. The Gilroy 1 (rock) motion, for example, produced higher spectral accelerations at low periods than did the Gilroy 2 (soil) motion, and lower spectral accelerations at higher periods. The higher long-period content of the Gilroy 2 (soil) motion produced spectral velocities and displacements much higher than those of the Gilroy 1 (rock) motion.

Response spectra may be plotted individually to arithmetic scales, or may be combined, by virtue of the relationships of equation (3.11), in tripartite plots (Section A.2.2). The tripartite plot displays spectral velocity on the vertical axis, natural frequency (or period) on the horizontal axis, and acceleration and displacement on inclined axes. The acceleration and displacement axes are reversed when the spectral values are plotted against natural period rather than natural frequency. The shapes of typical response spectra indicate that peak spectral acceleration, velocity, and displacement values are associated with different frequencies (or periods). At low frequencies the average spectral displacement is nearly constant; at high frequencies the average spectral acceleration is fairly constant. In between lies a range of nearly constant spectral velocity. Because of this behavior, response spectra are often divided into *acceleration-controlled* (high-frequency), *velocity-controlled* (intermediate-frequency), and *displacement-controlled* (low-frequency) portions.

Elastic response spectra assume linear structural force-displacement behavior. For many real structures, however, inelastic behavior may be induced by earthquake ground

motions. An inelastic response spectrum (i.e., one that corresponds to a nonlinear force-displacement relationship, can be used to account for the effects of inelastic behavior. Figure 3.16 shows inelastic response spectra for acceleration and yield displacement for various values of the *ductility factor* $\mu = u_{\max}/u_y$, where u_{\max} is the maximum allowable displacement and u_y is the yield displacement. A separate inelastic spectrum must be plotted to show total (elastic plus plastic) displacement. Spectral accelerations decrease with increasing ductility, but total displacements increase.

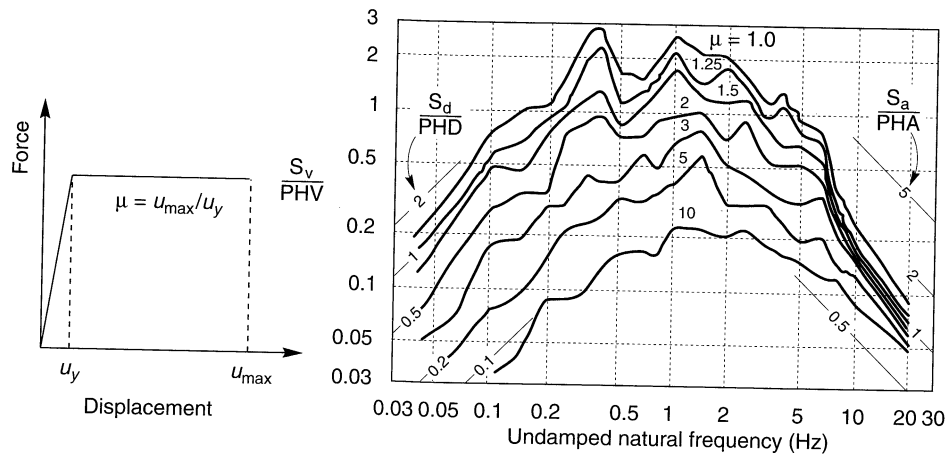


Figure 3.16 Inelastic response spectra for the El Centro N-S component of the 1940 Imperial Valley earthquake. Only the elastic component of the displacement is plotted. Spectral accelerations are correct, but spectral velocities are not. (After Newmark and Hall, 1982; used by permission of EERI.)

Response spectra reflect strong ground motion characteristics indirectly, since they are “filtered” by the response of a SDOF structure. The amplitude, frequency content, and to a lesser extent, duration of the input motion all influence spectral values. The different frequency contents of the Gilroy No. 1 (rock) and Gilroy No. 2 (soil) ground motions are clearly illustrated by the different shapes of their respective response spectra (Figure 3.15).

It is important to remember that response spectra represent only the maximum responses of a number of different structures. However, the response of structures is of great importance in earthquake engineering, and the response spectrum has proven to be an important and useful tool for characterization of strong ground motion.

3.3.2.2 Spectral Parameters

Section 3.3.2.1 described three types of spectra that can be used to characterize strong ground motion. The Fourier amplitude spectrum and the closely related power spectral density, combined with the phase spectrum, can describe a ground motion completely. The response spectrum does not describe the actual ground motion, but it does provide valuable additional information on its potential effects on structures. Each of these spectra is a complicated function and, as with time histories, a great many data are required to describe them completely. A number of *spectral parameters* have been proposed to extract important pieces of information from each spectrum.

Predominant Period. A single parameter that provides a useful, although somewhat crude representation of the frequency content of a ground motion is the *predominant period*, T_p . The predominant period is defined as the period of vibration corresponding to the maximum value of the Fourier amplitude spectrum. To avoid undue influence of individual spikes of the Fourier amplitude spectrum, the predominant period is often obtained from a smoothed spectrum. While the predominant period provides some information regarding the frequency content, it is easy to see (Figure 3.17) that motions with radically different frequency contents can have the same predominant period.

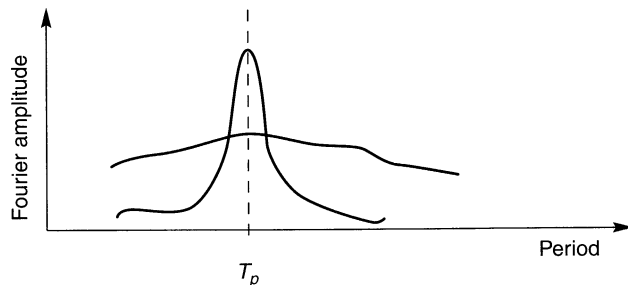


Figure 3.17 Two hypothetical Fourier amplitude spectra with the same predominant period but very different frequency contents. The upper curve describes a wideband motion and the lower a narrowband motion.

Example 3.3

Determine the predominant periods for the E-W components of the Gilroy No. 1 (rock) and Gilroy No. 2 (soil) ground motions.

Solution The Fourier amplitude spectra of most ground motions are quite jagged in the vicinity of their peaks, so some smoothing is required to identify the predominant period. The smoothing and predominant period identification is most easily accomplished by plotting the Fourier amplitude spectrum as a function of frequency. By numerically smoothing their Fourier amplitude spectra (Figure E3.3), the predominant periods are

$$\text{Gilroy No. 1 (rock): } T_p = 0.39 \text{ sec}$$

$$\text{Gilroy No. 2 (soil): } T_p = 0.53 \text{ sec}$$

Note that the predominant period of the Gilroy No. 2 (soil) motion is greater than that of the Gilroy No. 1 (rock) motion, thereby illustrating the relative strength of the longer period (lower-frequency) components of the Gilroy No. 1 (soil) motion.

Bandwidth. The predominant period can be used to locate the peak of the Fourier amplitude spectrum; however, it provides no information on the dispersion of spectral amplitudes about the predominant period. The *bandwidth* of the Fourier amplitude spectrum is the range of frequency over which some level of Fourier amplitude is exceeded. Bandwidth is usually measured at the level where the power of the spectrum is half its maximum value; this corresponds to a level of $1/\sqrt{2}$ times the maximum Fourier amplitude. The irregular shape of individual Fourier amplitude spectra often renders bandwidth difficult to evaluate. It is determined more easily for smoothed spectra.

Central Frequency. The power spectral density function can be used to estimate statistical properties of the ground motion. Defining the n th spectral moment of a ground motion by

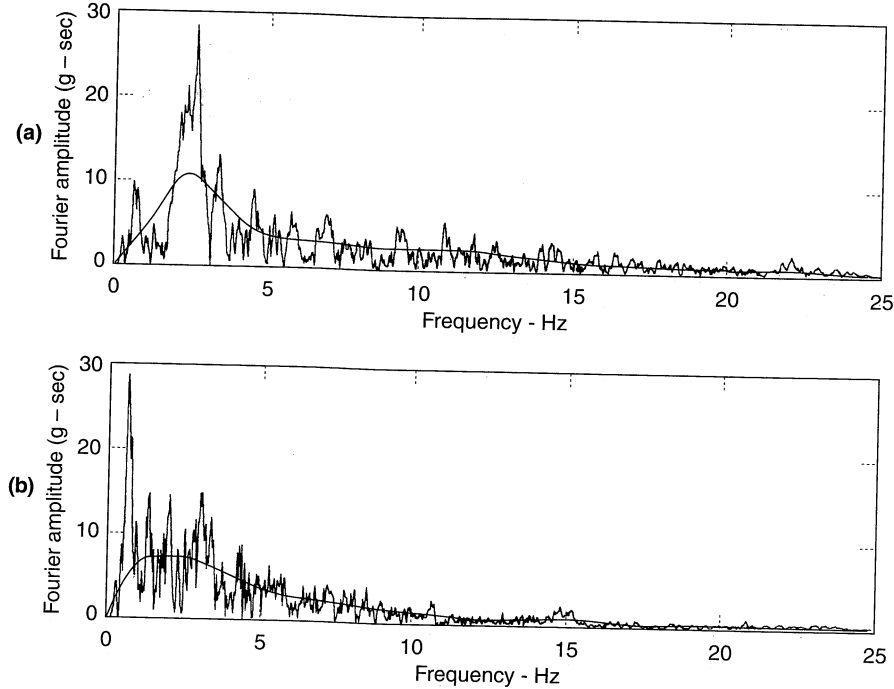


Figure E3.3 Raw and smoothed FAS for Gilroy No.1 (rock) and Gilroy No.2 (soil) motions.

$$\lambda_n = \int_0^{\omega_N} \omega^n G(\omega) d\omega \quad (3.11)$$

the *central frequency* Ω (Vanmarcke, 1976) is given by

$$\Omega = \sqrt{\frac{\lambda_2}{\lambda_0}} \quad (3.12)$$

The central frequency is a measure of the frequency where the power spectral density is concentrated. It can also be used, along with the average intensity and duration, to calculate the theoretical median peak acceleration

$$\ddot{u}_{\max} = \sqrt{2\lambda_0 \ln\left(2.8 \frac{\Omega T_d}{2\pi}\right)} \quad (3.13)$$

Shape Factor. The *shape factor* (Vanmarcke, 1976) indicates the dispersion of the power spectral density function about the central frequency:

$$\delta = \sqrt{1 - \frac{\lambda_1^2}{\lambda_0 \lambda_2}} \quad (3.14)$$

The shape factor always lies between 0 and 1, with higher values corresponding to larger bandwidths.

Kanai-Tajimi Parameters. Although individual power spectral density functions may have highly irregular shapes, averaging a number of normalized power spectral density functions for similar strong ground motions reveals a smooth characteristic shape. Kanai (1957) and Tajimi (1960) used a limited number of strong motion records to propose the following three-parameter model for power spectral density:

$$G(\omega) = G_0 \frac{1 + [2\xi_g(\omega/\omega_g)]^2}{[1 - (\omega/\omega_g)^2]^2 + [2\xi_g(\omega/\omega_g)]^2} \quad (3.15)$$

where the parameters G_0 , ξ_g , and ω_g determine the shape of the function (Figure 3.18).

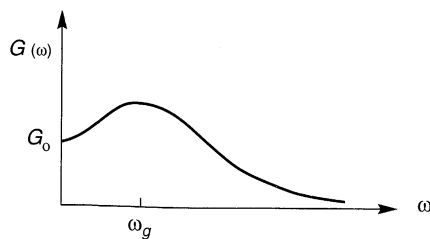


Figure 3.18 Shape of the Kanai-Tajimi power spectral density function.

The displacement response of a SDOF system with natural frequency ω_g and damping ratio ξ_g to white noise base motion would be described by a Kanai-Tajimi power spectral density function. As such, high-frequency components of the input motion will be attenuated, and frequency components in the vicinity of ω_g will be amplified. Typical values of Kanai-Tajimi parameters for various site conditions are shown in Table 3-1.

Clough and Penzien (1975) proposed a correction to the Kanai-Tajimi power spectral density function to prevent excessive velocities and displacements at very low frequencies. The corrected Kanai-Tajimi power spectral density function requires two additional parameters to describe the power spectral density.

3.3.2.3 v_{\max}/a_{\max}

Because peak velocities and peak accelerations are usually associated with motions of different frequency, the ratio v_{\max}/a_{\max} should be related to the frequency content of the motion (Newmark, 1973; Seed et al., 1976; McGuire, 1978). For a simple harmonic motion

Table 3-1 Ground Intensity, Ground Frequency, and Ground Damping for Various Site Conditions

Ground Motion	Site Conditions	Number of Records	Ground Intensity, G_0	Ground Frequency, ω_g	Ground Damping, ξ_g
Horizontal	Alluvium	161	0.102	18.4	0.34
	Alluvium on rock	60	0.078	22.9	0.30
	Rock	26	0.070	27.0	0.34
	Alluvium	78	0.080	26.2	0.46
	Alluvium on rock	29	0.072	29.1	0.46
	Rock	13	0.053	38.8	0.46

Source: Elghadamsi et al. (1988).

of period T , for example, $v_{\max}/a_{\max} = T/2\pi$. For earthquake motions that include many frequencies, the quantity $2\pi(v_{\max}/a_{\max})$ can be interpreted as the period of vibration of an equivalent harmonic wave, thus providing an indication of which periods of the ground motion are most significant. Seed and Idriss (1982) suggested the following representative average values for different site conditions less than 50 km from the source:

Site Condition	v_{\max}/a_{\max}
Rock	55 cm/sec/g = 0.056 sec
Stiff soils (<200 ft)	110 cm/sec/g = 0.112 sec
Deep stiff soils (>200 ft)	135 cm/sec/g = 0.138 sec

The corresponding periods of equivalent harmonic waves for the rock, stiff soil, and deep stiff soil site conditions are 0.35 sec, 0.70 sec, and 0.87 sec, respectively, which indicates a shift toward longer-period (lower-frequency) motion on softer soil deposits.

Example 3.4

Determine the ratio v_{\max}/a_{\max} for the N-S components of the Gilroy No. 1 (rock) and Gilroy No. 2 (soil) ground motions. Compare the quantities $2\pi(v_{\max}/a_{\max})$ with the predominant periods of the motions.

Solution Based on the v_{\max} and a_{\max} values from Example 3.1,

$$\text{Gilroy No.1 (rock): } \frac{v_{\max}}{a_{\max}} = \frac{33.7 \text{ cm/sec}}{0.442 (981 \text{ cm/sec}^2)} = 0.078 \text{ sec}$$

$$\text{Gilroy No.2 (soil): } \frac{v_{\max}}{a_{\max}} = \frac{39.2 \text{ cm/sec}}{0.322 (981 \text{ cm/sec}^2)} = 0.124 \text{ sec}$$

The quantity $2\pi(v_{\max}/a_{\max})$ is equal to the predominant period of a simple harmonic motion. To see how well it corresponds to the predominant period of the Gilroy No. 1 (rock) and Gilroy No. 2 (soil) ground motions,

$$\text{Gilroy No.1 (rock): } 2\pi \frac{v_{\max}}{a_{\max}} = 0.49 \text{ sec} \quad T_p = 0.39 \text{ sec}$$

$$\text{Gilroy No.2 (soil): } 2\pi \frac{v_{\max}}{a_{\max}} = 0.78 \text{ sec} \quad T_p = 0.53 \text{ sec}$$

Though the ratio v_{\max}/a_{\max} certainly indicates that the Gilroy No. 1 (rock) motion has a higher frequency content than the Gilroy No. 2 (soil) motion, it overestimates the predominant period of both the Gilroy No. 1 (rock) motion and Gilroy No.2 (soil) motions. Due to the approximate nature of the predominant period and the stochastic nature of both v_{\max} and a_{\max} , close agreement between v_{\max}/a_{\max} and predominant period should not be expected.

3.3.3 Duration

The duration of strong ground motion can have a strong influence on earthquake damage. Many physical processes, such as the degradation of stiffness and strength of certain types of structures and the buildup of porewater pressures in loose, saturated sands, are sensitive to the number of load or stress reversals that occur during an earthquake. A motion of short duration may not produce enough load reversals for damaging response to build up in a structure, even if the amplitude of the motion is high. On the other hand, a motion with moderate amplitude but long duration can produce enough load reversals to cause substantial damage.

The duration of a strong ground motion is related to the time required for release of accumulated strain energy by rupture along the fault. As the length, or area, of fault rupture increases, the time required for rupture increases. As a result, the duration of strong motion increases with increasing earthquake magnitude. While this relationship has been supported by empirical evidence for many years, advances in source mechanism modeling (Hanks and McGuire, 1981) have provided theoretical support, indicating that the duration should be proportional to the cube root of the seismic moment. When *bilateral rupture* [i.e., rupture that propagates in opposite directions from the focus (as in the case of the 1989 Loma Prieta earthquake)] occurs, the strong motion duration may be considerably lower.

An earthquake accelerogram generally contains all accelerations from the time the earthquake begins until the time the motion has returned to the level of background noise. For engineering purposes, only the strong-motion portion of the accelerogram is of interest. Different approaches have been taken to the problem of evaluating the duration of strong motion in an accelerogram. The *bracketed duration* (Bolt, 1969) is defined as the time between the first and last exceedances of a threshold acceleration (usually 0.05g). Another definition of duration (Trifunac and Brady, 1975b) is based on the time interval between the points at which 5% and 95% of the total energy has been recorded. Boore (1983) has taken the duration to be equal to the *corner period* (i.e., the inverse of the corner frequency). The rate of change of cumulative root-mean-square (rms) acceleration has also been used as the basis for evaluation of strong-motion duration (McCann and Shah, 1979). Power spectral density concepts can also be used to define a strong-motion duration (Vanmarcke and Lai, 1977). Other definitions of strong-motion duration have been proposed (Perez, 1974; Trifunac and Westermo, 1977). Because it implicitly reflects the strength of shaking, the bracketed duration is most commonly used for earthquake engineering purposes.

The duration of strong motion has been investigated by interpretation of accelerograms from earthquakes of different magnitudes. Using a 0.05g threshold acceleration, Chang and Krinitzsky (1977) estimated the bracketed durations for soil and rock sites at short (less than 10 km) epicentral distances shown in Table 3-2.

Duration has also been expressed in terms of equivalent cycles of ground motion. One such approach was developed in conjunction with an early procedure for evaluation of liquefaction potential (Seed et al., 1975). To represent an irregular time history of shear stress

Table 3-2 Typical Earthquake Durations at Epicentral Distances Less Than 10 km

Magnitude	Duration (sec)	
	Rock Sites	Soil Sites
5.0	4	8
5.5	6	12
6.0	8	16
6.5	11	23
7.0	16	32
7.5	22	45
8.0	31	62
8.5	43	86

Source: Chang and Krinitzsky (1977).

by a uniform series of harmonic stress cycles, the concept of an equivalent number of significant stress cycles was developed. The equivalent number of uniform stress cycles, shown in Table 3-3, was selected to cause pore pressure buildup equivalent to that of an actual shear stress-time history at a harmonic stress amplitude of 65% of the maximum actual shear stress.

Table 3-3 Equivalent Number of Uniform Stress Cycles

Earthquake Magnitude	Number of Significant Stress Cycles
$5\frac{1}{4}$	2–3
6	5
$6\frac{3}{4}$	10
$7\frac{1}{2}$	15
$8\frac{1}{2}$	26

Example 3.5

Determine the bracketed durations of the E-W components of the Gilroy No. 1 (rock) and Gilroy No. 2 (soil) ground motions.

Solution Based on a threshold acceleration of $0.05g$, the bracketed durations can be obtained graphically from the accelerograms shown in Figure E3.5.

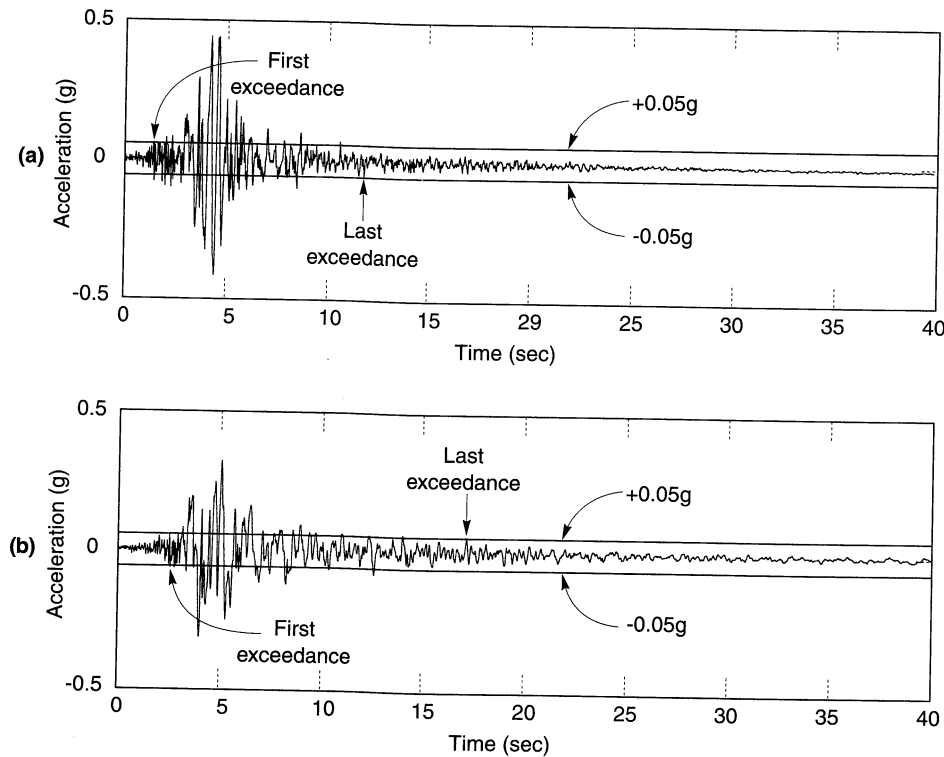


Figure E3.5

$$\begin{aligned} \text{Gilroy No.1 (rock):} & \quad T_d = 9.8 \text{ sec} \\ \text{Gilroy No.2 (soil):} & \quad T_d = 14.7 \text{ sec} \end{aligned}$$

3.3.4 Other Ground Motion Parameters

The preceding parameters related primarily to the amplitude, frequency content, or duration of a ground motion. Since all of these characteristics are important, ground motion parameters that reflect more than one are very useful. The following paragraphs present a number of parameters that reflect two or three important ground motion characteristics.

A single parameter that includes the effects of the amplitude and frequency content of a strong motion record is the *rms acceleration*, defined as

$$a_{\text{rms}} = \sqrt{\frac{1}{T_d} \int_0^{T_d} [a(t)]^2 dt} = \sqrt{\lambda_0} \quad (3.16)$$

where T_d is the duration of the strong motion and λ_0 is the average intensity (or mean-squared acceleration). Because the integral in equation (3.16) is not strongly influenced by large, high-frequency accelerations (which occur only over a very short period of time) and because it is influenced by the duration of the motion, the rms acceleration can be very useful for engineering purposes. Its value, however, can be sensitive to the method used to define strong motion duration.

A parameter closely related to the rms acceleration is the *Arias intensity* (Arias, 1970), defined as

$$I_a = \frac{\pi}{2g} \int_0^{\infty} [a(t)]^2 dt \quad (3.17)$$

The Arias intensity has units of velocity and is usually expressed in meters per second. Since it is obtained by integration over the entire duration rather than over the duration of strong motion, its value is independent of the method used to define the duration of strong motion.

Example 3.6

Determine the rms accelerations and Arias intensities of the E-W components of the Gilroy No. 1 (rock) and Gilroy No. 2 (soil) ground motions.

Solution By integrating the accelerograms of the Gilroy No. 1 (rock) and Gilroy No. 2 (soil) ground motions numerically, the rms accelerations and Arias intensities are

$$\begin{aligned} \text{Gilroy No.1 (rock):} & \quad a_{\text{rms}} = 0.112g \quad I_a = 1.667 \text{ m/sec} \\ \text{Gilroy No.2 (soil):} & \quad a_{\text{rms}} = 0.072g \quad I_a = 1.228 \text{ m/sec} \end{aligned}$$

The *characteristic intensity*, defined as

$$I_c = a_{\text{rms}}^{1.5} T_d^{0.5} \quad (3.18)$$

is related linearly to an index of structural damage due to maximum deformations and absorbed hysteretic energy (Ang, 1990).

The *cumulative absolute velocity* is simply the area under the absolute accelerogram:

$$\text{CAV} = \int_0^{T_d} |a(t)| dt \quad (3.19)$$

The cumulative absolute velocity has been found to correlate well with structural damage potential. For example, a CAV of 0.30g-sec (obtained after filtering out frequencies above 10 Hz) corresponds to the lower limit for MMI VII shaking (Benjamin and Associates, 1988).

Since many structures have fundamental periods between 0.1 and 2.5 sec, the response spectrum ordinates in this period range should provide an indication of the potential response of these structures. The *response spectrum intensity* (Housner, 1959) was therefore defined as

$$\text{SI}(\xi) = \int_{0.1}^{2.5} \text{PSV}(\xi, T) dT \quad (3.20)$$

(i.e., the area under the pseudovelocity response spectrum between periods of 0.1 sec and 2.5 sec. The response spectrum intensity, as indicated in equation (3.20), can be computed for any structural damping ratio. It captures important aspects of the amplitude and frequency content (in the range of primary importance for structures) in a single parameter.

Von Thun et al. (1988) referred to the response spectrum intensity for 5% damping as the *velocity spectrum intensity*. The velocity spectrum intensity was suggested as being useful for evaluation of the response of earth and rockfill dams, which typically have fundamental periods between 0.6 and 2.0 sec (Makdisi and Seed, 1978). To characterize strong ground motion for analysis of concrete dams, which generally have fundamental periods of less than 0.5 sec, Von Thun et al. (1988) introduced the *acceleration spectrum intensity*, defined as

$$\text{ASI} = \int_{0.1}^{0.5} S_a(\xi=0.05, T) dT \quad (3.21)$$

(i.e., the area under the acceleration response spectrum between periods of 0.1 sec and 0.5 sec).

The Applied Technology Council (1978) defined two factors by which standard response spectra could be normalized. The *effective peak acceleration* (EPA) was defined as the average spectral acceleration over the period range 0.1 to 0.5 sec divided by 2.5 (the standard amplification factor for a 5% damping spectrum). The *effective peak velocity* (EPV) was defined as the average spectral velocity at a period of 1 sec divided by 2.5. Determination of EPA and EPV is shown schematically in Figure 3.19. The process of averaging the spectral accelerations and velocities over a range of periods minimizes the influence of local spikes in the response spectrum on the EPA and EPV. The EPA and EPV have been used in the specification of smoothed design response spectra in building codes (Chapter 8).

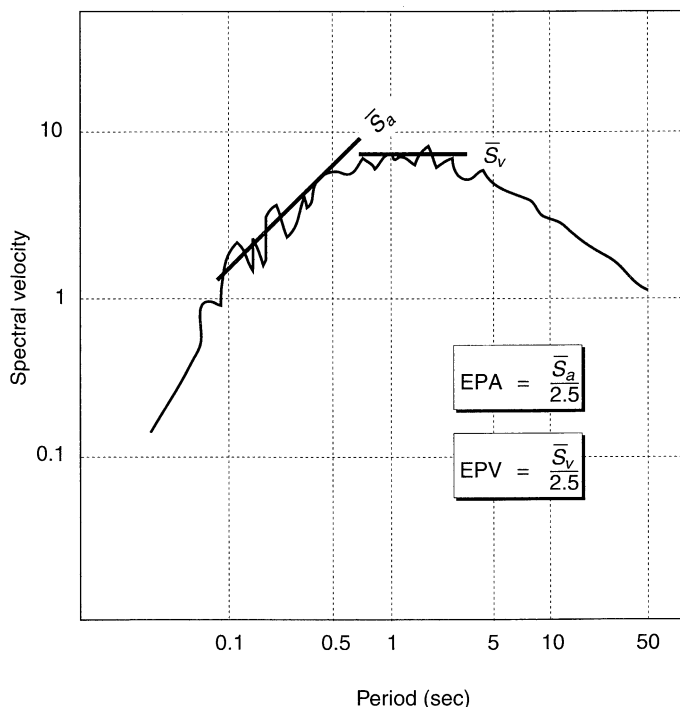


Figure 3.19 Determination of effective peak acceleration and effective peak velocity from response spectra. (After Applied Technology Council, 1978.)

3.3.5 Discussion

A wide variety of strong motion parameters have been presented. Some describe only the amplitude of the motion, others only the frequency content or duration. Some of these parameters are influenced by two or three of these important ground motion characteristics. Table 3-4 indicates which ground motion characteristics strongly influence the various ground motion parameters.

Seismic hazard analyses (Chapter 4) and the development of design ground motions (Chapter 8) rely heavily on the characterization of strong ground motion by ground motion parameters. Characterization by a single parameter is only rarely appropriate; the use of several parameters is usually required to describe adequately the important characteristics of a particular ground motion. Since different engineering problems are influenced by different ground motion characteristics, the significance of different parameters depends on the types of problems for which they are used.

3.4 ESTIMATION OF GROUND MOTION PARAMETERS

Proper design of earthquake-resistant structures and facilities requires estimation of the level of ground shaking to which they will be subjected. Since the level of shaking is most

Table 3-4 Ground Motion Characteristics That Are Strongly Reflected in Various Ground Motion Parameters

Ground Motion Parameter	Ground Motion Characteristic		
	Amplitude	Frequency Content	Duration
Peak acceleration, PHA and PHV	×		
Peak velocity, PHV	×		
Sustained maximum acceleration, SMA	×		
Effective design acceleration, EDA	×		
Predominant period, T_p		×	
Bandwidth		×	
Central frequency, Ω		×	
Shape factor, δ		×	
Power spectrum intensity, G_0	×	×	×
Ground frequency, ω_g		×	
Ground damping, ξ_g		×	
v_{\max}/a_{\max}		×	
Duration, T_d			×
rms acceleration, a_{rms}	×	×	
Characteristic intensity, I_c	×	×	×
Arias intensity, I_a	×	×	×
Cumulative absolute velocity, CAV	×	×	×
Response spectrum intensity, SI(ξ)	×	×	
Velocity spectrum intensity, VSI	×	×	
Acceleration spectrum intensity, ASI	×	×	
Effective peak acceleration, EPA	×	×	
Effective peak velocity, EPV	×	×	

conveniently described in terms of ground motion parameters, methods for estimating ground motion parameters are required. *Predictive relationships*, which express a particular ground motion parameter in terms of the quantities that affect it most strongly, are used to estimate ground motion parameters. Predictive relationships play an important role in seismic hazard analyses (Chapter 4) used for seismic design.

3.4.1 Magnitude and Distance Effects

Much of the energy released by rupture along a fault takes the form of stress waves. Since the amount of energy released in an earthquake is strongly related to its magnitude, the characteristics of the stress waves will also be strongly related to magnitude. Figure 3.20 illustrates the influence of earthquake magnitude on actual ground motion characteristics in the time domain. Each earthquake came from essentially the same source, and each accelerogram was measured at about the same distance from the source. The variations in amplitude, frequency content, and duration with magnitude are apparent.

As stress waves travel away from the source of an earthquake, they spread out and are partially absorbed by the materials they travel through. As a result, the *specific energy* (energy per unit volume) decreases with increasing distance from the source. Since the characteristics of stress waves are strongly related to specific energy, they will also be strongly related to distance. The distance between the source of an earthquake and a

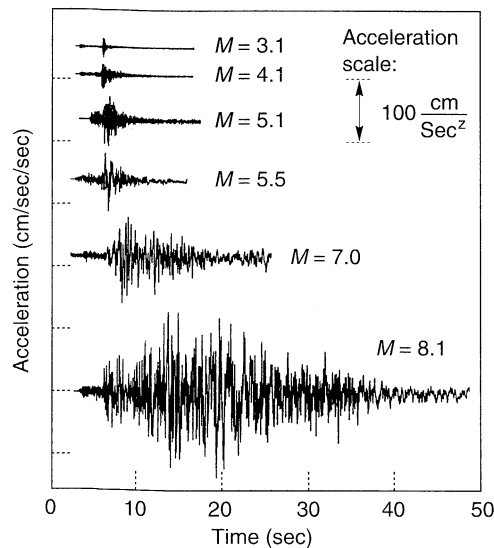


Figure 3.20 Accelerograms from six earthquakes off the Pacific coast of Mexico. Each accelerogram was measured at nearly the same epicentral distance. The record from the $M = 8.1$ (1985 Michoacan) earthquake continues for another 25 sec. (After Anderson, 1991, *Geotechnical News*, Vol. 9, No. 1, p. 35. Used by permission of BiTech Publishers, Ltd.)

particular site can be interpreted in different ways. Figure 3.21 illustrates some of the most commonly used measures of distance. R_1 and R_2 are the hypocentral and epicentral distances, which are the easiest distances to determine after an earthquake. If the length of fault rupture is a significant fraction of the distance between the fault and the site, however, energy may be released closer to the site, and R_1 and R_2 may not accurately represent the "effective distance." R_3 is the distance to the zone of highest energy release. Since rupture of this zone is likely to produce the peak ground motion amplitudes, it represents the best distance measure for peak amplitude predictive relationships. Unfortunately, its location is difficult to determine after an earthquake and nearly impossible to predict before an earthquake. R_4 is the closest distance to the zone of rupture (not including sediments overlying basement rock) and R_5 is the closest distance to the surface projection of the fault rupture. R_4 and R_5 have both been used extensively in predictive relationships.

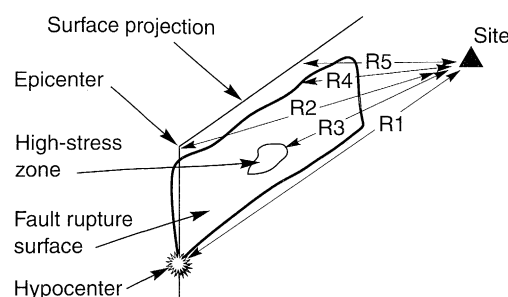


Figure 3.21 Various measures of distance used in strong-motion predictive relationships. (After Shakal and Bernreuter, 1981.)

3.4.2 Development of Predictive Relationships

Predictive relationships usually express ground motion parameters as functions of magnitude, distance, and in some cases, other variables, for example,

$$Y = f(M, R, P_i) \quad (3.22)$$

where Y is the ground motion parameter of interest, M the magnitude of the earthquake, R a measure of the distance from the source to the site being considered, and the P_i are other parameters (which may be used to characterize the earthquake source, wave propagation path, and/or local site conditions). Predictive relationships are developed by regression analyses of recorded strong motion databases. As such, they change with time as additional strong motion data become available. Most predictive relationships are updated in the literature every 3 to 5 years or shortly after the occurrence of large earthquakes in well-instrumented regions.

The functional form of the predictive relationship is usually selected to reflect the mechanics of the ground motion process as closely as possible. This minimizes the number of empirical coefficients and allows greater confidence in application of the predictive relationship to conditions (magnitudes and distances) that are poorly represented in the database. Common forms for predictive relationships are based on the following observations:

1. Peak values of strong motion parameters are approximately lognormally distributed (i.e., the logarithms of the parameters are approximately normally distributed). As a result, the regression is usually performed on the logarithm of Y rather than on Y itself.
2. Earthquake magnitude is typically defined as the logarithm of some peak motion parameter (Section 2.9.2). Consequently, $\ln Y$ should be approximately proportional to M .
3. The spreading of stress waves as they travel away from the source of an earthquake causes body wave [p- and s-wave (Section 5.2.2.5)] amplitudes to decrease according to $1/R$ and surface wave [primarily Rayleigh wave (Section 5.3.1)] amplitudes to decrease according to $1/\sqrt{R}$.
4. The area over which fault rupture occurs increases with increasing earthquake magnitude (Section 4.2.1.2). As a result, some of the waves that produce strong motion at a site arrive from a distance, R , and some arrive from greater distances. The effective distance, therefore, is greater than R by an amount that increases with increasing magnitude.
5. Some of the energy carried by stress waves is absorbed by the materials they travel through [material damping (Section 5.5.1)]. This material damping causes ground motion amplitudes to decrease exponentially with R .
6. Ground motion parameters may be influenced by source characteristics (e.g. strike-slip, normal, or reverse faulting) or site characteristics (e.g. hard rock, soft rock, alluvium, etc.).

Combining these observations, a typical predictive relationship may have the form

$$\begin{aligned} \ln Y = & \underbrace{C_1}_{(1)} + \underbrace{C_2 M + C_3 M^{C_4}}_{(2)} + \underbrace{C_5 \ln[R + C_6 \exp(C_7 M)]}_{(3)} + \\ & \underbrace{C_8 R}_{(5)} + \underbrace{f(\text{source}) + f(\text{site})}_{(6)} \quad \sigma_{\ln Y} = C_9 \quad (3.23) \end{aligned}$$

where the circled numbers indicate the observations associated with each term. Some predictive relationships utilize all these terms (and some have even more) and others do not.

The $\sigma_{\ln Y}$ term describes uncertainty in the value of the ground motion parameter given by the predictive relationship. Statistically, it represents an estimate of the standard deviation of $\ln Y$ at the magnitude and distance of interest. Historically, most $\sigma_{\ln Y}$ values have been constants, but several recent predictive relationships indicate $\sigma_{\ln Y}$ values that vary with magnitude. At a given magnitude, therefore, the probability that the ground motion parameter will exceed a value Y^* would be $1 - F_Z(z^*)$ where $F_Z(z^*)$ is the value of the standard cumulative distribution function (see Section C7.2 of Appendix C) at $z^* = (\ln Y^* - \bar{\ln Y})/\sigma_{\ln Y}$.

When using any predictive relationship, it is very important to know how parameters such as M and R are defined and to use them in a consistent manner. It is also important to recognize that different predictive relationships are usually obtained from different data sets. To make reasonable predictions of ground motion parameters, a predictive relationship based on data that are consistent with the conditions relevant to the prediction is required.

3.4.3 Estimation of Amplitude Parameters

Predictive relationships for parameters that decrease with increasing distance (such as peak acceleration and peak velocity) are often referred to as *attenuation relationships*. A few of a large number of useful attenuation relationships for different geographic and tectonic environments are described in the following sections.

3.4.3.1 Peak Acceleration

Since peak acceleration is the most commonly used ground motion parameter, many peak acceleration attenuation relationships have been developed. All are best suited to conditions similar to those in the databases from which they were developed. As additional strong motion data have become available, attenuation relationships have become more refined. Consider, for example, two attenuation relationships developed some 13 years apart.

In 1981, Campbell (1981) used worldwide data to develop an attenuation relationship for the mean PHA for sites within 50 km of the fault rupture in magnitude 5.0 to 7.7 earthquakes:

$$\begin{aligned} \ln \text{PHA}(g) &= -4.141 + 0.868M - 1.09 \ln[R + 0.0606 \exp(0.7M)] \\ \sigma_{\ln \text{PHA}} &= 0.37 \end{aligned} \quad (3.24)$$

where M is the local magnitude or surface wave magnitude for magnitudes less than or greater than 6, respectively, and R is the closest distance to the fault rupture in kilometers. In this relatively simple attenuation relationship, which represented the state of the art in 1981, the peak acceleration was taken as a function of M and R only and $\sigma_{\ln \text{PHA}}$ was constant. In 1994, Campbell and Bozorgnia (1994) used worldwide accelerograms from earthquakes of moment magnitude ranging from 4.7 to 8.1 to develop the attenuation relationship

$$\begin{aligned} \ln \text{PHA(gals)} &= -3.512 + 0.904M_w - 1.328 \ln \sqrt{R^2 + [0.149 \exp(0.647M_w)]^2} \\ &\quad + (1.125 - 0.112 \ln R - 0.0957M_w)F + (0.440 - 0.171 \ln R)S_{SR} \\ &\quad + (0.405 - 0.222 \ln R)S_{HR} \\ \sigma_{\ln \text{PHA}} &= \begin{cases} 0.889 - 0.0691M & M \leq 7.4 \\ 0.38 & M > 7.4 \end{cases} \end{aligned} \quad (3.25)$$

where R is the closest distance (≤ 60 km) to seismic rupture in kilometers (with minimum values of 7.3, 5.8, 3.5, and 3.0 km for magnitudes of 5.0, 5.5, 6.0, and 6.5, respectively); the source term, F , takes on values of 0 for strike-slip and normal faulting, and 1 for reverse, reverse-oblique, and thrust faulting; $S_{SR} = 1$ for soft-rock sites (sedimentary deposits of Tertiary age), $S_{HR} = 1$ for hard-rock sites (primarily older sedimentary deposits, metamorphic rock, and crystalline rock), and $S_{SR} = S_{HR} = 0$ for alluvium sites. The 1994 relationship, which is based on more data, is clearly more specific (and more complicated) than the 1981 relationship. The incorporation of additional terms reflecting source and site characteristics are typical of the refinement of predictive relationships that has taken place in recent years.

Boore et al. (1993) used data from western North America earthquakes of magnitude 5.0 to 7.7 at distances within 100 km (62 mi) of the surface projection of the fault to develop the predictive relationship

$$\log \text{PHA}(g) = b_1 + b_2(M_w - 6) + b_3(M_w - 6)^2 + b_4R + b_5 \log R + b_6G_B + b_7G_C \quad (3.26)$$

where $R = \sqrt{d^2 + h^2}$, d is the closest distance to the surface projection of the fault in kilometers, and

$$G_B = \begin{cases} 0 & \text{for site class A} \\ 1 & \text{for site class B} \\ 0 & \text{for site class C} \end{cases} \quad G_C = \begin{cases} 0 & \text{for site class A} \\ 0 & \text{for site class B} \\ 1 & \text{for site class C} \end{cases}$$

Note that the Boore et al. (1993) attenuation relationship is expressed in terms of the common (base 10) logarithm rather than the natural logarithm. The site classes are defined on the basis of the average shear wave velocity in the upper 30 m (100 ft) (Table 3-5). Coefficients for the Boore et al. (1993) attenuation relationship were developed for two measures of peak acceleration: the randomly oriented component and the larger horizontal component (the former considers two orthogonal horizontal records at a particular site as separate events and the latter considers only the larger of the two). The coefficients are given in Table 3-6.

Table 3-5 Definitions of Site Classes for Boore et al. (1993) Attenuation Relationship

Site Class	\bar{v}_s in Upper 30 m (100 ft)
A	> 750 m/sec (2500 ft/sec)
B	360–750 m/sec (1200–2500 ft/sec)
C	180–360 m/sec (600–1200 ft/sec)

Table 3-6 Coefficients for Boore et al. (1993) Attenuation Relationship

	Component								
	b_1	b_2	b_3	b_4	b_5	b_6	b_7	h	$\sigma_{\log \text{PHA}}$
Random	-0.105	0.229	0.0	0.0	-0.778	0.162	0.251	5.57	0.230
Larger	-0.038	0.216	0.0	0.0	-0.777	0.158	0.254	5.48	0.205

Since the continental crust in eastern North America is stronger and more intact than the crust in western North America, peak accelerations tend to be higher. For the mid-continent portion of eastern North America, Toro et al. (1994) developed an attenuation relationship for peak horizontal rock acceleration:

$$\begin{aligned} \ln \text{PHA}(g) = & 2.20 + 0.81(M_w - 6) - 1.27 \ln R_m \\ & + 0.11 \max\left(\ln \frac{R_m}{100}, 0\right) - 0.0021 R_m \quad \sigma_{\ln \text{PHA}} = \sqrt{\sigma_M^2 + \sigma_R^2} \end{aligned} \quad (3.27)$$

where $R_m = \sqrt{R^2 + 9.3^2}$, R is the closest horizontal distance to the earthquake rupture (in km), $\sigma_M = 0.36 + 0.07(M_w - 6)$, and

$$\sigma_R = \begin{cases} 0.54 & \text{for } R < 5 \text{ km} \\ 0.54 - 0.0227(R - 5) & \text{for } 5 \text{ km} \leq R \leq 20 \text{ km} \\ 0.20 & \text{for } R > 20 \text{ km} \end{cases}$$

Subduction zone earthquakes generally occur at greater hypocentral depths than earthquakes that occur on transform faults. Consequently, the seismic waves that emanate from subduction zone earthquakes follow different paths from those of transform faults. Youngs et al. (1988) used strong-motion measurements obtained on rock from 60 earthquakes and numerical simulations of $M_w \geq 8$ earthquakes to develop a subduction zone attenuation relationship:

$$\begin{aligned} \ln \text{PHA}(g) = & 19.16 + 1.045M_w - 4.738 \ln [R + 205.5 \exp(0.0968M_w)] \\ & + 0.54Z_t \quad \sigma_{\ln \text{PHA}} = 1.55 - 0.125M_w \end{aligned} \quad (3.28)$$

where R is the closest distance to the zone of rupture in kilometers and Z_t is 0 for interface events and 1 for intraslab events.

The four preceding attenuation relationships are shown graphically for earthquake magnitudes 5.5, 6.5, and 7.5 in Figure 3.22. The shapes of the attenuation relationships are similar, despite the fact that they represent different geographic regions and different source mechanisms and use different measures of distance.

Peak Velocity. Regression analysis of PHV data has provided a number of useful relationships describing the attenuation of that parameter. Joyner and Boore (1988), for example, used strong-motion records from earthquakes of moment magnitude between 5.0 and 7.7 to develop the attenuation relationship

$$\log \text{PHV(cm/sec)} = j_1 + j_2(M - 6) + j_3(M - 6)^2 + j_4 \log R + j_5 R + j_6 \quad (3.29)$$

where PHV can be selected as the randomly oriented or larger horizontal component, $R = \sqrt{r_0^2 + j_7^2}$, and r_0 is the shortest distance (in kilometers) from the site to the vertical projection of the earthquake fault rupture on the surface of the earth. The coefficients for the Joyner and Boore (1988) attenuation relationship are given in Table 3-7.

Table 3-7 Coefficients for Joyner and Boore (1988) Peak Horizontal Velocity Attenuation Relationship

Component	j_1	j_2	j_3	j_4	j_5	j_6	j_7	$\sigma_{\log \text{PHV}}$
Random	2.09	0.49	0.0	-1.0	-0.0026	0.17	4.0	0.33
Larger	2.17	0.49	0.0	-1.0	-0.0026	0.17	4.0	0.33

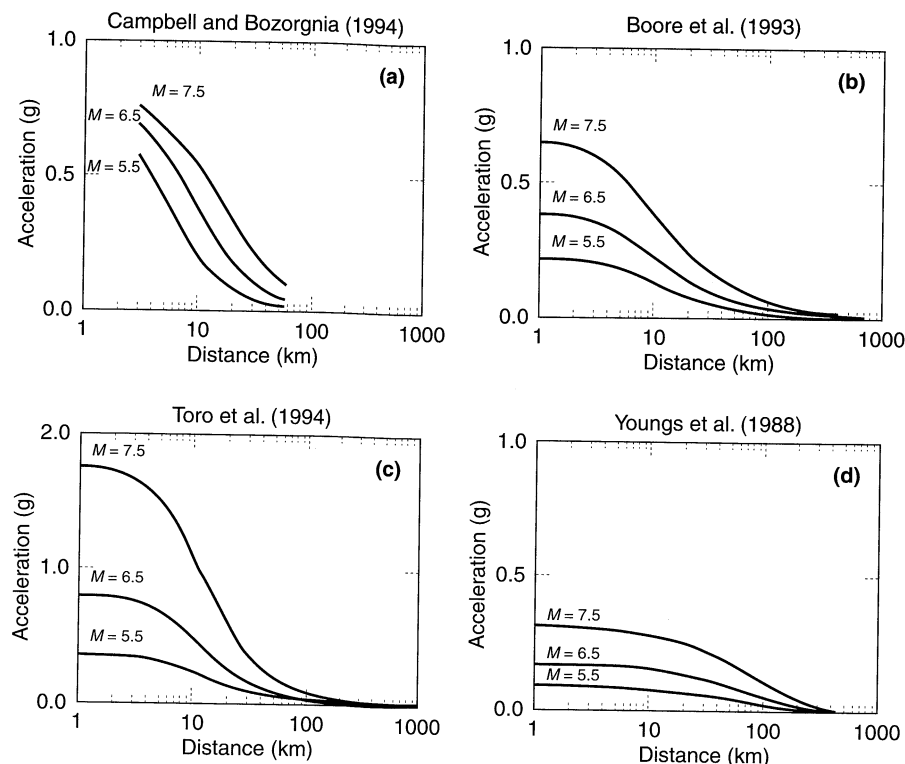


Figure 3.22 Variation of peak horizontal acceleration with distance for $M = 5.5$, $M = 6.5$, and $M = 7.5$ earthquakes according to various attenuation relationships: (a) Campbell and Bozorgnia (1994), soft rock sites and strike-slip faulting; (b) Boore et al. (1993), site class B; (c) Toro et al. (1994); and (d) Youngs et al. (1988), intraslab event.

3.4.4 Estimation of Frequency Content Parameters

Large earthquakes produce larger and longer-period ground motions than do smaller earthquakes; consequently, the frequency content of a ground motion is related to the earthquake magnitude. As seismic waves travel away from a fault, their higher-frequency components are scattered and absorbed more rapidly than are their lower-frequency components. As a result, the frequency content also changes with distance.

3.4.4.1 Predominant Period

One aspect of the change in frequency content with distance involves the shifting of the peak of the Fourier amplitude spectrum to lower frequencies (or higher periods). As a result, the predominant period increases with increasing distance, as illustrated in Figure 3.23.

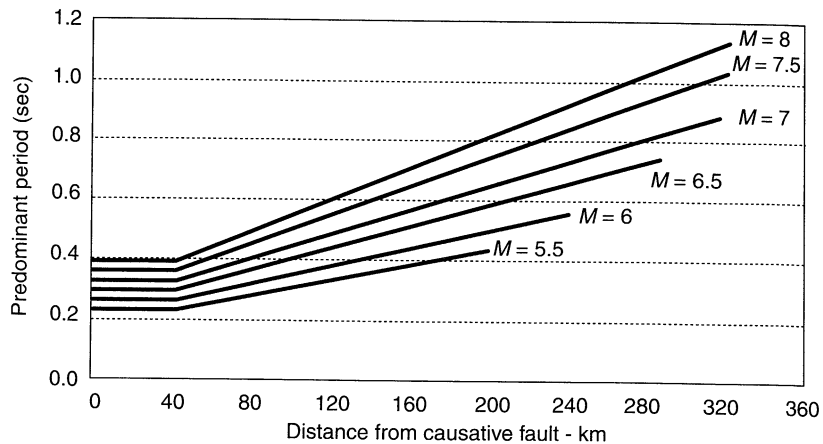


Figure 3.23 Variation of predominant period at rock outcrops with magnitude and distance. (After Seed et al., 1969.)

Example 3.7

Determine the predominant period that would have been expected for the recorded motion at the Gilroy No. 1 (rock) site.

Solution The Gilroy No. 1 (rock) motion was recorded at a site located at an epicentral distance of 21.8 km from the Loma Prieta ($M = 7.1$) earthquake. From Figure 3.23, the expected predominant period would be 0.33 sec. As determined in Example 3.3, the actual predominant period of the Gilroy No. 1 (rock) motion was 0.39 sec.

3.4.4.2 Fourier Amplitude Spectra

Ordinates of the Fourier amplitude spectrum can be estimated empirically by regression on the Fourier spectral ordinates of actual strong-motion data (e.g., Trifunac, 1976; McGuire et al., 1984; Trifunac and Lee, 1987; Castro et al., 1990). Alternatively, a physically based model of source, travel path, and site behavior may be calibrated to predict Fourier amplitude spectra.

Based on Brune's (1970, 1971) solution for instantaneous slip of a circular rupture surface, the Fourier amplitudes for a far-field event at distance R can be expressed (McGuire and Hanks, 1980; Boore, 1983) as

$$|A(f)| = \left[CM_0 \frac{f^2}{1 - (f/f_c)^2} \frac{1}{\sqrt{1 + (f/f_{\max})^8}} \right] \frac{e^{-\pi f R / Q(f) v_s}}{R} \quad (3.30)$$

where f_c is the corner frequency (see Figure 3.14), f_{\max} the cutoff frequency (Figure 3.14), $Q(f)$ is the frequency-dependent *quality factor* (inversely proportional to the damping ratio of the rock; see Section 5.5.1), and C is a constant given by

$$C = \frac{R_{0\phi} FV}{4\pi\rho v_s^3} \quad (3.31)$$

where R_{00} (~ 0.55) accounts for the radiation pattern, F ($= 2$) accounts for the free-surface effect, V ($= \sqrt{2}/2$) accounts for partitioning the energy into two horizontal components, ρ is the density of the rock along the rupture surface, and v_s is the shear wave velocity of the rock.

If f_{\max} is assumed constant for a given geographic region (15 Hz and 40 Hz are typical values for western and eastern North America, respectively), the spectra for different earthquakes are functions of the seismic moment, M_o , and f_c , which can be related (Brune, 1970, 1971) by

$$f_c = 4.9 \times 10^6 v_s \left(\frac{\Delta\sigma}{M_o} \right)^{1/3} \quad (3.32)$$

where v_s is in km/sec, M_o is in dyne-cm, and $\Delta\sigma$ is referred to as the *stress parameter* or *stress drop* in bars. Stress parameters of 50 bars and 100 bars are commonly used for sources in western and eastern North America, respectively. Figure 3.24a shows how the Fourier amplitude spectra predicted by equation (3.30) vary with magnitude. Note the strong influence of magnitude on both the amplitude and frequency content of the motion. As the magnitude increases, the bandwidth increases and the corner frequency decreases, implying that more low-frequency (long-period) motion will occur. Figure 3.24b shows time histories of acceleration generated from the spectra of equation (3.30) for magnitude 4 and magnitude 7 events. The stress parameter and seismic moment are commonly used to specify the *source spectrum*, given by the expression in brackets in equation (3.30). The final expression is the *travel path operator*, which describes attenuation of the Fourier amplitudes as the energy travels away from the site. An expression that describes the effects of soil response (a *site operator*) can be added to equation (3.31), if necessary, to account for near-surface effects. The response of soil deposits during earthquakes is discussed in detail in Chapter 7.

Since it is based on the mechanics of source rupture and wave propagation, equation (3.30) offers significant advantages over purely empirical methods for magnitudes and distances for which few or no data are available.

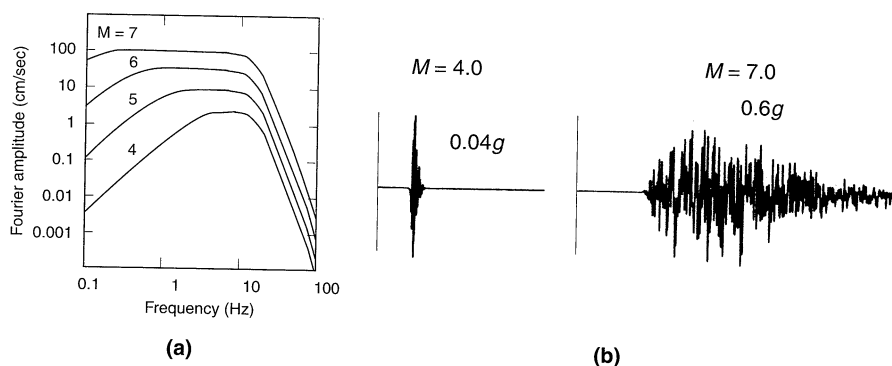


Figure 3.24 (a) Variation of Fourier amplitude spectra at $R = 10$ km for different moment magnitudes ($\Delta\sigma = 100$ bars); (b) accelerograms generated from the $M = 4$ and $M = 7$ spectra. (After Boore, 1983. Used by permission of the Seismological Society of America.)

3.4.4.3 Ratio v_{\max}/a_{\max}

As a measure of the frequency content of a ground motion, the ratio v_{\max}/a_{\max} is also related to earthquake magnitude and distance. This dependence has been studied by several investigators, with a summary of their results provided by McGuire (1978), who proposed the magnitude and distance dependencies shown in Table 3-8. The table indicates that, as expected, the v_{\max}/a_{\max} ratio increases with increasing earthquake magnitude and increasing source-to-site distance.

Table 3-8 Magnitude and Distance Dependence of v_{\max}/a_{\max} ^a

Site Conditions	Magnitude Dependence	Distance Dependence
Rock sites	$e^{0.40M}$	$R^{0.12}$
Soil sites	$e^{0.15M}$	$R^{0.23}$

Source: After McGuire (1978).

^aThe ratio v_{\max}/a_{\max} is proportional to these dependence relationships.

Example 3.8

Estimate the values of v_{\max}/a_{\max} that would be observed at rock and soil sites 40 km from the source of a $M = 6$ earthquake located near the 1989 Loma Prieta earthquake.

Solution Using the values from the Gilroy No. 1 (rock) and Gilroy No. 2 (soil) sites, and recalling that those sites were located 21.8 km and 22.8 km, respectively, from the $M = 7.1$ Loma Prieta earthquake,

$$\text{Rock site: } \frac{v_{\max}}{a_{\max}} \approx 0.078 \sec \frac{e^{(0.40)(6)}}{e^{(0.40)(7.1)}} \frac{40^{0.12}}{21.8^{0.12}} = 0.054 \text{ sec}$$

$$\text{Soil site: } \frac{v_{\max}}{a_{\max}} \approx 0.124 \sec \frac{e^{(0.15)(6)}}{e^{(0.15)(7.1)}} \frac{40^{0.23}}{22.8^{0.23}} = 0.120 \text{ sec}$$

3.4.4.4 Response Spectrum Ordinates

The importance of response spectra in earthquake engineering has led to the development of methods for predicting them directly. For many years, the shapes of all response spectra were, for a given class of soil conditions, assumed to be identical. Design spectra were developed by scaling standard spectral shapes by some ground motion parameter, usually the PHA. As more recorded motions became available, the magnitude dependence of spectral shapes was recognized increasingly. For example, Figure 3.25 shows the response spectra computed from the accelerograms shown in Figure 3.21. The difference in spectral shapes at different magnitudes, particularly in the long-period range, are apparent. This shape dependence was later accounted for, at least approximately, by using PHA, PHV, and peak displacement to scale design spectra in different frequency ranges (Newmark and Hall, 1978, 1982), as discussed in Section 8.3.2. More recently, regression analyses have been used to develop predictive relationships for spectral ordinates at various oscillator periods (e.g., Joyner and Boore, 1982, 1988; Crouse, 1991; Boore et al., 1993).

For example, Boore et al. (1993) determined values of coefficients that when used with equation (3.26), predict pseudospectral velocities for oscillators of different natural periods. These attenuation relationships, the coefficients of which are presented in

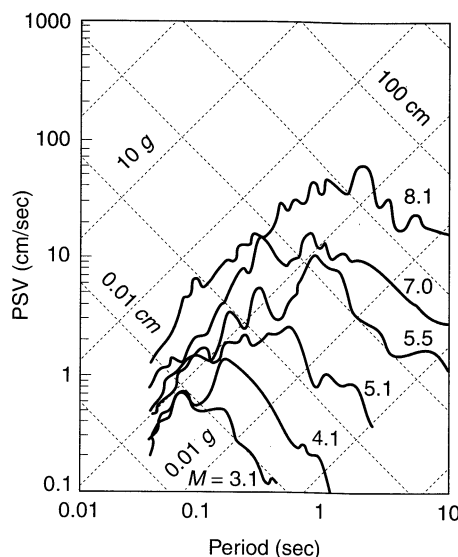


Figure 3.25 Response spectra computed from the accelerograms of Figure 3.20. Epicentral distances from each accelerogram were nearly equal. Note that the shapes, as well as the values, of the spectra vary with earthquake magnitude. (After Anderson, 1991. *Geotechnical News*, Vol. 9, No.1, p.35. Used by permission of BiTech Publishers, Ltd.)

Tables 3-9 and 3-10, are applicable to the same conditions as the attenuation relationship of equation (3.26). These coefficients produce smooth response spectra, as illustrated in Figure 3.26. Although the smooth response spectra are limited to periods of 2.0 sec, their general shapes are similar to those of actual spectra.

3.4.5 Estimation of Duration

The duration of strong ground motion increases with increasing earthquake magnitude. However, the manner in which strong motion duration varies with distance depends on how it is defined. Since acceleration amplitudes decrease with distance, durations based on absolute acceleration levels, such as the bracketed duration, would be expected to decrease with distance; at some distance all accelerations will drop below the threshold acceleration and the bracketed duration will be zero. Page et al. (1972) and Chang and Krinitzsky (1977) confirmed this, as shown in Figure 3.27. Durations based on relative acceleration levels (e.g., Trifunac and Brady, 1975b; Dobry et al., 1978) increase with increasing distance and may have long durations even when the acceleration amplitudes are very low. For engineering purposes, the bracketed duration appears to provide the most reasonable indication of the influence of duration on potential damage.

3.4.6 Estimation of Other Parameters

Parameters that reflect more than one important characteristic of strong ground motion are likely to see increasing use. For most, however, only limited data for the development of predictive relationships are currently available.

Table 3-9 Smoothed Coefficients of Predictive Relationships for the Larger Horizontal Component of 5% Damped PSV

<i>T</i>	<i>b</i> ₁	<i>b</i> ₂	<i>b</i> ₃	<i>b</i> ₄	<i>b</i> ₅	<i>b</i> ₆	<i>b</i> ₇	<i>h</i>	$\sigma_{\log Y}$
0.10	1.700	0.321	-0.104	0.0	-0.921	0.039	0.128	6.18	0.194
0.11	1.777	0.320	-0.110	0.0	-0.929	0.065	0.150	6.57	0.194
0.12	1.837	0.320	-0.113	0.0	-0.934	0.087	0.169	6.82	0.193
0.13	1.886	0.321	-0.116	0.0	-0.938	0.106	0.187	6.99	0.193
0.14	1.925	0.322	-0.117	0.0	-0.939	0.123	0.203	7.09	0.193
0.15	1.956	0.323	-0.117	0.0	-0.939	0.137	0.217	7.13	0.194
0.16	1.982	0.325	-0.117	0.0	-0.939	0.149	0.230	7.13	0.194
0.17	2.002	0.326	-0.117	0.0	-0.938	0.159	0.242	7.10	0.195
0.18	2.019	0.328	-0.115	0.0	-0.936	0.169	0.254	7.05	0.195
0.19	2.032	0.330	-0.114	0.0	-0.934	0.177	0.264	6.98	0.196
0.20	2.042	0.332	-0.112	0.0	-0.931	0.185	0.274	6.90	0.196
0.22	2.056	0.336	-0.109	0.0	-0.926	0.198	0.291	6.70	0.198
0.24	2.064	0.341	-0.105	0.0	-0.920	0.208	0.306	6.48	0.199
0.26	2.067	0.345	-0.101	0.0	-0.914	0.217	0.320	6.25	0.201
0.28	2.066	0.349	-0.096	0.0	-0.908	0.224	0.333	6.02	0.202
0.30	2.063	0.354	-0.092	0.0	-0.902	0.231	0.344	5.79	0.204
0.32	2.058	0.358	-0.088	0.0	-0.897	0.236	0.354	5.57	0.205
0.34	2.052	0.362	-0.083	0.0	-0.891	0.241	0.363	5.35	0.206
0.36	2.045	0.366	-0.079	0.0	-0.886	0.245	0.372	5.14	0.208
0.38	2.038	0.369	-0.076	0.0	-0.881	0.249	0.380	4.94	0.209
0.40	2.029	0.373	-0.072	0.0	-0.876	0.252	0.388	4.75	0.211
0.42	2.021	0.377	-0.068	0.0	-0.871	0.255	0.395	4.58	0.213
0.44	2.013	0.380	-0.065	0.0	-0.867	0.258	0.401	4.41	0.213
0.46	2.004	0.383	-0.061	0.0	-0.863	0.261	0.407	4.26	0.215
0.48	1.996	0.386	-0.058	0.0	-0.859	0.263	0.413	4.11	0.216
0.50	1.988	0.390	-0.055	0.0	-0.856	0.265	0.418	3.97	0.217
0.55	1.968	0.397	-0.048	0.0	-0.848	0.270	0.430	3.67	0.221
0.60	1.949	0.404	-0.042	0.0	-0.842	0.275	0.441	3.43	0.223
0.65	1.932	0.410	-0.037	0.0	-0.837	0.279	0.451	3.23	0.226
0.70	1.917	0.416	-0.033	0.0	-0.833	0.283	0.459	3.08	0.229
0.75	1.903	0.422	-0.029	0.0	-0.830	0.287	0.467	2.97	0.232
0.80	1.891	0.427	-0.025	0.0	-0.827	0.290	0.474	2.89	0.234
0.85	1.881	0.432	-0.022	0.0	-0.826	0.294	0.481	2.85	0.237
0.90	1.872	0.436	-0.020	0.0	-0.825	0.297	0.486	2.83	0.240
0.95	1.864	0.440	-0.018	0.0	-0.825	0.301	0.492	2.84	0.242
1.00	1.858	0.444	-0.016	0.0	-0.825	0.305	0.497	2.87	0.245
1.10	1.849	0.452	-0.014	0.0	-0.828	0.312	0.506	3.00	0.249
1.20	1.844	0.458	-0.013	0.0	-0.832	0.319	0.514	3.19	0.254
1.30	1.842	0.464	-0.012	0.0	-0.837	0.326	0.521	3.44	0.258
1.40	1.844	0.469	-0.013	0.0	-0.843	0.334	0.527	3.74	0.262
1.50	1.849	0.474	-0.014	0.0	-0.851	0.341	0.533	4.08	0.267
1.60	1.857	0.478	-0.016	0.0	-0.859	0.349	0.538	4.46	0.270
1.70	1.866	0.482	-0.019	0.0	-0.868	0.357	0.543	4.86	0.274
1.80	1.878	0.485	-0.022	0.0	-0.878	0.365	0.547	5.29	0.279
1.90	1.891	0.488	-0.025	0.0	-0.888	0.373	0.551	5.74	0.283
2.00	1.905	0.491	-0.028	0.0	-0.898	0.381	0.554	6.21	0.287

Source: After Boore et al., (1993).

Table 3-10 Smoothed Coefficients of Predictive Relationships for the Random Horizontal Component of 5% Damped PSV

<i>T</i>	<i>b</i> ₁	<i>b</i> ₂	<i>b</i> ₃	<i>b</i> ₄	<i>b</i> ₅	<i>b</i> ₆	<i>b</i> ₇	<i>h</i>	$\sigma_{\log Y}$
0.10	1.653	0.327	-0.098	0.0	-0.934	0.046	0.136	6.27	0.208
0.11	1.725	0.318	-0.100	0.0	-0.937	0.071	0.156	6.65	0.208
0.12	1.782	0.313	-0.101	0.0	-0.939	0.093	0.174	6.91	0.208
0.13	1.828	0.309	-0.101	0.0	-0.939	0.111	0.191	7.08	0.209
0.14	1.864	0.307	-0.100	0.0	-0.938	0.127	0.206	7.18	0.209
0.15	1.892	0.305	-0.099	0.0	-0.937	0.140	0.221	7.23	0.211
0.16	1.915	0.305	-0.098	0.0	-0.935	0.153	0.234	7.24	0.211
0.17	1.933	0.305	-0.096	0.0	-0.933	0.163	0.246	7.21	0.212
0.18	1.948	0.306	-0.094	0.0	-0.930	0.173	0.258	7.16	0.213
0.19	1.959	0.308	-0.092	0.0	-0.927	0.182	0.269	7.10	0.215
0.20	1.967	0.309	-0.090	0.0	-0.924	0.190	0.279	7.02	0.215
0.22	1.978	0.313	-0.086	0.0	-0.918	0.203	0.297	6.83	0.218
0.24	1.982	0.318	-0.082	0.0	-0.912	0.214	0.314	6.62	0.220
0.26	1.982	0.323	-0.078	0.0	-0.906	0.224	0.329	6.39	0.222
0.28	1.979	0.329	-0.073	0.0	-0.899	0.232	0.343	6.17	0.225
0.30	1.974	0.334	-0.070	0.0	-0.893	0.239	0.356	5.94	0.226
0.32	1.967	0.340	-0.066	0.0	-0.888	0.245	0.367	5.72	0.228
0.34	1.959	0.345	-0.062	0.0	-0.882	0.251	0.378	5.50	0.230
0.36	1.950	0.350	-0.059	0.0	-0.877	0.256	0.387	5.30	0.232
0.38	1.940	0.356	-0.055	0.0	-0.872	0.260	0.396	5.10	0.235
0.40	1.930	0.361	-0.052	0.0	-0.867	0.264	0.405	4.91	0.236
0.42	1.920	0.365	-0.049	0.0	-0.862	0.267	0.413	4.74	0.238
0.44	1.910	0.370	-0.047	0.0	-0.858	0.271	0.420	4.57	0.239
0.46	1.900	0.375	-0.044	0.0	-0.854	0.273	0.427	4.41	0.241
0.48	1.890	0.379	-0.042	0.0	-0.850	0.276	0.433	4.26	0.243
0.50	1.881	0.384	-0.039	0.0	-0.846	0.279	0.439	4.13	0.244
0.55	1.857	0.394	-0.034	0.0	-0.837	0.284	0.452	3.82	0.248
0.60	1.835	0.403	-0.030	0.0	-0.830	0.289	0.464	3.57	0.251
0.65	1.815	0.411	-0.026	0.0	-0.823	0.293	0.474	3.36	0.254
0.70	1.797	0.418	-0.023	0.0	-0.818	0.297	0.483	3.20	0.257
0.75	1.781	0.425	-0.020	0.0	-0.813	0.300	0.490	3.07	0.259
0.80	1.766	0.431	-0.018	0.0	-0.809	0.303	0.497	2.98	0.261
0.85	1.753	0.437	-0.016	0.0	-0.805	0.306	0.503	2.92	0.264
0.90	1.742	0.442	-0.015	0.0	-0.802	0.309	0.508	2.89	0.266
0.95	1.732	0.446	-0.014	0.0	-0.800	0.312	0.513	2.88	0.268
1.00	1.724	0.450	-0.014	0.0	-0.798	0.314	0.517	2.90	0.270
1.10	1.710	0.457	-0.013	0.0	-0.795	0.319	0.523	2.99	0.274
1.20	1.701	0.462	-0.014	0.0	-0.794	0.324	0.528	3.14	0.277
1.30	1.696	0.466	-0.015	0.0	-0.793	0.328	0.532	3.36	0.280
1.40	1.695	0.469	-0.017	0.0	-0.794	0.333	0.535	3.62	0.283
1.50	1.696	0.471	-0.019	0.0	-0.796	0.338	0.537	3.92	0.285
1.60	1.700	0.472	-0.022	0.0	-0.798	0.342	0.538	4.26	0.286
1.70	1.706	0.473	-0.025	0.0	-0.801	0.347	0.539	4.62	0.289
1.80	1.715	0.472	-0.029	0.0	-0.804	0.351	0.539	5.01	0.290
1.90	1.725	0.472	-0.032	0.0	-0.808	0.356	0.538	5.42	0.292
2.00	1.737	0.471	-0.037	0.0	-0.812	0.360	0.537	5.85	0.293

Source: After Boore et al., (1993).

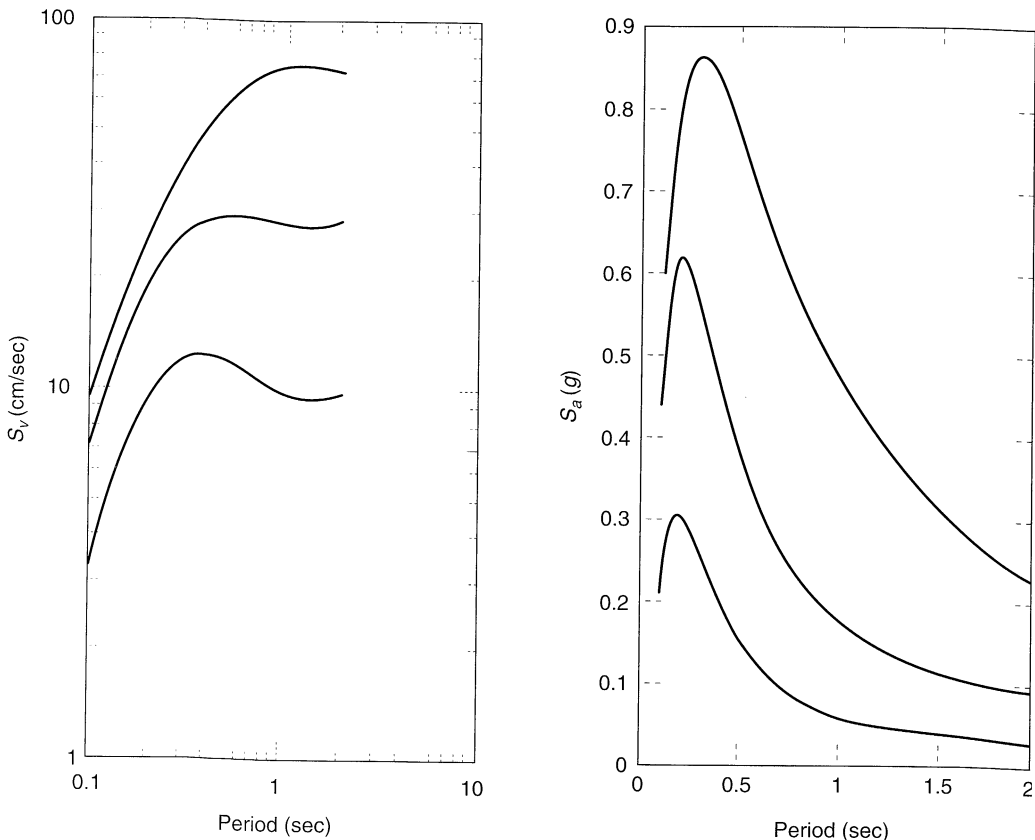


Figure 3.26 Response spectra for the random component of ground motion at a site class B site at $R = 10$ km according to the predictive relationship of Boore et al. (1993): (a) pseudospectral velocity computed directly from equation (3.27) and Table 3-10, and (b) pseudospectral acceleration computed from the pseudospectral velocities.

3.4.6.1 RMS Acceleration

Hanks and McGuire (1981) used a database of California earthquakes of local magnitude 4.0 to 7.0 to develop an attenuation relationship for rms acceleration for hypocentral distances between 10 and 100 km (6.2 and 62 mi):

$$a_{\text{rms}} = 0.119 \frac{\sqrt{f_{\max}/f_c}}{R} \quad (3.33)$$

where f_c is the corner frequency, f_{\max} is the cutoff frequency, and R is in kilometers.

Kavazanjian et al. (1985) used the definition of duration proposed by Vanmarcke and Lai (1980) with a database of 83 strong motion records from 18 different earthquakes to obtain

$$a_{\text{rms}} = 0.472 + 0.268M_w + 0.129 \log\left(\frac{0.966}{R^2} + \frac{0.255}{R}\right) - 0.1167R \quad (3.34)$$

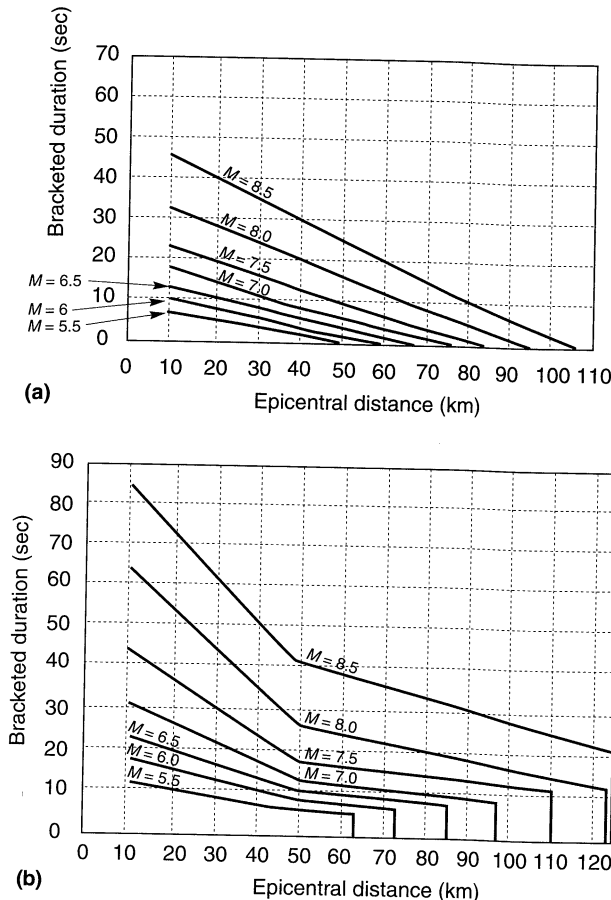


Figure 3.27 Variation of bracketed duration (0.05g threshold) with magnitude and epicentral distance: (a) rock sites; (b) soil sites. (After Chang and Krinitzsky, 1977.)

where R is the distance to the closest point of rupture on the fault. The database was restricted to $M_w > 5$, $R < 110$ km (68 mi), rupture depths less than 30 km (19 mi), and soil thicknesses greater than 10 m (33 ft).

3.4.6.2 Arias Intensity

Campbell and Duke (1974) used data from California earthquakes to predict the variation of Arias intensity within 15 to 110 km (9 to 68 mi) of magnitude 4.5 to 8.5 events.

$$I_a \text{ (m/sec)} = 313 \frac{e^{M_s(0.33M_s - 1.47)}}{R^{3.79}} S \quad (3.35)$$

$$\text{where } S = \begin{cases} 0.57R^{0.46} & \text{for basement rock} \\ 1.02R^{0.51} & \text{for sedimentary rock} \\ 0.37R^{0.81} & \text{for alluvium } \leq 60\text{ft thick} \\ 0.65R^{0.74} & \text{for alluvium } > 60\text{ft thick} \end{cases}$$

and R is the distance from the center of energy release in kilometers.

Wilson (1993) analyzed strong motion records from California to develop an attenuation relationship which, using the Arias intensity definition of equation (3.17), can be expressed as

$$\log I_a (\text{m/sec}) = M_w - 2\log R - kR - 3.990 + 0.365(1-P) \quad (3.36)$$

where $R = \sqrt{D^2 + h^2}$, D is the minimum horizontal distance to the vertical projection of the fault plane, h is a correction factor (with a default value of 7.5 km (4.7 mi)), k is a coefficient of anelastic absorption (with a default value of zero), and P is the exceedance probability.

Acceleration and Velocity Spectrum Intensities. Von Thun et al. (1988) used 30 strong motion records, primarily from rock outcrops in the western United States and Italy, to develop the attenuation relationships for acceleration spectrum intensity and velocity spectrum intensity shown graphically in Figure 3.28. Large earthquakes in these areas are generally accompanied by surface faulting. The use of these attenuation relationships is recommended only for areas with similar tectonic conditions.

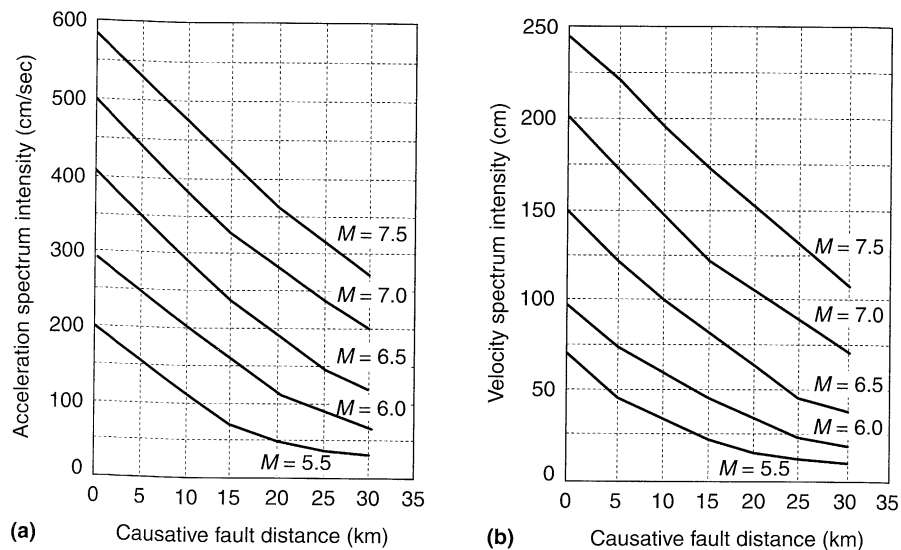


Figure 3.28 Attenuation of (a) acceleration spectrum intensity and (b) velocity spectrum intensity. (After Von Thun et al., 1988. Earthquake ground motions for design and analysis of dams, *Earthquake Engineering and Soil Dynamics II*. Reprinted by permission of ASCE.)

3.5 SPATIAL VARIABILITY OF GROUND MOTIONS

The preceding sections considered the spatial variation of ground motions on a regional scale. Ground motions also vary spatially on local scales, and this local variation can be important for certain types of structures. The longest dimension of most structures is usually small enough that the ground motion at one end is virtually the same as that at the other end. For structures such as bridges and pipelines that extend over considerable distances, different ground motions may occur beneath different parts of the structure. In such cases the

local spatial variation (or *incoherence*) of the ground motion may exert an important influence on the response of the structure.

Spatial incoherence can be caused by a number of factors. One is the traveling-wave or *wave-passage effect*, in which nonvertical waves reach different points on the ground surface at different times, producing a time shift between the motions at those points (Figure 3.29a). A cause of incoherence in the nearfield is the *extended source effect*, in which differences in the relative geometry of the source and sites produce different time shifts, and consequently different motions, at the sites (Figure 3.29b). Finally, *ray-path effects* caused by scattering (reflection, refraction, etc.) of waves by inhomogeneities along the travel path (Figure 3.30c) can cause incoherence.

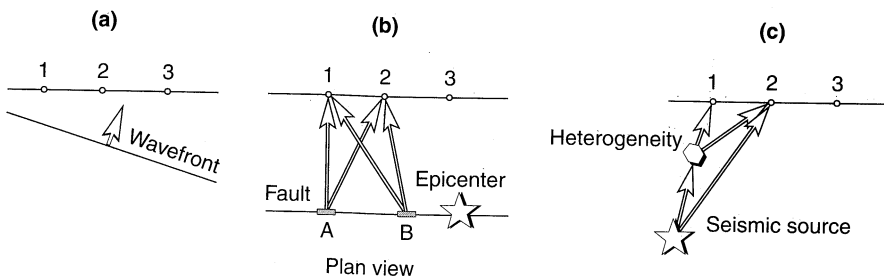


Figure 3.29 Sources of incoherent ground motions: (a) wave-passage effect causes inclined wavefront to reach locations 1, 2, and 3 at different times; (b) extended source effect causes waves due to rupture at A and B to reach points 1 and 2 at different times; (c) scattering of waves by heterogeneity causes different waves to arrive at different locations at different times. (After Abrahamson, 1991.)

The similarity between ground motions at different locations can be described in the time domain or the frequency domain. Consider two points j and k at which accelerograms $a_j(t)$ and $a_k(t)$ are recorded. The similarity of the motions can be described in the time domain by the *cross covariance*

$$C_{jk}(\tau) = \sum_{i=1}^N a_j(t_i)a_k(t_i + \tau) \quad (3.37)$$

where τ is a time increment and N is the number of time samples. The *autocovariance*, C_{jj} (or C_{kk}), is obtained by analyzing the covariance of an accelerogram against itself. The maximum value of the autocovariance will, obviously, correspond to a value of $\tau = 0$. The similarity of the motions in the frequency domain can be described by the *coherency*

$$\gamma_{jk}(\omega) = \frac{S_{jk}(\omega)}{\sqrt{S_{jj}(\omega)S_{kk}(\omega)}} \quad (3.38)$$

where the smoothed cross-spectrum, $S_{jk}(\omega)$, is the Fourier transform of the cross-covariance and the autospectra, $S_{jj}(\omega)$ and $S_{kk}(\omega)$, are the Fourier transforms of the autocovariances, $C_{jj}(\tau)$ and $C_{kk}(\tau)$. The coherency describes the degree of positive or negative correlation between the amplitudes and phase angles of two time histories at each of their component frequencies. A value of 1 indicates full coherence (or perfect correlation), while a value of

zero indicates full incoherence (or no correlation). The modulus of the coherency (the square root of the sum of the squares of the real and imaginary parts) is called the *lagged coherency*. Because the wave passage effect from a point source simply introduces a phase shift at each frequency, it does not influence the lagged coherency.

Ground motions recorded by dense arrays show that coherency decreases with increasing distance between measuring points and with increasing frequency, as shown in Figure 3.30. Measured coherency functions from dense arrays in California and Japan are similar to those from the SMART-1 array, suggesting that they may be applicable to other areas as well, although research in this area is continuing (Abrahamson, 1991). Smooth analytical coherency functions (coherency as a function of separation distance and frequency) that match the most significant trends in measured coherency functions have been proposed (Haricharan and Vanmarcke, 1986; Luco and Wong, 1986; Hao et al., 1989; Abrahamson et al., 1991).

3.6 SUMMARY

1. Complete description of a strong ground motion involves three components of translation and three components of rotation. In practice, only the translational components are usually measured, and they are usually measured in orthogonal directions.
2. A number of different instruments can be used for strong-motion measurement. Each has its own dynamic response characteristics that determine the conditions for which it is best suited. Older strong-motion instruments are likely to acquire data in analog form, while newer instruments often acquire data digitally.
3. Raw strong-motion data may include errors from several sources that require correction to produce accurate strong motion records. Strong motion processing is often required to minimize background noise, correct for the dynamic response of the transducer, and to correct for measurement errors.
4. Strong ground motions can be quite complicated, and their complete description involves a large amount of data. For engineering purposes, the essential characteristics of a strong ground motion can be described in much more compact form using ground motion parameters.
5. From an earthquake engineering standpoint, the most important characteristics of a strong ground motion are the amplitude, frequency content, and duration. All of these characteristics can significantly influence earthquake damage. Consequently, knowledge of the amplitude, frequency content, or duration alone may not be sufficient to describe accurately the damage potential of a ground motion.
6. A variety of parameters are available for description of strong ground motions. Some of these parameters describe ground motion amplitude, some describe frequency content, and others describe duration. Other parameters reflect two or more of these important characteristics. More than one parameter is generally required to characterize a strong ground motion.
7. Commonly used amplitude parameters include peak acceleration, peak velocity, and peak displacement. The peak acceleration provides a good indication of the high-frequency component of a ground motion. The peak velocity and peak displacement describe the amplitudes of the intermediate- and low-frequency components, respectively.

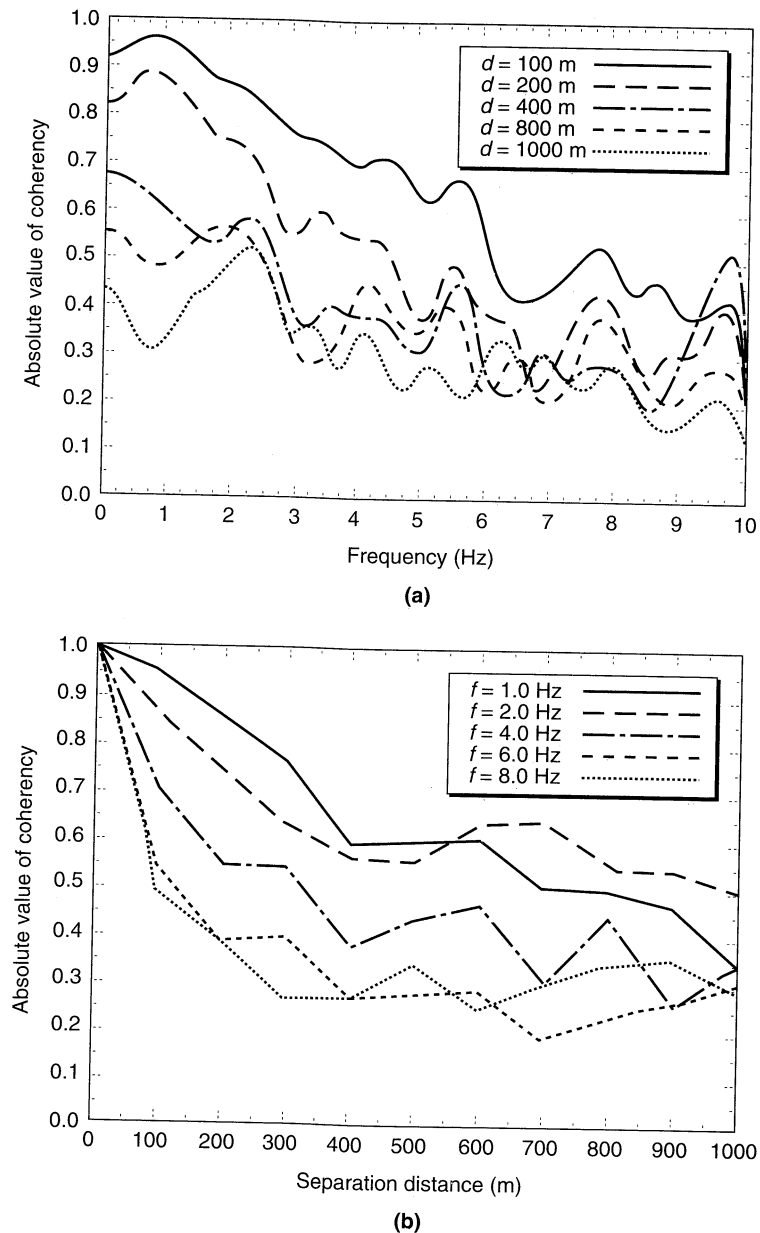


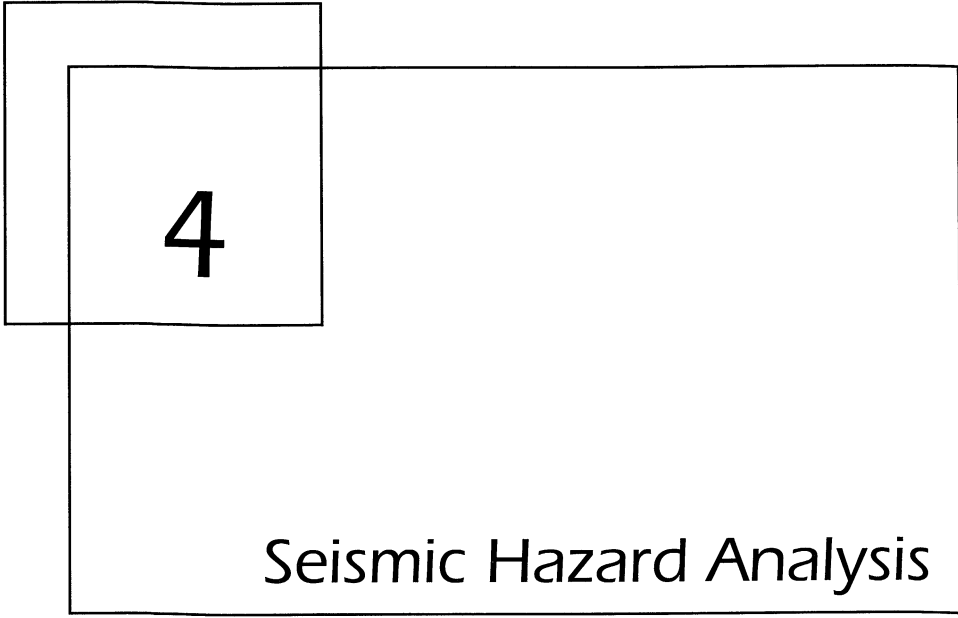
Figure 3.30 Measured decay of coherency with increasing frequency and separation distance for $M = 6.9$ event at hypocentral depth of 30.6 km and epicentral distance of 116.6 km from SMART-1 dense array at Lotung, Taiwan. (After Haricharan and Vanmarcke, 1986. Stochastic variation of earthquake ground motion in space and time, *Journal of Engineering Mechanics*, Vol. 112, No. 2. Reprinted by permission of ASCE.)

8. The frequency content of a strong ground motion is generally described through the use of different types of spectra. Fourier spectra and power spectra directly illustrate the frequency content of the motion itself. Response spectra reflect the influence of the ground motion on structures of different natural periods. A variety of spectral parameters are available to describe the frequency content of a strong ground motion.
9. Strong-motion durations can be described in absolute or relative terms. The bracketed duration, defined as the time between the first and last exceedances of a threshold acceleration, is based on an absolute measure of acceleration (the threshold acceleration). Measures of duration based on relative ground motion levels can define very long durations for weak ground motions. For engineering purposes, the bracketed duration is most commonly used.
10. Some parameters reflect the amplitude, frequency content, and duration of a strong ground motion. Although these parameters, such as rms acceleration, Arias intensity, and response spectrum intensity, may be more difficult to calculate than parameters more commonly used, they often reflect the potential of the motion to produce damage more accurately.
11. The characteristics of a ground motion at a particular site depend on earthquake magnitude and on the distance between the source of the earthquake and the site. Consequently, ground motion parameters also vary with earthquake magnitude and source-to-site distance.
12. Measured ground motion data have been used to develop relationships that predict values of ground motion parameters as functions of earthquake magnitude and source-to-site distance. Predictive relationships are generally empirical; each is obtained by regression on a specific set of data. Consequently, each predictive relationship is appropriate for conditions that are consistent with the conditions of the database.
13. Predictive relationships are not precise; they typically express the mean value of a ground motion parameter and include a measure of the distribution of values about the mean. The standard deviation of the parameter (or the natural logarithm of the parameter) is usually estimated in the development of the predictive relationship.
14. Predictive relationships for variables that decrease with increasing source-to-site distance are frequently referred to as attenuation relationships. Many attenuation relationships have been reported in the literature, and the most commonly used relationships are updated every few years.
15. Ground motions vary on local as well as regional scales. Local variations may cause differential movements of the supports of long structures such as bridges and pipelines. Design and analysis of such structures may require consideration of local variations.
16. The local variability of ground motions is usually expressed in terms of coherency. The coherency of two ground motions can be computed—it is a measure of the correlation of the amplitudes and phase angles of the motions at different frequencies. The coherency of two closely spaced ground motions is higher than that of two distant ground motions. Also, the coherency of the low-frequency (long-wavelength) components of a pair of motions is higher than that of the high-frequency (short-wavelength) components.

HOMEWORK PROBLEMS

Strong motion records can be obtained from a variety of sources over the Internet, often by anonymous ftp. Download the strong motion record indicated by your instructor and use it to solve Problems 3.1 - 3.6. The use of a mathematical analysis program such as MATLAB is highly recommended; it will greatly simplify the required computations.

- 3.1** Plot the time history of acceleration and determine:
 - (a) The peak acceleration.
 - (b) The sustained maximum acceleration (3rd cycle and 5th cycle).
 - (c) The bracketed duration.
- 3.2** Integrate the time history of acceleration to produce time histories of velocity and displacement. Plot the time histories of velocity and displacement and determine the peak velocity and peak displacement.
- 3.3** Compute and plot the Fourier amplitude spectrum of the strong motion record.
- 3.4** Determine the predominant period of the strong motion record.
- 3.5** Compute the rms acceleration for the strong motion record.
- 3.6** Compute the Arias intensity for the strong motion record.
- 3.7** Determine and plot the variations of peak horizontal acceleration with distance for a $M_w = 6.5$ earthquake using the attenuation relationship of Campbell (1981).
- 3.8** Determine and plot the variations of peak horizontal acceleration with distance for a $M_w = 6.5$ earthquake at soft rock, hard rock, and alluvium sites using the attenuation relationship of Campbell and Bozorgnia (1994). Which of these conditions agrees best with the attenuation relationship of Campbell (1981)?
- 3.9** Using the attenuation relationship of Toro et al. (1994), determine the probability that a $M_w = 7$ earthquake in mid-continent eastern North America would produce a peak acceleration greater than 0.30 g at a point located 50 km from the closest point of rupture.
- 3.10** Determine the peak horizontal velocity that would have a 10% probability of being exceeded by a $M_w = 7.5$ earthquake occurring at a distance of 40 km. Use the Joyner and Boore (1988) attenuation relationship.
- 3.11** Using the Boore et al. (1994) attenuation relationship, determine and plot the mean and mean \pm one standard deviation response spectra for a $M_w = 6.75$ earthquake that occurs at a distance of 70 km.
- 3.12** Determine the values of Arias intensity that have 10%, 25%, 50%, 75%, and 90% probabilities of being exceeded by a $M_w = 7.25$ earthquake at a distance of 45 km. Use the attenuation relationship of Wilson (1993) with zero anelastic absorption.



4

Seismic Hazard Analysis

4.1 INTRODUCTION

In many areas of the world, the threat to human activities from earthquakes is sufficient to require their careful consideration in the design of structures and facilities. The goal of *earthquake-resistant design* is to produce a structure or facility that can withstand a certain level of shaking without excessive damage. That level of shaking is described by a *design ground motion*, which can be characterized by *design ground motion parameters*. The specification of design ground motion parameters is one of the most difficult and most important problems in geotechnical earthquake engineering.

Much of the difficulty in design ground motion specification results from its unavoidable reliance on subjective decisions that must be made with incomplete or uncertain information. These decisions largely revolve around the definition of the boundary between acceptable and excessive damage, and uncertainty in the size, time, and location of future earthquakes. If very little damage is acceptable, a relatively strong level of shaking must be designed for, and the measures required to resist that shaking can be quite expensive. If greater levels of damage are tolerable, lower design levels of shaking may be considered and the resulting design will be less expensive. Obviously, there are trade-offs between the short-term cost of providing an earthquake-resistant design and the potential long-term cost (which, for many structures, may never be realized) of earthquake-induced damage.

Seismic hazard analyses involve the quantitative estimation of ground-shaking hazards at a particular site. Seismic hazards may be analyzed deterministically, as when a particular earthquake scenario is assumed, or probabilistically, in which uncertainties in earthquake size, location, and time of occurrence are explicitly considered. Although seismic hazard analysis is a critical part of the development of design ground motions, it is not the only part. This chapter presents different methods for analysis of seismic hazards; the broader problem of design ground motions is addressed in Chapter 8.

4.2 IDENTIFICATION AND EVALUATION OF EARTHQUAKE SOURCES

To evaluate seismic hazards for a particular site or region, all possible sources of seismic activity must be identified and their potential for generating future strong ground motion evaluated. Identification of seismic sources requires some detective work; nature's clues, some of which are obvious and others quite obscure, must be observed and interpreted.

The availability of modern seismographs and seismographic networks has made observation and interpretation of current earthquakes rather convenient. The occurrence of a large earthquake is now recorded by hundreds of seismographs around the world. Within hours, seismologists are able to determine its magnitude, locate its rupture surface, and even evaluate source parameters. In the 1990s, it is virtually impossible for a significant earthquake anywhere in the world to go undetected.

The current ability to identify and locate all earthquake sources is a relatively recent development, particularly when compared with the time scales on which large earthquakes usually occur. The fact that no strong motions have been instrumentally recorded in a particular area does not guarantee that they have not occurred in the past or that they will not occur in the future. In the absence of an instrumental seismic record, other clues of earthquake activity must be uncovered. These may take the form of geologic and tectonic evidence, or historical (preinstrumental) seismicity.

4.2.1 Geologic Evidence

The theory of plate tectonics assures us that the occurrence of earthquakes is written in the geologic record, primarily in the form of offsets, or relative displacements, of various strata. Study of the geologic record of past earthquake activity is called *paleoseismology* (Wallace, 1981). In some parts of the world, this geologic record is easily accessible and relatively easily interpreted by the trained seismic geologist. In other locations, however, the geologic record may be very complex or it may be hidden by thick layers of recent sediments that have not been displaced by seismic activity. The identification of seismic sources from geologic evidence is a vital, though often difficult part of a seismic hazard analysis.

The search for geologic evidence of earthquake sources centers on the identification of faults. A variety of tools and techniques are available to the geologist, including the review of published literature; interpretation of air photos and remote sensing (e.g., infrared photograph) imagery; field reconnaissance including logging of trenches (Figure 4.1); test pits and borings; and geophysical techniques. Criteria for identification of faults are described in numerous textbooks on structural geology, field geology and geomorphology (Adair, 1979). The following list of features that suggest faulting is that of Reiter (1990):

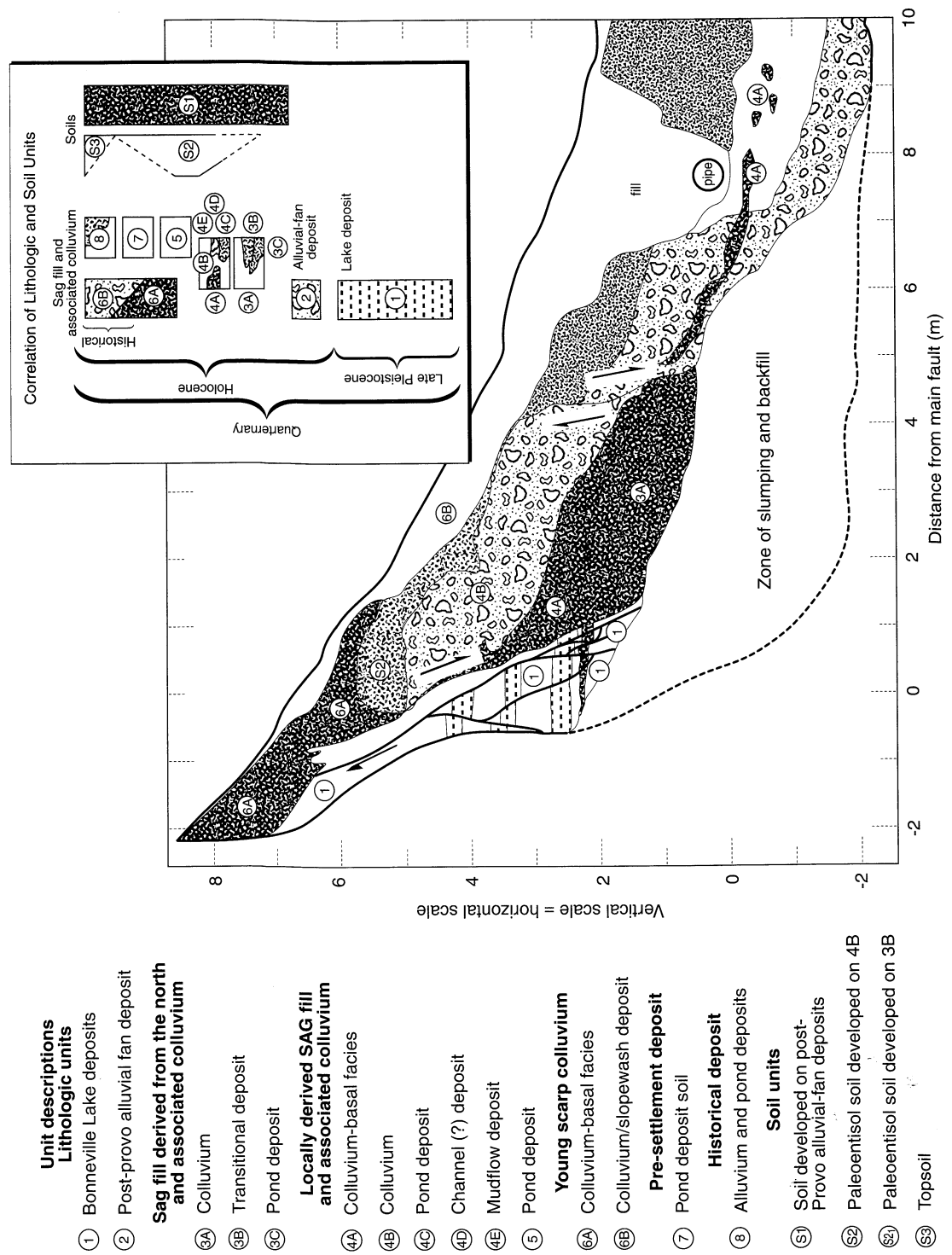


Figure 4.1 Trench log across the Wasatch fault near Kaysville, Utah. Colluvial units 3A, 4A/4B/S2, and 6A are three separate deposits. Each resulted from erosion of the scarp produced by a surface-faulting earthquake. (After Swan et al., 1980; Schwartz, 1988.)

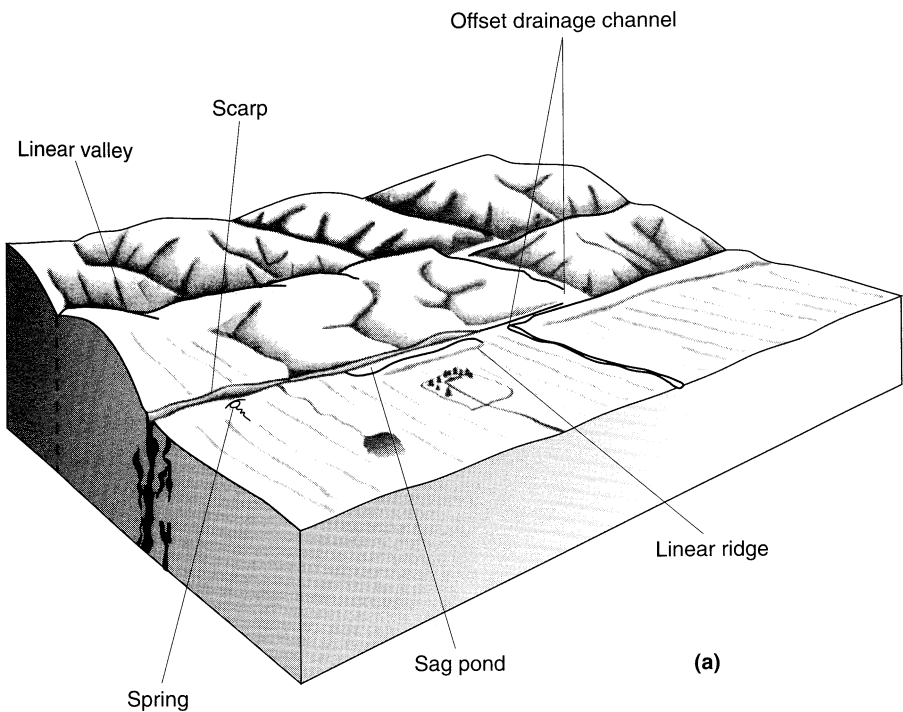
1. Directly observable fracture surfaces and indicators of fracturing. These include disruption of the ground surface and evidence of the movement and grinding of the two sides of the fault (*slickensides*, *fault gouge*, and *fault breccia*).
2. Geologically mappable indicators. These include the juxtaposition of dissimilar materials, missing or repeated strata and the truncation of strata or structures.
3. Topographic and *geomorphic* (surface landform) indicators [Figure 4.2]. These include topographic scarps or triangular facets on ridges, offset streams or drainage, tilting or changes in elevation of terraces or shorelines, *sag ponds* (water ponded by depressions near strike-slip faults) and anomalous stream gradients.
4. Secondary geologic features. These include abrupt changes in groundwater levels, gradients, and chemical composition, alignment of springs or volcanic vents and the presence of hot springs.
5. Lineaments on remote sensing imagery. These may be caused by topography, vegetation, or tonal contrasts.
6. Geophysical indicators of subsurface faulting. These include steep linear gravity or magnetic gradients, differences in seismic wave velocities, and offset of seismic reflection horizons.
7. Geodetic indicators. These include fault movement appearing in geodetic surveys as tilting and changes in the distance between fixed points.

4.2.1.1 Fault Activity

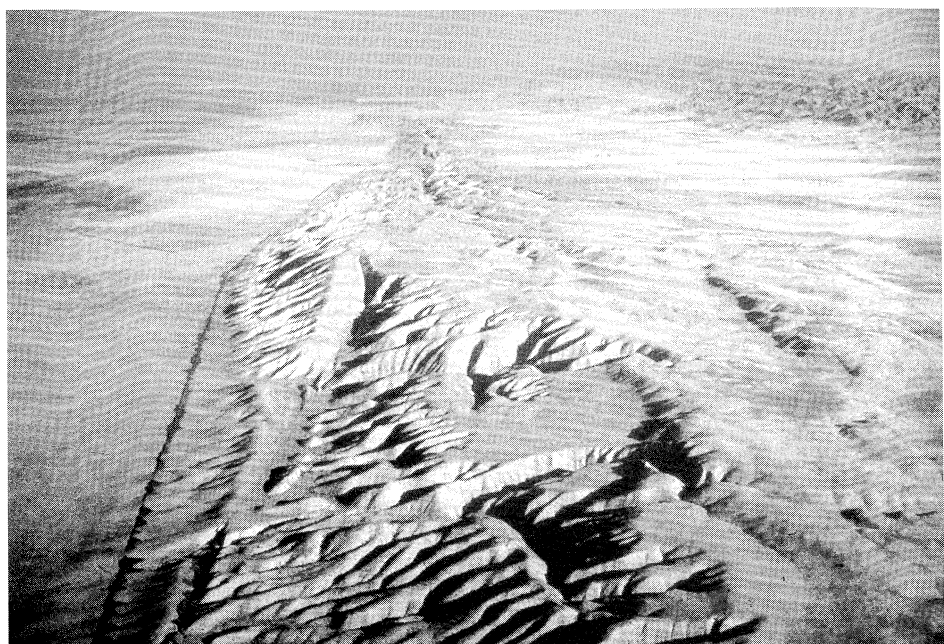
The mere presence of a fault, however, does not indicate the likelihood of future earthquakes. The notion of *fault activity* is important and has been a topic of considerable discussion and controversy over the years. Although there is general agreement concerning the use of the terms *active fault* to describe a fault that poses a current earthquake threat and *inactive fault* to describe one on which past earthquake activity is unlikely to be repeated, there is no consensus as to how fault activity should be evaluated.

Formal definitions of fault activity are important because they often trigger legal requirements for special investigations or special design provisions. However, there are wide variations in the criteria for fault activity in the commonly used definitions. Slemmons and McKinney (1977), for example, found 31 different definitions of the term *active fault*. Most were based on the elapsed period of time since the most recent fault movement. The California Division of Mines and Geology defines an active fault as one that has produced surface displacement within Holocene time (approximately the past 10,000 years). For dams, the U.S. Army Corps of Engineers has used a time period of 35,000 years, and the U.S. Bureau of Reclamation has used 100,000 years (Idriss, 1985). The U.S. Nuclear Regulatory Commission (*Code of Federal Regulations*, 1978), on the other hand, has used the term *capable fault* (rather than active fault) for those that exhibit

1. movement at or near the ground surface at least once within the past 35,000 years or movement of a recurring nature within the past 500,000 years;
2. macroseismicity instrumentally determined with records of sufficient precision to demonstrate a direct relationship with the fault; or



(a)



(b)

Figure 4.2 Typical terrain in the vicinity of a fault (a) showing topographic and geomorphic indicators of faulting (After Wesson et al., 1975.) and (b) an aerial view of such terrain along the San Andreas fault in the Carrizo Plain (photo by Robert Wallace; used by permission of U.S. Geological Survey.)

3. a structural relationship to a capable fault according to characteristics (1) or (2) above, such that movement on one could reasonably be expected to be accompanied by movement on the other.

Actually, the specification of fault activity by specific time intervals is not very realistic (Cluff et al., 1972; Cluff and Cluff, 1984); faults do not suddenly become inactive on the 10,000th or 35,000th anniversary of their last movement. Rather, fault activity is relative and can change as faults move from active to inactive states over geologic time. Cluff and Cluff (1984) suggested six classes (and five subclasses) of fault activity based on characteristics such as slip rate, slip per event, rupture length, earthquake size, and recurrence interval. Approaches of this type offer a more satisfying framework for characterization of fault activity but can be difficult to implement in the political and economic environment in which many seismic hazard analyses are conducted.

4.2.1.2 Magnitude Indicators

Geologic evidence can also be used to estimate the magnitude of past earthquakes by correlating observed deformation characteristics with the known magnitudes of recorded earthquakes. Studies of worldwide earthquakes have shown that faults do not rupture over their entire lengths or areas during individual events. Instead, individual fault segments with physically controlled boundaries (Schwartz and Coppersmith, 1986; Schwartz, 1988) rupture repeatedly. Rupture length, rupture area, and fault displacement can be evaluated by postearthquake, field geological investigations. Correlation of magnitude with such quantities involves regression on limited data sets and, consequently, produces an estimate of the expected value of the magnitude. The uncertainty in these estimates, which can be considerable, must be recognized when applying them.

Fault rupture length has often been used to estimate earthquake magnitude. A number of studies (e.g., Tocher, 1958; Bonilla and Buchanan, 1970; Mark and Bonilla, 1977; Slemmons, 1977, 1982; Acharaya, 1979; Chen, 1984; Bonilla et al., 1984; Wells and Coppersmith, 1994) have illustrated the general nature of the relationship between fault rupture length and magnitude. Estimation of magnitude based on fault rupture length does not account for variations in the width of the rupture surface; rupture length methods are best suited to cases in which the rupture surface is fairly narrow, typically less than about 20 km (12.4 mi) (Bonilla et al., 1984). Obviously, they are not useful for cases in which rupture does not extend to the ground surface. Fault rupture area, by virtue of its relationship to seismic moment, would appear to be more fundamentally related to magnitude than fault rupture length alone. Indeed, for faults of width greater than about 20 km (12.4 mi), magnitudes are more closely correlated to fault rupture area than are any other parameter (Wyss, 1979; Wells and Coppersmith, 1994). Although the average fault displacement is used to evaluate the seismic moment, the unavailability of fault displacement measurements over an entire rupture surface renders its determination impossible. Instead, maximum surface displacements (Slemmons, 1982; Wells and Coppersmith, 1994) have been correlated to magnitude. Empirical relationships based on statistical analyses of worldwide historical earthquake data are presented in Table 4-1 and Figure 4.3.

The relationships in Table 4-1 can be used to predict mean values of the dependent variables (M_w , $\log L$, $\log A$, and $\log D$); the standard deviations of the dependent variables can be used (see Appendix C) to compute values other than the mean.

Table 4-1 Empirical Relationships between Moment Magnitude, M_w , Surface Rupture Length, L (km), Rupture Area, A (km^2), and Maximum Surface Displacement, D (m)

Fault Movement	Number of Events	Relationship	σ_{M_w}	Relationship	$\sigma_{\log L, A, D}$
Strike slip	43	$M_w = 5.16 + 1.12 \log L$	0.28	$\log L = 0.74M_w - 3.55$	0.23
Reverse	19	$M_w = 5.00 + 1.22 \log L$	0.28	$\log L = 0.63M_w - 2.86$	0.20
Normal	15	$M_w = 4.86 + 1.32 \log L$	0.34	$\log L = 0.50M_w - 2.01$	0.21
All	77	$M_w = 5.08 + 1.16 \log L$	0.28	$\log L = 0.69M_w - 3.22$	0.22
Strike Slip	83	$M_w = 3.98 + 1.02 \log A$	0.23	$\log A = 0.90M_w - 3.42$	0.22
Reverse	43	$M_w = 4.33 + 0.90 \log A$	0.25	$\log A = 0.98M_w - 3.99$	0.26
Normal	22	$M_w = 3.93 + 1.02 \log A$	0.25	$\log A = 0.82M_w - 2.87$	0.22
All	148	$M_w = 4.07 + 0.98 \log A$	0.24	$\log A = 0.91M_w - 3.49$	0.24
Strike slip	43	$M_w = 6.81 + 0.78 \log D$	0.29	$\log D = 1.03M_w - 7.03$	0.34
Reverse ^a	21	$M_w = 6.52 + 0.44 \log D$	0.52	$\log D = 0.29M_w - 1.84$	0.42
Normal	16	$M_w = 6.61 + 0.71 \log D$	0.34	$\log D = 0.89M_w - 5.90$	0.38
All	80	$M_w = 6.69 + 0.74 \log D$	0.40	$\log D = 0.82M_w - 5.46$	0.42

Source: Wells and Coppersmith (1994).

^a Regression relationships are not statistically significant at a 95% probability level (note inconsistency of regression coefficients and standard deviations).

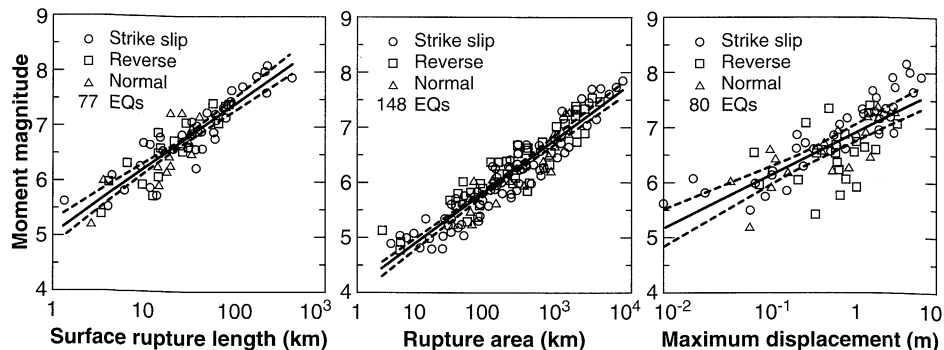


Figure 4.3 Scatter inherent in databases from which correlations of Table 4-1 were developed. (After Wells and Coppersmith, 1994. Used by permission of the Seismological Society of America.)

Example 4.1

Compute the probability that a moment magnitude 7.0 earthquake on the San Andreas fault would cause a surface rupture longer than 100 km.

Solution The San Andreas fault is known to produce strike-slip movement (Section 2.4.2.2). From Table 4-1, the mean surface rupture length for a $M_w = 7.0$ earthquake would be computed as

$$\log L = 0.74M_w - 3.55 = 0.74(7.0) - 3.55 = 1.63$$

Then the mean, or expected, value of L is given by

$$L = 10^{1.63} = 42.7 \text{ km}$$

The standard normal variate (Section C.7.2 of Appendix C) for a 100-km-long surface rupture would be

$$z = \frac{\log 100 - \log 42.7}{0.28} = 1.32$$

From Table C-1, the probability that the surface rupture length would exceed 100 km is 0.0934 or 9.34%.

4.2.2 Tectonic Evidence

Plate tectonics and elastic rebound theory tell us that earthquakes occur to relieve the strain energy that accumulates as plates move relative to each other. The rate of movement, therefore, should be related to the rate of strain energy accumulation and also to the rate of strain energy release (Smith, 1976; Woodward-Clyde Consultants, 1979; Idriss, 1985). For major subduction zones, Ruff and Kanamori (1980) related maximum magnitude to both the rate of convergence and the age of the subducted slab according to

$$M_w = -0.0089T + 0.134V + 7.96 \quad (4.1)$$

where T is the age in millions of years and V is the rate of convergence in cm/yr. Heaton and Kanamori (1984) used this relationship to suggest that the Cascadia subduction zone off the coasts of Oregon, Washington, and British Columbia could be capable of generating great earthquakes of magnitude well above 8 (Figure 4.4). Subsequently, geologic evidence of historical great earthquakes was discovered (e.g., Atwater, 1987; Atwater et al., 1987) along the coasts of Washington and Oregon.

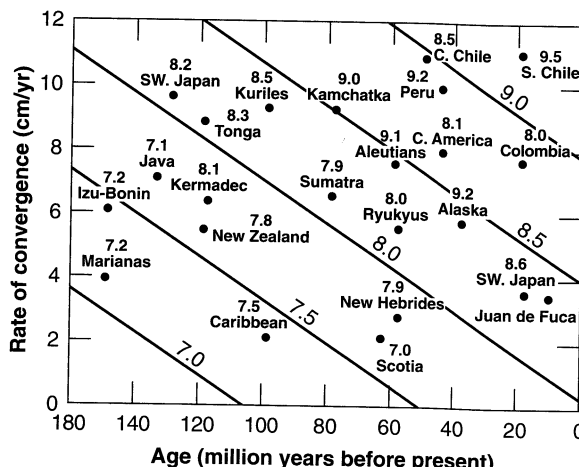


Figure 4.4 Relationship between earthquake magnitude, age, and rate of convergence in subduction zone environments. Diagonal lines correspond to equation (4.1). Data points represent actual earthquakes. (After Heaton and Kanamori, 1984. Used by permission of the Seismological Society of America.)

4.2.3 Historical Seismicity

Earthquake sources may also be identified from records of historical (preinstrumental) seismicity. The written historical record extends back only a few hundred years or less in the United States; in Japan and the Middle East it may extend about 2000 years and up to 3000 years or so in China (Ambraseys, 1971, 1978; Allen, 1975; Bolt, 1988).

Historical accounts of ground-shaking effects can be used to confirm the occurrence of past earthquakes and to estimate their geographic distributions of intensity. When sufficient data are available, the maximum intensity can be determined and used to estimate the location of the earthquake epicenter and the magnitude of the event. Although the accuracy of locations determined in this way depends strongly on population density and the rate of

earthquake recurrence, a geographic pattern of historic epicenters provides strong evidence for the existence of earthquake source zones. Since historical records are dated, they can also be used to evaluate the rate of recurrence of earthquakes, or *seismicity*, in particular areas.

4.2.4 Instrumental Seismicity

Over the past 80 or 90 years, about 10 earthquakes of $M_s > 7$ have occurred somewhere in the world each year (Kanamori, 1988). Instrumental records from large earthquakes have been available since about 1900, although many from before 1960 are incomplete or of uneven quality. Nevertheless, instrumental recordings represent the best available information for the identification and evaluation of earthquake sources. Their most significant limitation is the short period of time, compared with the average period of time between large earthquakes, for which they have been available. Again, the alignment of instrumentally located epicenters or hypocenters indicates the existence of earthquake sources. Analysis of aftershocks can also aid in the delineation of earthquake source zones.

4.3 DETERMINISTIC SEISMIC HAZARD ANALYSIS

In the early years of geotechnical earthquake engineering, the use of *deterministic seismic hazard analysis* (DSHA) was prevalent. A DSHA involves the development of a particular seismic scenario upon which a ground motion hazard evaluation is based. The scenario consists of the postulated occurrence of an earthquake of a specified size occurring at a specified location. A typical DSHA can be described as a four-step process (Reiter, 1990) consisting of:

1. Identification and characterization of all earthquake sources capable of producing significant ground motion at the site. Source characterization includes definition of each source's geometry (the *source zone*) and earthquake potential.
2. Selection of a source-to-site distance parameter for each source zone. In most DSHAs, the shortest distance between the source zone and the site of interest is selected. The distance may be expressed as an epicentral distance or hypocentral distance, depending on the measure of distance of the predictive relationship(s) used in the following step.
3. Selection of the *controlling earthquake* (i.e., the earthquake that is expected to produce the strongest level of shaking), generally expressed in terms of some ground motion parameter, at the site. The selection is made by comparing the levels of shaking produced by earthquakes (identified in step 1) assumed to occur at the distances identified in step 2. The controlling earthquake is described in terms of its size (usually expressed as magnitude) and distance from the site.
4. The hazard at the site is formally defined, usually in terms of the ground motions produced at the site by the controlling earthquake. Its characteristics are usually described by one or more ground motion parameters obtained from predictive relationships of the types presented in Chapter 3. Peak acceleration, peak velocity, and response spectrum ordinates are commonly used to characterize the seismic hazard.

The DSHA procedure is shown schematically in Figure 4.5. Expressed in these four compact steps, DSHA appears to be a very simple procedure, and in many respects it is.

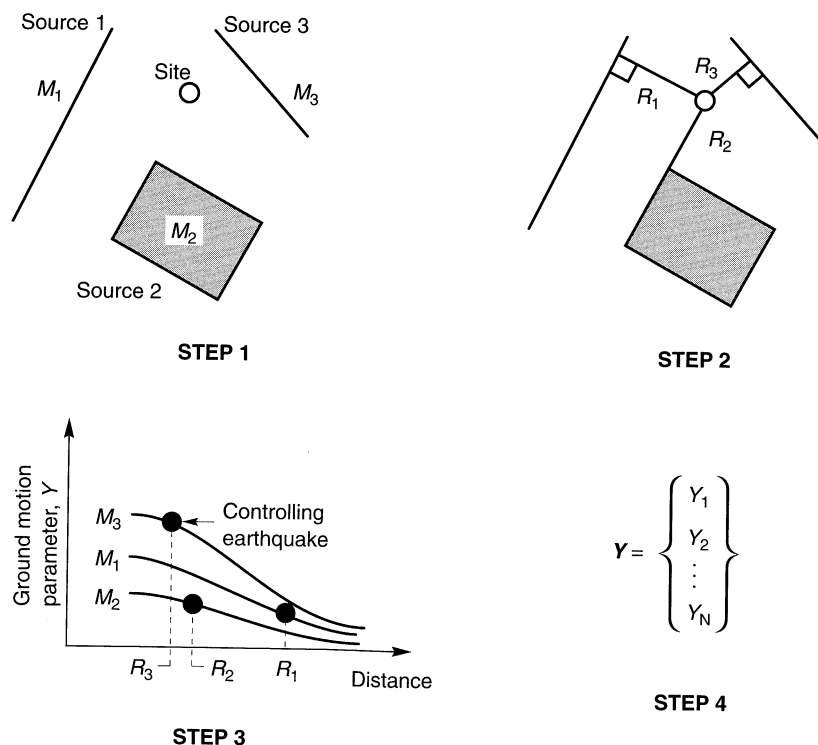


Figure 4.5 Four steps of a deterministic seismic hazard analysis.

When applied to structures for which failure could have catastrophic consequences, such as nuclear power plants and large dams, DSHA provides a straightforward framework for evaluation of worst-case ground motions. However, it provides no information on the likelihood of occurrence of the controlling earthquake, the likelihood of it occurring where it is assumed to occur, the level of shaking that might be expected during a finite period of time (such as the useful lifetime of a particular structure or facility), or the effects of uncertainties in the various steps required to compute the resulting ground motion characteristics.

Perhaps most important, DSHA involves subjective decisions, particularly regarding earthquake potential (step 1), that can require the combined expertise and opinions of seismologists, seismic geologists, engineers, risk analysts, economists, social scientists, and government officials. The broad range of backgrounds and often divergent goals of such professionals can cause difficulty in reaching a consensus on earthquake potential. Over the years there have been many terms used to describe earthquake potential; among them the *maximum credible earthquake* (MCE), *design basis earthquake* (DBE), *safe shutdown earthquake* (SSE), *maximum probable earthquake* (MPE), *operating basis earthquake* (OBE), and *seismic safety evaluation earthquake*. The MCE, for example, is usually defined as the maximum earthquake that appears capable of occurring under the known tectonic framework. The DBE and SSE are usually defined in essentially the same way. The MPE has been defined as the maximum historical earthquake and also as the maximum earthquake

likely to occur in a 100-year interval. Many DSHAs have used the two-pronged approach of evaluating hazards for both the MCE and MPE (or SSE and OBE). Disagreements over the definition and use of these terms have forced the delay, and even cancellation, of a number of large construction projects. The Committee on Seismic Risk of the Earthquake Engineering Research Institute (EERI) has stated that terms such as MCE and MPE "are misleading . . . and their use is discouraged" (Committee on Seismic Risk, 1984).

Example 4.2

The site shown in Figure E4.2 is located in the vicinity of three independent seismic sources represented by source zones 1, 2, and 3. Using a deterministic seismic hazard analysis, compute the peak acceleration.

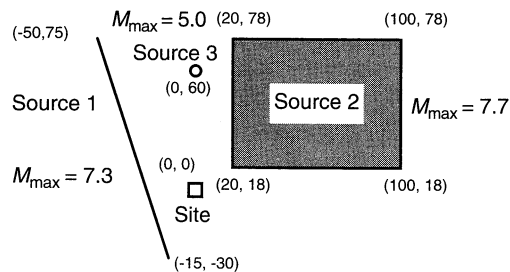


Figure E4.2

Solution Taking the site as the center of a local x - y coordinate system, the coordinates of the source zone boundaries (in kilometers) are given in parentheses. Source zone 1 is a 111-km-long linear source zone that can produce a maximum magnitude of 7.3 at any point along its length. Source zone 2 is an areal source zone of 4800 km^2 capable of generating a magnitude 7.7 earthquake anywhere within its boundaries. Source zone 3 is a point source that can produce a maximum magnitude of 5.0. Following the four-step procedure described earlier:

1. The problem statement provides the location and maximum magnitude of each source zone. In real DSHAs, this is often an extremely complex and difficult task.
2. The source-to-site distance can be represented by the minimum between the site and any part of each source zone. On that basis, the distances are:

Source Zone	Distance, R (km)
1	23.7
2	25.0
3	60.0

3. If the level of shaking is assumed to be adequately characterized by the peak horizontal acceleration, an appropriate attenuation relationship can be used to select the controlling earthquake. Using the relationship of Cornell et al. (1979), developed with data from $M = 3.0$ to 7.7 earthquakes at distances of 20 to 200 km in the western United States,

$$\ln \text{PHA (gals)} = 6.74 + 0.859M - 1.80 \ln(R + 25)$$

the PHA values generated by each of the source zones would be:

Source Zone	<i>M</i>	<i>R</i> (km)	PHA
1	7.3	23.7	0.42g
2	7.7	25.0	0.57g
3	5.0	60.0	0.02g

On this basis, the source zone 2 event would be selected as the controlling earthquake. (Note: Though currently out of date, the Cornell et al. relationship is used here because of its simplicity which will make a subsequent example on probabilistic seismic hazard analysis much easier to understand.)

4. The hazard would be taken as that which would result from a magnitude 7.7 earthquake occurring at a distance of 25 km. This motion would produce a peak acceleration of 0.57g; other ground motion parameters could be obtained from the predictive relationships described in Chapter 3.

4.4 PROBABILISTIC SEISMIC HAZARD ANALYSIS

In the past 20 to 30 years the use of probabilistic concepts has allowed uncertainties in the size, location, and rate of recurrence of earthquakes and in the variation of ground motion characteristics with earthquake size and location to be explicitly considered in the evaluation of seismic hazards. *Probabilistic seismic hazard analysis* (PSHA) provides a framework in which these uncertainties can be identified, quantified, and combined in a rational manner to provide a more complete picture of the seismic hazard.

Understanding the concepts and mechanics of PSHA requires familiarity with some of the terminology and basic concepts of probability theory. Such background information can be found in Appendix C. The PSHA methodology described in this section is similar in many respects to the well-established methods developed by Cornell (1968), and Algermissen et al. (1982).

The PSHA can also be described as a procedure of four steps (Reiter, 1990), each of which bear some degree of similarity to the steps of the DSHA procedure, as illustrated in Figure 4.6.

1. The first step, identification and characterization of earthquake sources, is identical to the first step of the DSHA, except that the probability distribution of potential rupture locations within the source must also be characterized. In most cases, uniform probability distributions are assigned to each source zone, implying that earthquakes are equally likely to occur at any point within the source zone. These distributions are then combined with the source geometry to obtain the corresponding probability distribution of source-to-site distance. The DSHA, on the other hand, implicitly assumes that the probability of occurrence is 1 at the points in each source zone closest to the site, and zero elsewhere.
2. Next, the seismicity or temporal distribution of earthquake recurrence must be characterized. A *recurrence relationship*, which specifies the average rate at which an earthquake of some size will be exceeded, is used to characterize the seismicity of each source zone. The recurrence relationship may accommodate the maximum size earthquake, but it does not limit consideration to that earthquake, as DSHAs often do.

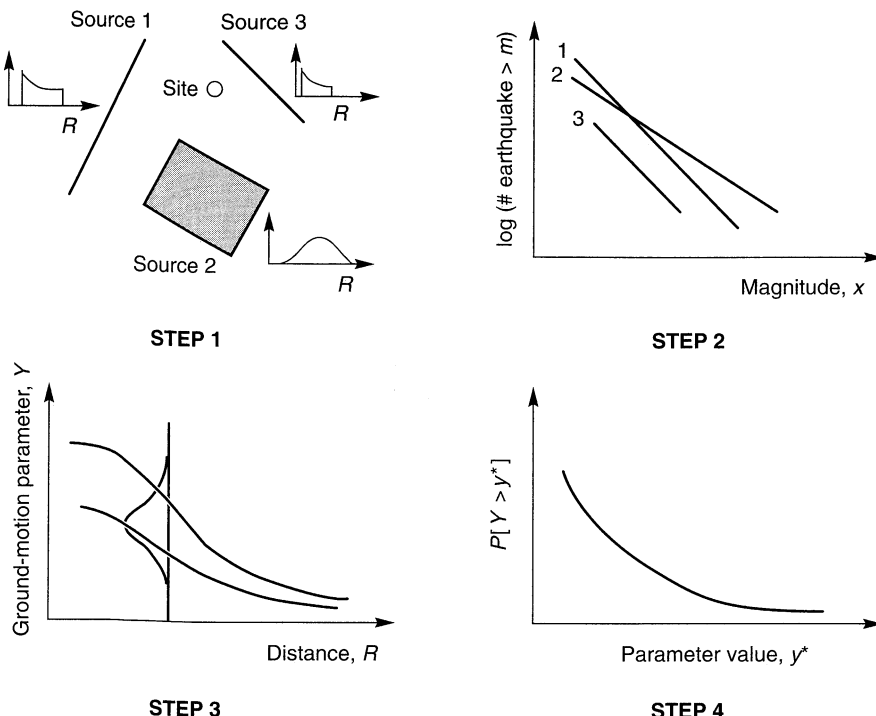


Figure 4.6 Four steps of a probabilistic seismic hazard analysis.

3. The ground motion produced at the site by earthquakes of any possible size occurring at any possible point in each source zone must be determined with the use of predictive relationships. The uncertainty inherent in the predictive relationship is also considered in a PSHA.
4. Finally, the uncertainties in earthquake location, earthquake size, and ground motion parameter prediction are combined to obtain the probability that the ground motion parameter will be exceeded during a particular time period.

The proper performance of a PSHA requires careful attention to the problems of source characterization and ground motion parameter prediction and to the mechanics of the probability computations.

4.4.1 Earthquake Source Characterization

Characterization of an earthquake source requires consideration of the spatial characteristics of the source and of the distribution of earthquakes within that source, of the distribution of earthquake size for each source, and of the distribution of earthquakes with time. Each of these characteristics involves some degree of uncertainty.

4.4.1.1 Spatial Uncertainty

The geometries of earthquake sources depend on the tectonic processes involved in their formulation. Earthquakes associated with volcanic activity, for example, generally

originate in zones near the volcanoes that are small enough to allow them to be characterized as *point sources*. Well-defined fault planes, on which earthquakes can occur at many different locations, can be considered as two-dimensional *areal sources*. Areas where earthquake mechanisms are poorly defined, or where faulting is so extensive as to preclude distinction between individual faults, can be treated as three-dimensional *volumetric sources*.

For the purposes of a seismic hazard analysis, the *source zones* may be similar to or somewhat different than the actual source, depending on the relative geometry of the source and site of interest and on the quality of information about the sources. For example, the relatively short fault in Figure 4.7a can be modeled as a point source since the distance between any point along its length and the site is nearly constant. Similarly, the depth of the fault plane shown in Figure 4.7b is sufficiently small that variations in hypocentral depth have little influence on hypocentral distance. In such a case the hazard analysis can be simplified with negligible loss of accuracy by approximating the planar source as a linear source zone. In Figure 4.7c, the available data are insufficient to determine accurately the actual geometry of the source, so it is represented as a volumetric source.

Earthquakes are usually assumed to be uniformly distributed within a particular source zone (i.e., earthquakes are considered equally likely to occur at any location). The assumption of uniformity is by no means required; nonuniform distributions may be used when sufficient information to justify them exists. A uniform distribution within the source zone does not, however, often translate into a uniform distribution of source-to-site distance. Since predictive relationships express ground motion parameters in terms of some measure of source-to-site distance, the spatial uncertainty must be described with respect to the appropriate distance parameter. The uncertainty in source-to-site distance can be described by a probability density function.

For the point source of Figure 4.8a, the distance, R , is known to be r_s ; consequently, the probability that $R = r_s$ is assumed to be 1 and the probability that $R \neq r_s$, zero. Other cases are not as simple. For the linear source of Figure 4.8b, the probability that an earthquake occurs on the small segment of the fault between $L = l$ and $L = l + dl$ is the same as the probability that it occurs between $R = r$ and $R = r + dr$; that is,

$$f_L(l) dl = f_R(r) dr \quad (4.2)$$

where $f_L(l)$ and $f_R(r)$ are the probability density functions for the variables L and R , respectively. Consequently,

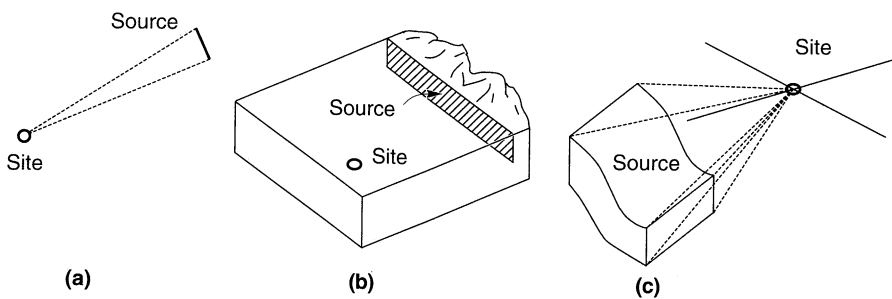


Figure 4.7 Examples of different source zone geometries: (a) short fault that can be modeled as a point source; (b) shallow fault that can be modeled as a linear source; (c) three-dimensional source zone.

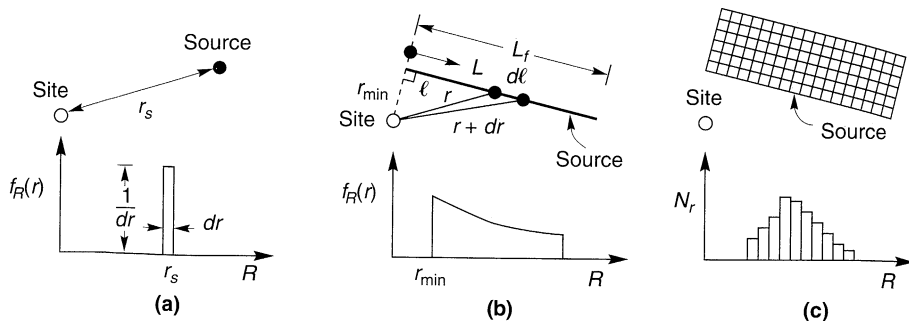


Figure 4.8 Examples of variations of source-to-site distance for different source zone geometries. The shape of the probability distribution can be visualized by considering the relative portions of the source zone that would fall between each of a series of circles (or spheres for three-dimensional problems) with equal differences in radius.

$$f_R(r) = f_L(l) \frac{dl}{dr} \quad (4.3)$$

If earthquakes are assumed to uniformly distributed over the length of the fault, $f_L(l) = l/L_f$. Since $l^2 = r^2 - r_{\min}^2$ the probability density function of R is given by

$$f_R(r) = \frac{r}{L_f \sqrt{r^2 - r_{\min}^2}} \quad (4.4)$$

For source zones with more complex geometries, it is easier to evaluate $f_R(r)$ by numerical rather than analytical methods. For example, dividing the irregular source zone of Figure 4.8c into a large number of discrete elements of equal area, a histogram that approximates $f_R(r)$ can be constructed by tabulating the values of R that correspond to the center of each element.

The preceding discussion assumes that all the energy is released at the hypocenter of the earthquake. However, energy is released over the entire fault rupture surface, parts of which may be much closer to the site than the hypocenter. Der-Kiureghian and Ang (1977) noted that the rupture surface of a large earthquake with a distant hypocenter could release energy much closer to the site, and developed methods to account for rupture surface dimensions in PSHA.

4.4.1.2 Size Uncertainty

Once an earthquake source is identified and its corresponding source zone characterized, the seismic hazard analyst's attention is turned toward evaluation of the sizes of earthquakes that the source zone can be expected to produce. All source zones have a maximum earthquake magnitude that cannot be exceeded; it can be large for some and small for others. In general, the source zone will produce earthquakes of different sizes up to the maximum earthquake, with smaller earthquakes occurring more frequently than larger ones. The strain energy may be released aseismically, or in the form of earthquakes. Assuming that all strain energy is released by earthquakes of magnitude 5.5 to 9.0 and that the average fault displacement is one-half the maximum surface displacement, Slemmons (1982) showed how the rate of movement was related to earthquake magnitude and recurrence interval (Figure 4.9). The distribution of earthquake sizes in a given period of time is described by

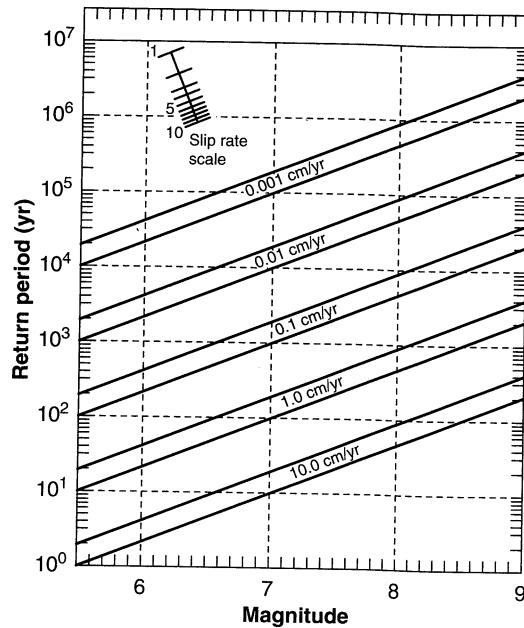


Figure 4.9 Effect of fault slip rate and earthquake magnitude on return period. (After Slemmons, 1982.)

a *recurrence law*. A basic assumption of PSHA is that the recurrence law obtained from past seismicity is appropriate for the prediction of future seismicity.

Gutenberg–Richter Recurrence Law. Gutenberg and Richter (1944) gathered data for southern California earthquakes over a period of many years and organized the data according to the number of earthquakes that exceeded different magnitudes during that time period. They divided the number of exceedances of each magnitude by the length of the time period to define a *mean annual rate of exceedance*, λ_m of an earthquake of magnitude m . As would be expected, the mean annual rate of exceedance of small earthquakes is greater than that of large earthquakes. The reciprocal of the annual rate of exceedance for a particular magnitude is commonly referred to as the *return period* of earthquakes exceeding that magnitude. When the logarithm of the annual rate of exceedance of southern California earthquakes was plotted against earthquake magnitude, a linear relationship was observed. The resulting *Gutenberg–Richter law* for earthquake recurrence was expressed as

$$\log \lambda_m = a - bm \quad (4.5)$$

where λ_m is the mean annual rate of exceedance of magnitude m , 10^a is the mean yearly number of earthquakes of magnitude greater than or equal to zero, and b (the *b value*) describes the relative likelihood of large and small earthquakes. The Gutenberg–Richter law is illustrated schematically in Figure 4.10a. As the *b value* increases, the number of larger magnitude earthquakes decreases compared to those of smaller magnitudes. The Gutenberg–Richter law is not restricted to the use of magnitude as a descriptor of earthquake size; epicentral intensity has also been used. Worldwide recurrence data are shown in Figure 4.10b.

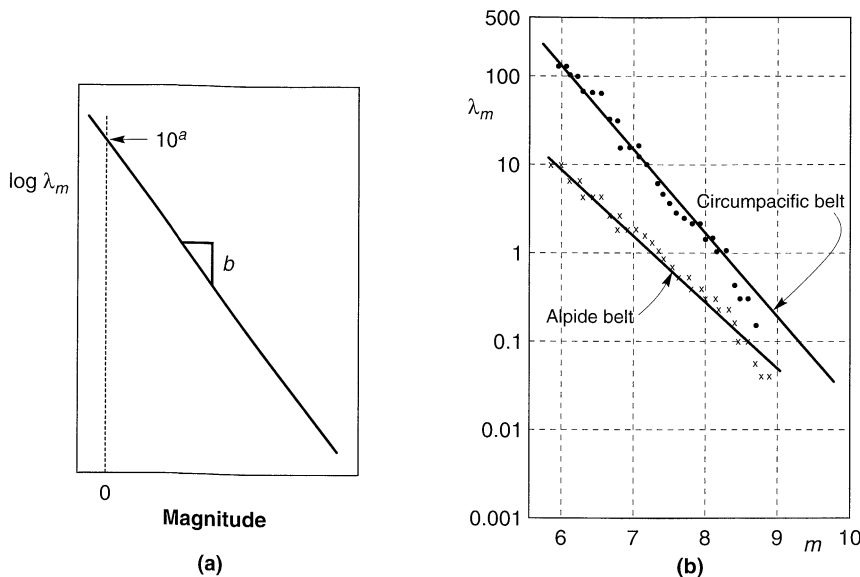


Figure 4.10 (a) Gutenberg–Richter recurrence law, showing meaning of a and b parameters; and (b) application of Gutenberg–Richter law to worldwide seismicity data. (After Esteva, 1970.)

Example 4.3

Using Figure 4.10b, compute the return period of $M = 8$ earthquakes on the Circumpacific and Alpide belts.

Solution At a magnitude of 8, Figure 4.10b indicates that the Circumpacific and Alpide belts have mean annual rates of exceedance of 1.76 per year and 0.31 per year, respectively. Therefore, the corresponding return periods are

$$\text{Circumpacific: } T_R = \frac{1}{\lambda_m} = \frac{1}{1.76/\text{yr}} = 0.6 \text{ year}$$

$$\text{Alpide: } T_R = \frac{1}{\lambda_m} = \frac{1}{0.31/\text{yr}} = 3.2 \text{ years}$$

The a and b parameters are generally obtained by regression on a database of seismicity from the source zone of interest. Unless the source zone is extremely active, the database is likely to be relatively sparse. Since the use of both instrumental and historical events is usually required, the database may contain both magnitude (possibly based on different scales) and intensity data, necessitating the conversion of one measure of size to the other. In some areas, the record of seismicity may be distorted by the presence of *dependent events* such as aftershocks and foreshocks (Merz and Cornell, 1973). Although such dependent events can cause significant damage, a PSHA is intended to evaluate the hazard from discrete, independent releases of seismic energy. Therefore, dependent events must be removed from the seismicity database and their effects accounted for in separate analyses. Completeness of the database must also be considered. The historical record is usually more complete for large earthquakes than for small earthquakes; small earthquakes can go undetected for a

variety of physical and demographic reasons. Fitting a straight line such as that implied by the Gutenberg–Richter law through recurrence data in which the mean rate of exceedance of small earthquakes is underestimated will tend to flatten the line. As a result, the actual mean rate of small earthquakes will be underpredicted and the mean rate of large earthquakes will be overpredicted. Different methods have been proposed (Stepp, 1972; Weichert, 1980; EPRI, 1986) to correct incomplete records.

Bounded Gutenberg–Richter Recurrence Laws. The standard Gutenberg–Richter recurrence law of equation (4.5) may also be expressed as

$$\lambda_m = 10^{a-bm} = \exp(\alpha - \beta m) \quad (4.6)$$

where $\alpha = 2.303a$ and $\beta = 2.303b$. Equation (4.6) shows that the Gutenberg–Richter law implies that earthquake magnitudes are exponentially distributed. The standard Gutenberg–Richter law covers an infinite range of magnitudes, from $-\infty$ to $+\infty$. For engineering purposes, the effects of very small earthquakes are of little interest and it is common to disregard those that are not capable of causing significant damage. If earthquakes smaller than a lower threshold magnitude m_0 are eliminated, the mean annual rate of exceedance can be written (McGuire and Arabasz, 1990) as

$$\lambda_m = v \exp[-\beta(m - m_0)] \quad m > m_0 \quad (4.7)$$

where $v = \exp(\alpha - \beta m_0)$. In most PSHAs, the lower threshold magnitude is set at values from about 4.0 to 5.0 since magnitudes smaller than that seldom cause significant damage. The resulting probability distribution of magnitude for the Gutenberg–Richter law with lower bound can be expressed in terms of the *cumulative distribution function* (CDF):

$$F_M(m) = P[M < m | M > m_0] = \frac{\lambda_{m_0} - \lambda_m}{\lambda_{m_0}} = 1 - e^{-\beta(m - m_0)} \quad (4.8)$$

or the probability density function (PDF):

$$f_M(m) = \frac{d}{dm} F_M(m) = \beta e^{-\beta(m - m_0)} \quad (4.9)$$

At the other end of the magnitude scale, the standard Gutenberg–Richter law predicts nonzero mean rates of exceedance for magnitudes up to infinity. This implies, for example, that the Circumpacific belt (Figure 4.10b), would produce a magnitude 10 earthquake at a mean annual exceedance rate of about 0.02 per year (a return period of only 50 years), even though earthquakes of that size have never been observed. Some maximum magnitude, m_{\max} , is associated with all source zones. If it is known or can be estimated, the mean annual rate of exceedance can be expressed (McGuire and Arabasz, 1990) as

$$\lambda_m = v \frac{\exp[-\beta(m - m_0)] - \exp[-\beta(m_{\max} - m_0)]}{1 - \exp[-\beta(m_{\max} - m_0)]} \quad m_0 \leq m \leq m_{\max} \quad (4.10)$$

The bounded recurrence law of equation (4.10) is shown in Figure 4.11a for conditions of constant rate of seismicity (i.e., constant mean annual rate of exceedance of m_0). An alternative interpretation, based on a constant rate of seismic moment (hence energy) release, produces the recurrence curves of Figure 4.11b. In the constant moment rate model, increasing the maximum magnitude requires a substantial decrease in the mean annual rate of exceedance of

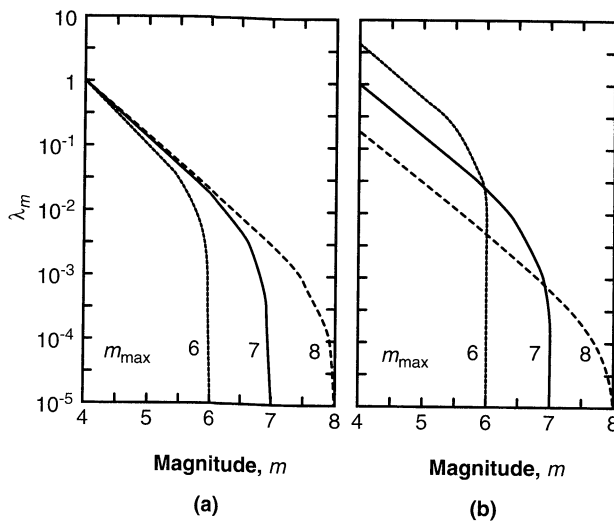


Figure 4.11 Bounded Gutenberg–Richter recurrence laws for $m_0 = 4$ and $m_{\max} = 6, 7$, and 8 constrained by (a) constant seismicity rate and (b) constant moment rate. (After Youngs and Coppersmith, 1985.)

lower magnitude events to account for the extra energy released in large earthquakes. Since the seismic moment is proportional to the amount of slip (displacement) that occurs in an earthquake, the moment rate is proportional to the slip rate. Hence the constant-moment-rate model is equivalent to a constant-slip-rate model and can be used when the slip rate is known to be constant. The extent to which actual slip rates vary with time, however, appears to be different for different faults and can even fluctuate with time along the same fault.

The CDF and PDF for the Gutenberg–Richter law with upper and lower bounds can be expressed as

$$F_M(m) = P[M < m | m_0 \leq m \leq m_{\max}] = \frac{1 - \exp[-\beta(m - m_0)]}{1 - \exp[-\beta(m_{\max} - m_0)]} \quad (4.11)$$

$$f_M(m) = \frac{\beta \exp[-\beta(m - m_0)]}{1 - \exp[-\beta(m_{\max} - m_0)]} \quad (4.12)$$

Characteristic Earthquake Recurrence Laws. The Gutenberg–Richter law was developed from a set of regional data that included many different seismic sources. Since PSHAs are usually conducted for specific sites rather than large regions, the earthquake-generating characteristics of individual faults is important. In recent years the ability of the Gutenberg–Richter law to represent the behavior of a single source has been called into question (Schwartz and Coppersmith, 1984; Schwartz, 1988).

Paleoseismic studies indicate that individual points on faults and fault segments tend to move by approximately the same distance in each earthquake. This has been interpreted to suggest that individual faults repeatedly generate earthquakes of similar (within about one-half magnitude unit) size, known as *characteristic earthquakes*, at or near their maximum magnitude. Alternatively, the apparently repetitive nature of fault movement at individual points may be controlled by localized geologic constraints and, consequently, not reflect earthquake magnitude very accurately. Resolution of these alternative interpretations awaits further paleoseismic research.

By dating these characteristic earthquakes, their historical rate of recurrence can be estimated. Geologic evidence indicates the characteristic earthquakes occur more frequently than would be implied by extrapolation of the Gutenberg–Richter law from high exceedance rates (low magnitude) to low exceedance rates (high magnitude). The result is a more complex recurrence law that is governed by seismicity data at low magnitudes and geologic data at high magnitudes, as shown in Figure 4.12.

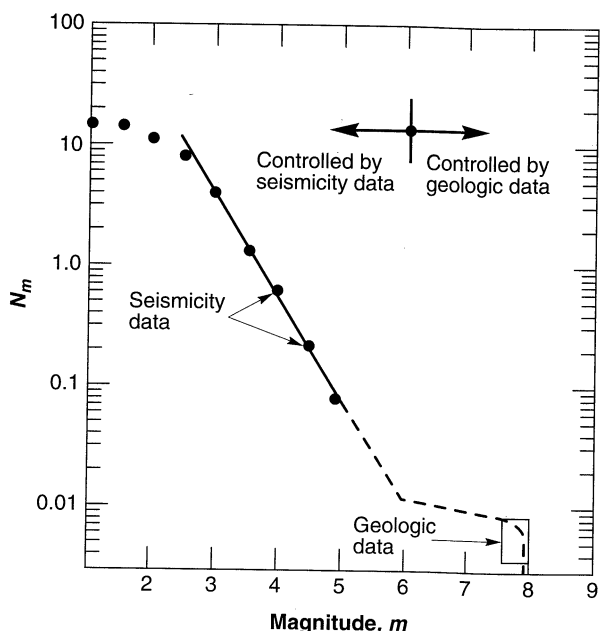


Figure 4.12 Inconsistency of mean annual rate of exceedance as determined from seismicity data and geologic data. (After Youngs and Coppersmith, 1985.)

Youngs and Coppersmith (1985) developed a generalized magnitude-frequency density function that combined an exponential magnitude distribution at lower magnitudes with a uniform distribution in the vicinity of the characteristic earthquake. Recurrence relationships derived from the Youngs and Coppersmith model and the bounded Gutenberg–Richter model, assuming the same m_{\max} , b value, and slip rate, are shown in Figure 4.13. The characteristic earthquake model predicts higher rates of exceedance at magnitudes near the characteristic earthquake magnitude and lower rates at lower magnitudes. Other models that account for characteristic earthquakes have been developed by Wesnorsky et al. (1984) and Wu et al. (1995).

Other Recurrence Laws. A number of other recurrence laws have been proposed. Merz and Cornell (1973a) used a quadratic expression to describe the mean annual rate at which earthquakes of magnitude greater than m_0 and less than m_{\max} are exceeded. Shah et al. (1975) used a bilinear recurrence law in an evaluation of seismic risk for Nicaragua. In another approach, the Gutenberg–Richter law was modified on the basis of seismic moment and fault slip (Lomnitz-Adler and Lomnitz, 1979).

Discussion. Available evidence is insufficient to determine whether the Gutenberg–Richter, characteristic earthquake, or some other recurrence law is correct. Evaluation of which model is most appropriate for a given source is hampered by the brevity of historical

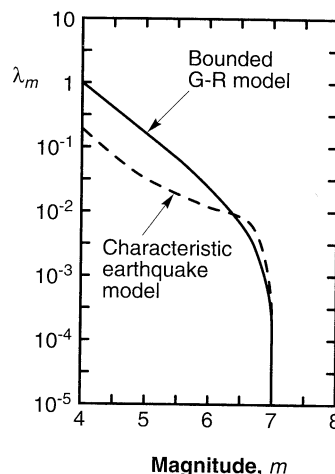


Figure 4.13 Comparison of recurrence laws from bounded Gutenberg–Richter and characteristic earthquake models. (After Youngs and Coppersmith, 1985.)

and/or instrumental records. Based on five decades of seismicity records for the major seismic sources of southern California, Wesnousky (1994) concluded that while the available data were not sufficient to disprove the Gutenberg–Richter recurrence law, the characteristic earthquake model better represented the observed distribution of earthquake magnitudes. Additional research in this area is in progress and will undoubtedly be an active topic of discussion in the forthcoming seismology literature.

4.4.2 Predictive Relationships

Predictive relationships are nearly always obtained empirically by least-squares regression on a particular set of strong motion parameter data. Despite attempts to remove questionable data and the use of quality-based weighting schemes, some amount of scatter in the data is inevitable. The scatter results from randomness in the mechanics of rupture and from variability and heterogeneity of the source, travel path, and site conditions. Scatter in the data can be quantified by confidence limits (Campbell, 1985) or by the standard deviation of the predicted parameter. Reflecting the form of most predictive relationships, the standard deviation of the (natural) logarithm of the predicted parameter is usually computed. This considerable uncertainty must be accounted for in computation of seismic hazards. The probability that a particular ground motion parameter Y exceeds a certain value, y^* , for an earthquake of a given magnitude, m , occurring at a given distance, r , is illustrated graphically in Figure 4.14. In probabilistic terms, it is given by

$$P [Y > y^* | m, r] = 1 - F_Y(y^*) \quad (4.13)$$

where $F_Y(y)$ is the value of the CDF of Y at m and r . The value of $F_Y(y)$ depends on the probability distribution used to represent Y . In general, ground motion parameters are usually assumed to be lognormally distributed (the logarithm of the parameter is normally distributed); however, the unbounded characteristics of that distribution can attribute a nonzero probability to unrealistic values of the ground motion parameter. For example, a hypothetical PHA attenuation relationship that predicts a mean PHA of $0.5g$ with $\sigma_{\ln y} = 0.5$ would imply a 0.06% probability that the PHA would exceed $2.5g$. The use of distributions that impose an upper limit on Y have been studied by Kulkarni et al. (1979), Bender (1984), and Zemell (1984).

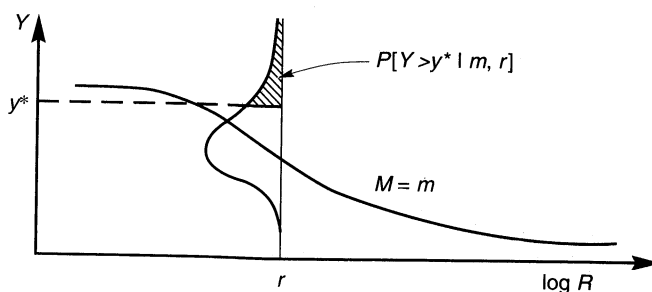


Figure 4.14 Schematic illustration of conditional probability of exceeding a particular value of a ground motion parameter for a given magnitude and distance.

Example 4.4

Using the predictive relationship of Campbell and Bozorgnia (1994) given as equation (3.25), compute the probability that a $M_w = 7$ earthquake on a strike-slip fault would cause a peak horizontal acceleration greater than $0.4g$ at a soft-rock site 15 km from the closest point on the rupture surface.

Solution. For equation (3.26), the parameters $F = 0$ and $S_{HR} = 0$ and $S_{SR} = 1$, so the mean value of the natural logarithm of peak horizontal acceleration is given by

$$\begin{aligned}\overline{\ln \text{PHA}} (\text{gal}) &= 3.512 + 0.904M_w - 1.328\sqrt{R^2 + [0.149 \exp(0.647M_w)]^2} \\ &\quad + 0.904 - 0.171 \ln R \\ &= 3.512 + (0.904)(7) - 1.328\sqrt{15^2 + [0.149 \exp(0.647 \times 7)]^2} \\ &\quad + 0.904 - 0.171 \ln (15) \\ &= 6.31\end{aligned}$$

from which $\text{PHA} = e^{6.31} = 552 \text{ gal}$. Then, from Section C.7.2 of Appendix C, the standard normal variate is

$$z = \frac{\ln \text{PHA} - \overline{\ln \text{PHA}}}{\sigma_{\ln \text{PHA}}} = \frac{\ln [(0.40g)(981 \text{ gal/g})] - \ln (552 \text{ gal})}{0.405} = -0.843$$

From Table C-1,

$$F_z(-0.843) = P[z < -0.843] = P[a_{\max} < 0.4g] = 0.200$$

so the desired probability

$$P[\text{PHA} > 0.40g | M = 7.0, R = 15 \text{ km}] = 1 - 0.200 = 0.800$$

4.4.3 Temporal Uncertainty

To calculate the probabilities of various hazards occurring in a given time period, the distribution of earthquake occurrence with respect to time must be considered. Earthquakes have long been assumed to occur randomly with time, and in fact, examination of available seismicity records has revealed little evidence (when aftershocks are removed) of temporal patterns in earthquake recurrence. The assumption of random occurrence allows the use of simple probability models, but is inconsistent with the implications of elastic rebound theory (Section 2.5.1).

4.4.3.1 Poisson Model

The temporal occurrence of earthquakes is most commonly described by a Poisson model. The Poisson model provides a simple framework for evaluating probabilities of events that follow a *Poisson process*, one that yields values of a random variable describing the number of occurrences of a particular event during a given time interval or in a specified spatial region. Since PSHAs deal with temporal uncertainty, the spatial applications of the Poisson model will not be considered further. Poisson processes possess the following properties:

1. The number of occurrences in one time interval are independent of the number that occur in any other time interval.
2. The probability of occurrence during a very short time interval is proportional to the length of the time interval.
3. The probability of more than one occurrence during a very short time interval is negligible.

These properties indicate that the events of a Poisson process occur randomly, with no “memory” of the time, size, or location of any preceding event.

For a Poisson process, the probability of a random variable N , representing the number of occurrences of a particular event during a given time interval is given by

$$P[N = n] = \frac{\mu^n e^{-\mu}}{n!} \quad (4.14)$$

where μ is the average number of occurrences of the event in that time interval. The time between events in a Poisson process can be shown to be exponentially distributed. To characterize the temporal distribution of earthquake recurrence for PSHA purposes, the Poisson probability is usually expressed as

$$P[N = n] = \frac{(\lambda t)^n e^{-\lambda t}}{n!} \quad (4.15)$$

where λ is the average rate of occurrence of the event and t is the time period of interest. Note that the probability of occurrence of at least one event in a period of time t is given by

$$\begin{aligned} P[N \geq 1] &= P[N = 1] + P[N = 2] + P[N = 3] + \dots \\ &+ P[N = \infty] = 1 - P[N = 0] = 1 - e^{-\lambda t} \end{aligned} \quad (4.16)$$

When the event of interest is the exceedance of a particular earthquake magnitude, the Poisson model can be combined with a suitable recurrence law to predict the probability of at least one exceedance in a period of t years by the expression

$$P[N \geq 1] = 1 - e^{-\lambda_m t} \quad (4.17)$$

4.4.3.2 Other Models

Elastic rebound theory suggests that the occurrence of earthquakes on a particular fault or fault segment should *not* be independent of past seismicity. If earthquakes occur to release strain energy that builds up over extended periods of time, the occurrence of a large earthquake should substantially reduce the chances of another independent, large earthquake

(from the same source) occurring shortly thereafter. If earthquakes are triggered when the stress on a fault reaches some limiting value, the chances of occurrence should depend on the times, sizes, and locations of preceding events.

A number of models that account for prior seismicity have been proposed (Anagnos and Kiremidjian, 1988). *Nonhomogeneous Poisson models* (e.g., Vere-Jones and Ozaki, 1982) allow the annual rate of exceedance to vary with time. *Renewal models* (Esteva, 1970; Hagiwara, 1974; Savy et al., 1980; Kiremidjian and Anagnos, 1984; Cornell and Winterstein, 1986) use arrival-time distributions other than exponential (implied by the homogeneous Poisson model) to allow the hazard rate to increase with time since the last event; gamma and Weibull distributions are most common. *Time-predictable models* specify a distribution of the time to the next earthquake that depends on the magnitude of the most recent earthquake; *slip-predictable models* consider the distribution of earthquake magnitude to depend on the time since the most recent earthquake. *Markov models* incorporate a type of memory that describes the chances that a process moves from some past “state” to a particular future state. The time for which the process stays in a particular state before moving to another state is exponentially distributed; *semi-Markov models* are not restricted to the exponential distribution. Both Markov models (Vere-Jones, 1966; Vagliente, 1973; Veneziano and Cornell, 1974; Nishioka and Shah, 1980) and semi-Markov models (Patwardhan et al., 1980; Cluff et al., 1980; Coppersmith, 1981; Guagenti-Grandori and Molina, 1984) have been used in seismic hazard analysis. The semi-Markov models of Patwardhan et al. (1980) and Cluff et al. (1980), for example, relate the probability of future earthquakes of various sizes to the size of the most recent event and the elapsed time since its occurrence. *Trigger models* (Vere-Jones and Davies, 1966; Shlien and Tokosz, 1970; Merz and Cornell, 1973b; Lai, 1977) can account for clusters of events (aftershocks) that occur after triggering events.

4.4.3.3 Model Applicability

Investigations of the applicability of Poisson and non-Poissonian models (Cornell and Winterstein, 1986) have shown that the Poisson model is useful for practical seismic risk analysis except when the seismic hazard is dominated by a single source for which the time interval since the previous significant event is greater than the average interevent time and when the source displays strong “characteristic-time” behavior. For this and other reasons related to simplicity, ease of use, and lack of sufficient data to support more sophisticated models, the Poisson model is the most widely used in contemporary PSHA.

Each of the more sophisticated models uses a “pattern” of earthquake occurrence to reconcile their computed probabilities with the mechanics of the elastic rebound process of earthquake generations. As a result, each requires additional parameters whose values must be evaluated from historical and instrumental seismicity records that are, in most cases, too sparse to permit accurate evaluation. As time passes and additional data becomes available, the use of these models will undoubtedly increase.

4.4.4 Probability Computations

The results of a PSHA can be expressed in many different ways. All involve some level of probabilistic computations to combine the uncertainties in earthquake size, location, frequency, and effects to estimate seismic hazards. A common approach involves the development of *seismic hazard curves*, which indicate the annual probability of exceedance of

different values of a selected ground motion parameter. The seismic hazard curves can then be used to compute the probability of exceeding the selected ground motion parameter in a specified period of time.

4.4.4.1 Seismic Hazard Curves

Seismic hazard curves can be obtained for individual source zones and combined to express the aggregate hazard at a particular site. The basic concept of the computations required for development of seismic hazard curves is fairly simple. The probability of exceeding a particular value, y^* , of a ground motion parameter, Y , is calculated for one possible earthquake at one possible source location and then multiplied by the probability that that particular magnitude earthquake would occur at that particular location. The process is then repeated for all possible magnitudes and locations with the probabilities of each summed. The required calculations are described in the following paragraphs.

For a given earthquake occurrence, the probability that a ground motion parameter Y will exceed a particular value y^* can be computed using the total probability theorem, that is,

$$P[Y > y^*] = P[Y > y^* | \mathbf{X}] P[\mathbf{X}] = \int P[Y > y^* | \mathbf{X}] f_x(\mathbf{X}) dx \quad (4.18)$$

where \mathbf{X} is a vector of random variables that influence Y . In most cases the quantities in \mathbf{X} are limited to the magnitude, M , and distance, R . Assuming that M and R are independent, the probability of exceedance can be written as

$$P[Y > y^*] = \iint P[Y > y^* | m, r] f_M(m) f_R(r) dm dr \quad (4.19)$$

where $P[Y > y^* | m, r]$ is obtained from the predictive relationship and $f_M(m)$ and $f_R(r)$ are the probability density functions for magnitude and distance, respectively.

If the site of interest is in a region of N_S potential earthquake sources, each of which has an average rate of threshold magnitude exceedance, $\nu_i [= \exp(\alpha_i - \beta_i m_0)]$, the total average exceedance rate for the region will be given by

$$\lambda_{y^*} = \sum_{i=1}^{N_S} \nu_i \iint P[Y > y^* | m, r] f_{Mi}(m) f_{Ri}(r) dm dr \quad (4.20)$$

The individual components of equation (4.20) are, for virtually all realistic PSHAs, sufficiently complicated that the integrals cannot be evaluated analytically. Numerical integration, which can be performed by a variety of different techniques, is therefore required. One approach, used here for simplicity rather than efficiency, is to divide the possible ranges of magnitude and distance into N_M and N_R segments, respectively. The average exceedance rate can then be estimated by

$$\lambda_{y^*} = \sum_{i=1}^{N_S} \sum_{j=1}^{N_M} \sum_{k=1}^{N_R} \nu_i P[Y > y^* | m_j, r_k] f_{Mi}(m_j) f_{Ri}(r_k) \Delta m \Delta r \quad (4.21)$$

where $m_j = m_0 + (j - 0.5)(m_{\max} - m_0)/N_M$, $r_k = r_{\min} + (k - 0.5)(r_{\max} - r_{\min})/N_R$, $\Delta m = (m_{\max} - m_0)/N_m$, and $\Delta r = (r_{\max} - r_{\min})/N_R$. This is equivalent to assuming that each source is capable of generating only N_M different earthquakes of magnitude, m_j , at only N_R different source-to-site distances, r_k . Equation (4.21) is then equivalent to

$$\lambda_{y^*} \approx \sum_{i=1}^{N_S} \sum_{j=1}^{N_M} \sum_{k=1}^{N_R} v_i P[Y > y^* | m_j, r_k] P[M = m_j] P[R = r_k] \quad (4.22)$$

The accuracy of the crude numerical integration procedure described above increases with increasing N_M and N_R . More refined methods of numerical integration will provide greater accuracy at the same values of N_M and N_R .

Example 4.5

The basic procedures of a typical PSHA can be illustrated for the site shown in Figure 4-6 if the recurrence relationships for each of the source zones is known. Assuming that the seismicity of the respective source zones are described by

$$\text{Source zone 1: } \log \lambda_m = 4.4 - 1.0M$$

$$\text{Source zone 2: } \log \lambda_m = 3.5 - 0.8M$$

$$\text{Source zone 3: } \log \lambda_m = 2.7 - 1.2M$$

the PSHA can be performed in the four previously described steps:

1. The problem statement provides the location, geometry, and maximum magnitude of each source zone. The distribution of source-to-site distance must also be characterized. To limit the number of computations involved in this simple example, we will characterize the distribution of source-to-site distance by a relatively coarse histogram. Consider first source zone 1. It is a simple matter to show that the shortest possible source-to-site distance will be 23.72 km and that the longest will be 90.12 km. We can divide this total range into 10 distance intervals of length $(90.12 \text{ km} - 23.72 \text{ km})/10 = 6.64 \text{ km}$. If we divide the source zone into a large number of segments of equal length, we can characterize the distribution of source-to-site distance by determining how many of the segments fall within each distance interval. For 1000 segments, the normalized histogram of source-to-site distance is shown in Figure E4.5a. The ordinates of the normalized histogram represent the relative frequency that would be equal to the probability if an infinite number of segments were used, but which is an approximation to the probability in this case. The probability that the source-to-site distance is between 23.72 and 30.36 km (or about equal to the midpoint of that range, 27.04 km) is approximately 0.336. For source zone 2, the source-to-site range 25 to 125 km can be divided into 10 intervals of 10-km length; dividing the areal source zone into 2500 elements of equal area, the normalized histogram of Figure E4.5b is obtained. Since there is only one possible source-to-site distance, obtaining the normalized histogram of Figure E4.5c for source zone 3 is trivial matter.

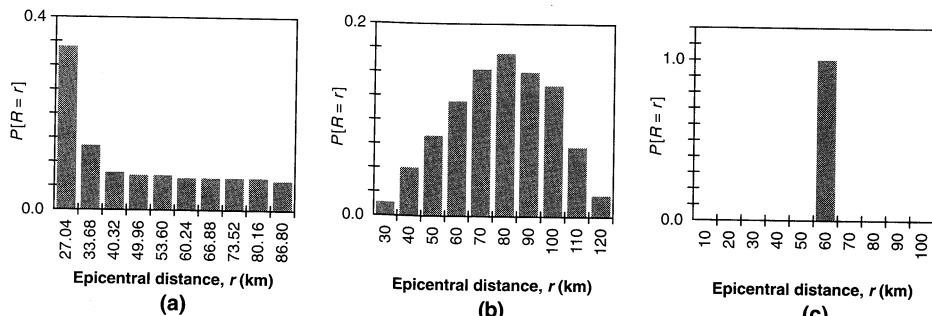


Figure E4.5a–c Approximations to source-to-site probability distributions for source zones (a)1, (b)2, and (c)3.

2. The temporal distribution of earthquake recurrence can be characterized using the recurrence relationships provided in the problem statement. Assuming that earthquakes of magnitude less than 4.0 do not contribute to the seismic hazard, the mean rates of exceedance of magnitude 4.0 events from each of the source zones are

$$\text{Source zone 1: } \nu_1 = 10^{4.4 - 1.0(4.0)} = 2.512$$

$$\text{Source zone 2: } \nu_2 = 10^{3.5 - 0.8(4.0)} = 1.995$$

$$\text{Source zone 3: } \nu_3 = 10^{2.7 - 1.2(4.0)} = 0.008$$

giving $\nu_{\text{total}} = 4.515$. For each source zone, the probability that the magnitude will be within an interval between a lower bound m_l and an upper bound m_u is given by

$$P[m_l < M < m_u] = \int_{M=m_l}^{M=m_u} f_M(m) dm \approx f_M\left(\frac{m_l + m_u}{2}\right)(m_u - m_l)$$

where $f_M(m)$ is given in equation (4.12). If $N_M = 10$, the lowest magnitude interval for source zone 1 will be from $M = 4.0$ to $M = 4.33$. The probability that the magnitude would fall within that interval would be

$$P[4.0 < M < 4.33] \approx \frac{2.303 e^{-2.303(4.165 - 4.0)}}{1 - e^{-2.303(7.3 - 4.0)}} (4.33 - 4.0) = 0.522$$

The probabilities of various magnitudes for each source zone are as shown in Figure E4.5d-f.

3. To compare the results of this PSHA with those from the DSHA example, we will use the same predictive relationship: that is, the Cornell et al. (1979) relationship

$$\ln \text{PHA (gals)} = 6.74 + 0.859M - 1.80 \ln(R + 25)$$

Uncertainty in this relationship is expressed by the standard deviation $\sigma_{\ln y} = 0.57$.

4. Finally, we compute the total seismic hazard as the sum of the contributions from each possible combination of source-to-site distance and earthquake magnitude on each of the three source zones. First, we consider source zone 1. For the lowest magnitude interval ($j = 1$),

$$P[M = m_1] = P[M = 4.165] = 0.522$$

as computed in step 2. For the lowest distance interval ($k = 1$),

$$P[R = r_1] = P[R = 27.04 \text{ km}] = 0.336$$

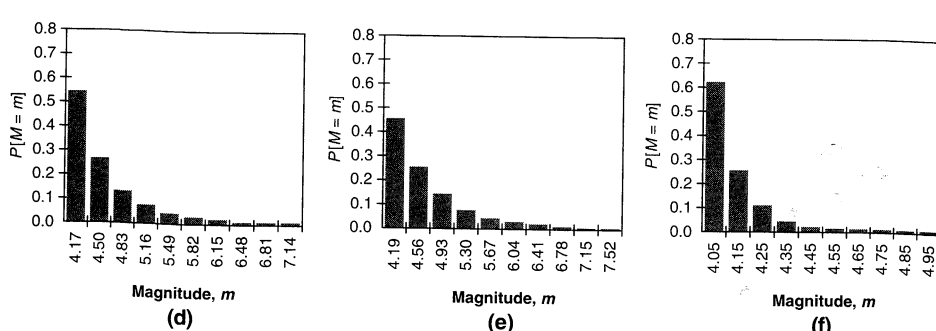


Figure E4.5d-f Approximations to magnitude probability distributions for source zones (d)1, (e)2, and (f)3.

as computed in step 1. This combination of magnitude and distance indicates an expected value of $\ln \text{PHA}$ of

$$\overline{\ln \text{PHA}} = 3.204$$

Now we can calculate the probabilities that various target peak acceleration levels will be exceeded. For $a^* = 0.01g$ (9.81 gals), the corresponding standard normal variable is

$$z^* = \frac{\ln a^* - \overline{\ln \text{PHA}}}{\sigma_{\ln y}} = \frac{\ln (9.81) - 3.204}{0.57} = -1.63$$

Then the probability that the peak acceleration is greater than $0.01g$, using Table 4-2, is

$$\begin{aligned} P[\text{PHA} > 0.01g | M = 4.165, R = 27.04 \text{ km}] &= P[z^* > -1.63] \\ &= 1 - P[z^* < -1.63] \\ &= 1 - F_z(-1.63) \\ &= 0.9484 \end{aligned}$$

Annual rate of exceedance of a peak acceleration of $0.01g$ by an earthquake of magnitude 4.165 at a distance of 27.04 km on source zone 1 (given that an earthquake of $M > m_0$ occurs on source zone 1) will be

$$\begin{aligned} \lambda_{0.01g} &= v_1 P[\text{PHA} > 0.01g | M = 4.165, R = 27.04 \text{ km}] \\ &\quad \times P[M = 4.165] P[R = 27.04] \\ &= 2.512 (0.9484) (0.522) (0.336) \\ &= 0.4181 \end{aligned}$$

If the preceding calculations are repeated for the 99 other possible combinations of magnitude and distance for source zone 1, the contributions of each will be

Magnitude	Distance (km)									
	27.04	33.68	40.32	46.96	53.60	60.24	66.88	73.52	80.16	86.80
4.165	0.4181	0.1501	0.0805	0.0676	0.0559	0.0456	0.0369	0.0293	0.0231	0.0179
4.495	0.2027	0.0753	0.0424	0.0376	0.0331	0.0289	0.0250	0.0213	0.0181	0.0149
4.825	0.0957	0.0363	0.0209	0.1092	0.0177	0.0162	0.0148	0.0134	0.0120	0.0106
5.155	0.0452	0.0172	0.0100	0.0093	0.0088	0.0084	0.0079	0.0074	0.0070	0.0065
5.485	0.0212	0.0081	0.0047	0.0045	0.0042	0.0041	0.0040	0.0038	0.0037	0.0035
5.815	0.0099	0.0037	0.0022	0.0021	0.0020	0.0019	0.0019	0.0018	0.0018	0.0018
6.145	0.0045	0.0018	0.0010	0.0010	0.0010	0.0010	0.0009	0.0009	0.0009	0.0009
6.475	0.0023	0.0009	0.0005	0.0005	0.0005	0.0005	0.0005	0.0004	0.0004	0.0004
6.805	0.0011	0.0004	0.0003	0.0002	0.0002	0.0002	0.0002	0.0002	0.0002	0.0002
7.135	0.0005	0.0002	0.0001	0.0001	0.0001	0.0001	0.0001	0.0001	0.0001	0.0001

Summing all of these contributions indicates that the mean annual rate at which an acceleration of $0.01g$ will be exceeded by an earthquake on source zone 1 will be 1.923. Repeating all of these calculations for the other source zones yields equivalent exceedance rates of 1.016 for source zone 2 and 0.005 for source zone 3. Consequently, the probability that a target acceleration of $0.01g$ will be exceeded by an earthquake of $M > m_0$ on any of the three source zones will be $1.923 + 1.016 + 0.005 = 2.944$. This implies a return period of 0.34 year for this low acceleration. By repeating this process for different target accelerations, the seismic hazard curves of Figure E4.5g can be developed.

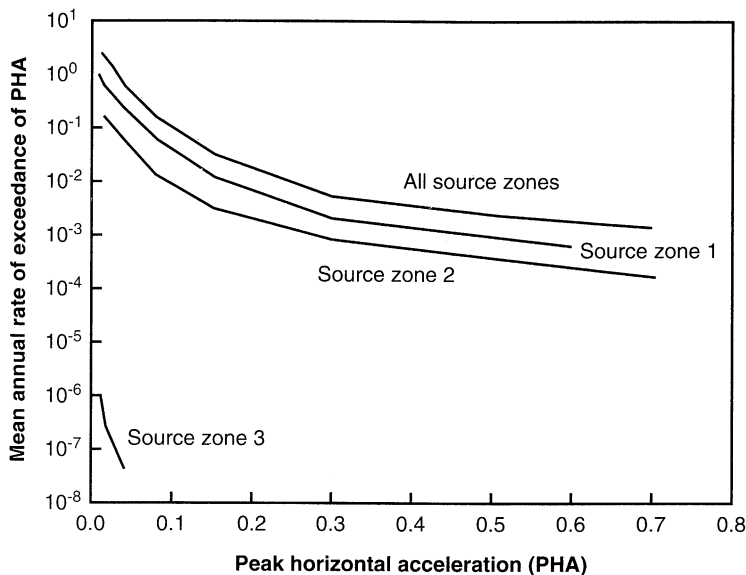


Figure E4.5g Seismic hazard curves for source zones 1, 2, and 3 and total seismic hazard curve for all sources.

4.4.4.2 Finite Time Periods

The seismic hazard curve can easily be combined with the Poisson model to estimate probabilities of exceedance in finite time intervals. From equation (4.17), the probability of exceedance of y^* in a time period T is

$$P [Y_T > y^*] = 1 - e^{-\lambda_{y^*} T} \quad (4.23)$$

Example 4.6

Returning to Example 4.5, the probability that an acceleration of $0.10g$ would be exceeded in a 30-year period would be

$$P [\text{PHA} > 0.10g \text{ in 30 years}] = 1 - e^{-\lambda_{y^*} T} = 1 - e^{-(0.0822)(30)} = 0.915 = 91.5\%$$

It is often necessary to compute the value of a ground motion parameter corresponding to a particular probability of exceedance in a given time period. For example, the acceleration level that has a 10% probability of exceedance in a 50-year period would be that with an annual rate of exceedance, obtained by rearranging equation (4.23), of

$$\lambda_{y^*} = \frac{-\ln(1 - P[Y_T > y^*])}{T} = \frac{-\ln(1 - 0.1)}{50} = 0.00211$$

From the total seismic hazard curve of Figure 4.18, that acceleration level would be approximately $0.63g$.

These types of analyses have been performed for a variety of seismically active areas within the United States. As the exposure time, T , increases, the probability of exceeding a particular ground motion parameter value also increases. Similarly, the value of a ground motion parameter with a particular probability of exceedance increases with increasing exposure time. Figure 4.15 illustrates the peak acceleration with a 10% probability of

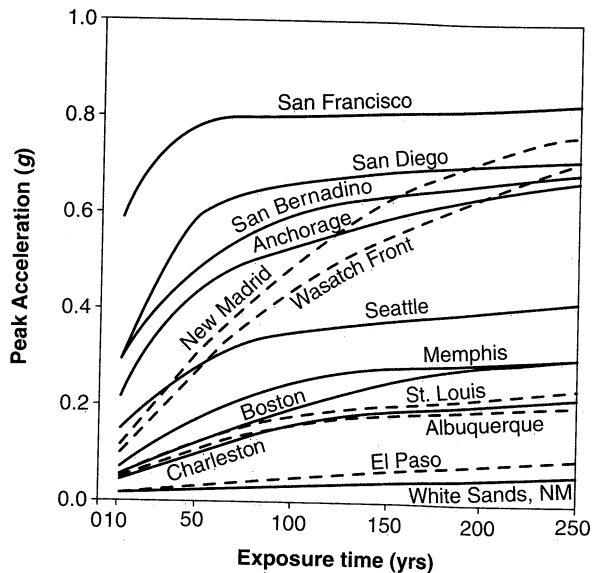


Figure 4.15 Peak horizontal bedrock accelerations with 10% probability of exceedance over various exposure times for 14 areas in North America. (After NEHRP, 1993.)

exceedance for a number of metropolitan areas within the United States. Seismic hazard maps, such as that shown in Figure 4.16, have been developed to express the relative seismicity of different regions in building codes (Chapter 8).

4.4.4.3 Deaggregation

The PSHA procedures described in the preceding sections allow computation of the mean annual rate of exceedance at a particular site based on the aggregate risk from potential earthquakes of many different magnitudes occurring at many different source-site distances. The rate of exceedance computed in a PSHA, therefore, is not associated with any particular earthquake magnitude or source-site distance.

In some cases, however, it may be useful to estimate the most likely earthquake magnitude and/or the most likely source-site distance. These quantities may be used, for example, to select existing ground motion records (recorded in earthquakes of similar magnitude at similar source-site distance) for response analyses. This process of *deaggregation* requires that the mean annual rate of exceedance be expressed as a function of magnitude and/or distance. Computationally, this simply involves the removal of terms from the summations of Equation 4.22. For example, the mean annual rate of exceedance can be expressed as a function of magnitude by

$$\lambda_{y^*}(m_j) \approx P[M = m_j] \sum_{i=1}^{N_S} \sum_{k=1}^{N_R} v_i P[Y > y^* | m_j, r_k] P[R = r_k] \quad (4.24)$$

Similarly, the mean annual rate of exceedance can be expressed as a function of source-site distance by

$$\lambda_{y^*}(r_k) \approx P[R = r_k] \sum_{i=1}^{N_S} \sum_{j=1}^{N_M} v_i P[Y > y^* | m_j, r_k] P[M = m_j] \quad (4.25)$$



Figure 4.16 Contours of mean horizontal acceleration on rock (expressed as a percentage of gravity) with 10% probability of exceedance in 50 years.
(After Algermissen et al., 1990.)

Finally, it is possible to compute the mean annual rate of exceedance as functions of both earthquake magnitude and source-site distance, i.e.

$$\lambda_{y^*}(m_j, r_k) \approx P[M = m_j] P[R = r_k] \sum_{i=1}^{N_S} \nu_i P[Y > y^* | m_j, r_k] \quad (4.26)$$

4.4.4.4 Logic Tree Methods

The probability computations described previously allow systematic consideration of uncertainty in the values of the parameters of a particular seismic hazard model. In some cases, however, the best choices for elements of the seismic hazard model itself may not be clear. The use of *logic trees* (Power et al., 1981; Kulkarni et al., 1984; Coppersmith and Youngs, 1986) provides a convenient framework for the explicit treatment of model uncertainty.

The logic tree approach allows the use of alternative models, each of which is assigned a weighting factor that is interpreted as the relative likelihood of that model being correct. It consists of a series of nodes, representing points at which models are specified and branches that represent the different models specified at each node. The sum of the probabilities of all branches connected to a given node must be 1. The simple logic tree shown in Figure 4.17 allows uncertainty in selection of models for attenuation, magnitude distribution, and maximum magnitude to be considered. In this logic tree, attenuation according to the models of Campbell and Bozorgnia (1994) and Boore et al. (1993) are considered equally likely to be correct, hence each is assigned a relative likelihood of 0.5. Proceeding to the next level of nodes, the Gutenberg–Richter magnitude distribution is considered to be 50% more likely to be correct than the characteristic earthquake distribution. At the final level of nodes, different relative likelihoods are assigned to the maximum magnitude. This logic tree terminates with a total of $2 \times 2 \times 3 = 12$ (no. of attenuation

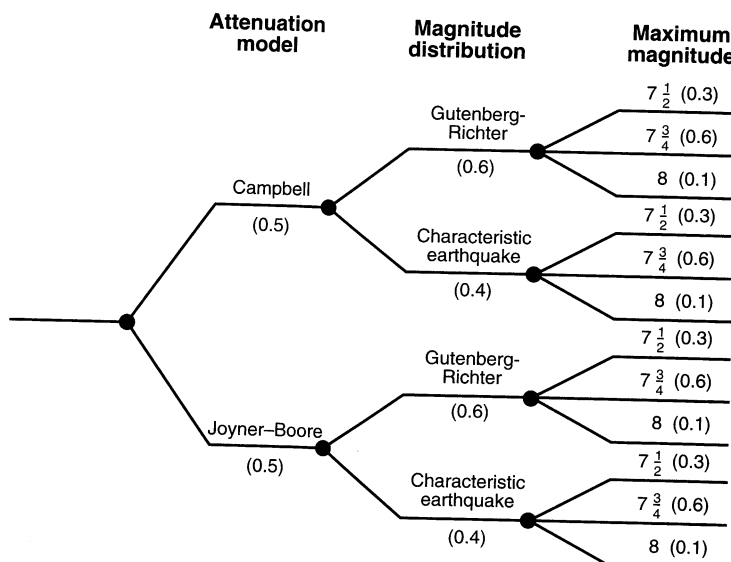


Figure 4.17 Simple logic tree for incorporation of model uncertainty.

models \times no. of magnitude distributions \times no. of maximum magnitudes) branches. The relative likelihood of the combination of models and/or parameters implied by each terminal branch is given by the product of the relative likelihood of the terminal branch and all prior branches leading to it. Hence the relative likelihood of the combination of the Campbell attenuation model, Gutenberg–Richter magnitude distribution, and maximum magnitude of 7.5 is $0.5 \times 0.6 \times 0.3 = 0.09$. The sum of the relative likelihoods of the terminal branches, or of those at any prior level, is equal to 1.

To use the logic tree, a seismic hazard analysis is carried out for the combination of models and/or parameters associated with each terminal branch. The result of each analysis is weighted by the relative likelihood of its combination of branches, with the final result taken as the sum of the weighted individual results.

It is easy to see that the required computational effort increases quickly with increasing numbers of nodes and branches. Parameters best characterized by continuous distributions (e.g., the maximum magnitude in the example of Figure 4.17) are difficult to treat in the logic tree without resorting to large numbers of branches. Nevertheless, the logic tree is a very useful tool for the analysis of seismic hazards.

4.5 SUMMARY

1. Earthquake-resistant design seeks to produce structures that can withstand a certain level of shaking without excessive damage. That level of shaking is described by a design ground motion which is usually determined with the aid of a seismic hazard analysis.
2. Seismic hazard analyses involve the quantitative estimation of ground motion characteristics at a particular site. They may be conducted deterministically or probabilistically.
3. Seismic hazard analyses require the identification and characterization of all potential sources of seismic activity that could produce significant ground motions at the site of interest. Earthquake sources may be identified on the basis of geologic, tectonic, historical, and instrumental evidence.
4. Deterministic seismic hazard analyses involve the assumption of some scenario—the occurrence of an earthquake of a particular size at a particular location—for which ground motion characteristics are determined. In practice, DSHAs often assume that earthquakes of the largest possible magnitude occur at the shortest possible distance to the site within each source zone. The earthquake that produces the most severe site motion is then used to compute site-specific ground motion parameters.
5. When applied to structures for which failure could have catastrophic consequences, such as nuclear power plants and large dams, DSHA provides a straightforward framework for evaluation of “worst-case” ground motions. However, it provides no information on the likelihood of occurrence of the controlling earthquake, the likelihood of it occurring where it is assumed to occur, the level of shaking that might be expected during a finite period of time (such as the useful lifetime of a particular structure or facility), or the effects of uncertainties in the various steps required to compute the resulting ground motion characteristics.

6. Probabilistic seismic hazard analyses allow uncertainties in the size, location, rate of recurrence, and effects of earthquakes to be explicitly considered in the evaluation of seismic hazards. A PSHA requires that uncertainties in earthquake location, size, recurrence, and ground shaking effects be quantified.
7. For each source zone, uncertainty in earthquake location is characterized by a probability density function of source-to-site distance. Evaluation of the probability density function requires estimation of the geometry of the source zone and of the distribution of earthquakes within it.
8. Uncertainty in the sizes of earthquakes produced by each source zone can be described by various recurrence laws. The Gutenberg–Richter recurrence law, which assumes an exponential distribution of magnitude, is commonly used with modifications to account for minimum and maximum magnitudes. A more recent interpretation of fault activity has produced the characteristic earthquake recurrence law. Which of these two recurrence laws is more correct has not yet been determined; it is not uncommon to incorporate both into a PSHA by means of a logic tree.
9. The level of shaking produced by an earthquake of a given size occurring at a given source-to-site distance is determined from predictive relationships. The uncertainty in these ground motions is a function of the scatter in the databases from which the predictive relationships were developed.
10. The probabilities of earthquakes of various sizes occurring in finite periods of time are usually computed assuming that earthquakes occur as Poisson processes. Although the Poisson model assumes an independence of events that is not consistent with elastic rebound theory, it remains the most commonly used model in contemporary PSHA.
11. Standard methods of probability analysis can be used to combine the quantified uncertainties in earthquake size, location, recurrence, and effects to compute ground motion levels with various probabilities of exceedance in different periods of time. Because of the complex and empirical nature of the probability density functions, exceedance probabilities are usually computed by numerical, rather than analytical, methods.
12. The accuracy of a PSHA depends on the accuracy with which uncertainty in earthquake size, location, recurrence, and effects can be characterized. Although models and procedures for characterization of uncertainty of these parameters are available, they may be based on data collected over periods of time that, geologically, are very short. Engineering judgment must be applied to the interpretation of PSHA results.
13. Model uncertainties can be incorporated into a PSHA by means of a logic tree. A logic tree allows the use of alternative models, each of which is assigned a weighting factor related to the likelihood of that model being correct. The weighting factors are usually assigned subjectively, often using expert opinion.

HOMEWORK PROBLEMS

- 4.1 Estimate the surface rupture lengths, rupture areas, and maximum surface displacements for earthquakes of $M_w = 6$ and $M_w = 8$.

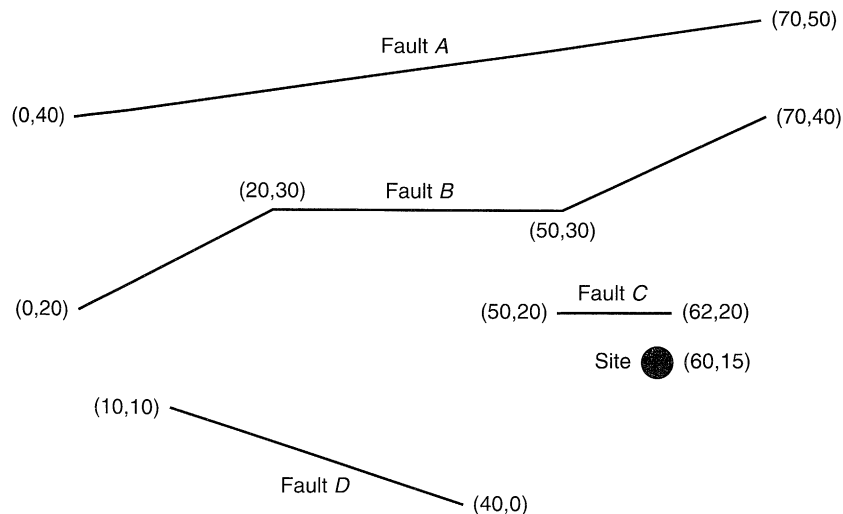


Figure P4.2

4.2 The site shown in Figure P4.2 is located near four active faults in California. Fault A is a normal fault. Faults B and C are strike-slip faults, and Fault D is a reverse fault. The coordinates of the site and faults shown above are in km. Assuming that only linear segments can rupture in an individual event, perform a deterministic seismic hazard analysis to:

- Determine the anticipated peak acceleration at the site. Use the attenuation relationship(s) from Chapter 3 you believe are most appropriate and briefly justify your selection.
- Determine and plot the anticipated response spectrum at the site.
- Assuming that the site consists of a bedrock outcrop, determine the anticipated duration of strong motion at the site.
- Estimate the anticipated Arias Intensity at the site.

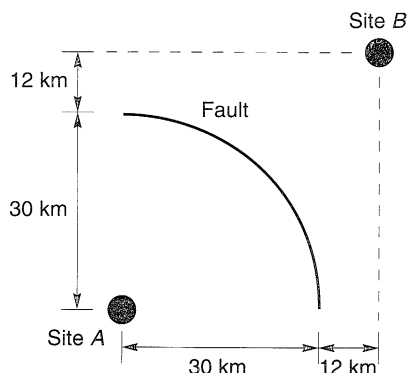


Figure P4.3

- 4.3** The hypothetical vertical fault segment shown in Figure P4.3 is represented as a quarter-circle. On the same graph, plot histograms of expected epicentral distance for motions at Site A and Site B assuming:
- Earthquakes are equally likely to occur at any point on the fault segment.
 - Earthquakes are twice as likely to occur at the midpoint of the fault segment as at either end and the likelihood is linearly distributed between the midpoint and the ends.
- 4.4** In a hypothetical seismically active region, earthquakes have been recorded over an 80-year period. Part of the record is instrumental, but part is not. Combining all available data, it appears that the earthquakes have been distributed as follows:

MOMENT MAGNITUDE	NUMBER OF EARTHQUAKES
3–4	~1800
4–5	~150
5–6	11
> 6	1

- Estimate the Gutenberg–Richter parameters for the region.
 - Neglecting earthquakes of magnitude less than 3, compute the probability that an earthquake in the region will have a moment magnitude between 5.5 and 6.5.
 - Repeat Part(b) assuming that paleoseismic evidence indicates that the region is not capable of producing earthquakes of moment magnitude greater than 6.5.
- 4.5** The seismicity of a particular region is described by the Gutenberg–Richter recurrence law:
- $$\log \lambda_m = 4.0 - 0.7M$$
- What is the probability that at least one earthquake of magnitude greater than 7.0 will occur in a 10-year period? In a 50-year period? In a 250-year period?
 - What is the probability that exactly one earthquake of magnitude greater than 7.0 will occur in a 10-year period? In a 50-year period? In a 250-year period?
 - Determine the earthquake magnitude that would have a 10% probability of being exceeded at least once in a 50-year period.
- 4.6** A hypothetical site is located at the end of a hypothetical 300 km long linear feature known as Holtz's Fault. Historical data indicates that the seismicity of Holtz's Fault can be described by the relationship

$$\log \lambda_m = 3.0 - 0.75M$$

Peak accelerations in the region of Holtz's Fault can be described by the simple attenuation relationship of Campbell (1981), even for distances greater than 50 km.
Given the above information:

- Develop a seismic hazard curve for peak acceleration at the site.
- Determine the probability that an acceleration of 0.25 g will be exceeded at least once in a 100-year period.
- Determine the peak acceleration that would have a 10% probability of being exceeded at least once in a 50-year period.

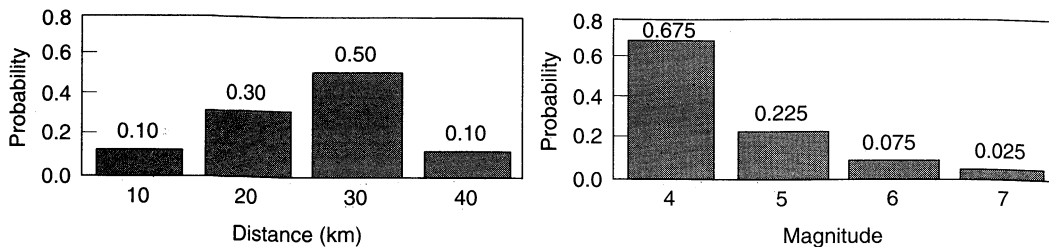
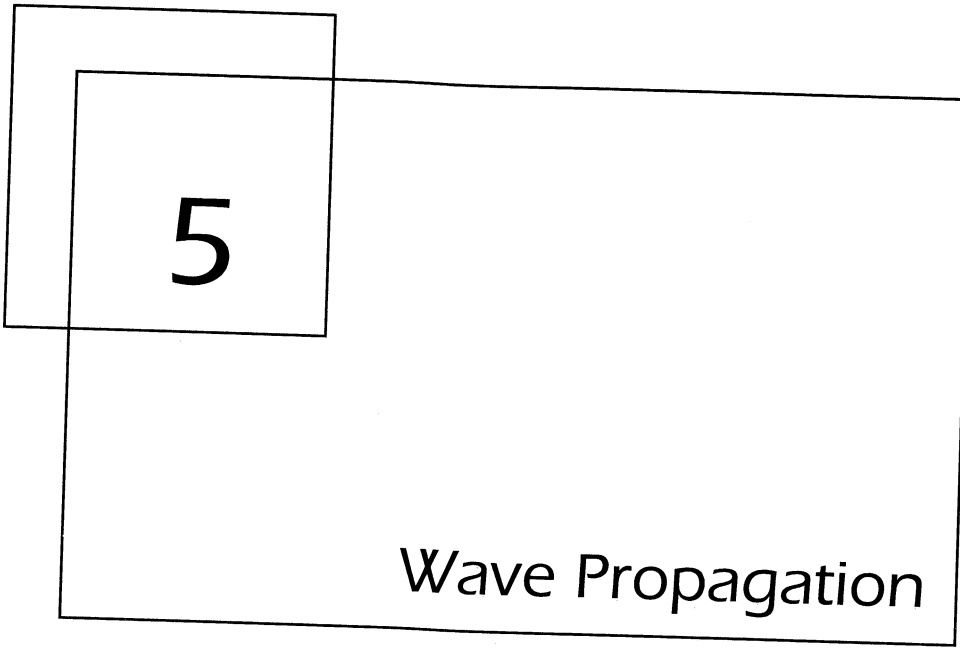


Figure P4.7

- 4.7** A new seismic source is identified in the vicinity of the site described in Problem 6. The geometry of the source is such that the source-site distance is distributed as indicated by the simple histogram above. The source is expected to produce an earthquake of magnitude 4 or more every 5 years, on average, and the magnitudes are expected to be distributed as indicated in the simple histogram above. Assuming that earthquakes of magnitude 4, 5, 6, or 7 can occur at distances of 10, 20, 30, or 40 km, and using the attenuation relationship given in Problem 6,
- (a) Develop and plot a seismic hazard curve for peak acceleration at the site that considers both Holtz's Fault and the new seismic source. Plot the individual seismic hazard curves on the same graph.
 - (b) Considering both sources, determine the probability that an acceleration of 0.25 g will be exceeded at least once in a 100-year period.
 - (c) Considering both sources, determine the peak acceleration that would have a 10% probability of being exceeded at least once in a 50-year period.



5

Wave Propagation

5.1 INTRODUCTION

It is the continuous nature of geologic materials that causes soil dynamics and geotechnical earthquake engineering to diverge from their structural counterparts. While most structures can readily be idealized as assemblages of discrete masses with discrete sources of stiffness, geologic materials cannot. They must be treated as continua, and their response to dynamic disturbances must be described in the context of wave propagation.

Some basic concepts of wave propagation have been alluded to in previous chapters; a more fundamental treatment of the basic concepts is presented in this chapter. The presentation follows a repeated pattern of simple-to-complex applications. The relatively simple problem of waves in unbounded media is followed by the more complicated problem of waves in bounded and layered media. Within each, the concepts are presented first for the simple case of one-dimensional wave propagation, and then for the more general three-dimensional case. The careful reader will note that the basic techniques and principles used to solve the more complicated cases are generally the same as those used for the simple cases; the additional complexity simply results from the need to consider more dimensions.